MASTER

Modeling, designing and characterizing a micro fluidic cell stretcher to measure cell elasticity

van Rijen, M.W.J.M.

Award date:
2006

Modeling, designing and characterizing a micro fluidic cell stretcher to measure cell elasticity

M.W.J.M van Rijen

Report MT 06.14

Technical University Eindhoven
Department: Mechanical Engineering
Section: Polymer Technology
Specialization: Micro and Nano Technology
Graduation coaches: Prof. J.M.J. den Toonder and Dr. P.D. Anderson
Student number: (0531080)

May 1, 2006

Preface

This thesis was written for my master degree at the department MaTerials Technology (MaTe) of the University of Technology of Eindhoven. My specialization is micro and nano technology. Before I decided which project I wanted to do, I had talked to several professors and sent several e-mails. My interest went out to a project with a theoretical as well a possible experimental approach. With a project having both aspects a validation could be made of the theoretical results to the experimental results.

After a meeting with Prof. J.M.J. den Toonder, I was curious and excited about this project, that was proposed to me. The project has a theoretical part of creating a model for the deformation of a biological cell through a micro fluidic cell stretcher. Besides the theoretical part a micro fluidic cell stretcher will be made, so that experimental measurements can be preformed. With the experimental data and the theoretical model a comparison can be made between the theory and the experimental results.

This project also allowed me to get an introduction to biomedical engineering. Before my master thesis I did not have any experience with biological cells or techniques used in the medical world. It took some time to learn about the structure of cells and the behavior of mechanical stimuli on cells, but it has increased my overview of the possibilities after my study. Also no know research had been done on this project, which makes this project even a bigger challenge to me.

The project is a cooperation between Philips and the University of Eindhoven of the departments material science, biomechanical engineering and micro- and nano-technology. This allowed me to work with many people and get an inside view of the company Philips and the work going on at the Technical University Eindhoven. I also participated at the meetings of Philips biosensor and meetings of the fluid-structure group, micro- and nano-technologie group and polymer group at the Technical University of Eindhoven. This has increased my knowledge of several available techniques and research in these regions.

Because many people worked with me on this project, I want to thank all the people that make this project possible. As specially I want to thank my graduation coaches Prof. J.M.J. den Toonder and Dr. P.D. Anderson for their support and enthusiasm. I want to thank Dr. C.V.C. Bouten for her support and knowledge about biological cells. I want to thank Dr. R. van Loon and Dr. V.V. Khatavkar for their support on the Sepran software. Also I want to thank Ir. L. Meijer for her help with the experiments and preparation of the cells and H. Timmermans (Phillips) who made all the components for the micro fluidic cell stretcher. I want to thank G. Peters for his support to find all the equipment to make the experimental setup possible. Also I want to thank W. Buysse, R. van Aalst, B. van Daal and M. Thissen for their contribution on the experimental setup. All the other people I did not mention but helped me also with this project, thank you all.

Eindhoven, April 2006,

Tommie van Rijen

Summary

All tissues in mammalian organisms are composed of an assembly of cells. The cells are subjected to mechanical stimuli arising from either the external or the internal environment. Cells positively respond to mechanical stimuli by changing their own behavior and by modifying their environment. If forces are applied to the cell, the response can either lead to cell adaption or to cell damage or death when the applied forces exceeds the adaptive capacity of the cell. The most important cellular structures, that are relevant for the mechanical properties of the cell are the plasma membrane, cytoplasm, cytoskeleton and nucleus.

The elasticity of cells is mainly determined by their cytoskeleton. Changes in cellular function are reflected in the amount of cytoskeleton proteins and their associated networks. Diseases that influence the cytoskeleton could be detected by measuring the elasticity of the cell. A drastic change in elasticity is caused by diseases such as cancer, in which the altered cytoskeleton can be used for diagnostic purposes. A cell hosted by a disease, such as cancer, has a lower elasticity than a cell that is normal. Other deceases, such as malaria, increase the elasticity compare to the healthy cell.

There are several techniques that can be used to measure the elastic properties of a cell. The techniques can be divided into two groups. The first group consists of techniques designed for local loading of single cells, which contains the partial micropipette aspiration, cell poking or cell indentation and atomic force microscopy (AFM). The seconde group are techniques designed for global loading of single cells which contains full micropipette aspiration, micromanipulation, micro-plates, optical tweezers and magnetic bead twister. Each technique gives different results in elasticity for the same type of cell. This can be explained by the variety of loading methods, different cell cultures or different testing environments. These parameters all have an influence on the measured mechanical cell properties.

Existing techniques for measuring the elasticity of cells have a drastic limitation. The tedious sample preparation limits the number of cells investigated, ruling out applications in clinical diagnostics. To overcome the limitation, an optical tweezer has been developed recently. The optical stretcher aims also to detect cancerous cells before they become cancerous. The optical stretcher is still in development, but some experiments are carried out in a hospital in Germany. One disadvantage is the influence of the laser light on the cell. The laser light could give radiation problems on the cells. To minimize the influence of the measurement technique the laser could be replaced by an elongating flow. The project assignment was to develop a single cell stretch device through an elongating flow, which can detect the deformation of the cell. A high throughput is preferred for a possible clinical diagnostics application to determine if a cell is precancerous or normal.

A numerical model has been made to predict the influence of several dimensional numbers on the deformation of the cell. The deformation of the cell is defined by the Taylor deformation rate D_{xy}, which is the ration between the difference of the x and y dimension divided by the sum of the x and y dimension. The following assumptions were made for the numerical model. The problem is two-dimensional and the initial shape of the cell is circular. The numerical model was made with the finite element package Sepran. The flow is described in the fluid domain Ω_f and the cell is described in the structure domain (Ω_s). A laminar flow is assumed which behaves isothermal, incompressible and Newtonian. The cell is assumed to be hyperelastic and isotropic and is described by a Neo-Hookean constitutive model. The model calculated the different equations for the fluid domain Ω_f, structure domain Ω_s and interaction between the fluid and solid domain. The result of the simulation was the deformation of the cell during flow inside the micro fluidic cell stretcher. The dimensionless numbers that characterize the micro fluidic cell stretcher were the Deborah number (De), the Reynolds number (Re) and the fraction number F_{RW}. The influence of the dimensionless numbers (De, Re, F_{RW}) on the deformation of the cell were investigated. The De-number and the F_{RW}-number have significant influence on the deformation of the cell inside the micro fluidic cell stretcher. The model predicted that a cell could be deformed inside the micro fluidic cell stretcher if the viscosity and velocity of the fluid were high enough and the width of the micro channel was small enough. The results of the simulation were used to design the micro fluidic cell stretcher.

An experimental setup has been designed and made. The geometry of the micro fluidic cell stretcher is based on a cross slot geometry. Inside the cross slot a cell can be positioned at the stagnation point by controlling the exit flows of the cross slot. The flow is controlled using a camera and software that actuate two micro valves at the exits of the cross slot. With continuously control of the flow, the cell can be held in the middle and the flow velocity can be increased. Due to the increasing flow the cell will deform and images can be taken from the deformed and normal state of the cell. When images are taken from the cell in deformed and normal state, a Matlab routine determines the Taylor deformation rate of the cell. For this system, the cross slot, the micro valves with software to control them and the software to determine the Taylor deformation rate had to be designed. The cells can be inserted inside the cross slot with a T-junction. The main flow and the flow of the cells are both controlled individually with syringe pumps, that are controlled with a computer or manually. Some cells were made fluorescent to enhance the contrast and improve the measurement of the deformation of the cell. The cross slot channels are closed with a vacuum system, which makes it easy to clean the channels after the experiments.

For the experiments Fibroblasts are chosen as a model cell, because many studies have already been carried out using these cells. Fibroblasts are easy to grow in culture and have a finite line of 50 generations. Also the fibroblasts are employing immunofluorescence, which means that the properties of fibroblasts do not change if they are fluorescent and they can live for a relative long time if they are fluorescent. The cell's geometric properties are relatively constant between the cells, which gives better statistics results. The size of a 3T3-fibroblasts is around 10 μm and the average elastic modulus is 380 Pa and was measure by E. Peters with micromanipulation, following [Peeters, 2004].

Many experiments were done to prove the principle of stretching cells with micro fluidic

flow. Cells flowing through a sudden contraction, and cells flowing through the cross slot geometry were studied. The sudden contraction resulted in little deformation of the cell even for the contraction width of 400 μm to 25 μm. Another problem was the limited time for imaging the deformation of the cell. This problem was solved with a high speed camera of Kodak (sr 1000), but still the deformation of the cell was too little. Small contraction had been designed, but the production of the foil mask had problems.

The second kind of experiments are for the cross slot geometry. Three dimensions of the cross slot were made, namely cross slots with a main channel of 500μm, 200μm and 100μm. The 500 μm cross slot is too big to induce any deformation of the cells. Some experiments were done with the 200μm and 100 μm channel. During the experiments many problems occurred. The main problem in all the experiments was the leakage of the fluid to the vacuum system. The channels where not closing properly and a second vacuum system was developed. But also the second vacuum system causes leakage of fluid out of the cross slot. The channels could be closed with grease between the glass cover plate and the cross slot chip, but this could also come inside the micro channels. On top of the 100 μm cross slot a cover glass had been glued and was closing the channels nice. Besides leakage problems also air bubbles causes problems with the control of the flow inside the cross slot. The Matlab Simulink model to control of the micro valves was not ready to use, so some experiments were preformed with actuation of the micro valve manually. In these experiments small deformation of fibroblasts occurred. The fibroblast could be positioned in the stagnation point, but the flow could not been increased, because of the continuous control of the flow to keep the fibroblast inside the stagnation point. The experimental setup needs to be improvements before the cross slot setup could work properly.

The numerical model can be improved by replacing the hyperelastic model of the cell by a structural model of the filaments and action between them. This is basically a model of the cytoskeleton. Also the model needs to be expanded to the third dimension which will make the model more realistic. The boundary of the fluid solid interaction loses the smoothness during the simulation, this could be resolve by refining the fluid and/or solid mesh but better will be to use mesh adaptation. If the micro fluidic cell stretcher is working, the shear modulus input has to be studied if it is validate for this experiment. Also a study have to be done if the surface tension of the cell should be taken into account.

One of the points of discussion with respect to the experimental setup is the material PMMA (poly-methyl-methacrylate). All components are made out of PMMA, which is by origin hydrophobic. If the material of micro fluidic channels is hydrophobic, air bubbles can get stuck inside the micro channel, which will block the micro channel due the surface tension of the water air interaction. A plasma treatment of PMMA can decrease the contact angle between water an PMMA, but it is still not hydrophilic. A consideration should be made to make the micro fluidic cell stretcher out of glass or perhaps SU-8, which are both hydrophilic. Besides the material, also the design should be adapted to avoid sudden wall geometry changes. At sharp corners air bubbles could easily get stuck and cause problems. The surface roughness of the micro fluidic channels could have influence on the flow inside the micro fluidic cell stretcher and can be reduced if other production methodes are used.

The micro valve can also be improved. The actuators are much too strong for the actua-

tion of the membrane. From experiments only a small difference of resistance in the channels can control the flow inside the cross slot. Perhaps piezo-electric actuation of a membrane can be intergraded inside the micro fluidic system. If the micro valves are intergraded to the cross slot geometry, also the leakage between the two components is solved. To improve the control of the flow, the two micro valves should be replaced by one valve that keeps the flow through the cross slot constant.

The environment of the experimental setup has to be improved. The fluid PBS prevent the cells from osmotic swelling and keeps the cells a live for several hours and provides a humidity environment. The temperature still needs to be controlled to 37 °C, to get an in vivo environment. This can be achieved with LED-lighting or with heating channels.

Permanent closing of the cross slot chip can be done with UV-hardening glue. The closing of the micro channel with a removable cover glass needs to be improved. The vacuum channel leaks fluid from the micro channel to the vacuum channel. This can be resolve if a rubber like material is between the glass cover plate and the chip. The rubber functions like a sealing ring.

In the future the micro fluidic cell stretcher can be used to determine if possible disease will develop or not. Not only cancer can be detected, but also other diseases could be possibly detected with this device. It will be the less destructive way to measure the cell elasticity. If it is possible to deform cells, it maybe also be possible to stretch cells beyond the adaptive region, so the cell wall will break an cell lysing can be possible. When the cell wall and nucleus breaks, DNA is released from the cell. The DNA can be used for further analysis. This technique can be intergraded in a micro fluidic system for a controlled way of cell lysing. Another application could be for research of break up an coalescence of droplets on micro scale. An advantage of droplets break up and coalescence on micro scale compared to other experimental setups is the use of small amount of materials, which are relative expensive. An advantage of the strong actuators is that the fluid used inside the cross slot can be high viscous. The higher the viscosity of the fluid, the more force is needed to deflect the membrane. The valve can therefore also be used for droplets break up and coalescence experiments.

Samenvatting

Alle weefsels in dierlijke of humane organismes zijn opgebouwd uit verschillende cellen. De cellen worden mechanisch belast door zowel de externe als de interne factoren. Cellen reageren op mechanische belasting door middel van een interne verandering in hun gedrag en/of door verandering van zijn omgeving. Als een kracht wordt uitgeoefend op een cel, kan dit leiden tot aanpassing van de cel, beschadiging van de cel of zelfs de dood van de cel. De cel zal dood gaan als de belasting een kritieke waarde overschrijdt. De belangrijkste cel structuren, die de mechanische eigenschappen van de cel bepalen, zijn het plasma membraan, cytoplasma, cytoskelet en de nucleus.

De elasticiteit van de cel wordt voor een groot deel bepaald door het cytoskelet. Verandering in de functie van de cel wordt gereflecteerd in de hoeveelheid cytoskelet protiens en hun geassocieerde netwerken. Ziektes die invloed hebben op het cytoskelet kunnen worden gedetecteerd door het meten van de elasticiteit van de cel. Een drastische verandering van de elasticiteit wordt onder ander veroorzaakt door een ziekte als kanker en hier kan het cytoskelet gebruikt kan worden voor diagnostische analyse. Een cel die geïnfecteerd door een ziekte, zoals kanker, heeft een lagere Young's modulus dan een normale cel. Andere ziekten, zoals malaria, verhogen de Young's modulus van de cel ten opzichte van een gezonde cel.

Er zijn verschillende technieken om de elasticiteit van een cel te meten. Deze technieken kunnen in twee groepen worden opgedeeld. De eerste groep is bedoeld voor het lokaal meten van de elasticiteit van individuele cellen. Hieronder vallen 'partial micropipet aspiration', 'cell indentation', 'atomic force microscopy (AFM)'. De tweede groep is bedoeld voor globale belasting van individuele cellen. Hieronder vallen 'whole micropipet aspiration', 'micro manipulation', 'micro plates', 'optical tweezer' en 'magnetic bead twister'. Elke techniek geeft andere resultaten voor de elasticiteit voor dezelfde soort cel. Dit kan worden verklaard aan de hand van de verschillende belasting technieken, verschillende cel cultuur of verschillen in test omgeving. Al deze parameters hebben invloed op de gemeten mechanische eigenschappen van de cel.

Bestaande meettechnieken voor het bepalen van de elasticiteit van cellen hebben beperkingen. De zorgvuldige monster voorbereiding beperkt het aantal te meten cellen, waardoor klinische toepassing onmogelijk is. Om deze beperking te overwinnen is recentelijk een optical tweezer ontwikkeld. Met de optical tweezer zou het ook mogelijk zijn om kanker cellen te detecteren al voordat ze kanker cellen worden. De optical tweezer is nog in ontwikkeling, maar er worden al experimenten uitgevoerd in een ziekenhuis in Duitsland. Een nadeel is dat de laser invloed heeft op het gedrag van de cel. Het licht van de laser kan stralingsbeschadiging bij de cel veroorzaken. Om de invloed van de meettechniek te verminderen kan

de laser worden vervangen door een vloeistof rek stroming. De opdracht van dit project was dan ook het ontwerpen van een techniek waarmee individuele cellen kunnen worden uitgerekt met behulp van een rek stroming, voor het meten van de deformatie van de cel. Dit apparaat is de 'micro fluidic cell stretcher'. Een hoge doorzet van cellen heeft de voorkeur voor een mogelijke klinische opstelling.

Een numeriek model is gemaakt om te voorspellen wat de invloed is van verschillende dimensieloze getallen op de deformatie van de cel. De deformatie van de cel is gedefiniëerd door de Taylor deformatie graad D_{xy}. Omdat een voortbewegende cel met deformatie moeilijk te modelleren is, zijn de volgende aannames gemaakt voor het numerieke model. Het probleem wordt twee dimensionaal beschreven. De beginvorm van de cel is cirkelvormig. Het numerieke model is gemaakt met behulp van het eindige elementen pakket Sepran. Sepran is een eindige elementen pakket ontworpen voor gas, vloeistof en vaste stof simulaties. Met Sepran kunnen ook interacties tussen vaste stof en vloeistoffen worden gemodelleerd. De stroming wordt beschreven in het vloeistof domein (Ω_f). Voor de vloeistof wordt een laminaire stroming verondersteld, welke zich isotherm, incompressibel en Newtonian gedraagt. De cel wordt beschreven in het structuur domein (Ω_s). Voor de deformatie van de cel is aangenomen dat de cel zich hyper elastisch, isotoop gedraagt volgens het Neo-Hookean constitutief model. Met behulp van Sepran berekeningen zijn uitgevoerd voor het vloeistof domein Ω_f, structuur domein Ω_s en de interacties tussen het vloeistof domein en de structuur domein. Het resultaat van de berekeningen was de deformatie van de cel tijdens het transport door de 'micro fluidic cell stretcher'. De dimensieloze getallen die in de 'micro fluidic cell stretcher' een rol kunnen spelen zijn het Deborah getal (De), Reynolds getal (Re) en het fractie getal F_{RW}. De invloed van de dimensieloze getallen (De, Re, F_{RW}) op de deformatie van de cel is gesimuleerd. Het De getal en het F_{RW} getal hebben significant invloed op de deformatie van de cel in de 'micro fluidic cell stretcher'. Het model voorspelde dat een cel mogelijk gedeformeerd kan worden door de 'micro fluidic cell stretcher' als de viscositeit en de snelheid van de vloeistof hoog genoeg zijn en de breedte van de 'micro fluidic cell stretcher' smal genoeg is. Het resultaat van de simulaties is gebruikt bij het ontwerpen van de 'micro fluidic cell stretcher'.

Een experimentele opstelling is geconstrueerd. De geometrie voor de 'micro fluidic cell stretcher' is gebaseerd op een zogenaamde 'cross slot flow' (i.e. kruispuntstroming). In een kruispunt kan een cel worden gepositioneerd in het stagnatie punt als de twee uitstromingen van het kruispunt worden geregeld. De stroming wordt bestuurd door middel van een camera en software die twee micro kleppen aanstuurt. De micro kleppen zijn verbonden aan de uitgangen van het kruispunt. Door een continue besturing van de stroming kan de cel in het midden van het kruispunt worden gehouden tijdens opvoeren van de stroming. Doordat de stroming wordt opgevoerd zal de cel deformeren. Wanneer foto's worden genomen voordat de cel wordt gedeformeerd en als de cel is gedeformeerd, kan met behulp van een Matlab routine de Taylor deformatie graad bepaald worden. Voor deze opstelling moesten de micro kleppen met besturing software en de software om de Taylor deformatie graad te bepalen zelf ontwikkeld worden. De cellen worden in het kruispunt geleid door middel van een T-split.

Voor de experimenten zijn fibroblasten gebruikt als model cel, omdat vele studies op deze cellen zijn uitgevoerd. Fibroblasten zijn gemakkelijk te kweken en hebben een eindige lijn na 50 generaties. Fibroblasten kunnen goed tegen een fluorescente label en de eigenschappen van fibroblasten veranderen niet als ze worden gemarkeerd. Ook leven fibroblasten relatief lang

als ze zijn gelabeld met een fluorescente label. De cel geometrische eigenschappen zijn relatief constant tussen de cellen, wat ten goede komt aan het statistische resultaat. De grootte van een 3T3-fibroblasts is ongeveer 10 μm en de gemiddelde Young's modulus is 380 Pa.

Vele experimenten zijn gedaan om het principe van het oprekken van cellen door middel van micro vloeistof stroming te bewijzen. Cellen stomend door een plotselinge contractie en cellen stromend door een kruispunt geometrie. Het resultaat van de plotselinge contractie was een kleine deformatie van de cel. Zelfs bij een contractie van 1 : 16, met een kleinste breedte van het kanaal van 25 μm vervormde de cel niet veel. Een ander probleem was de geringe tijd voor het maken van een foto tijdens de deformatie in de contractie. Dit probleem is opgelost door gebruik te maken van een hoge snelheid camera van Kodak (sr 1000), maar nog steeds was de deformatie van de cel klein. Kleinere contracties zijn geconstrueerd, maar de productie van het folie masker zorgde voor problemen waardoor deze niet meer geproduceerd konden worden.

De tweede soort van experimenten zijn gedaan met een kruispunt geometrie. Drie dimensies van kruispunten zijn gemaakt. Kruispunten met een kanaal breedte van 500μm, 200μm en 100μm. Het 500 μm kruispunt was te groot om significante deformatie van cellen te induceren. Sommige experimenten zijn gedaan met de 200 μm en 100 μm kanaal. Tijdens de experimenten waren er vele problemen. Het hoofdprobleem met alle experimenten was het vacuüm systeem waarmee de micro vloeistof kanalen zouden worden afgesloten. Er lekte vloeistof vanuit het micro kanaal naar het vacuüm kanaal. Een nieuw ontwerp was gemaakt, maar deze lekte nog steeds. De kanalen zijn vervolgens afgesloten door middel van vet, echter gaf dit weer problemen tijdens het schoon maken en kwam er soms vet in het kanaal zelf. Naast de lek gaven ook luchtbellen in de micro kanalen een probleem voor de besturing van de flow in het kruispunt. Het 100 μm kanaal was afgesloten door middel van UV lijm. Het Matlab Simulink model voor de aansturing van de micro kleppen was nog niet klaar om toegepast te worden. De micro kleppen zijn voor de experimenten handmatig aangestuurd. Tijdens the experimenten kleine deformatie van de fibroblasten gebeurden in het kruispunt en tijdens de invoer van de fibroblasten in de hoofd stroming. De fibroblasten konden in het stagnatie punt van de kruispunt stroming worden gehouden. De experimentele opstelling zou moeten worden verbeterd, willen er deformatie metingen aan cellen kunnen worden gedaan.

Het numerieke model kan worden verbeterd. Het hyper elastisch model van de cel zou vervangen kunnen worden door een structureel model van de filaments en de interactie tussen de verschillende filaments gemoduleerd worden. In principe is dit een model van het cytoskelet. Ook moet het model worden uitgebreid naar de derde dimensie, zodat het model meer realistisch wordt. Ook zou de oppervlakte spanning van de cel in het model geïmplementeerd moeten worden. De grens tussen de vloeistof en de vaste stof verliest zijn gladheid tijdens de simulatie, dit kan worden verbeterd door middel van mesh verfijning. Ook kan gedacht worden een mesh aanpassing om zodoende een betere oplossing te krijgen.

De experimentele opstelling kan ook worden verbeterd. Het materiaal dat gebruikt was voor de kruispunt opstelling was PMMA. Alle ander componenten zijn ook gemaakt uit PMMA, dat van nature hydrofoob is. Als het materiaal van micro vloeistof kanalen hydrofoob is de kans groter dat lucht bellen het kanaal verstoppen. Een plasma behandeling van het PMMA kan de contact hoek tussen water en PMMA verlagen, maar PMMA is dan nog

steeds niet hydrofiel. Een afweging moet gemaakt worden om de 'micro fluidic cell stretcher' uit glas of misschien SU-8 te gaan maken, welke beide hydrofiel zijn. Naast het materiaal kan ook het ontwerp worden verbeterd door scherpe overgangen te reduceren. In scherpe hoeken kunnen gemakkelijk lucht bellen blijven hangen wat weer tot problemen leid tijden het regelen van de stroming. De oppervlakte ruwheid van de micro kanalen kan invloed hebben op de stroming in de 'micro fluidic cell stretcher' en zou verminderd kunnen worden door andere productie technieken.

De micro klep kan ook verbeterd worden. De actuator is te sterk voor de besturing van water stromingen. De micro klep kan worden geïntegreerd met de micro klep aan de kruispunt geometrie, waardoor tevens een lek word verholpen. Uit experimenten blijkt dat een kleine verandering in de weerstand van het kanaal voldoende is om de stroming in het kruispunt te bepalen. Misschien zou een piezo-elektrische aansturing van het membraan geïntegreerd kunnen worden in het micro vloeistof systeem.

De omgeving van de meet opstelling is nog niet ideaal. Door de vloeistof PBS worden de cellen in leven gehouden voor enkele uren blijven leven en niet uitdrogen. De temperatuur van de meet omgeving is alleen nog kamer temperatuur (20 °C) en zou (37 °C) moeten zijn. De temperatuur moet worden geregeld om een meer realistische omgeving te realiseren. Dit kan worden gerealiseerd door middel van led-lampjes of door middel van warmte kanaaltjes langs het micro kanaal.

Het afdichten van de micro kanalen door middel van lijm ging goed. Moet de afdichting niet permanent zijn dan zou het vacuüm systeem verbeterd moeten worden, zodat het niet meer lekt. Vloeistof uit het micro vloeistof kanaal lekt naar het vacuüm kanaal. Dit zou opgelost kunnen worden door een flexibel materiaal tussen het dek glaasje en de chip te construeren. Dit kan fungeren als afdichtring.

In de toekomst zou de 'micro fluidic cell stretcher' gebruikt kunnen worden voor analyse van cellen op mogelijke kans op ontwikkeling van kanker. Daarnaast zou de opstelling ook kunnen dienen om cellen op te rekken, verder dan dat de cellen aan kunnen, zodat de cel wand breekt. Hierdoor komt DNA uit de cel die gebruikt kan worden voor verder analyse. Deze opstelling zou dan geïntegreerd kunnen worden in een lab-on-chip applicatie. Een heel andere toepassing zou zijn voor onderzoek naar druppel opbreken en samensmelting op micro schaal. Hierdoor zou met relatief weinig 'duur' materiaal, testen uitgevoerd kunnen worden. Een voordeel dat de actuator sterk is, is dat ook hoog viskeuze vloeistoffen gebruikt kunnen worden in het kruispunt. Door de hoge viscositeit van de vloeistof, meer kracht is nodig om het membraan te actueren. De klep kan daarom gebruikt worden voor experimenten naar het op breken van druppels.

Contents

List of Figures

List of Tables

Chapter 1

Introduction

1.1 Cell biomechanics

Mammalian organisms are all warm blooded animals, like humans. All tissues in mammalian organisms are composed of an assembly of cells. The cells are subjected to mechanical stimuli either arising from the external or internal environment [Peeters, 2004]. An example of an external stimulus is the motion generated by muscular contractions which mechanically stimulates the cells within muscles and bones. Especially in attached cells, which are physically connected to the surrounding extracellular matrix, the mechanical stimuli of the external environment are directly transferred to the cell. Mechanical energy is actively generated during processes such as attachment, spreading, and motility of cells. The internal environment of the cells imposes mechanical stimuli by the conversion of chemical energy into mechanical energy.

Cells positively responds to mechanical stimuli by changing their own behavior and by modifying their environment. If forces are applied to the cell, the cellular deformations induce a variety of processes, including morphological changes, growth, differentiation, secretion, gene expression and altered extracellular matrix production [Peeters, 2004]. This response can either lead to cell adaption to counteract the effect of the applied stimuli or to cell damage or even cell death when the applied stimuli exceed the adaptive capacity of the cell [Peeters, 2004].

The field of cell biomechanics studies how cells move, deform, and interact, as well as how they sense, generate, and respond to mechanical stimuli. Both experimental and numerical approaches are used to investigate these processes. The former use a variety of loading techniques to deform the cell and to determine its mechanical properties or the damage phenomena. Also mechanical structural framework approaches are used to understand cell mechanics [Lamoureux et al., 2000]. Numerical approaches of the mechanical stimuli and the response of cells are made to predict the distribution of mechanical stimuli through cells. These results not only include the response of healthy cells, but also give insight into the behavior of specific diseases by examining the mechanical response of diseased cells [Peeters, 2004].

1.2 Cell architecture

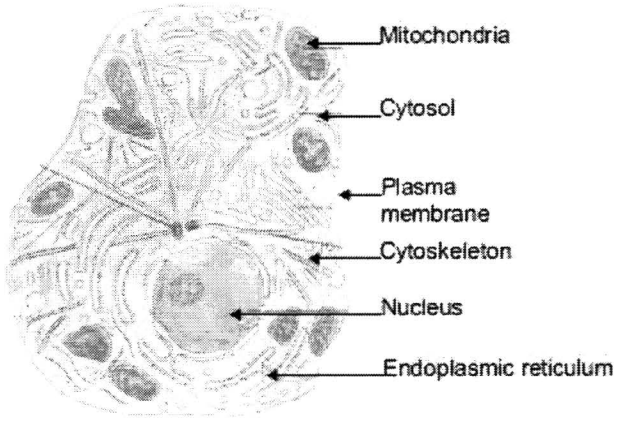

Figure 1.1: Cellular structure [Lewis et al., 1994]

The most important cellular structures (figure 1.1), that are relevant for the mechanical properties of the cell are, following [Lewis et al., 1994, Peeters, 2004]:

Plasma membrane All mammalian cells are surrounded by a plasma membrane (figure 1.2), providing a barrier between the internal and external environment. The plasma membrane consist of a lipid bilayer and proteins. Some of these proteins serve as pumps and channels for transporting specific molecules into and out of the cell.

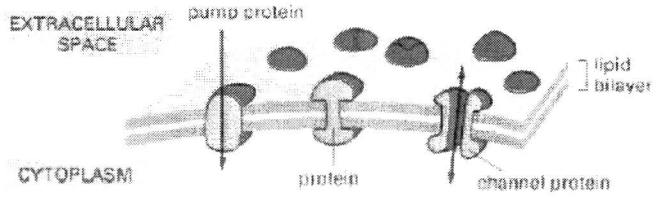

Figure 1.2: Plasma membrane [Lewis et al., 1994]

Cytoplasm Is also called the cell interior (excluding the nucleus), and is composed of the cytosol and cell specific organelles, such as mitochondria and the endoplasmic reticulum.

Cytoskeleton Inside de cytosol, arrays of protein filaments form networks, the cytoskeleton, that give the cell its shape and provide a basic framework for its movements. The protein filaments extend throughout the entire cell and/or are bound to the plasma membrane. It provides a continuous, dynamic connection between nearly all cellular structures. The cytoskeleton is involved in regulating cell shape, resistance to deformation and elasticity. The cytoskeleton also involves active processes such as cell division, locomotion and the transport of intracellular particles.

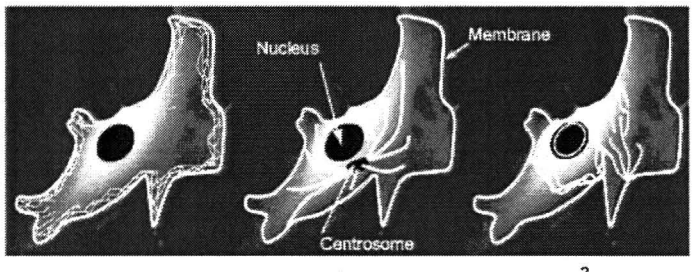

Figure 1.3: Cytoskeleton: 1 actin filaments; 2 micro tubules; 3 intermediate filaments [Peeters, 2004]

The cytoskeleton consist of three main kinds of cytoskeleton filaments (figure 1.3):

Micro tubules These are hollow, rigid cylinders around 25 nm diameter [Lewis et al., 1994] with a length up to 100 μm or more [Peeters, 2004]. They determine the location of organelles and of other parts inside the cell. The hypothesis is that the micro tubules serve as stabilizing elements between the other two filaments of the cytoskeleton. A single microtubule is stiff and rigid over cellular dimensions, but microtubule networks easily deform [Peeters, 2004].

Actin filaments These are around 8 nm thick, flexible and appear to be the most resistant to deformation compared to the other cytoskeleton elements. The actin filaments can be found near the plasma membrane of the cell. The actin filaments can have a variety of structures including isotropic networks, contractile bundles (also called stress fibres) and highly organized parallel arrays (micro spikes or lamellipodia)

Intermediate filaments These are stringlike arrays with a diameter around 10 nm. They are located around the nucleus and stretch out to the cell membrane. The intermediate filaments form close associations with the cell membrane at the cell adhesion sites. They are believed to connect the nuclear membrane to the other cytoskeleton elements [Peeters, 2004]. Intermediate filaments are specifically found in cells which are regularly subjected to mechanical stresses, like cells of muscles.

Nucleus The nucleus (figure 1.4) is the most noticeable organelle in the cell. It is separated form the cytoplasm by an envelope consisting of two membranes, an inner and an outer membrane that form the nuclear envelope. All of the chromosomal DNA is held in the nucleus. The nuclear contents communication with the cytosol takes place through openings in the nuclear envelope called nuclear pores. The nucleus is mechanically stiffer than the cell cytoplasm [Peeters, 2004].

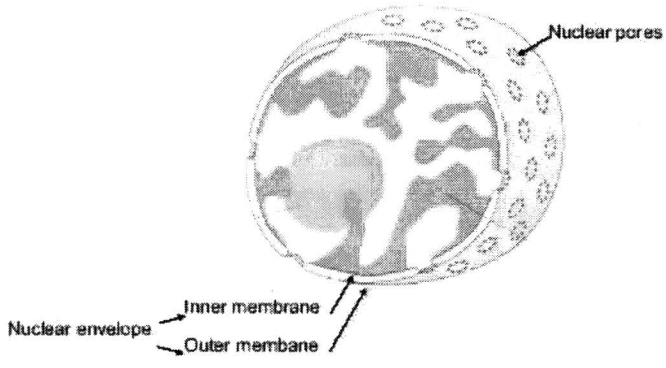

Figure 1.4: Nucleus [Lewis et al., 1994]

1.3 Cell biomechanics v.s. diseases

The elasticity of cells is determined by their cytoskeleton. Changes in cellular function are reflected in the amount of cytoskeleton proteins and their associated networks. Diseases that influence the cytoskeleton could be detected by measuring the elasticity of the cell. A drastic change in elasticity is caused by diseases such as cancer, so that the altered cytoskeleton may be used for diagnostic purpose. Cancer cells tend to de-differentiate, losing the special characteristics of the organ where they started life. Because of this, they no longer need the rigid cytoskeleton which holds them in shape, making them stretchier than normal cells [Lewis et al., 1994]. This connection between cellular function and cytoskeleton mechanical properties suggests using the deformability of cells as a novel inherent cell marker. The progress of a disease could be estimated if the elasticity of the cell is measured and compared with a normal cell. A cell hosted by a disease, such as cancer, has a lower elasticity than a cell that is normal [Schinkinger et al., 2003, Mahmood et al., 2001, Moon et al., 2000]. Other deceases, such as malaria, increase the elasticity compare to the healthy cell [Shelby et al., 2003]. The effect on the elasticity of the cell is depending on the kind of diseases that is hosted by the cell.

1.4 Techniques to study cell elasticity

Several techniques have been developed to study the elasticity of cells. This project will focus on the techniques where the mechanical elasticity of single cells are measured. Whole cell elasticity can be indirectly investigated by measuring the compression and shear modulus of densely packed cell pellets. However, these measurements only represent an average value, rather than a true single-cell measurement, and also depend on non-cytoskeleton forces such as cell-cell adhesion [Cunningham et al., 2002]. The techniques developed to study mechanical behavior of single cells can be divided into two groups:

1. Techniques designed for local loading of single cells
    - Partial micropipette aspiration [Hochmuth, 2000, Laursen et al., 2005b,a]
    - Cell poking or cell indentation [Goldmann, 2000]
    - Atomic Force Microscopy (AFM) [Dufrêne, 2000, Antonik et al., 1998, Gil et al., 1999, Athanasiou et al., 2003]
2. Techniques designed for global loading of single cells
    - Full micropipette aspiration [Hochmuth, 2000, Laursen et al., 2005b,a]
    - Micromanipulation [Zhang et al., 2000, Peeters, 2004]
    - Micro-plates [Tardy et al., 2002]
    - Optical tweezer [Moon et al., 2000, Cunningham et al., 2002, Schinkinger et al., 2003]
    - Magnetic bead twister [Zivkovic-Ben et al., 2002, Planus-Redouan et al., 2002]

The techniques are explained in detail in appendix A. Each of these techniques has several limitations. Due to small size (10 μm), low modulus and mechanical strength ($\approx$ 10 - 1000 Pa) of cells, its difficult to obtain reliable and precise data [Cunningham et al., 2002, Zhang et al., 2000]. Some of these techniques use small probes (AFM, cell poking) while others use probes as large as the cell size (micro-plates, micromanipulation). Micropipette aspiration experiments can provide inaccurate measurements if the plasma membrane becomes detached form the cytoskeleton. The partial micropipette aspiration, cell poking, AFM and magnetic bead twister only measure the elasticity of the cells over a relatively small area of its surface. The laser light of the optical tweezer could also have influence on the cell behavior. Through radiation from the laser the cell could even been killed if the power of the laser is too high.

In all of these techniques, cells are loaded in variety of ways and environments to simulate the vivo environment. All these techniques give different results in elasticity for the same type of cell [Peeters, 2004, Knight et al., 2002, Bouten, 2004, Sheih and Athanasiou, 2003].

Table 1.1: Table different techniques and cell properties: E : Young's modulus, $k1$: lineair elastic spring, $k2$: non linear elastic spring, μ : apparent viscosity, T : cortical tension [Bouten, 2004]

technique	cell type	model	force	deformation	properties
AFM	Fibroblast		< 0.6 nN	< 140 nm	E = 0.5 – 17 kPa
	Fibroblasts	Hertz model	0.05-0.3 nN	50-200 nm	E = 4 – 100 kPa
Cell poker	Fibroblasts	Elastic solid	up to 2.5 μm	up to 40 nN	E = 7.5 kPa T = 25 mN/m
Micropipette; large deformation	Fibroblasts	Newtonian fluid + cort. tension	1-3 nN	-50%	μ = 10 kPa·s, T=0.04 mN/m
Microplate manipulation	Fibroblasts	Viscoelastic solid	50-100 nN	-80%	k1+k2=1kPa, μ =10 kPa·s
	Fibroblasts	Viscoelastic solid	20 - 100 nN		k1= 960 Pa k2= 840 Pa τ =13 s

Table 1.1 shows that for the same type of cell (fibroblasts), different elastic properties are measured with different techniques. This can be explained by the difference of the measure techniques used. For example, AFM deforms a part of a cell while the optical tweezer deforms a whole cell. Different structures inside de cell (§1.2) could be deformed by the different techniques. AFM could only deform the nucleus, membrane or specific filaments of the cytoskeleton, while the micro-plates will deform the total cell structure.

Another explanation for the difference in measured elastic properties could be the measurement conditions of the environment of the technique. Some techniques use room temperature (20 °C) while other use an more in vivo environment temperatures (37 °C). Cells behave differently when the environmental temperature is changing. Several studies have shown the influence of temperature on the mechanical properties [Peeters, 2004, Antonik et al., 1998]. Also some techniques provide an optimal, physiological environment to keep the cells alive for several hours. Important parameters of the environment to keep the cell alive are:

- Temperature
- Humidity (avoiding evaporation)
- Level of CO_2

Also different kinds of models of a single cell are used to calculate the elastic properties of cells, see figure 1.5. The continuum models used to describe the deformation of a single cell are:

Elastic solid The whole cell is described with one elastic element.

Non lineair viscoelastic solid This is commonly used to describe the results of micropipette aspiration of cells. Application of a step aspiration pressure results in an elastic initial deformation followed by a slow-creeping phase. Creep and recovery behavior are described by a non lineair viscoelastic sold. The model is derived form the elastic solid,

consisting of a Maxwell element parallel to a spring k_1. The Maxwell element consist of a dashpot τ with relaxation time and a non-linear spring with spring constant $k_2(z)$.

Newtonian fluid with cortical tension In this model the cell is described as a homogeneous Newtonian liquid core encapsulated by a distinct cortical shell. Cortical tension generated within a thin actin-rich layer underneath the plasma membrane.

Hyper elastic Includes both nonlinear kinematics and nonlinear material behavior. This model is used for very large strains and is commonly used to described plastic or rubber-like substances.

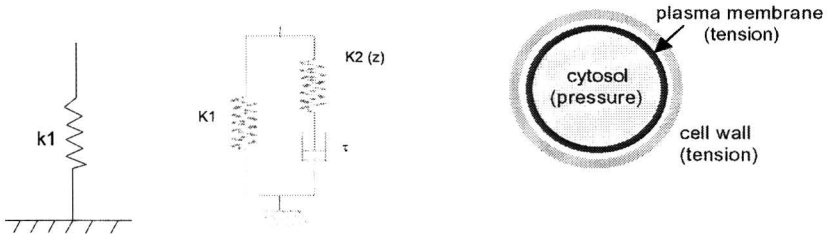

(a) Linear spring (b) Viscoelastic (c) Newtonian fluid with cortical tension

Figure 1.5: Continuum modulation of cell deformation [Bouten, 2004]

Multi-phase models are another category of models which regard the cells and extracellular matrix as a combination of fluid, solid elements and positive and negative ions. This theory is commonly used to describe the overall mechanical environment of cells in an extracellular matrix (tissue equivalents) and is not used to describe the mechanical properties of individual cells. An numerical example of a multi phase model, of a Chondrocyte inside a fluid, is given in figure 1.6(a).

Also structural models are used to model single cells. In contrast to the continuum models, structural models are based on the properties, architecture and interactions of the individual components of the cell. Unfortunately, the spatial organization and especially the mechanical properties of the components of the cell are not well understood. For example, from §1.2 it is clear that the internal structure of a cell is extremely complex. An example of a structural model is given in figure 1.6(b). Figure 1.6(b) shows a possible three-layered structural model for the entire fibroblast, consisting of actin cortex, interior polymer network of micro tubules, intermediate filaments and actin, and nucleus.

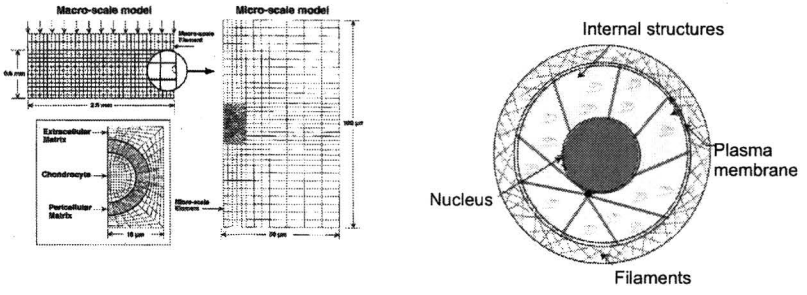

(a) Multi-phase model [Bouten, 2004] (b) Structural model [Ananthakrishnan et al., 1998]

Figure 1.6: Other modulation of cell deformation

Different models also lead to different descriptions of the properties of the cells. Characteristics of loading techniques designed for global and local loading of cells are given in appendix B.

Visual observations of the deformation of the cell are made with conventional brightfield microscopy, providing only two-dimensional information of the cell deformation. In the single cell compression device developed by E. Peeters [Peeters, 2004], micromanipulation have been combined with a confocal microscope to measure three-dimensional deformations of cells (see figure 1.7). The principle of the confocal microscope is that it takes (x,y)-pictures of several layers in z-dimension. After assembling the pictures with a software package a three-dimensional picture of the cell is made. (see figure 1.8)

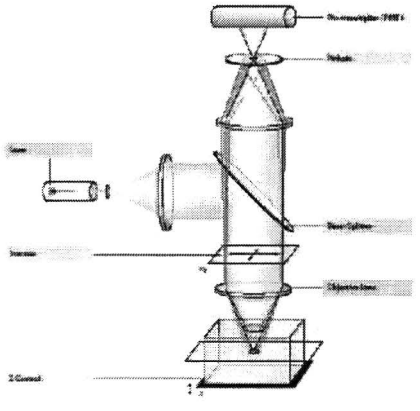

Figure 1.7: Confocal microscope

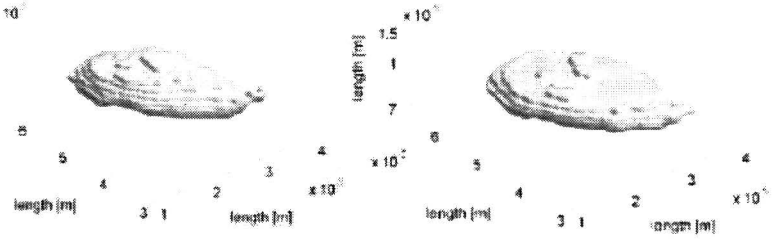

Figure 1.8: Three-dimensional image of a cell obtained with a confocal microscope. Left: before indentation and right: after indentation using a glass probe with the micromanipulation device developed by Peeters [Peeters, 2004]

1.5 Problem

It is well known that cytoskeleton properties of biological cells are correlated with cell function [Schinkinger et al., 2003, Mahmood et al., 2001, Moon et al., 2000]. It has been shown that the cytoskeleton elasticity changes significantly as a function of cancer progression (see figure 1.9 for Young's modulus of a normal cell and a cancerous cell).

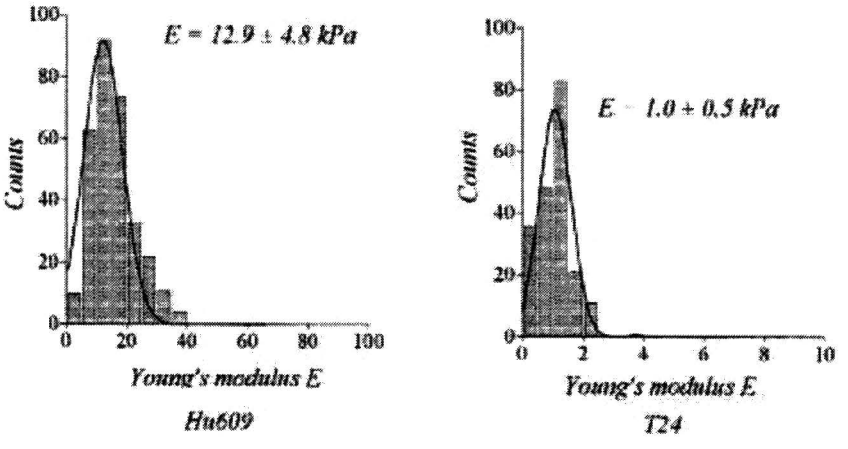

(a) Normal cell

(b) Cancerous cell

Figure 1.9: Histogram of mean value and the distribution of the Young's modulus of cells measured by AFM [Gil et al., 1999]

Figure 1.9(a) and figure 1.9(b) show that normal cells have a Young's modulus of about one order of magnitude higher than cancerous ones. The Young's modulus was measured with atomic force microscopy. Such change in the Young's modulus might be attributed to a difference in the organization of cell cytoskeleton. By measuring the cell elasticity, it is in principle possible to detect single malignant cells and precancerous cells. Malignantly transformed cells are easier to stretch than normal cells. The difference in elasticity opens the possibility to monitor the progress of cancer from preinvasive to invasive.

Existing techniques for measuring the elasticity of cells have a drastic limitation. The tedious sample preparation limits the number of cells investigated a sample, ruling out applications in clinical diagnostics. To overcome this limitation, an optical tweezer has been developed. This device deformans cells with a laser beam. The deformation of the cell is measured by a phase contrast microscope. A micro fluidic setup is used to provide the laser with cells allowing samples with many cells to be handled. The optical tweezer may possibly be simplified significantly by using fluid flow to stretch the cell, instead of using the laser beams. This eliminates the need for the optical cell stretch device and avoids possible radiation damage of cells.

1.6 Project assignment

Design a fluid flow device to stretch a single cell. The device must have the following features:

- A single cell is strained in an elongation flow.
- Deformation is detected, which can be related to the state of the cell. (malignant / precancerous)

1.7 Objective

Design of a fluid flow device to stretch cells and which can be used to determine if a cell is precancerous or normal.

1.8 Strategy

First we start with a literature search, to make an inventory of preceding research in this area. After the literature search a concept for the micro fluidic cell stretcher is determined. When the geometry of the micro fluidic cell stretcher is known, a numerical model is made that simulates the cell deformation inside the micro fluidic cell stretcher. Dimensionless numbers are determined and the effect of these dimensionless numbers on the cell deformation are predicted. A design is made for the micro fluidic cell stretcher and fabricated. The fabricated parts are tested and the experimental setup is assembled. Test are done with the designed micro fluidic cell stretcher and the results are compared with the numerical results. At the end some points of discussion and conclusions are made.

1.9 Assumptions

Because the deformation of the cell is complex to model, a simple model will be used to predict the influence of several parameters on the deformation of the cell. In the model the following assumptions are made:

- The problem is two-dimensional.
- The cell initially has a circular shape.
- The cell properties are assumed to be hyperelastic and isotropic according to a Neo-Hookean constitutive model.
- The flow is laminar and the fluid is Newtonian.

1.10 Outline

This chapter gave an introduction into the cell structure and cell mechanics. This chapter also pointed out the problem of measuring the cell mechanics and the purpose of this project. Chapter 2 gives an overview of the requirements for the cell stretcher and possible solutions. There is a distinction made in features needed for the proof of principle and the clinical application, since first the proof of principle needs to be delivered. In chapter 2 the concept of the micro fluidic cell stretcher is determined with literature study and some calculations. From chapter 2, two different geometric concepts had potential. The contraction geometry was worked out, but unfortunately in the production practical difficulties were encountered. The concept of the contraction geometry can be found in the appendix C. The cross slot concept is worked out to an experimental setup. The design and fabrication of the micro fluidic cell stretcher will be discussed in chapter 4. Chapter 3 shows how the numerical simulation is built and used to predict the influence of several dimensionless numbers on the deformation of the cell in the micro fluidic cell stretcher. Chapter 5 gives the results of the experiments of the micro fluidic cell stretcher. Chapter 7 is used for the conclusions and discussion. After the chapters the bibliography can be found, followed by the appendices.

Chapter 2

Requirements for the cell stretcher and possible solutions

2.1 Requirements

To design a micro fluidic cell stretcher, first the features of the micro fluidic cell stretcher have to be determined:

- A fluid flow that applies a force to the cell.
- Measurement of the cell deformation, which can be related to the state of the cell (normal or cancerous).
- The in vitro environment must be representative of the in vivo environment.
- A final design of the micro fluidic cell stretcher should be suitable for clinical applications.

These features are not specific enough to make a design of the micro fluidic cell stretcher. The features will be turned to quantitative features.

2.1.1 The cell is strained in an elongating flow.

The idea of the micro fluidic cell stretcher is based on previous studies of droplets in elongational flows [Janssen, 1991, Stegeman, 2002]. Figure 2.1(a) shows the principle of a cross slot flow. In this concept a droplet with a different viscosity compared to the surrounding fluid, is centered inside a cross slot flow. A control system controls the flow in the four channels. With the control of the four channels the droplet is held in the middle of the cross slot. With the droplet in the middle of the cross slot and the flow controlled, the elongating flow is acting on the droplet can be controlled. Due to the elongating flow, the droplet is deformed and may even break up. Figure 2.1(b) depicts the experimental setup of the cross slot used by Y. Stegeman.

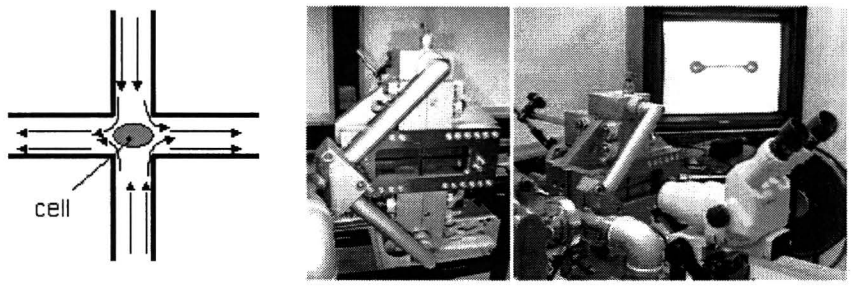

(a) Principle (b) Experimental setup

Figure 2.1: Cross flow setup of Y. Stegeman [Stegeman, 2002]

If the droplets could be deformed by an elongating flow, a cell could possibly also be deformed with an elongating flow.

2.1.2 Measurement of cell deformation

The diameter of different cells is not identical, i.e. there is always a natural variation in the mean diameter of the cell. If a deviation between a normal or cancerous cell must be proven, statistics could provide a solution. A significant difference should be found between the deformation of a normal or cancerous cell. For better statistical results, sufficiently many measurements are needed. If the throughput of the device is high, the measurement time could be minimized. The throughput of several techniques are around 30 cells a day. The optical stretcher aims to have a throughput of several hundreds of cells a minute [Kas and Gunk, 2005]. Just 50 tumor cells are needed in a sample for the optical stretcher to diagnose cancer (with accuracy 90 %), contrasting with traditional methods which need 10.000 to 100.000 cells [Kas and Gunk, 2005]. The optical stretcher aims also to detect cancerous cells before they become cancerous [Kas and Gunk, 2005]. The optical stretcher is still in development, but some experiments are carried out in a hospital in Germany [Kas and Gunk, 2005]. To compete with the optical stretcher, the final clinical application of the micro fluidic cell stretcher should have a comparable throughput to the optical stretcher.

To detect the difference between a normal and a cancerous cell, one should be able to measure a difference of an order of magnitude of the elastic modulus [Gil et al., 1999]. In section §1.5 figure 1.9(a) and figure 1.9(b) show the histogram of mean value and the distribution of the Young's modulus of a normal and cancerous cell. If pre-cancerous cells also need to be detected, one should be able to measure a difference in elastic modulus less than one order.

To measure the cell deformation, first the dimensions of the cell in no-loading conditions have to be measured. Every technique listed in section §1.4 uses a microscope to observe the deformation of the cell during loading. If microscopy is used to measure the cell, at least one side of the micro fluidic cell stretcher must be transparent.

From the cell the x-dimension and the y-dimension are measured before loading and during loading.

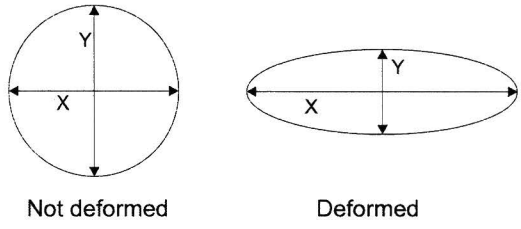

Figure 2.2: Measured dimensions cell deformation

With the x-dimension and the y-dimension a measure for the deformation can be defined. The deformation of the cell is described by the Taylor deformation parameter D_{xy} which can be calculated with equation 2.1, following [Eggleton and Popel, 1998] [Pozrikidis, 2003]:

$$D_{xy} = \frac{X - Y}{X + Y} \tag{2.1}$$

If $D_{xy} = 0$ the cell has a circular shape and if $0 < Dxy < 1$ than the cell is elliptical. The cell is assumed to be incompressible which means that the area of the elliptical cell will be the same during deformation. If a circular cell with a diameter of 10 μm is deformed in the x-dimension from 10 to 18 μm the shape of the cell and the Taylor deformation parameter are shown in figure 2.3(a).

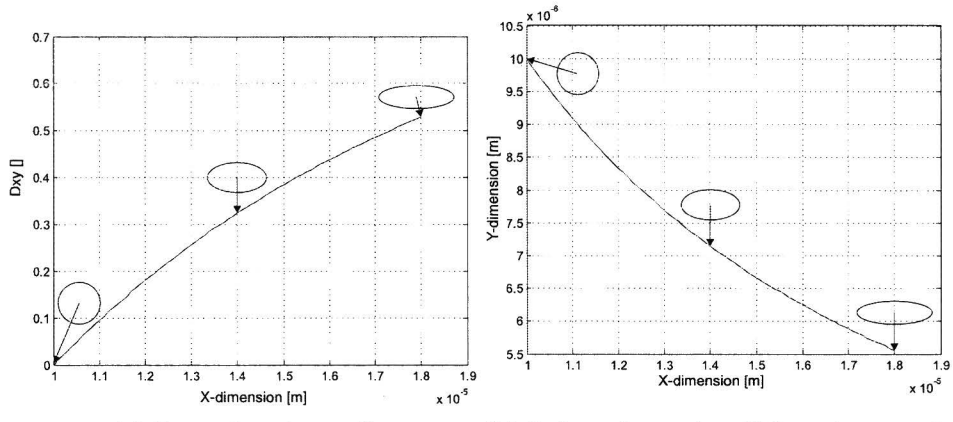

(a) D_{xy} against shape cell

(b) X-dimension against Y-dimension, area is constant

Figure 2.3: D_{xy} compared to the shape of the cell (x,y-dimension)

2.1.3 The in vitro environment must be close to the in vivo environment

The environment of the cells is crucial for the mechanical properties of the cells. The relaxation time is strongly dependent on temperature [Antonik et al., 1998]. Following [Antonik et al., 1998] the time constants which are one to three orders of magnitude larger at 22 °C ($\approx$ several seconds) than at 37 °C. A more rapid recovery was reported from sustained stress at 37 °C than at 25 °C [Petersen et al., 1982]. Also the initial stiffness of the cell decreases a factor of two between 33 °C and 37 °C [Petersen et al., 1982]. The environment could also influence the lifetime of a cell. Depending on the environment the cell could die after several days, hours or even minutes. The in vivo environment of a cell depends on the type of cell. Important parameters of the in vivo environment are:

- Temperature of 37 °C
- Humidity (avoiding evaporation)
- Certain level of CO_2

The in situ environment should be as close as possible to these parameters. Humidity is not relevant, because the fluid cell stretcher is filled with a liquid and evaporation will not occur.

Because of the need to measure the cell, a fluorescent die could be added to the in situ environment. Cell tracker green or orange fluorescent could be used. The plasma of the cell is marked by the color green or orange. The advantage of fluorescent die is that the cells are observed more easily. The disadvantaged is that the cells could die faster with the fluorescent dye than without the fluorescent dye. Some cells are employing immunofluorescence, which means that the properties of the cell do not change if they are fluorescent and therefore they can live for a relatively long time if they are fluorescent. An disadvantage of fluorescence is that the cell will die in time due to the fluorescent marker.

2.1.4 Micro fluidic cell stretcher should be used for clinical applications in the end

The micro fluidic cell stretcher should be practical to use, which means that it would need to be able to stretch different cells with a minimum of change of components. If it is possible a range of cells should be characterized with the same device. A range of cells is selected from 10 μm (diameter fibroblasts) to 50 μm (diameter of chondrocyte).

For clinical use the device should be easy to clean or be disposable. Cells from a previous measurement should not get stuck inside the channel, since this could influence the measurement. If the fluid velocity is not high enough, the chance that cells will bind on the walls of the micro channel will be greater. A disposable solution for the micro fluidic cell stretcher is preferred.

Because the micro fluidic cell stretcher could become disposable, the costs of the micro fluidic cell stretcher should be taken into in account. For the experimental setup the cost are not extremely important, but for a clinical application the cost will certainly play a role.

2.1.5 Quantitative requirements

For quantitative features, a difference will be made between the experimental setup and the clinical application. Since first the principle has to be proven, some features would take a lot of effort, but are not necessary to prove the principle of the micro fluidic cell stretcher. The quantitative features of the experimental setup of the micro fluidic cell stretcher are:

- A fluid flow that applies a force to the cell.
- Measurement of the cell deformation, which can be related to the state of the cell (normal or cancerous).
  - At least one side transparent
  - Cross sectional
  - Fluorescent marker can be applied for cell to enhance the contrast
- The in situ environment must be close to the in vivo environment.
  - Surrounding liquid
- Micro fluidic cell stretcher should be used for clinical applications.
  - Range of cells diameter 10 μm to 50 μm
  - Easy to clean

The extra quantitative features for the clinical setup of the micro fluidic cell stretcher are:

- Measurement of the cell deformation, which can be related to the state of the cell (normal or cancerous).
  - Throughput of several hundreds of cells a minute
  - An accuracy of 90 % with 50 tumor cells
- The in situ environment must be close to the in vivo environment.
  - Temperature of 37 °C
  - Level of CO_2
- Micro fluidic cell stretcher should be used for clinical applications.
  - Disposable
  - Low cost

The quantitative features for the clinical setup are taken into account with the development of the experimental setup of the micro fluidic cell stretcher.

2.2 Possible solutions micro fluidic cell stretcher

The functions that the micro fluidic cell stretcher should have are:

- Input of cells in micro fluidic cell stretcher.
- Stretching of cells with elongation flow.
- Measurement technique for the cell deformation.
- Create an in vivo environment.

The possible solutions for a function are discussed in next paragraphs.

2.2.1 Input of cells in micro fluidic cell stretcher

The cells need to be inserted inside the micro fluidic cell stretcher. The input of the cells can be divided into two groups:

Direct The cells are already put inside the solvent before the fluid is entering into the micro fluidic cell stretcher. The cells are already inside the main flow that also deforms the cells.

Indirect A separate flow of the suspension with cells is put inside the main flow from outside. The main flow will deform the cells, while a separate flow only provides the cells to the micro fluidic cell stretcher.

Besides direct or indirect input of the cells, also manual or automatic control can be chosen. Automatic control is preferred above the manual input of cells. A separate automatic flow controlled the input of the cells is preferred above a direct input of cells. In a separate automatic flow, cells will come through the structure in a more controlled way than with a direct automatic flow.

2.2.2 Stretching of cells with elongating flow

One of the features of the micro fluidic cell stretcher is that the cells have to be stretched with a fluid elongation flow. No contact surface may be used to deform the cells. Possibilities to deform the cells with only fluid are described below:

Contraction Through a geometric change of the outer boundary of the channel, the flow will increase or decrease speed. If the outer boundary of the channel changes such that the hydraulic diameter of the micro channel decreases, the velocity of the fluid will increase. This increasing flow will deform the cell when it enters the contraction. See figure 2.4(a) for an example of a contraction.

Geometric boundary inside channel If inside a channel, a geometric boundary is created, the flow will also increase speed caused by a decreasing hydraulic diameter of the micro channel. Due to the increasing speed, the cell will deform. See figure 2.4(b) for a cylindrical boundary inside a micro channel.

Cross slot If a cross slot geometry is used, two flows will enter the cross slot. These two equal fluids streams will interact with each other in the middle of the cross slot and will leave the cross slot through two exits. The two flows create a stagnation point. If the cell is positioned at the stagnation point, the cell will deform because of the elongating flow created by the two flows. See figure 2.4(c) for an example of a cross slot.

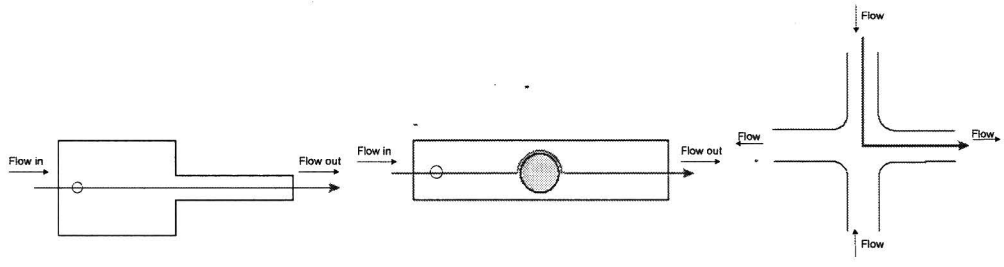

(a) Contraction

(b) Geometric boundary inside channel, for instance a cylinder

(c) Cross slot

Figure 2.4: Concepts of geometry micro fluidic cell stretcher

For the selection of the best flow geometry, the amount of stretching of the cell must be determined. The strain rate $\dot{\varepsilon}$ against time $[s]$ for different geometric channels and different Weissenberg (Wi) numbers can be seen in figure 2.5. The Wi-number represent the fraction of the visco-elastic force of the flow to the viscous force of the flow [Massey, 1971]. This Wi-number is a dimensionless number that is defined by equation 2.2.

$$Wi = \frac{U\lambda}{H} \tag{2.2}$$

Where:

U : Velocity of fluid

λ : Characteristic relaxation time

H : Height of the channel in planar section

If Wi>1 the fluid has a high elasticity and if Wi<1 the fluid has a low elasticity. In this report viscoelastic fluid (polyisobutylene) is flowing through these geometric channels. From figure 2.5 it can be concluded that the cross slot flow will induce more strain for a longer period of time than the contraction and obstruction inside the channel.

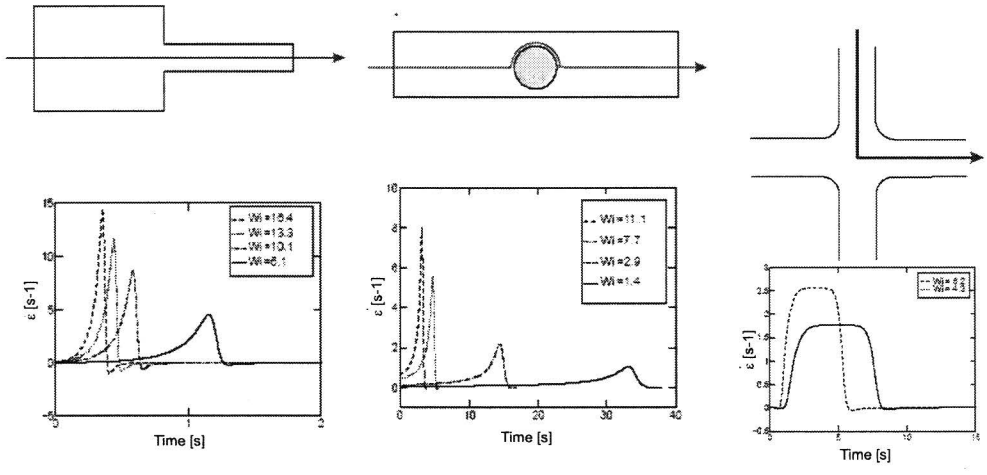

(a) Contraction (b) Cylinder (c) Cross slot)

Figure 2.5: Strain rate $\dot{\varepsilon}$ against time for different Wi-numbers [Schoonen, 1998]

The amount of strain N against the time s, for different geometric channels and Weissenberg numbers is plotted in figure 2.6.

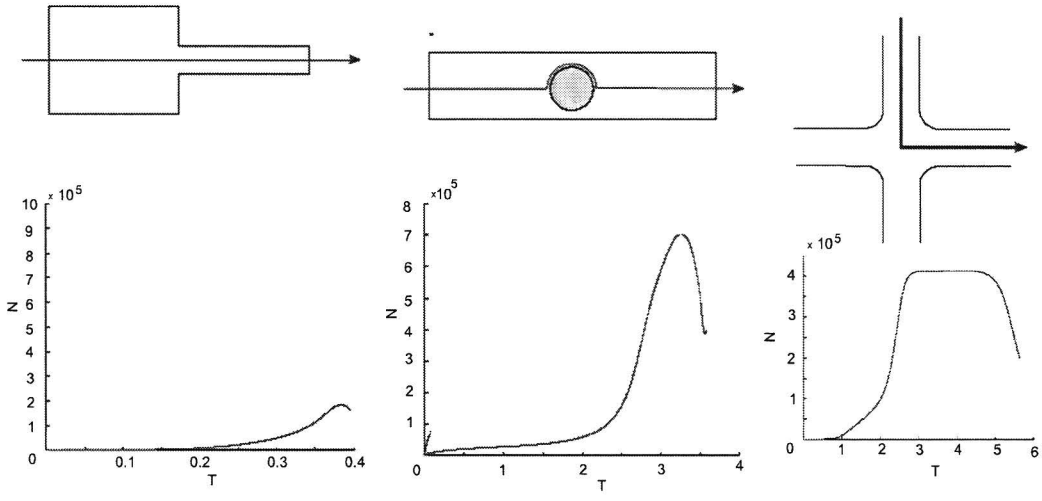

(a) Contraction (b) Cylinder (c) Cross slot

Figure 2.6: Strain rate against time for different Wi-numbers [Schoonen, 1998]

From figure 2.6 it can be seen that the contraction reaches a strain N = $2 \cdot 10^5$ for a relative short time 0.5. The cylinder reach a higher strain N = $7 \cdot 10^5$ for a longer periode of time 1. The cross slot reached a same strain rate N = $4.5 \cdot 10^5$, but for a much longer period of time of 3.5. The contraction has the same strain rate as the cross slot geometry, see figure 2.5(a), but because the cross slot has a longer period of high strain rate than the contraction, see figure 2.5(a), the total strain of the cell will be higher in a cross slot geometry than in a contraction. That is why the cross slot geometry is preferred to the contraction geometry. The through put of a contraction could be higher than the cross slot geometry, because the cell has to be positioned and held stationary in the stagnation point of the cross slot. In a contraction the cells only flow through. But important is that the cell will deform and the best chance will be with a cross slot geometry.

Because some contraction geometries were already available, some experiments were done. Based upon the experience of those experiments some new contraction geometries were designed, but unfortunately the production of the mask needed for production of the contraction had problems. All development of the contraction and ideas can be read in appendix C. In appendix C the experimental results can also be found. From here on this report will concentrate on the cross slot geometry.

2.2.3 Measurement techniques for cell deformation

To measure the cell deformation, first the dimensions of the cell in no-loading conditions have to be measured. Every technique in section §1.4 uses a microscope to observe the deformation of the cell during loading. If microscopy is used to measure the cell, at least one side of the micro fluidic cell stretcher must be transparent.

If light is shining on a surface, an interaction takes place between the passing light rays

and the object. If light with a certain wave length λ and intensity I is shining on a surface, the different following interactions can be possible (see figure 2.7), following [James and Tanke, 1991]:

Absorption The light is absorbed by the surface and releases with the same wave length λ but with lower intensity I.

Refraction The light is moving through the material and is released with the same wave length λ and with the same intensity I. It can be seen as a phase shift of the light.

Fluorescence The light is absorbed and released with another wave length λ but with the same intensity I.

Reflection The light is totaly reflected from a surface. Depending on the kind of surface (irregular or smooth) the reflected light is scattered or not.

Diffraction If the light passes a narrow whole, with a diameter smaller than the wave length, the light will generate a diffraction pattern after passing the hole.

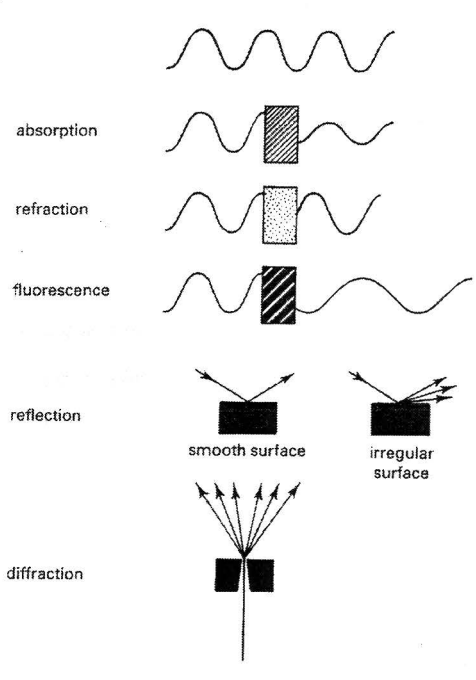

Figure 2.7: Schematic view of possible interactions between passing light rays and an object [James and Tanke, 1991]

The techniques available to visualize the cell are:

Bright field microscopy Bright field microscopy uses reflection of visible light. If the contrast between the cell contour and the background is not sufficient to measure the cell size, other techniques can be used.

Fluorescent microscopy Fluorescent microscopy uses a light source for excitation of the fluorescent marker. The cells need to be marked by a fluorescent die, which will attach to the cell surface. A fluorescent marker will have a specific excitation wave length. The fluorescent marker absorbs the energy and releases a light array with another wave length. (See figure 2.8)

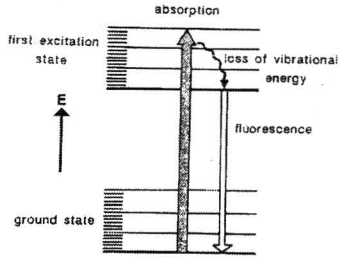

Figure 2.8: Absorption and emission of fluorescent marker [James and Tanke, 1991]

If the right filters are used, only the emitted ray of light from the fluorescent marker is visualized. By this fluorescent microscopy the contrast between the background and the cell can be higher than with brightfield microscopy.

Absorption microscopy This technique uses a laser that shines through the channel and the cell. The intensity of the light increases or decreases if a cell passes by the measure point. If a line is measured the dimension and speed of the cell can be measured. The disadvantage of absorption microscopy is that the cell is measured only in one dimension in time. For absorption microscopy the channel needs to have full optical access, which means the channel has to be fully transparent.

The best solution for the imaging of the cell would be to use a brightfield microscope to image the shape of the cell. If the contrast between the cell and the background is not sufficient, a fluorescence marker can be used to increase the contrast. If a contraction will be used for deformation of the cells, a high speed camera will be necessary to make images of the cells. The speed of the cells are increased in the contraction. From experimental results with a normal camera (15 fps (frames per seconde)) the resolution time is not fast enough to make sharp images of the cell flowing through the contraction. With the use of a high speed camera, the amount of recorded data is a limitation of the measurement time. If the speed or capacity of the camera do not fulfill the requirements, another measurement technique should be used. A laser absorption technique can be used to measure the length of the cell. If the laser passes through the cell, the laser loses intensity, which can be measured by a photo detector behind the cell. This technique measured only in one dimension in time. To measure two dimensions, two sensors are needed to detect the two dimensions (x,y) of the cell. To construct two sensors is more difficult than to measure the dimensions with a brightfield

microscope.

If a cross slot flow deforms the cells, a normal camera can make images of the cell deformation. The speed in the stagnation point is close to zero. If the cell can be positioned inside the stagnation point with a control system, the speed of de cell will also be close to zero. A normal camera has a imaging speed of 15 fps, which will be enough to make an image of the cell before deformation an at the deformed state.

2.2.4 Create an in vivo environment

For the first experiments, the cell has to be in an environment which does not influence the elastic behavior of the cell. In the section §2.1.3 it was mentioned that the temperature, level of CO_2 and humidity play a key role in the elastic behavior. In the clinical application this environment needs to be controlled. For the first experiments the liquid in the micro fluidic cell stretcher will have the same osmotic value as the culture of the cell. Osmosis is diffusion of molecules through a semipermeable membrane (cell wall) from a place of higher concentration to a place of lower concentration until the concentration on both sides is equal [van Donkelaar et al., 2003]. If the cells are placed in an osmotic low concentration fluid, cells will expand or even burst. If cells are placed in an osmotic high concentration fluid, cells will shrink in size. The fluid of the micro fluidic cell stretcher will have the same osmotic value as the inside of the cell, so the fluid will not influence the elasticity of the cell. This fluid can be made with PBS (salt solution).

2.3 Final concept

The final concept of the micro-fluidic cell stretcher is:

- Input of cells in micro fluidic cell stretcher.
  - A separate flow with automatic control
- Stretching of cells with an elongation flow.
  - Cross slot
- Measurement technique for the cell deformation.
  - Brightfield microscope
- Create an in vivo environment.
  - Fluid with same osmotic value as the inside of the cell made with PBS.

Chapter 3

Simulation of fluidic cell stretcher

Before a simulation of the micro fluidic cell stretcher can be carried out, the model cell need to be selected. With the experience of dr. C.V.C Bouten, fibroblasts are chosen as model cells. The motivation can be found in section §5.1.1. First, the fibroblasts are used to prove the principle of the micro fluidic cell stretcher. The fibroblasts are also used for the first experiments and simulations. The basis for the simulation is formed by the model of R. van Loon, who modeled the deformation and stresses of a heart valve in a pulsating blood flow [van Loon et al., 2004].

3.1 Assumptions

For the simulation of the fibroblast deformation inside the micro fluidic cell stretcher, the follow assumptions are made:

- The problem is two-dimensional.
- The cell initially has a circular shape.
- The cell properties are assumed to be hyperelastic and isotropic according to a Neo-Hookean constitutive model.
- The flow is laminar and the fluid is Newtonian.

3.2 Fluid domain: flow

The flow is described in the fluid domain Ω_f. A laminar flow is assumed for the fluid which behaves isothermal, incompressible and Newtonian. The momentum and continuity equations that govern the mathematical formulation of the fluid domain Ω_f are given by:

$$\rho_f \frac{\partial \mathbf{v}_f}{\partial t} + \rho_f \mathbf{v}_f \cdot \nabla \mathbf{v}_f = \nabla \cdot (-p_f \mathbf{I} + \boldsymbol{\tau}_f) \tag{3.1}$$

$$\nabla \cdot \mathbf{v}_f = 0 \tag{3.2}$$

Where:

ρ_f : Density of fluid

$\mathbf{v}_f$: Velocity of fluid

p_f : Hydrostatic pressure in fluid

$\boldsymbol{\tau}_f$: Extra stress tensor

∇ : The gradient operator

For Newtonian fluids the extra stress tensor $\boldsymbol{\tau}_f$ can be written as a function of the rate of deformation tensor $\mathbf{D} = \frac{1}{2}(\nabla \mathbf{v}_f + (\nabla \mathbf{v}_f)^T)$:

$$\boldsymbol{\tau}_f = 2\eta_f \mathbf{D} \tag{3.3}$$

Where:

η_f : The dynamic viscosity of the fluid

Note that the subscript $_f$ and $_s$ will be used in this thesis to distinguish between fluid and solid, respectively.

3.3 Structure domain: cell

The cell is described in the structure domain Ω_s. The deformation of the cell is assumed to be elastic and isotropic. The Cauchy stress $\boldsymbol{\sigma}_s$ can be described by equation 3.4.

$$\boldsymbol{\sigma}_s = p_s \mathbf{I} + \boldsymbol{\tau}_s \tag{3.4}$$

Where:

p_s : Hydrostatic pressure in cell

$\boldsymbol{\tau}_s$: Extra stress tensor

$\mathbf{I}$: Unit tensor

The cell is assumed to behaves hyperelastic and isotropic according to a Neo-Hookean constitutive model. The extra stress tensor can be described by equation 3.5.

$$\boldsymbol{\tau}_s = G_s(\mathbf{B} - \mathbf{I}) \tag{3.5}$$

where:

G_s : Shear modulus

$\mathbf{B}$: Finger or Cauchy-Green strain tensor ($\mathbf{B} = \mathbf{F} \cdot \mathbf{F}^T$ where $\mathbf{F} = (\vec{\nabla}_0 \vec{x}_s)^T$). ∇_0 is the gradient operator and x_s is the cell position vector.

$\mathbf{I}$: Unit tensor.

The density of the cell is chosen equal to the density of the fluid, so buoyancy forces can be neglected. The mass of the cell will not be taken into account, since it is much smaller than the mass of the fluid flowing around it. In absence of any body forces the equation of motion and the continuity equation for the structure domain Ω_s thus yields.

$$\nabla \cdot \boldsymbol{\sigma}_s = \nabla \cdot \boldsymbol{\tau}_s - \nabla \cdot p_s \mathbf{I} = 0 \tag{3.6}$$

$$det(\mathbf{F}) - 1 = 0 \tag{3.7}$$

3.4 Fluid-structure interaction

There is a distinct difference between equations 3.1 and 3.6 that in the momentum equation of the fluid the domain is known and fixed in space (Eulerian), while the position of the structure domain is a priori unknown (Lagrangian). As a consequence the gradient operator in equation 3.6 depends on the solution of the cell position, while the gradient operator in equation 3.1 is independent of the velocity field $\mathbf{v}_f$. This situation changes whenever the computational domain of the fluid is adapted to the computed velocity field, for instance to follow the motion of the immersed structure. The method used assumes the fluid domain as a fixed space. The equations (3.1), (3.2), (3.5), (3.6) and (3.7) will be complemented with appropriate coupling and boundary conditions.

In the Lagrange formulation of the structure the displacement field $\mathbf{u}_s$ is the unknown. The structure velocity $\mathbf{v}_s$ during time interval $t_n \rightarrow t_{n+1}$ is taken to be related to the structure displacement $\mathbf{u_s}$ by the following approximation:

$$\mathbf{v_s} = \frac{\mathbf{u_s}}{\Delta t} \tag{3.8}$$

with time step $\Delta t = t_{n+1} - t_n$. Coupling between the fluid and structure is done by a fluid-structure interface boundary $\delta\Omega_s$, with a velocity constraint:

$$\mathbf{v}_f - \mathbf{v}_s = \mathbf{0} \tag{3.9}$$

Straight forward coupling of the fluid and structure domain requires that their boundaries and nodal points coincide along the interface, which means equal order finite elements for both domains. Coincident boundaries with non-conforming discretizations can be realized by the use of a Lagrange multiplier. This method is called the Arbitrary Lagrangian-Eulerian algorithm (ALE) [Donea et al., 2004]. With the equations 3.1, 3.6 and 3.9, the weak form of the full set of equations is given by, following [de Hart et al., 2003, van Loon, 2005]:

$$\int_{\Omega_f} w_f \cdot ((\rho_f \frac{\partial \mathbf{v}_f}{\partial t} + \mathbf{v}_f \cdot \nabla \mathbf{v}_f) - \nabla \cdot \boldsymbol{\tau}_f + \nabla \cdot p_f \mathbf{I}) d\Omega_f + \int_{\delta\Omega_s} w_f \cdot \boldsymbol{\lambda} d\delta\Omega_s = 0 \tag{3.10}$$

$$\int_{\Omega_s} w_s \cdot (\nabla \cdot \boldsymbol{\tau}_s - \nabla \cdot p_s \mathbf{I}) d\Omega_s - \int_{\delta\Omega_s} w_s \cdot \boldsymbol{\lambda} d\delta\Omega_s = 0 \tag{3.11}$$

$$\int_{\delta\Omega_s} w_\lambda \cdot (\mathbf{v}_f - \mathbf{v}_s) d\delta\Omega_s = 0 \tag{3.12}$$

Which must hold for all admissible weighting functions w_f w_s and w_λ. The Lagrange multiplier $\boldsymbol{\lambda}$ may be interpreted as the surface force exerted on the fluid and structure along $\delta\Omega_s$ to maintain the coupling between them.

3.5 Sepran model

For the calculation of the different equations for the fluid domain Ω_f, structure domain Ω_s and interaction between the fluid en solid domain, Sepran is used. Sepran is a finite element package which is designed for simulations of flow, gasses and material calculations. Sepran is also capable of simulating solid and fluid interactions. First the mesh needs to be generated. After the meshing the problem needs to be applied to the mesh. The boundary of the moving structure domain is coupled to the fluid domain with the ALE method. In Sepran this boundary is called the fictitious boundary. Also the properties of the fluid and solid need to be applied to the mesh. The output of the program needs to be defined. If the mesh and the problem with properties and the wanted results are loaded, the simulation can begin. A graphical representation of the solution proces can be seen in figure 3.1.

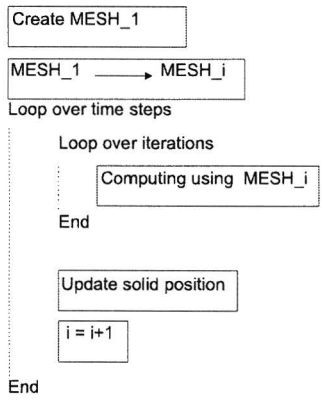

Figure 3.1: Schematic representation of the Sepran program.

After the mesh is generated, every time step another mesh will be created and used for the next time step. The non-linear set of equations is linearized and solved in a Newton-Raphson iterative scheme [van Loon, 2005].

3.6 Dimensionless numbers

The simulation provide more insight into the effect of the different properties of the fluid, solid or geometry of the cell stretcher. In reality the cell properties can only be changed if an other cell is chosen as model cell. The fluid or the geometry of the micro fluidic cell stretcher can be varied to control the deformation of the cell. In the model, the following input values are needed:

- Geometry micro fluidic cell stretcher
- Fluid viscosity η_f
- Fluid density ρ_f
- Fluid velocity v_f
- Shear modulus cell G_s

Because a change in only one of the values could have effect on several parts of the equations and will have effect on different kind of dimensionless numbers. In the micro fluidic cell stretch model dimensionless numbers allow us to experiment and predict the behavior of the micro fluidic cell stretcher under actual conditions. First the dimensionless numbers for the micro fluidic cell stretcher need to be determined. This has be done with reference to [Dantzig and Tucker, 2001] and can be found in appendix D. The model used for the determination of the dimensionless numbers for the micro fluidic cell stretcher can be seen in figure 3.2. The geometry of the cross slot will be two input flows and two exit flows, with an equal width of W.

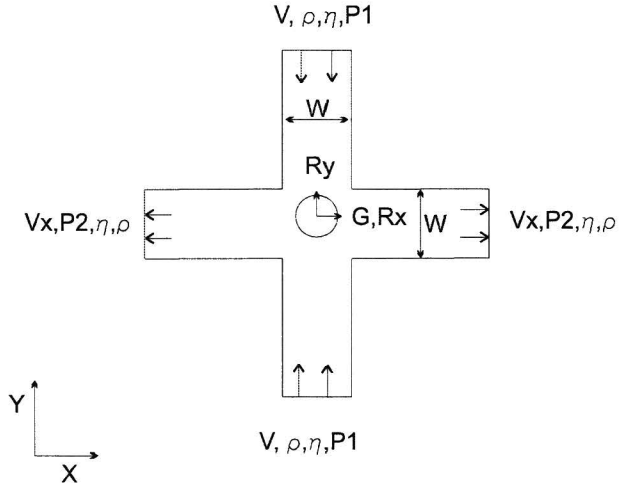

Figure 3.2: Schematic model micro fluidic cell stretcher

The flow is stationary and the fluid is Newtonian with a constant density ρ and a constant viscosity η. The model is two dimensional in the x-y plane. Known parameters of the fluid are P_2, V, η and ρ. Unknown parameters of the fluid are P_1 and V_x. The solid is characterized as a hyperelastic, Neo-Hookean and incompressible. Known parameters of the solid are the shear modulus G, dimensions of the solid in the x-y direction (R_x, R_y). Unknown parameters of the solid are the dimensions of the solid in the x-y direction after deformation (r_x, r_y), see figure 3.3.

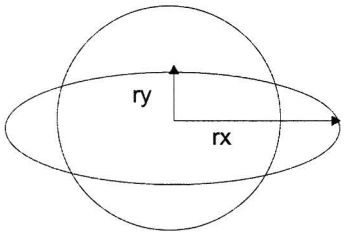

Figure 3.3: Schematic r_x and r_y cell

The surface tension of the cell will assumed to be negligibly small, following [Laursen et al., 2005a]. If the deformation of the cell is small, then the radius of the cell R after deformation is $\approx$ R. This leads to the following dimensionless numbers that characterize the model of the micro fluidic cell stretcher in figure 3.2:

- $F_{RW} = \frac{R}{W}$
- $Re = \frac{\rho_f v_f W}{\eta_f}$
- $De = \frac{\eta_f \frac{v_f}{R}}{G_s}$

The parameters for a realistic model are:

ρ_f : Density of fluid 1000 kg/m^3 [Leijendeckers et al., 1998]

η_f : Dynamic viscosity of fluid 0.001 Pa $\cdot$ s [Leijendeckers et al., 1998]

G_s : Shear modulus of cell 380 Pa

v_f : Velocity of the fluid when going inside the micro fluidic cell stretcher 1000 μm/s

The liquid surrounding the cells has almost the same properties as water. For the shear modulus of the structure (cell), micromanipulation test (AFM) of E. Peters on fibroblasts results were used. From the experiments an elastic modulus of $E_{fibroblast} = 1140$ kPa was found [Peeters, 2004]. If is assumed that the cell is incompressible, the Poisson ratio is $\nu = 0.5$, and with the equation 3.13, following [Peeters, 2004]:

$$G = \frac{E_{fibroblast}}{2(1+\nu)} \tag{3.13}$$

Following equation 3.13, the shear modulus of a fibroblasts is 380 Pa. The elastic modulus of the fibroblast, following [Peeters, 2004], was based on a model of a hyperelastic isotropic deformation of a solid, and can be used as a reference for this model. Another advantage of using fibroblasts is that the elasticity of the cells is high, compared to other cells like Chondrocyte. Chondrocyte have a Young's modulus of 2.7 kPa, which results in a shear modulus of 900 Pa. These values were also measured with AFM, following [Knight et al., 2002]. The size of a 3T3-fibroblast is around 10μm [Thoumine et al., 1999, Uhal et al., 1998]. If the width of the cross slot (W) is 100 μm, the dimensionless numbers for the experiment will be:

$$Re = 0.1 \tag{3.14}$$

$$De = 5.26 \cdot 10^{-4} \tag{3.15}$$

$$F_{RW} = 0.05 \tag{3.16}$$

The Reynolds number is low, which means that the flow is laminar. Since Re=< 1 it can be assumed that the fluid flow is dominated by viscous forces. Because De=< 1 the characteristic time of the cell against deformation is higher than of the resistance time of the fluid. The F_{RW} will always be < 0.5, because otherwise the cell diameter will be higher than the width of the channel. After proper scaling of the $W, R, \rho_f, v_f, G_s, \eta_f$, simulations are started and the Taylor deformation parameter D_{xy} was determined in time. The definition of the Taylor deformation parameter can be found with equation 2.1 in section §2.1.2. With the simulations variations on the geometry F_{RW}, De and Re are made to estimate the influence on the Taylor deformation rate of the cell.

3.7 Simulation results

The mesh of the micro fluidic stretcher can be seen in figure 3.4(a).

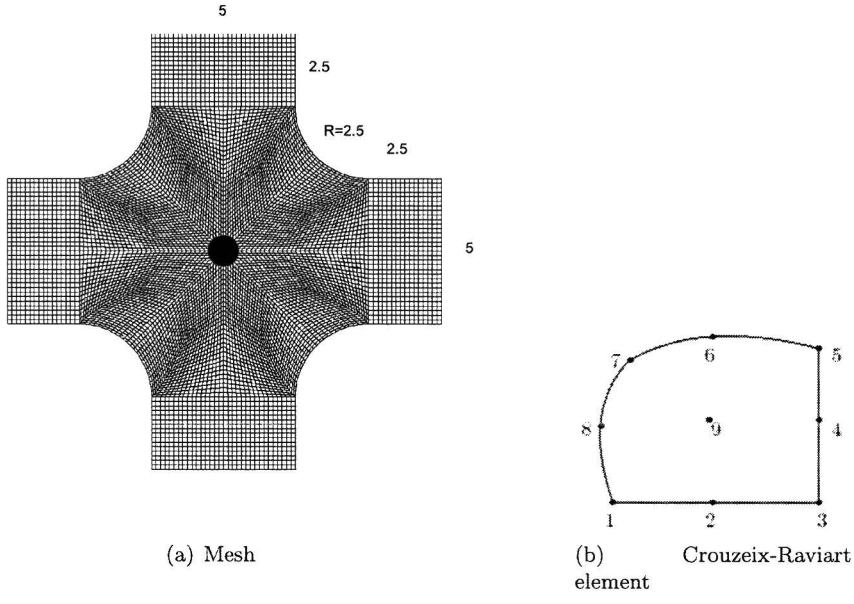

(a) Mesh

(b) Crouzeix-Raviart element

Figure 3.4: Mesh model Sepran

The number of elements in the fluid domain is ♯8064. The solid domain is described with ♯3125 elements. The elements are chosen that two or more elements of the solid fit inside a fluid element, which gives the best results for the interaction between the fluid and solid domain [van Loon, 2005]. The type of element for the fluid domain is a rectangular bi-quadratic quadrilateral, also called Crouzeix-Raviart element which can be seen in figure 3.4(b) [Segal, 2004]. The solution vector contains two velocity components in each node. Furthermore in the centroid (point 9), the pressure and the gradient of the pressure are available. In this point we have v_1, v_2, p, $\frac{\delta p}{\delta x}$ and $\frac{\delta p}{\delta y}$. For the solid domain a general bi-quadratic quadrilateral element is used, which contains the same information as the fluid domain.

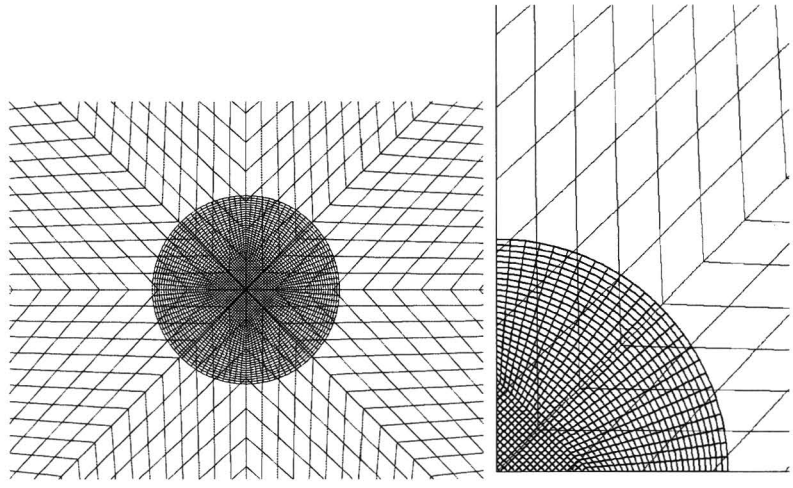

(a) Mesh solid (b) Part of solid mesh

Figure 3.5: Mesh solid model Sepran

The mesh of the solid can be seen in figure 3.5(a). The mesh of the fluid is defined such that at least two solid nodes will fall inside one fluid element. This results in the best solution for the boundary of the interface between the solid and fluid [van Loon, 2005]. This can be seen in figure 3.5(b). The time step of the simulations is taken 0.01. For this time step maximum of three iterations are needed to solve the equations. The width of the cross slot is 5 and the radius of the cell is 0.5. The radius of the corners of the cross slot is 2.5. The length of the inlet of the cross slot is 2.5. A short inlet of the cross slot is chosen because Re $\approx$ 0, which leads to a short development length of the flow. The field of the area of the cross is 15x15. On the top and bottom boundary a plug flow is defined with an average velocity $v_f = 1$. The result of the simulation is a velocity field, with a solid particle inside that deforms. An example can be seen in figure 3.6(a) and figure 3.6(b).

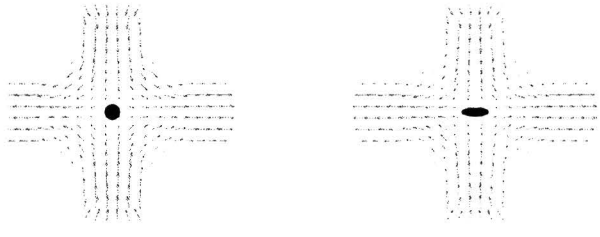

(a) Cell (b) Deformed cell

Figure 3.6: Example cross slot: velocity field of flow and with cell in the middle

3.7.1 Influence of the Deborah number on the deformation of the cell

The Deborah represents the relation between the relaxation time constant of the fluid a the relaxation time constant of the solid [Squires and Quake, 2005, Massey, 1971]. If De=1, the solid behaves like the fluid and wil deform equally with the fluid. Thats why the simulation represent De< 1. The Reynolds number is kept constant at 0.05 and the Fraction number F_{RW} is kept constant at 0.1. The Deborah number is increased from 0.01 to 1 by decreasing the shear modulus of the cell. In figure 3.7 images are shown of the deformation of the solid inside the cross slot for different Deborah numbers at time 2. The first image of figure 3.7 shows the starting position of the simulation at t=0.

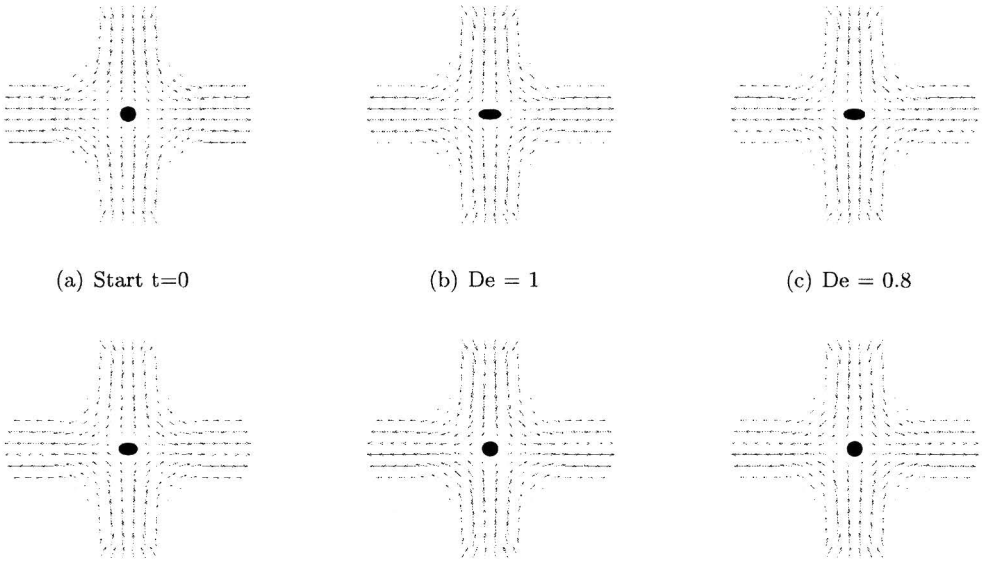

(a) Start t=0 (b) De = 1 (c) De = 0.8

(d) De = 0.5 (e) De = 0.1 (f) De = 0.01

Figure 3.7: Images simulation for different Deborah numbers at t=2

The Taylor deformation parameter (D_{xy}) of the solid as a function of the Deborah number, after t=2, can be seen in figure 3.8.

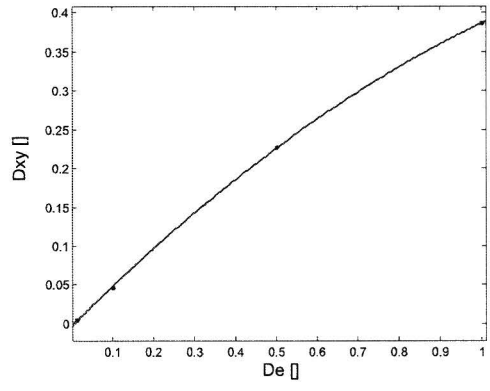

Figure 3.8: D_{XY} against De-number at t=2

The Taylor deformation parameter (D_{xy}) increases in time for the different Deborah number, this relation can be seen in figure 3.9.

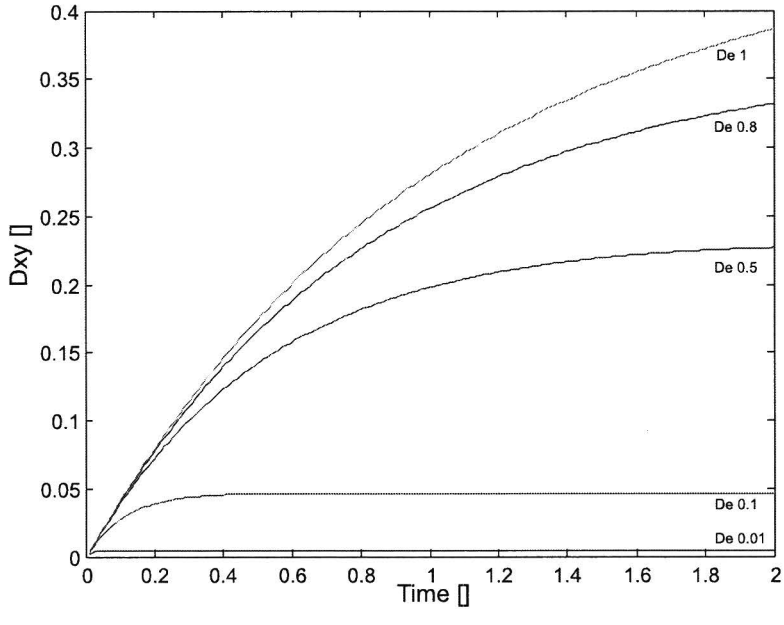

Figure 3.9: D_{XY} against time for different De-numbers

In figure 3.9 it can be seen that the D_{XY} increases in time, and the force of the fluid on the cell and the shape of the cell on the fluid go to an equilibrium value.

3.7.2 Influence of the Reynolds number on the deformation of the cell

The Reynolds number is a non-dimensional parameter that compares the inertial to viscous forces [Squires and Quake, 2005, Massey, 1971]. If the Reynolds number is low, then viscosity plays an important part in the simulations. The Deborah number is kept constant at 0.5 and the Fraction number F_{RW} is kept constant at 0.1. In the simulation, the Reynolds number was changed from Re=0.0025 to Re=2.5. In figure 3.10 images are shown of the deformation of the solid inside the cross slot for different Reynolds numbers at time 2. The first image of figure 3.10 shows the start position of the simulation at t=0.

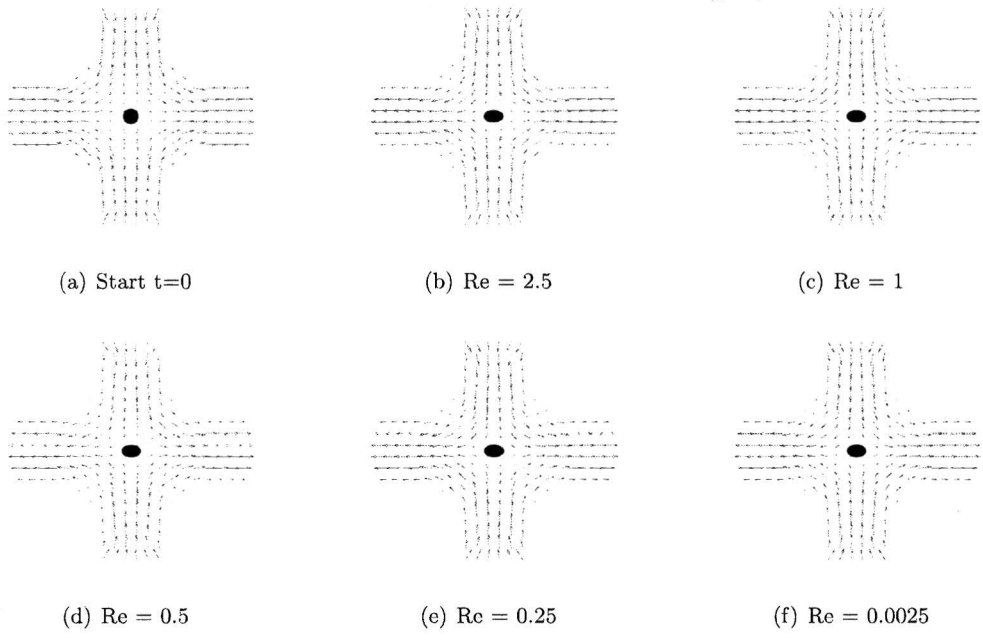

(a) Start t=0 (b) Re = 2.5 (c) Re = 1

(d) Re = 0.5 (e) Re = 0.25 (f) Re = 0.0025

Figure 3.10: Images simulation for different Reynolds numbers at t=2

Due the increasing Reynolds number form Re=0.0025 to Re=2.5, the Taylor deformation parameter (D_{xy}) increases form 0.2269 to 0.22927, which can be seen in figure 3.11.

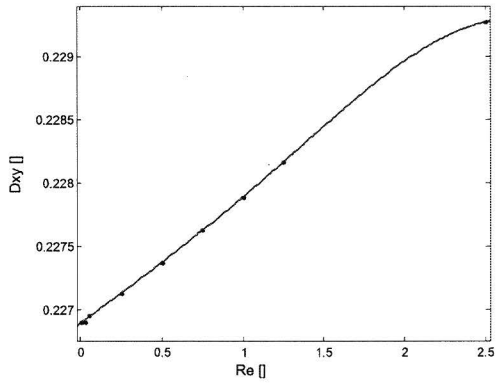

Figure 3.11: D_{XY} against Re-number at t=2

The Taylor deformation parameter (D_{xy}) increases in time for the different Reynolds number, this relation can be seen in figure 3.12.

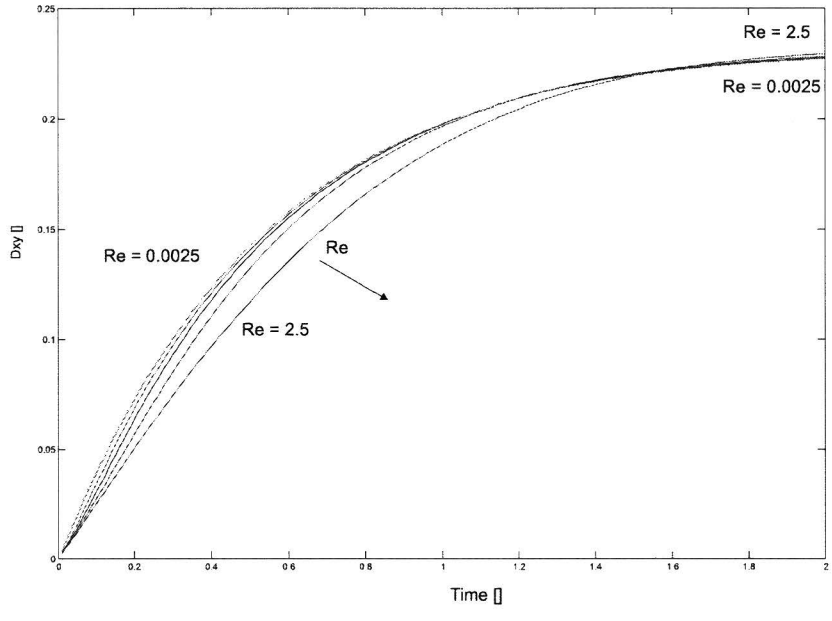

Figure 3.12: D_{XY} against time for different Re-numbers

After Re=2.5, the Taylor deformation parameters drops, which indicates that the deformation of the cell decreases. This is because the flow is no longer fully developed. The inlet length of the channel is 0.5 times the height of the channel, which is pretty low for a fully developed flow for Reynolds numbers greater than 1. If the inlet length is increased, the flow has a longer time to get fully developed and higher Reynolds number can be simulated. A solution to this problem could be to give another description of the flow on the inlet boundaries. Plug flow no longer can be applied. A Poiseuille flow on the inlet could increase the region of Reynolds numbers for the simulation. Another solution can be to make the inlet a function of the outlet of the cross slot.

3.7.3 Influence of fraction number on the deformation of the cell

The fraction number is a non-dimensional parameter that is determined by the geometry of the cross slot and the radius of the cell. If the fraction number is low, the cell is small compare to the width of the cross slot. The fraction number can never be higher than 0.5, because the radius of the cell could maximum be 0.5 times the width of the channel. In the simulations the size of the cell has been changed. The size of the mesh elements is kept constant and the Deborah number is also kept constant at 0.5, by changing the shear modulus of the cell. In the simulation the fraction number was changed from $F_{RW} = 0.2$ to $F_{RW} = 0.02$. If the fraction number is increases form $F_{RW} = 0.02$ to $F_{RW} = 0.2$. In figure 3.13 images are shown of the deformation of the solid inside the cross slot for different fraction numbers at time t=2. In image 3.13 first an image is shown in the initial situation t=0 and the second image is of the deformation at t=2.

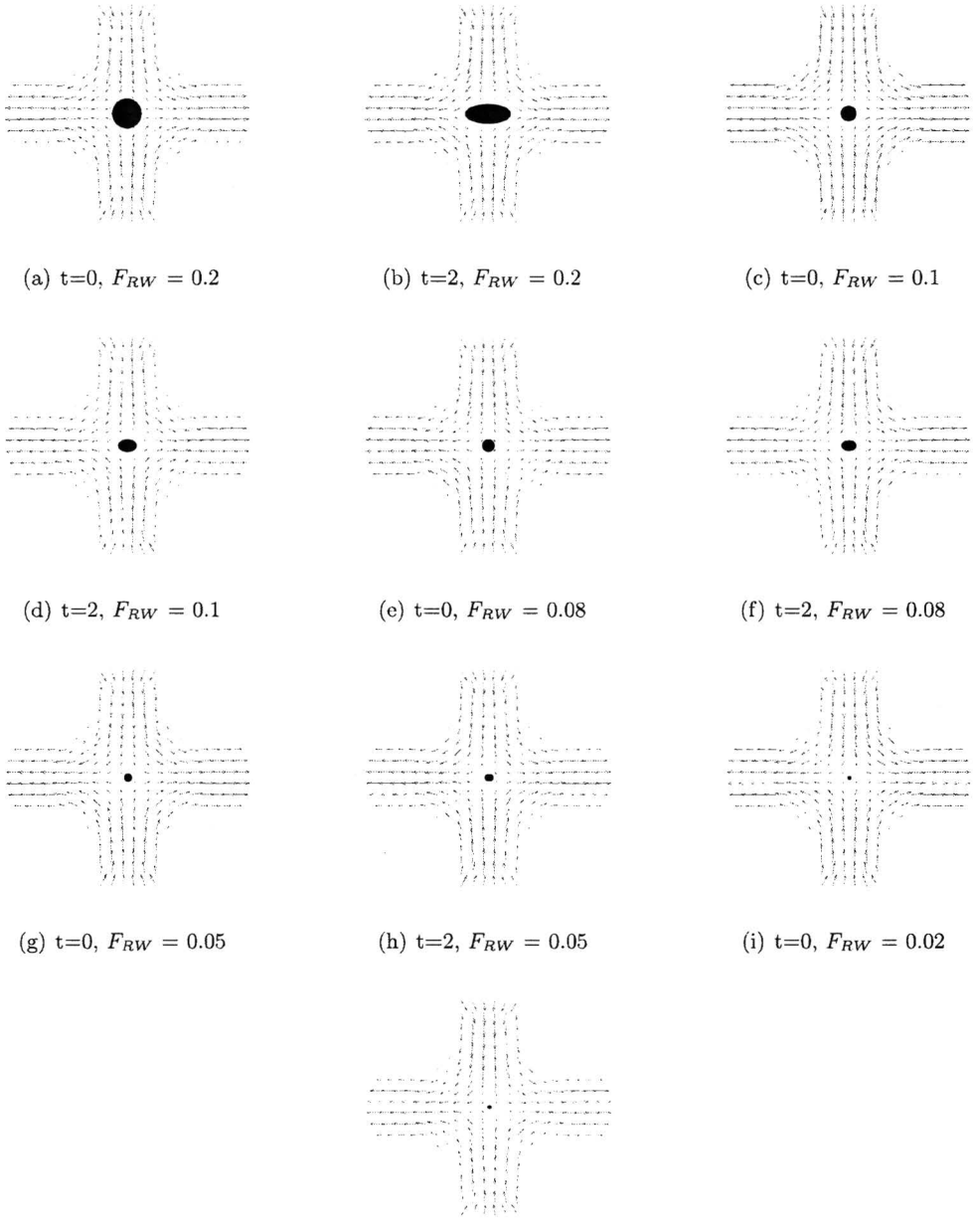

(a) t=0, $F_{RW} = 0.2$ (b) t=2, $F_{RW} = 0.2$ (c) t=0, $F_{RW} = 0.1$

(d) t=2, $F_{RW} = 0.1$ (e) t=0, $F_{RW} = 0.08$ (f) t=2, $F_{RW} = 0.08$

(g) t=0, $F_{RW} = 0.05$ (h) t=2, $F_{RW} = 0.05$ (i) t=0, $F_{RW} = 0.02$

(j) t=2, $F_{RW} = 0.02$

Figure 3.13: Images simulation for different fraction numbers at t=2

The number of fluid elements is kept constant at ♯8064. The number of elements, making up the solid are ♯4500 (F_{RW} = 0.2), ♯3125 (F_{RW} = 0.1), ♯2000 (F_{RW} = 0.08), ♯845 (F_{RW} = 0.05) and ♯125 (F_{RW} = 0.02). Due the increasing fraction number from F_{RW} = 0.02 to F_{RW} = 0.2 , the Taylor deformation parameter (D_{xy}) increases from 0.046022 to 0.4166 at time 2, which can be seen in figure 3.14.

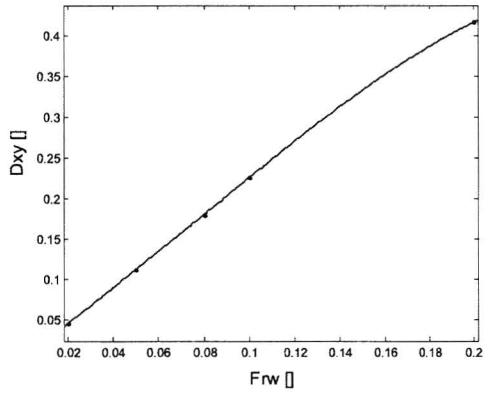

Figure 3.14: D_{XY} against F_{RW}-number at t=2

The Taylor deformation parameter D_{xy} increases in time for different fraction numbers, as can be seen in figure 3.15.

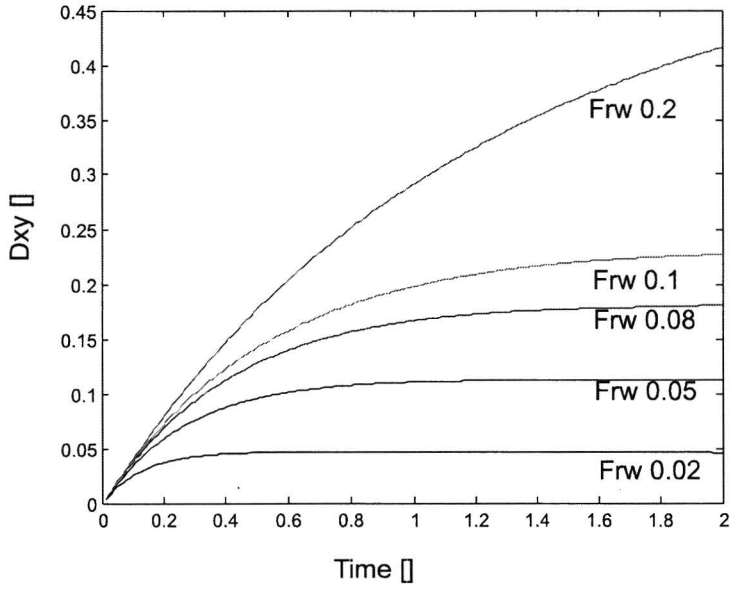

Figure 3.15: D_{XY} against time for different F_{RW}-numbers

If the width is decreased compared to the size of the cell, more deformation can be expected.

3.8 Conclusions

The influence of the mesh is determined by reducing the mesh size of the solid and observe whether the deformation of the cell is influenced. As an example a simulation is used in which Re = 0.05, De = 0.5, $F_{RW} = 0.05$. The number of solid elements and the effect on the Taylor deformation rate can be seen in figure 3.16.

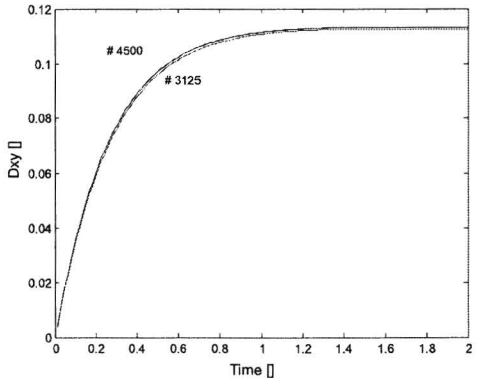

Figure 3.16: D_{XY} against time for different number of solid elements

From image 3.16 the effect on the Taylor deformation rate, if we increase the number of elements, is minimum. If the number of elements is increased from ♯3125 to ♯4500, the Taylor deformation rate increases form 0.11238 to 0.11311. If the time step is decreases, the influence on the Taylor deformation rate can be seen in figure 3.17.

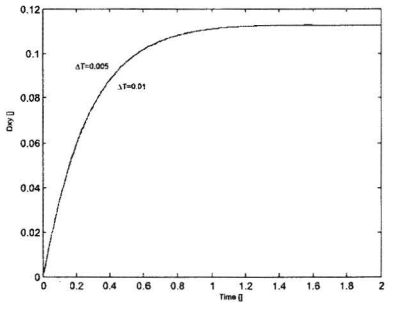

Figure 3.17: D_{XY} against time for different time steps

From image 3.17 the effect on the Taylor deformation rate is also minimum. If the time step decreases form 0.01 to 0.005, the Taylor deformation rate changes form 0.11238 to 0.11239. This means that the time step of the simulation is well chosen.

A simulation was made with the same dimensionless numbers as in reality mentioned in equations 3.14, 3.15, 3.16 namely: Re = 0.1, De = 0.000526 and $F_{RW} = 0.05$. The Taylor deformation rate of the cell for this case is shown in figure 3.18 with curve (1).

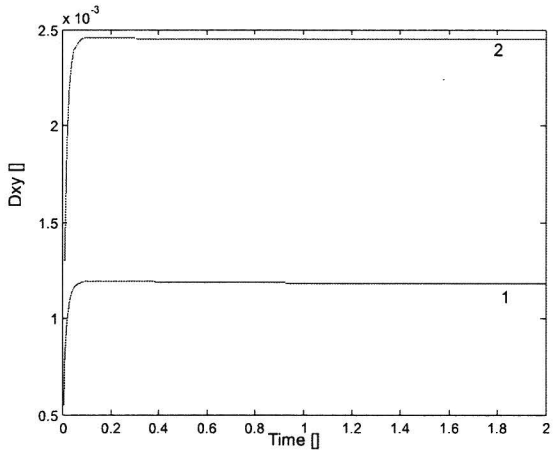

Figure 3.18: D_{XY} against time for micro fluidic cell stretcher

The deformation of the solid is very low. The Taylor deformation rate of curve (1) is 0.0011789. To increase the deformation of the solid, the fraction number of the cross slot can be increased. The can be realized by changing the width of the cross slot from 100 μm to 50 μm. The fraction number changes to $F_{RW} = 0.1$. The Taylor deformation rate in time for a fraction number of 0.1 can be seen in curve (2) of figure 3.18. Curve (2) reaches a maximum of 0.0024524. This is still a small deformation of the cell. To increase the deformation of the cell, the viscosity of the fluid can be increased by adding Dextran to the culture of the cells [Ainslie et al., 2005]. Dextran has a viscosity of 0.001 to 10 Pa·s depending on the molecular weight and concentration of Dextran in the solution, see figure 3.19.

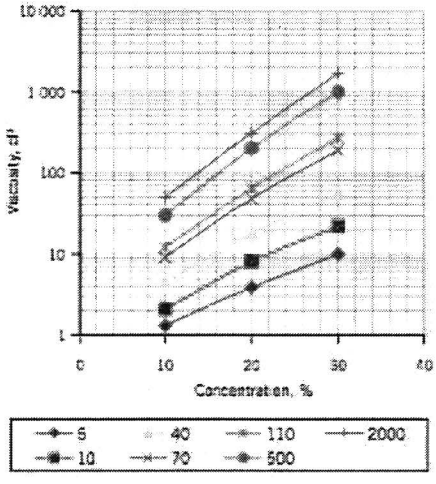

Figure 3.19: Dependence of viscosity of Dextran fractions on concentration [Dextran, 2005]

In figure 3.19 the viscosities are measured at 25 °Cand 1 Cp. One Centi poise) equals to 0.001 Pa·s. The concentration must be multiplied by 1000 Daltons, for example 5 stands for 5.000 Daltons. Dextran is a salt based solution and has no influence on the behavior of the cell. If the viscosity is increased also the velocity can be increased with the same factor, without increasing the Reynolds number. Since the viscosity of the fluid and the velocity are in the Deborah number, his wil increase with a multiplication of the two factors, resulting in more deformation of the cell.

If the viscosity is increased with a factor 10 and the velocity is increased with a factor 10, this should result in more deformation. The real value of the velocity will be 10 mm/s and the viscosity of the fluid has to be 0.01 Pa·s. Then Re = 0.1 and the Deborah number increases to De = 0.0526. The influence on the Taylor deformation rate for the cross slot of 100 μm is shown in figure 3.20(a).

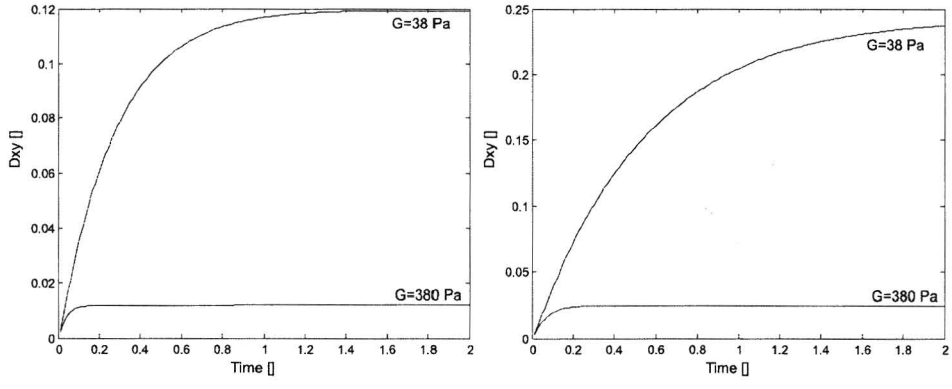

(a) Cross slot 100 μm

(b) Cross slot 50 μm

Figure 3.20: D_{XY} against time for micro fluidic cell stretcher with increased viscosity and velocity of fluid

The upper line in figure 3.20 is the Taylor deformation rate of a cancerous fibroblast (G=38 Pa), the lower line is the Taylor deformation rate of a healthy fibroblast (G = 380 Pa). The shear modulus is estimated with the found literature [Gil et al., 1999] in section §1.5. This leads for a shear modulus of 38 Pa (De = 0.526) to a Taylor deformation rate of 0.11914 and for a shear modulus of 380 Pa (De = 0.0526) to a Taylor deformation rate of 0.011947. If also the fraction number is increased to 0.1, the influence of on the Taylor deformation rate of the cross slot of 50 μm is shown in figure 3.20(b). This leads for a shear modulus of 38 Pa (De = 0.526) to a Taylor deformation rate of 0.23749 and for a shear modulus of 380 Pa (De = 0.0526) to a Taylor deformation rate of 0.024492.

The pressure gradients resulting from the simulation with shear modulus (G = 38 Pa) in figure 3.20(a) and figure 3.20(b) are shown in figure 3.21 and figure 3.22.

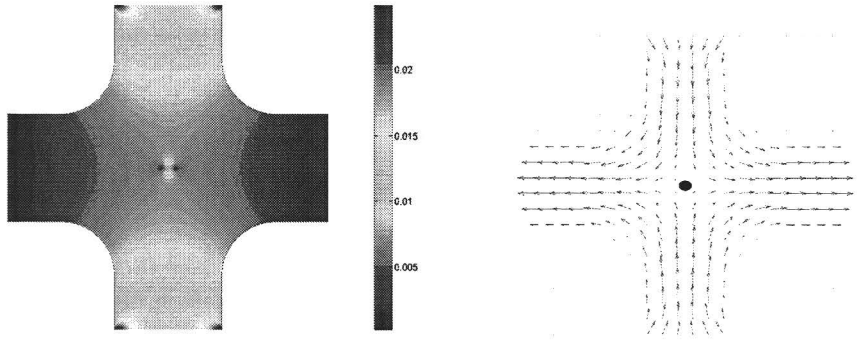

(a) Pressure gradient (b) Image at t=2

Figure 3.21: Pressure gradient at t=2 for situation in figure 3.20(a)

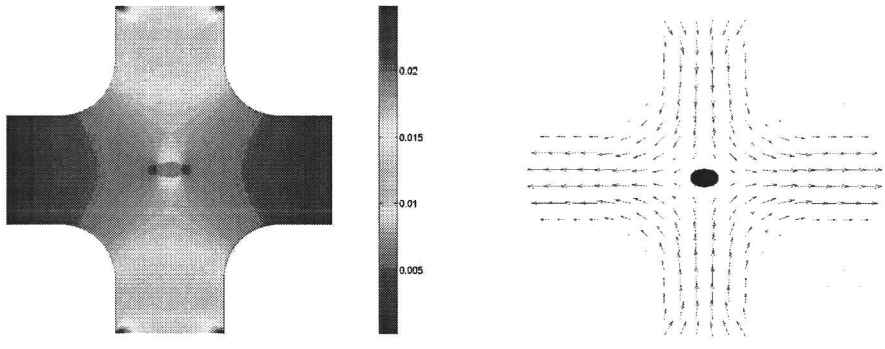

(a) Pressure gradient (b) Image at t=2

Figure 3.22: Pressure gradient at t=2 for situation in figure 3.20(b)

It can be seen that the cell will deform at a dimensionless pressure of around 0.014, created by the fluid on the surface of the cell. If this is calculated to a real value, the pressure of the fluid on the cell is around 26.6 Pa. In this situation the area of a cell with a radius of 10 μm, the force on the cell is estimated to be 0.42 mN, following equation 3.17;

$$F_{cell} = \frac{1}{2}\pi DP \tag{3.17}$$

Where P is the pressure on the surface of the cell (26.6 Pa) and D is the diameter of the cell (10 μm).

The parameters D and P are visualized in figure 3.23. In the corners of the top and

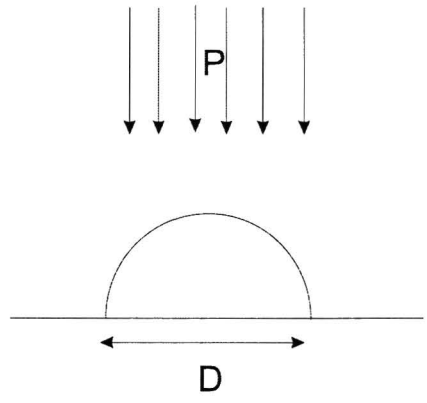

Figure 3.23: Schematic view estimated force on cell

bottom of the inlet channels, high pressures are shown. This will be explained in the next section. The tension inside the hyperelastic solid cell is shown for both situations in figure 3.24. The dimensionless tension at the left and right edge of the cell can rise to $3{\cdot}10^{-3}$. If

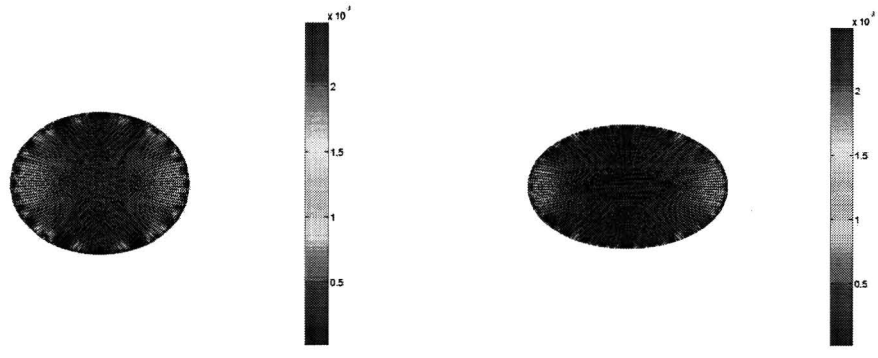

(a) Pressure gradient 100 μm

(b) Pressure gradient 50 μm

Figure 3.24: Pressure gradient at t=2 in hyperelastic solid

this is calculated to a real value, the tension inside the cell can rise to 5.7 Pa, which equals 5.7 mN/mm^2. From figure 3.24 can be seen that the left and the right edge of the cell suffers the highest tension due to the deformation of the cell. The tension in the cell increases with the decreasing radius of the cell.

The streamlines of the flow are shown in figure 3.25. In figure 3.25 also the inlet of the

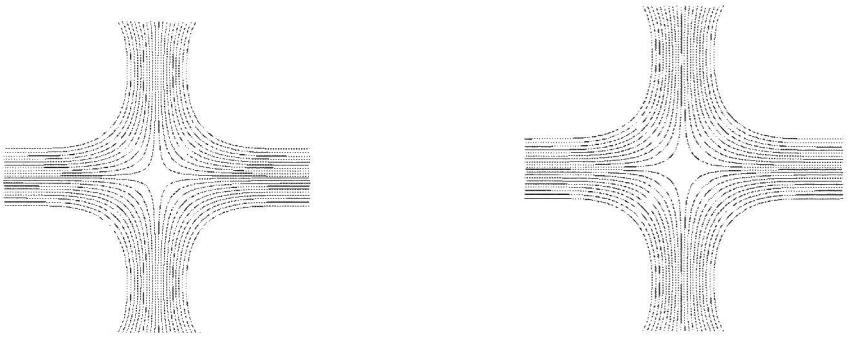

(a) 100 μm (b) 50 μm

Figure 3.25: Streamlines at t=2

flow can be seen in the top and bottom of the streamlines. Also can be seen that the flow is fully developed when leaving the cross slot (left and right exit).

3.9 Evaluation and discussion

In the simulations there is a strange velocity profile in the flow. In the model a plug flow is described, but no seen in the figure. On the inflow boundary only the second degree of freedom was defined and the first degree of freedom was not defined. Figure 3.26 shows which degree of freedom was undefined.

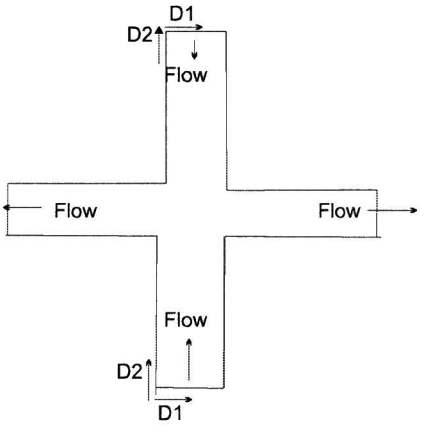

Figure 3.26: undefined degree of freedom

Therefore the flow was free to move in the tangent direction and the plug flow was gone. The inflow of the fluid inside (top/bottom) of the cross slot is different and can be seen in figure 3.27. Since no time was left to simulate all the simulations again, only one have been

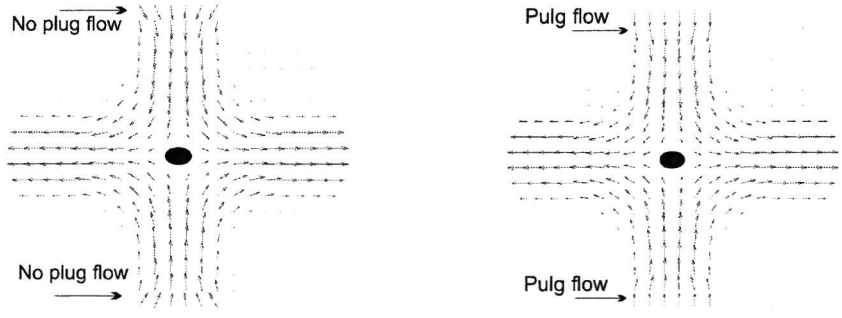

(a) Velocity profile wrong t=1.2

(b) Velocity profile right t=1.2

Figure 3.27: Simulation correction 50 μm

done again to look at the influence on the deformation of the cell. A simulation had been done with the right boundary conditions to look at the influence of this. The simulation used was of the cross slot of 50 μm with a fraction number F_RW =0.1, Reynolds number 0.1 and Deborah number De = 0.526. The simulation stopped at time 1.2, because an mesh element with no volume was found of the solid mesh. The velocity profile at time 1.2 can be seen in figure 3.27(b). The pressure gradient in the flow can be seen in figure 3.28.

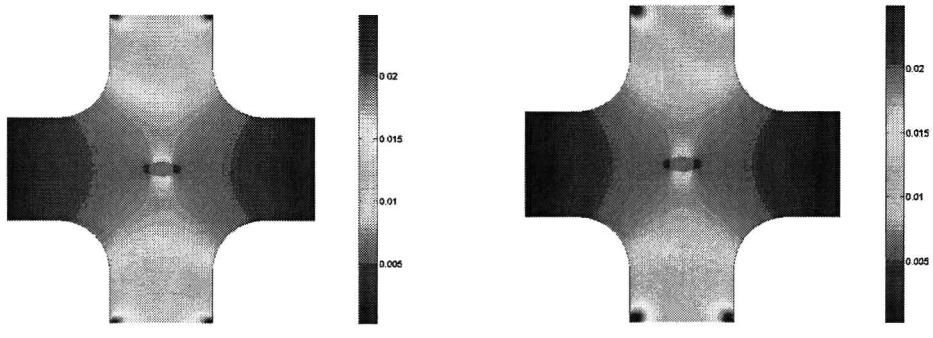

(a) Wrong t=1.2

(b) Right t=1.2

Figure 3.28: Simulation correction pressure gradient 50 μm cross slot

In the corners is of the inlet boundaries there is still a high pressure. This is because the flow has to be developed in this region to a fully developed flow. The pressure at the boundary increase a little from 0.025 to 0.028, but it has no effect of the pressure around the cell. The stress induced on the cell is also the same and can be seen in figure 3.29. The

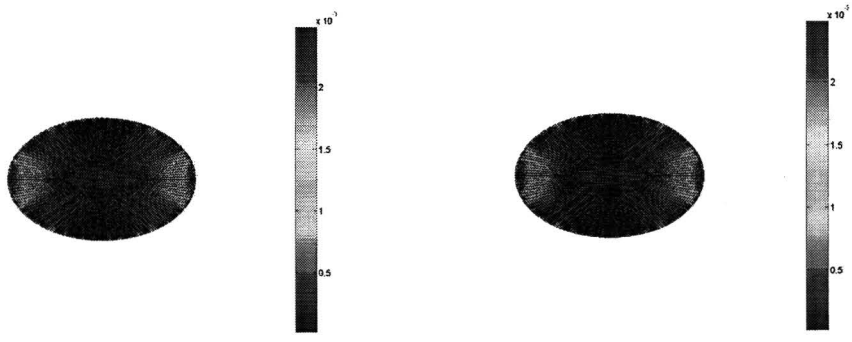

(a) Wrong t=1.2 (b) Right t=1.2

Figure 3.29: Simulation correction stress cell 50 μm cross slot

difference of the stream lines can be seen in figure 3.30 Important is to know if de deformation

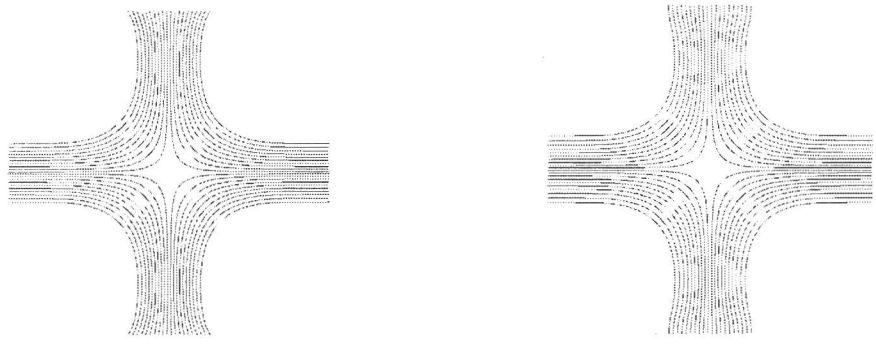

(a) Wrong t=1.2 (b) Right t=1.2

Figure 3.30: Simulation correction streamlines 50 μm cross slot

of the cell has been changed between the right and wrong boundary condition. Figure 3.31 shows the Taylor deformation rate of the cell for this case ($F_{RW} = 0.1$, Re $= 0.1$ and De $=$ 0.526).

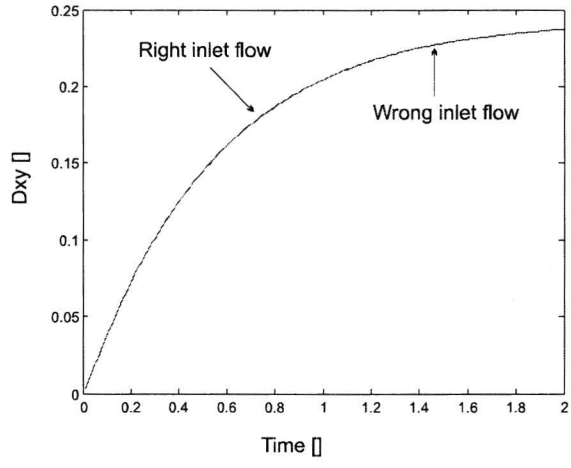

Figure 3.31: D_{XY} against time for micro fluidic cell stretcher, different inlet flows

The deformation of is not effected by the different boundary condition and has no influence at all on the cell. All experiments that are done with the 'wrong' boundary condition can be used for the conclusions on the influence of the several dimensional numbers on the deformation of the cell.

This model can only be used for Reynolds number below one. The equations and dimensionless numbers used in the model will change if higher Reynolds numbers are used. To improve the flow inside the model, two things can be improved. The inlet of the flow is 0.5 times the diameter of the channel, this is enough to get a fully developed flow inside the cross slot, but a increasing inlet of the cross slot could lead to higher possible Reynolds numbers that can be simulated. Besides increasing the inlet, the plug flow can be changed to a parabolic profile (Poiseuille), so the flow is already fully developed at the inlet boundary of the model.

The assumption that the cell has hyperelastic properties that can be described with only a shear modulus. Inside the cell several organs determine the elastic properties of the cell. Also there is a communication on the plasma membrane, which can release fluid in or out of the cell. The assumption that the cell is incompressible is also valid in reality because of the communication between the inside and outside of the cell. For obtaining a better model for the deformation of a cell, every organ inside the cell has to be characterize and connect to each other. Many researchers in the world are working on a model to describe the deformation of the cell. Not all behavior of the cell is known and science is trying to understand the physics inside a cell. A better description of the cell deformation may be reached if the cell is not assumed to be hyperelastic, but is described with a structural model of all the filaments of the cytoskeleton and the connection between them.

The numerical model is the assumption that the surface tension of the cell is negligible small, compare to the shear modulus of the cell. If a dimensionless analysis is performed with a found surface tension $\Gamma \approx 0.03$ mN/m, following [Morris and Homann, 2000, Raucher and Sheetz, 2000, Markosyan et al., 1999, Engler et al., 2004], the Deborah number De and the Capillary number Ca scale with the same order $O(10^{-7})$. The calculation can be found in appendix D. This means that the surface tension of the cell is equally important as the shear modulus of the cell. With the micro fluidic cell stretcher tests need to be preformed to look at the deformation of the cell and determine if the surface tension indeed has influence on the deformation of the cell inside the micro fluidic cell stretcher. The surface tension needs to be implemented in the model to study the influence of the surface tension of the cell in relation to the Taylor deformation rate of the cell inside the micro fluidic cell stretcher.

The numerical results can be used to determine what the possible influence of Re, De and F_{RW} are on the Taylor deformation rate D_{xy}. The model describes the situation only in two dimensions, this model has to be extended to a three dimensionally situation. A cell is initial spherical in the three dimensional model and will deform different than a initial circle shape in a two dimensional situation. After some iterations the boundary of the solid-fluid interaction loses the smoothness, because the fluid mesh and the solid mesh are not conform. This can be seen in figure 3.32.

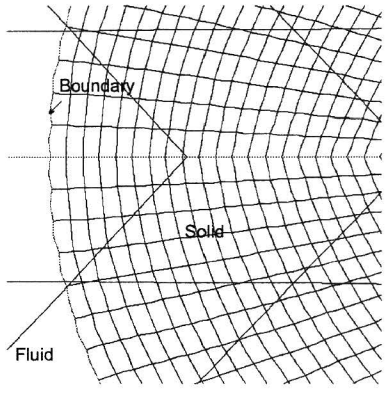

Figure 3.32: Smoothness losses of boundary solid

The maximum Taylor deformation rate D_{xy} which was reached with the model is 0.58. If the deformation increases $D_{XY} = 0.58$, the mesh of the solid was deformed to much creating an error during the simulation. The maximum deformation of the cell that can be reached was depending on the Re, De and F_{RW} numbers used in the model. The error represented that the fluid-solid boundary was disturbed to much and no solution was found for the constitute equation $\int_{\delta\Omega_s} \boldsymbol{\lambda}(\mathbf{v}_s - \mathbf{v}_f) d\delta\Omega_s = 0$. This problem can possibly solved if the mesh grid of the fluid and solid is refined. This will result in an increasing time of the calculation and more memory buffer is needed to calculate the equations. Another even better solution is to use mesh adaptation after every time step or after several time steps, following [van Loon, 2005].

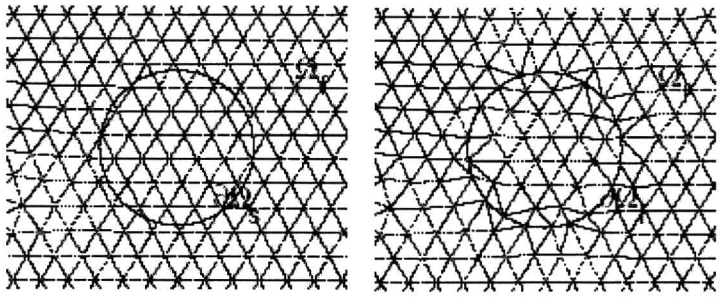

(a) Before adaptation (b) After adaptation

Figure 3.33: Mesh adaptation; a)Fluid domain Ω_f intersected by obstacle curve $\delta\Omega_s$ b) Adapted Ω_s to inner fluid boundary $\delta\Omega_f$ in Ω_f coincide $\delta\Omega_s$ [van Loon, 2005]

With an constant adaptation boundary of the solid mesh is created inside the fluid mesh. The fluid mesh is adapted to match the boundary of the solid so the interaction between the boundary of the solid and fluid mesh will coincide.

From the results of the simulation it should be possible to deform a cell with a micro fluidic flow. The experimental setup should have a cross slot with a width of 50 μm. The speed of the main fluid has to be 10 mm/s and the viscosity of the fluid has to be 0.01 Pa·s. To increase the viscosity of the fluid inside the cross slot, Dextran an be used. The influence of Dextran on the properties of the cell has to be investigated, but literature [Ainslie et al., 2005] confirms that it has no influence on the properties of the cell. However this is only a two dimensional model and in the three dimensions the situation is different, because of shape of the cell in the third dimension. In practise the characteristic values for the deformation locally can change, because of scaling effects. This could lead to other effects that are not taken in account in the model for the deformation of the cell inside the micro fluidic cell stretcher. Experiments are needed to study the deformation of the cell in the micro fluidic cell stretcher and confirm if the model is correct.

Chapter 4

Micro fluidic cell stretcher experimental setup and procedures

4.1 Experimental setup

Images of the experimental setup of the micro fluidic cell stretcher can be seen in figure 4.1(a) and 4.1(b).

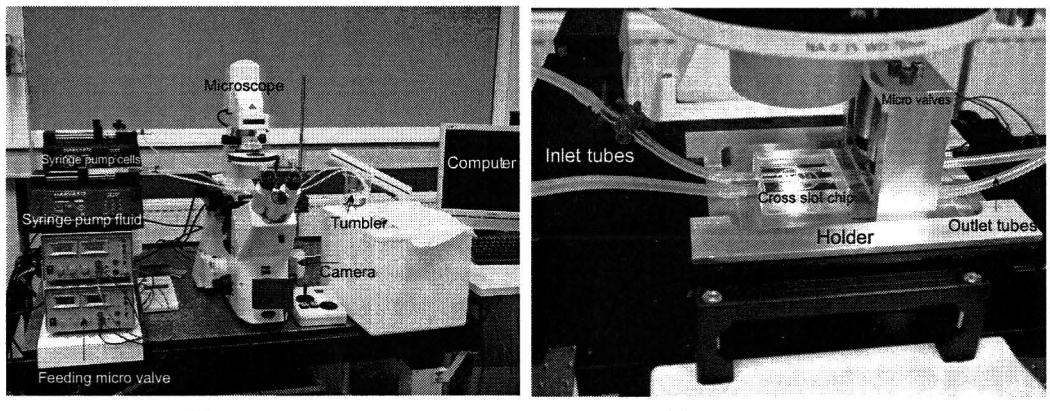

(a) Total setup

(b) Under the microscope

Figure 4.1: Image of experimental setup cross slot flow

The micro fluidic cell stretcher is constructed with the software Unigraphics. The design of the micro fluidic cell stretcher can be seen in figure 4.2.

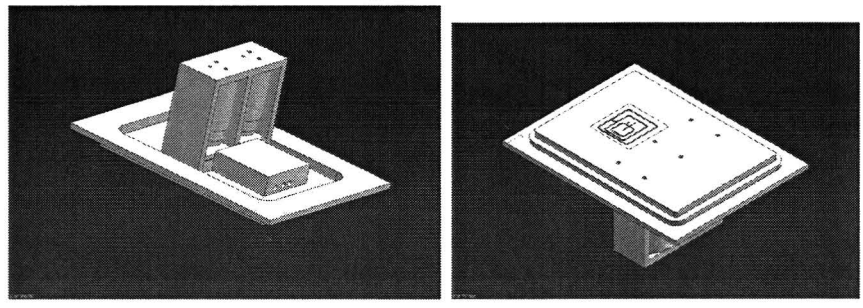

(a) Top (b) Bottom

Figure 4.2: Micro fluidic cell stretcher design with Unigraphics

Besides the geometry of the cross slot, the control system for the micro flow has to be developed. The design and fabrication of the components will be discussed if needed. The technical drawings of the micro fluidic cell stretcher can be found in the appendix E.

4.2 Cross slot chip

The concept design of the cross slot chip can be seen in figure 4.3.

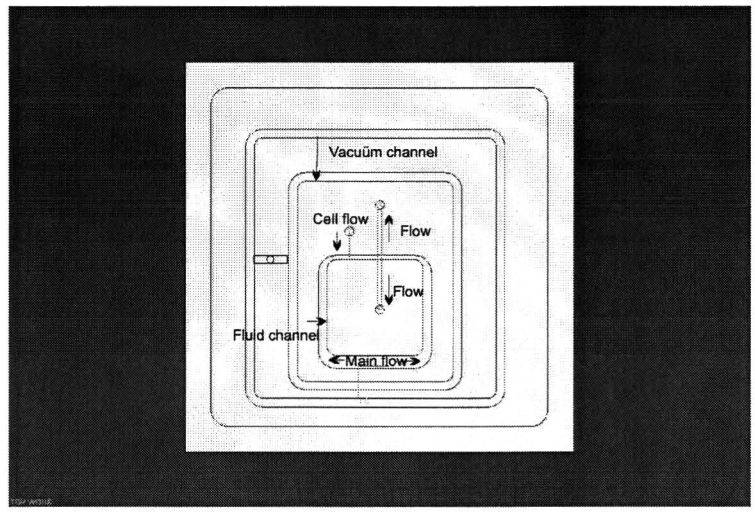

Figure 4.3: Concept of the cross slot

In the cross slot the flow enters the geometric through a hole and will be equal divided between left and right. The flow continues and one flow has a dispersion flow where cells can enter the main channel of the cross slot. The flows will interact in the middle of the cross slot and leave the cross slot geometry through two exit holes. The size of the main channel and cell entrance channel of the cross slot is depending on the minimal sizes of the tooling used to manufacture the cross slot. The cells enter the cross slot through a T-junction. A SEM image and a sketch of a T-junction can be seen in figure 4.4.

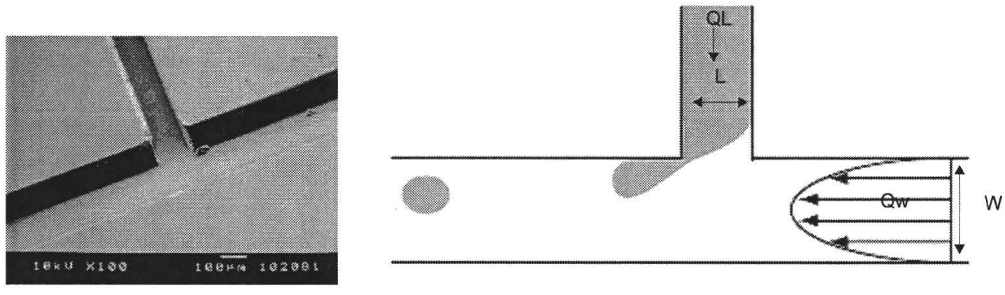

(a) SEM image [Nisisako et al., 2002]

(b) Schematic model

Figure 4.4: T-junction

The T-junction has already been used to make water droplets inside a micro channel network [Nisisako et al., 2002]. Important for the design of the T-junction is the width of the dispersion flow (L) has to be smaller than the width of the main flow (W). The droplets created by the T-junction are three to five times bigger than the width of the T-junction. Besides the size of the micro channels, also the difference between the two flow rates (Qw,QL) has influence on the size of the droplets created by the T-junction. The viscosity of the dispersion flow and the main flow also influence the formation of the droplets. Under shear of the continuous flow, the droplet is being torn form the material in the channel. In equation 4.1 the capillary number represents the shear forces ($\tau = \eta_c \cdot \dot{\gamma}$) of the continuous phase on the droplet compared to the surface tension of the droplet.

$$Ca = \eta_c \cdot \dot{\gamma} \cdot \frac{R}{\sigma} \tag{4.1}$$

In this equation η_c is the viscosity of the continuous medium, $\dot{\gamma}$ is the shear rate, R the droplet diameter and σ the surface tension between the two media. When the capillary number goes beyond a certain limit, Ca_c, shear forces overcome the surface tension of the droplet and break up takes place. This will occur for $Ca_c \approx 1$ [Nisisako et al., 2002]. An image of an oil flow with created water droplets can be seen in figure 4.5.

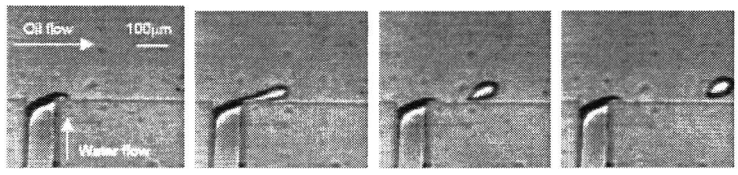

(a) t = 0.000 s (b) t = 0.002 s (c) t = 0.004 s (d) t = 0.006 s

Figure 4.5: Formation of a water droplet in a oil stream with the T-junction [Nisisako et al., 2002]

If the T-junction can be used to make droplets inside a micro channel, it is expected that it also can be used for a controllable input of cells inside the main channel of the cross slot. If a solution with a low density of cells is put inside the dispersion channel, like the water in figure 4.5, only a few cells at the same time will enter the main channel of the cross slot. After the cells are put inside the cross slot, the flow of the cells is stopped, so no new cells can enter the main channel of the cross slot. From the few cells that enter the cross slot, one cell can be positioned in the stagnation point. It is important that, when a cell is stretched inside the cross slot, other cells do not influence the deformation of that cell. With the T-junction it should be possible to control the input of the cells into the main channel of the cross slot. Because the minimum size of a milling tool is 100 μm, the T-junction is also made 100 μm. Because it is uncertain which dimension the main channel of the cross slot should have, three different sizes of cross slots will be made. For the controlled input of cells in the main channel of the cross slot the width of the T-junction can be the same as the main channel. The width of the different cross slot geometries are 100 μm, 200 μm and 500 μm. A picture of the design of the T-junction of the 500 μm cross slot can be seen in figure 4.6.

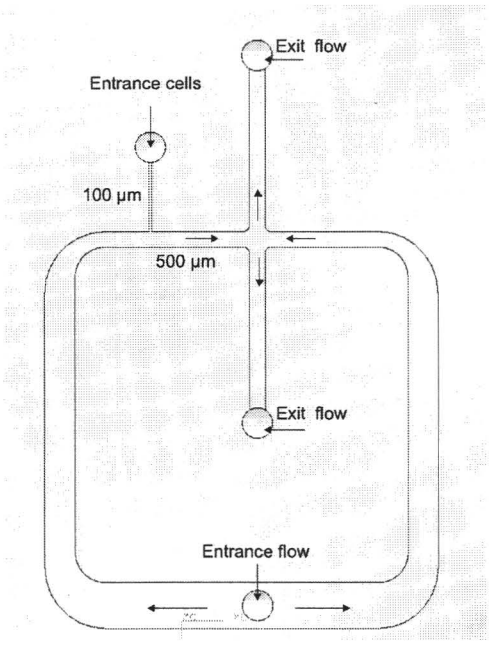

Figure 4.6: Design of the T-junction for the cross slot (500 μm)

The depth of the channel is made equal to the width of the channel. The depth of the T-junction is made equal to the depth of the main channel. The flow enters the cross slot in one entrance hole and is divided into two equal channels with a width and depth of 1 mm. This can be seen in figure 4.6. The length of both inlets of the cross slot is equal, resulting in an equal resistance between both channels. If both resistance are equal the flow will also be divided equal over the two channels of the cross slot. Both outlets of the cross slot are connected separately to micro valves that will control the flow. The T-junction has a separate inlet which will be connected to the syringe pump. With the pump and the T-junction the inlet of the cells inside the cross slot will be controlled. An image of the T-junction of the 500 μm cross slot chip is shown in figure 4.7.

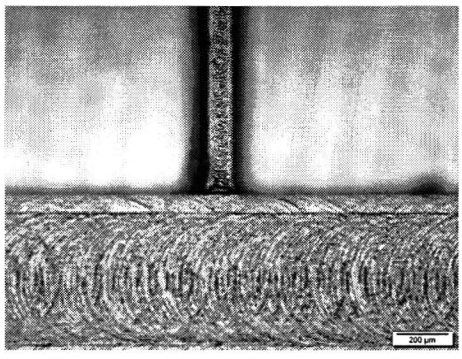

Figure 4.7: Image of the T-junction of cross slot (500 μm)

The length of the cross slot should be long enough to have a fully developed flow in the center of the cross slot. The development length ($L_{develop}$) of the flow inside a micro channel can be calculated with equation 4.2, following [Bruus, 2005]:

$$L_{develop} = (0.3125 + 0.011Re)D_h \tag{4.2}$$

D_h is the hydraulic diameter of the channel. For a rectangular micro channel the hydraulic diameter can be calculated with equation 4.3, following [Bruus, 2005]:

$$D_h = \frac{2WH}{W + H} \tag{4.3}$$

W and H are the width and height of the micro channel. If water is flowing with a speed of 1 mm/s through a channel with $W = 0.5$ mm and $H = 0.5$ mm, the Reynolds number will be $Re = 0.5$ and the development length $L_{develop}$ of the flow will be 0.16 mm. This means that the flow is fully developed and a distance of 0.16 mm from the inlet. The development length of micro channels is less than the hydraulic diameter of the channel. In macro systems the flow development length is usual larger than the hydraulic diameter. The T-junction is constructed 3 mm from the cross slot center, which should be enough to have a fully developed flow in the center of the cross slot. If the speed of the main flow in both channels of the cross slot (500 μm) is 1 mm/s, than the flow rate of the inlet of the cross slot needs to be equal to 30 μL/min.

4.2.1 Manufacturing technique

The cross slot geometry is made with mechanical speed milling with a milling tooling which has a diameter of 100 μm. The depth of the micro channel is the same as the width. This is a depth ratio of 1, which is no problem for mechanical mill cutting. The inlet and outlet of the cross slot chip are drilled. The cross slot chip is made out of poly-methyl-methacrylate (PMMA). PMMA is chosen because it has almost the same optical quality as glass. The refractive index of PMMA is 1.49 and of glass it is 1.52, which is nearly the same [Leijendeckers et al., 1998]. PMMA is optically transparent and the chemical resistance is also good. An image of the cross slot chip can be seen in figure 4.8(a). In figure 4.8(b), the cutting of the speed milling tool can be seen in the bottom of the channel. The fabricated cross slots had a main channel of 100 μm, 200 μm and 500 μm.

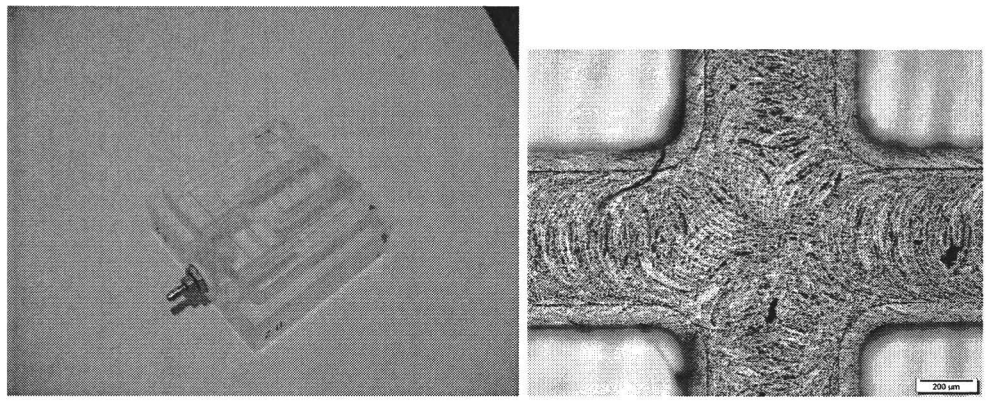

(a) Image of the chip (b) Microscopic image of the center

Figure 4.8: Cross slot chip $500\mu m$

The chip is put inside a scanning electron microscope (SEM) and images where taken, by L. Tufano at the Technical University of Eindhoven, to measure the surface roughness. The principle of an electron microscope is based on a microscope, but uses no light, but electrons to make an object visible. By applying voltage to a metal plate, the plate becomes positively-charged so that it attracts the electrons. Some of the electrons flow through a small hole that is inside the plate, creating a beam of electrons that is aimed to our object with the help of magnetic lenses. When the electrons hits the sample, the interaction is detected and transformed into an image. The scanning part of the electron microscope will send the beam of electrons across the surface of the sample. With the SEM the height differences of the surface can be measured. A SEM image of the middle part of the cross slot 200 μm can be seen in figure 4.9.

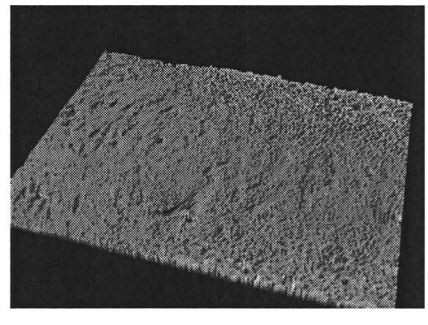

Figure 4.9: SEM image of the middle cross slot 200 μm

From the image in figure 4.9 a line is selected to measure the depth (z). The selected line and measurement can be seen in figure 4.10.

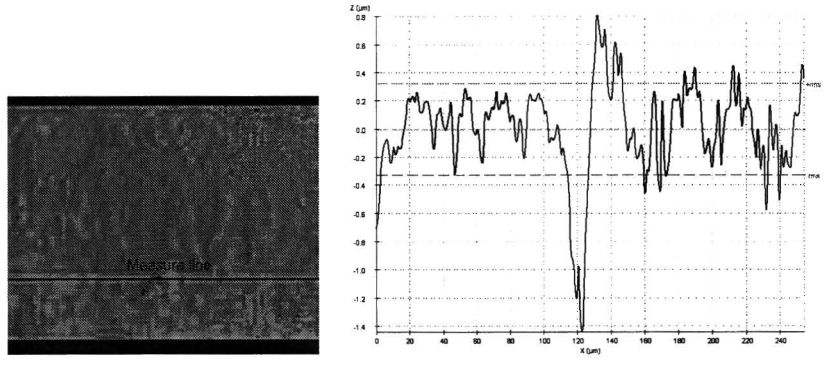

(a) Line selection

(b) Depth measurement

Figure 4.10: Roughness measurement with SEM of cross slot 200 μm

The total length of the measured surface was 254.64 μm. From the measurement in figure 4.10(b) it can be concluded that the dept of the surface variaties between 0.8 μm and -1.4 μm. The mean value of the depth (z) was -4.53 nm. The root mean square (rms) of the measurement was 0.32688 μm. The measured surface roughness inside the micro fluidic channel has an Ra value of 0.23404 μm.

The system is closed by a thin glass plate that is fixed to the cross slot chip by vacuum applied to specially designed channels. The thickness of the glass is 0.17 mm. This thickness is chosen, because the used lens of Zeiss is calibrated for a glass cover plate with a thickness of 0.17 mm. This means that the light path through the glass cover plate of 0.17 mm is corrected by the lens. The design and an image of the cross slot vacuum system can be seen in figure 4.11.

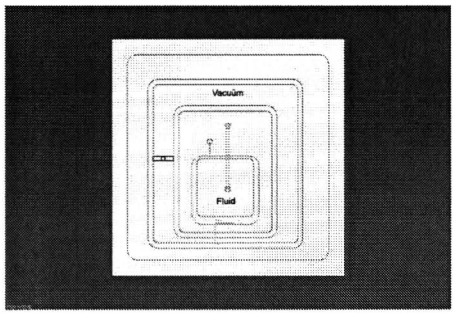

(a) Top view

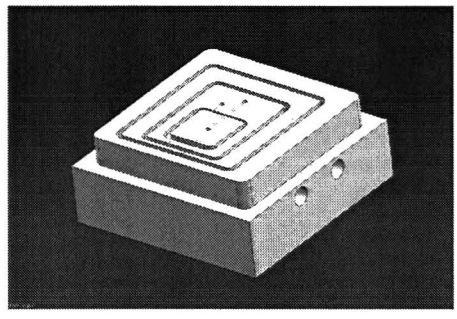

(b) Iso view

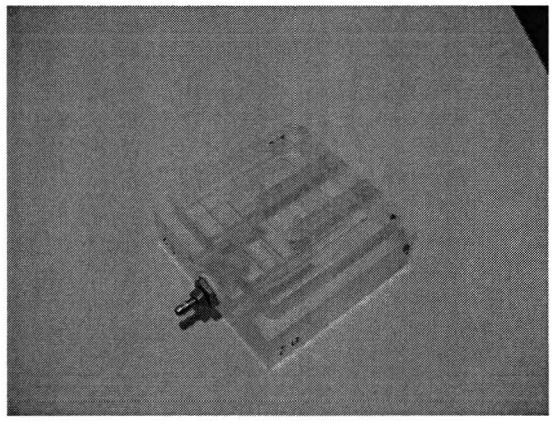

(c) Image 200 μm

Figure 4.11: Design of vacuum system cross slot 200 μm and 500 μm

The design of figure 4.11 did not close the micro fluidic channels. Possible the glass cover plate could bend over the surface, because it is not pulled down in the middle of the cross slot chip. Another design has been made to see if the problem is solved if the vacuum channels are constructed on both sides of the micro fluidic channel. The design and an image of the new vacuum system is shown in figure 4.12.

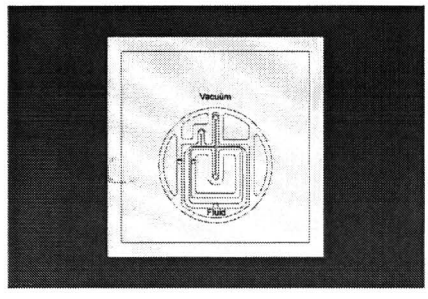

(a) Top view

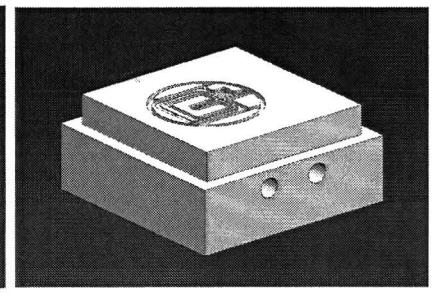

(b) Iso view

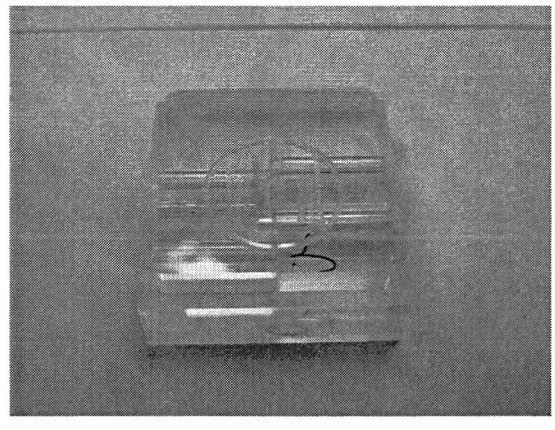

(c) Image

Figure 4.12: Design of vacuum system cross slot 100 μm

The cross slot chip is placed inside an aluminium holder that fits inside the microscope table. An image of the holder with the cross slot chip inside can be seen in figure 4.28(a).

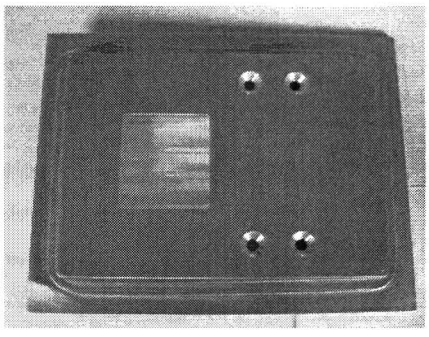

Figure 4.13: Cross slot chip inside holder

The total micro fluidic setup will be assembled on this holder, so the experimental setup can easily be assembled and transported to another microscope. The micro fluidic structures are point out to the bottom of the holder, because the experiments are planned on an inversion microscope where the lens is located on the bottom of the holder.

4.2.2 Characteristics vacuum system

Because the first vacuum system did not close the micro fluidic channel. Two thing has been improved compared to the first vacuum system. First the surface of the second vacuum system has been made very smooth, so the glass should close better on the PMMA surface. Also will the micro channel be enclosed by the vacuum system on both sides. This new cross slot design of 100 μm was also leaking fluid from the micro fluidic channel to the vacuum channel. Some images are taken from parts of the cross slot of 100 μm and shown in figure 4.14.

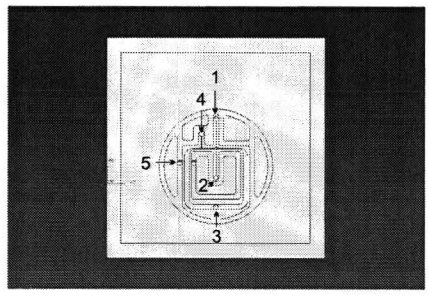

(a) Positions

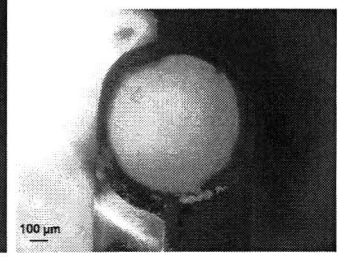

(b) 1

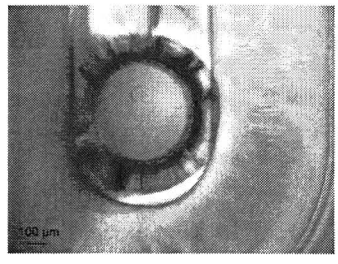

(c) 2

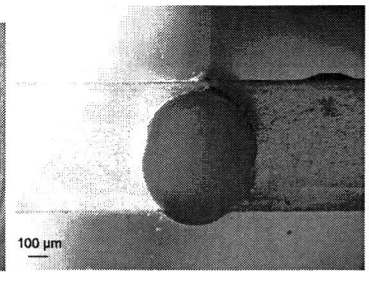

(d) 3

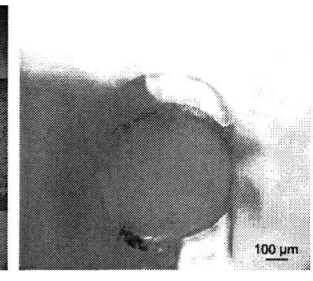

(e) 4

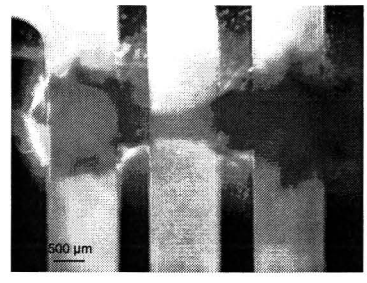

(f) 5

Figure 4.14: Images of cross slot 100 μm

In figure 4.14(b) and figure 4.14(e) the distance form the micro fluidic channel to the vacuum channel is very small. In figure 4.14(e) its even looks that in some parts there is no wall between the micro fluidic channel and the vacuum channel. This can explain why the fluid is sucked out of the micro fluidic channel to the vacuum channel.

There was also a cross slot of 200 μm fabricated, with a micro fluidic channel enclosed by a vacuum channel. Here the holes were drilled with more care. Images of the cross slot of 200 μm are shown in figure 4.15.

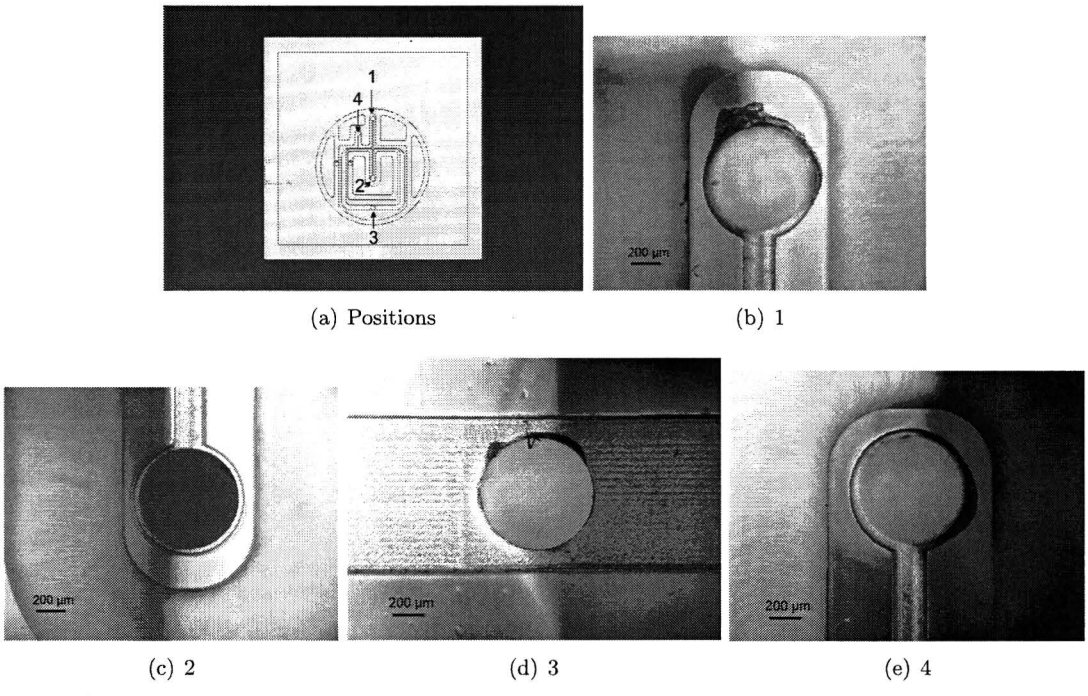

(a) Positions (b) 1

(c) 2 (d) 3 (e) 4

Figure 4.15: Images of cross slot 200 μm

In figure 4.15 it can be seen that there is always some PMMA between the micro fluidic channel and the vacuum channel. This channel should not leak fluid from the micro fluidic channel to the vacuum channel. During testing this chip was stil leaking, which can only mean that the glass cover plate is not properly closing on to the PMMA. Perhaps the material PMMA versus glass is to hard to enclose any small defect between the cover plate and the cross slot chip.

4.2.3 Characteristics flow

The flow inside the cross slot geometry can be measured using particle image velocimetry measurement. Particle image velocimetry (PIV) is a well established technique used to measure fluid velocity fields [Westerweel, 1997]. The technique works by measuring the displacement of small particles that follow the flow field. Images are made of the flow through the micro channels, by seeding small particles in the liquid flow. The particles are illuminated with a light source and images are taken at various times. The scattering pattern is recorded with a CCD camera. The basic principle of PIV is shown in figure 4.16.

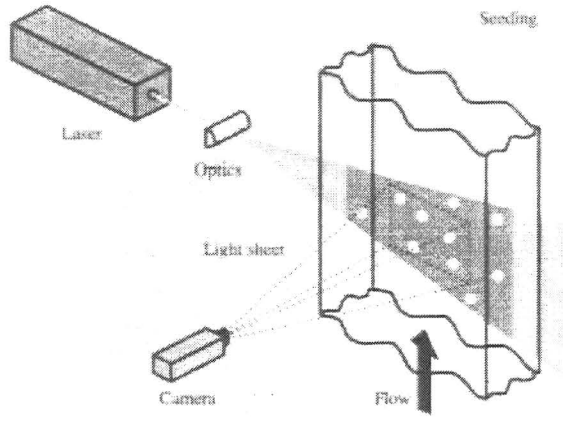

Figure 4.16: Basic principle of PIV

Velocity measurements are obtained by recording two images of the particles in the flow field separated by a specified time delay. The images are divided into smaller cells know as interrogation regions. The mean displacement of the particle images in each interrogation region is estimated by cross-correlation of each interrogation region between the two particle image fields. The local velocity is estimated for each interrogation region. The flow was measured for the cross slot of 500μm, with PMMA particles with a diameter of 10μm by W. Buysse and M. Thissen at the Technical University of Eindhoven. The size of the particles is depending on the size of the micro fluidic channel where the velocity is measurement. The flow rate was set to 20 μL/h adjusting by the syringe pump, which results in a velocity of 11 μm/s inside the channel and a Reynolds number of 0.0055. For 100 images the velocity field can be seen in figure 4.17.

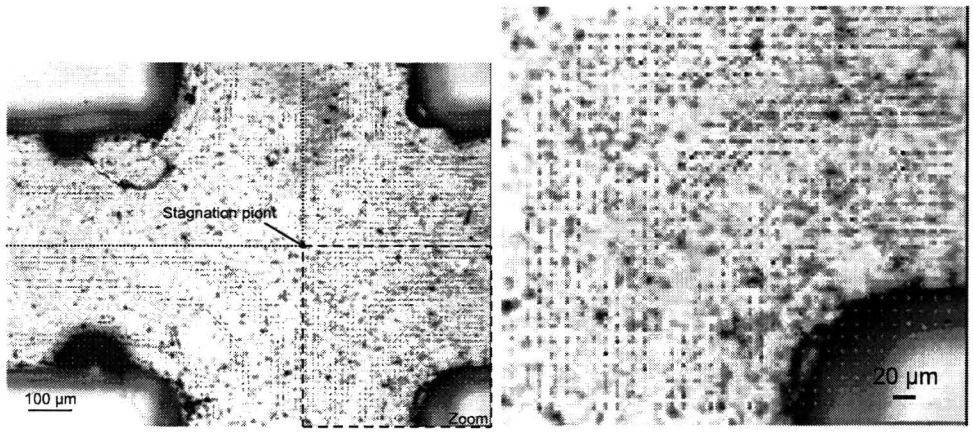

(a) Total cross slot (b) Magnified part of cross slot

Figure 4.17: PIV measurement of cross slot 500 μm

Figure 4.17 shows that the stagnation point of the flow is constant in time and the flow is divided equally between left and right. The length of the vector represent the velocity of the flow inside the channel, which seems to be around 11 μm/s. The particles of 10μm seems to have no influence on the flow inside the 500 μm width cross slot. Some vectors are missing because the density of the PMMA parts inside the fluid was to low to measure a velocity in every interrogation region.

4.3 Micro valve

To control the flow in the cross slot chip, use is made of micro valves as shown in figure 4.1(b). Recently, novel micro machining technologies have been applied not only to the fabrication of micro sensors but also to the fabrication of micro actuators. Very small devices controlling or sensing flow rates in the order of μl/min are called micro flow devices. Micro machining was applied to fabricate a gas flow sensor in the early age of this field. Micro valves and micro pumps are very promising devices of the micro machining products. Some micro pumps are commercially available but actively controlled micro valves are not commercially available. The supplier "Bartels mikrotechnik" has micro valves for flow control, but these valve only have the function of a passive dynamic check valve. These valves are designed as a three layer system built up by two plastic materials. See figure 4.18 for some examples of design variations. Bartels mikrotechnik is working on an active dynamic check valve, but the

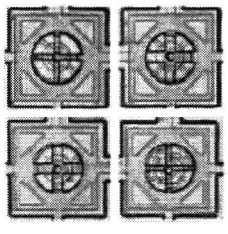

Figure 4.18: Examples of design variations

expectations are that the valve will be commercially available at spring 2006. Since no micro valve is commercial available, a design has to be made for the micro valve to control the flow inside the cross slot.

4.3.1 Principle of the micro valve

For the principle of the micro valve, several designs are investigated. In this section the final micro valve design is shown, the other ideas are described in appendix F. A sketch of the principle of the micro valve is shown in figure 4.19.

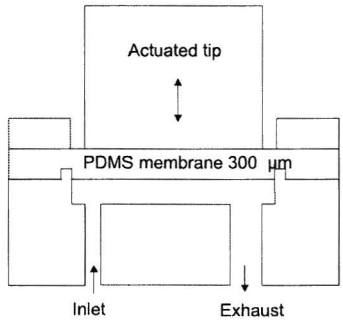

Figure 4.19: Micro valve schematic

The micro valve uses an actuated flexible membrane, which can be actuated to vary the hight of the gap between the inlet and the outlet of the micro valve. When the membrane is not actuated, the height of the gap is 200 μm. The distance between the inlet and outlet of the chamber inside micro valve is 2.5 mm. These values are determined in section §4.3.2. The holes of the inlet and outlet have a diameter of 0.5 mm and 1 mm. The outlet diameter is bigger compared to the inlet diameter to release the pressure build up by the closing valve. When the valve is closing the fluid will leave the valve through the biggest hole, because of its lower flow resistance than the small hole. Fluctuations of the flow inside the cross slot are not wanted, because the cell must be positioned at the stagnation point and this is why the outlet of the micro valve is bigger than the inlet. Fluctuation of the flow will leave the micro fluidic system through the valve outside the micro fluidic system.

The membrane needs to be high flexible and should be thin. The thickness of the membrane will be chosen 300 μm. The force needed to actuate the membrane can be calculated with equations 4.4, 4.5, 4.6, 4.7, 4.8, following [Leijendeckers et al., 1998]:

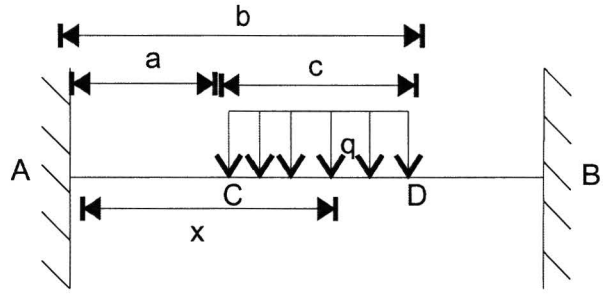

Figure 4.20: Dimensions calculation force on membrane

$$f = \frac{1}{6EI}\{R_a \cdot x^3 - 3M_a \cdot x^2 - \frac{Q(x-a)^4}{4c}\} \tag{4.4}$$

$$R_a = \frac{Q}{4l^2}(12d^2 - \frac{8d^3}{l} - \frac{2bc^2}{l} - \frac{c^3}{l} - c^2) \tag{4.5}$$

$$M_A = \frac{Q}{24l}(24\frac{d^3}{l} - 6\frac{bc^2}{l} - 3\frac{c^3}{l} + 4c^2 - 24d^2) \tag{4.6}$$

$$d = l - \frac{a}{2} - \frac{b}{2} \tag{4.7}$$

$$Q = q \cdot c \tag{4.8}$$

Where:

a, b, c: Dimensions of the membrane

A, B, C, D: Defined points of the membrane

q: Distribution load on membrane from actuator

x: Distance to the middle of the membrane

l: Total length of the membrane

E: Young's modulus material of the membrane

I: Moment of inertia which can be calculated with $\frac{b_{mem}*(h_{mem})^3}{12}$

The maximum bending f of the membrane can be calculated with equation 4.4. R_a is the force in point A created by the distributed force Q. M_A is the bending momentum at point A created by the distributed force Q. An important feature for the material of the membrane is a high flexibility. A commonly used material for membrane in micro systems is Poly-dimethyl-siloxane PDMS [Olsson, 1998, Yamahata et al., 2005]. PDMS is a commercial available clean room compatible type of silicon rubber. This material is frequently used for production of valve-less diffuser micro pumps because of its low elastic modulus and bending properties [Olsson, 1998]. The Young's modulus of PDMS is depending on the mass fraction of curing agent [Armani et al., 1999] and curing efficiency. An efficient curing of the PDMS results in more cross links and a higher Young's modulus. For the calculation the Young's modulus of PDMS is 1731 KPa, which has been measured by M. Yavuz at Phillips with a tensile test. If the force on the membrane increases form 0 N to 0.02 N, the deflection is shown in figure 4.21.

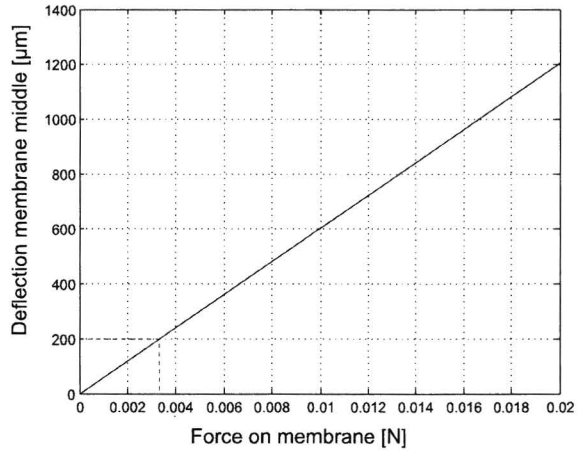

Figure 4.21: Membrane deflection against force on membrane

The displacement of the membrane must be at least 200 μm. With the given dimensions and material, the force needed to bend the PDMS membrane 200 μm is 0.0033 N, as can be seen in figure 4.21.

4.3.2 Fluid resistance

Important for the construction of the cross slot is that the flow should be controlled with the micro valve. If the micro valve is located 'far' from the cross slot, the fluid resistance of the control valve needs to be higher than the total fluid resistance of the cross slot channels. The fluid resistance depends on the geometry of the micro channel. The resistance of a circular channel can be calculated using equation 4.9, following [Beebe et al., 2002].

$$R = \frac{8\mu L}{\pi r^4} \tag{4.9}$$

Where:

μ : Fluid viscosity

L : Channel length

r : Channel radius

For a rectangular channel with a low aspect ration (i.e. $W \approx H$), the resistance can be found by equation 4.10, following [Beebe et al., 2002].

$$R = \frac{12\mu L}{WH^3}[1 - \frac{H}{W}(\frac{192}{\pi^5}\sum_{n=1,3,5}^{\infty}\frac{1}{n^5}\tanh(\frac{n\pi W}{2H}))]^{-1} \tag{4.10}$$

Where tanh is the hyperbolic tangent. The resistance of a rectangular micro channel with a high aspect ratio (i.e., $W \ll H$ or $H \ll W$) can be described by equation 4.11 [Beebe et al., 2002].

$$R = \frac{12\mu L}{WH^3} \tag{4.11}$$

The pressure drop over the channel can be calculated with the Hagen-Poiseuille law defined by equation 4.12.

$$\Delta p = Q \cdot R \tag{4.12}$$

Where:

Q: Flow rate of fluid

The resistance of the cross slot channels and the pressure drop over the cross slot system are calculated and can be seen in appendix G. From the calculations of possible geometric dimensions for the micro valve, some feasible dimensions were found. If the valve has a narrow part with a length of $L = 2.5$ mm, width of $W = 500$ μm and height of $H = 200$ μm, the resistance of the micro valve can be calculated with equation 4.10. The resistance of the micro valve is $R_{microvalve} = 8.0 \cdot 10^9$ Pa·s·m^{-3}, which is higher than the resistance of the cross slot $R_{crossslot} = 3.8 \cdot 10^9$ Pa·s·m^{-3}. This meas that the resistance of the micro valve is dominant over the micro fluidic system and should control the flow inside the cross slot. If the height of the channel decreases, the resistance increases and less fluid will flow through the valve. If the height of the micro valve is controlled, the flow can be controlled. Since the height of the micro valve is assumed to be 200 μm, the maximum displacement is 200 μm. With a height control of 200 μm the valve can even be closed completely. The flow rate inside the micro valve will be the same as half the flow rate of the inlet of the cross slot at a flow speed of 1 mm/s inside the cross slot of 500 μm (Re=0.5). The flow rate in each channel of the cross slot will be 15 μL/min. This results in a pressure dorp over the micro valve, at a height of H = 200 μm, of 2 Pa. This calculation can be found in appendix G. An actuator has to be found for the displacement of the membrane of the micro valve.

4.3.3 Fluid resistance, fluid flow of micro valve during actuation

If the micro valve is decreasing the gap of 200 μm, the hydraulic resistance of the micro valve will also change. The hydraulic resistance depends on the height of the gap of the micro valve. If it is assumed that the pressure over the micro valve will be the same as at a height of 200 μm, the hydraulic resistance increases and the velocity of the fluid inside the micro channel will decrease. The hydraulic resistance during control can be estimated with equations 4.11 and 4.12. The pressure drop over the micro valve, at a height of the gap of 200 μm, is $\Delta P_{microvalve} = 2$ Pa. If the height of the gap is decreased from 200 μm to 50μm and the pressure drop over the valve is constant, the resistance increases from $8.0 \cdot 10^9$ Pa·s·m^{-3} to $4.8 \cdot 10^{11}$ Pa·s·m^{-3} like shown in figure 4.22, according equations 4.10 and 4.12.

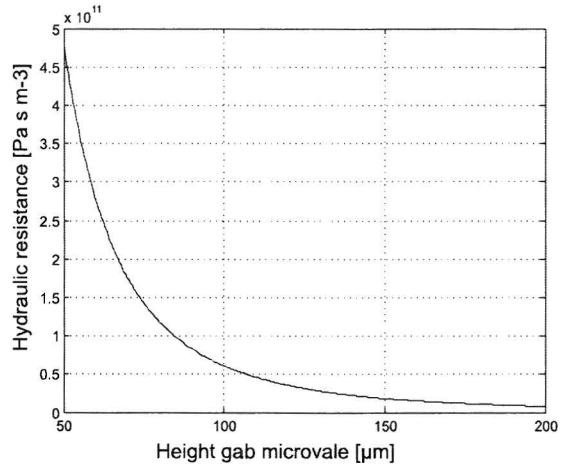

Figure 4.22: Valve hydraulic resistance against height of the gap of the micro valve

If the pressure drop is constant ($\Delta P_{microvalve} = 2Pa$), the flow rate through the valve will decreases from 15 μL/min to 0.25 μL/min, like shown in figure 4.23, according equation 4.12:

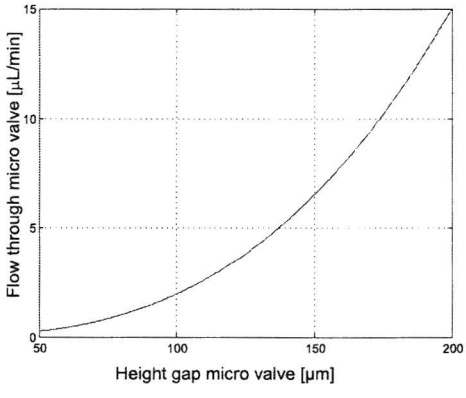

Figure 4.23: Valve flow against height of the gap of the micro valve

4.3.4 Actuation of the micro valve

Some important features for the selection of the actuator are:

- Displacement
- Force
- Speed
- Accuracy

The displacement of the actuator should be 200 μm. The speed of the actuator is chosen to be > 50 Hz. There are several techniques available to actuate in a micro scale environment. Micro fluidic valveless pumps are an example of micro actuated systems. Micro fluidic valveless pumps are developed to be integrated into micro fluidic systems. The kind of actuators used for micro fluidic valveless pumps are:

- Voice coil actuator
- Piezoelectric actuator
- Pneumatic actuation
- Hydraulic actuation

From the literature the frequency of a pneumatic or hydraulic actuation for a valve is < 5 Hz [Shoji and Esashi, 1994]. A piezoelectric actuator is fast but only has a maximum displacement of 10 μm [Shoji and Esashi, 1994]. The solution for a relatively long and fast stroke, as well as a high force is a voice coil actuator [Shoji and Esashi, 1994]. The other benefit of the voice coil actuator is the linear relation between the applied force with the applied current on the voice coil actuator.

The force needed for the displacement of 200 μm of the PDMS membrane is calculated with equation 4.4, 4.5, 4.6, 4.7, 4.8 and is 0.0033 N as mentioned before. The pressure needed to close the membrane is depending on the internal pressure under the membrane. The force needed to close the micro valve can be calculated with equation 4.13

$$F = P_{insidevalve} \cdot A_{pres} \tag{4.13}$$

Where:

A_{pres} : pressure area tip of actuator

$P_{insidevalve}$: pressure inside the micro valve

The circular area of the actuator has a diameter of 5 mm, which corresponds to an area of 4.9 mm ^{2}. The pressure inside the micro valve is almost the same as the pressure on the exit of the micro valve. The pressure drops over the micro channels are in the order of some Pa. The micro valve is the last component at located at the end of the micro fluidic system. Therefor the pressure inside the micro valve is almost the same as the pressure outside the system 10^5 Pa, see figure 4.24.

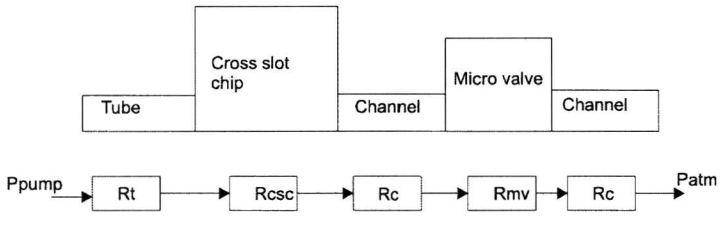

Figure 4.24: Schematic view of hydraulic resistance cross slot system

The force needed to close the valve will be 0.49 N. The total force needed to actuate the valve will be 0.49 N + 0.0033 N = 0.4933 N. So the actuator should be able to apply a force of 0.4933 N continuously. Some calculations are made to choose the right voice coil actuator. The force induced by the actuator is increased to 1 N, which leads to a certain safety factor for the calculation. The moving mass of the actuator is the mass of the coil, screws, indenting nipple and the lineair guiding of the actuator. The total moving mass of the actuator and components is estimated on 600 gram. The actuator should translate 200 μm back and forward. This frequency is chosen to be 50 Hertz. From calculations found in appendix H, the total peak force needed for this load and frequency will be 2.2 N, following [Kimco, 2005]. The lineair voice coil actuator that satisfy the requirements is the linear voice coil actuator LA08-10-000A of Bei Kimco. Specifications of this actuator can also be found in appendix H.

Because of a mistake in the first calculations of the pressure inside the micro channels, another actuator was used for the micro valve. The A12-17-000A of Bei Kimco. Specifications can be found in appendix H. This choice was based on a required force of 10 N. This leaded to a piek force of 11.2 N. This is a much stronger actuator than actually needed. The calculations for this actuator can be seen in appendix H. An image of the actuator A12-17-000A for the micro valve can be seen in figure 4.25.

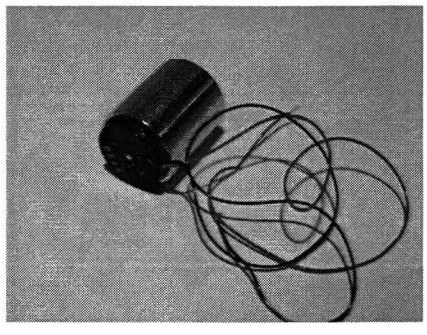

Figure 4.25: Actuator A12-17-000A of Bei Kimco

4.3.5 Manufacturing techniques

The PDMS membrane is made with a mold. The mold consist of a metal plate with a thickness of 300 μm in which square openings of 31 mm times 31 mm were cut by a laser. First the PDMS with $\frac{1}{10}$ mass fraction of curing agent. The mold is filled with the uncured PDMS. When the mask was filled, the air inside the PDMS was removed with vacuum and compressed afterwards. After curing of 24 hours the membrane was ready. See figure 4.26(a) for a picture of the mold with the PDMS membranes inside.

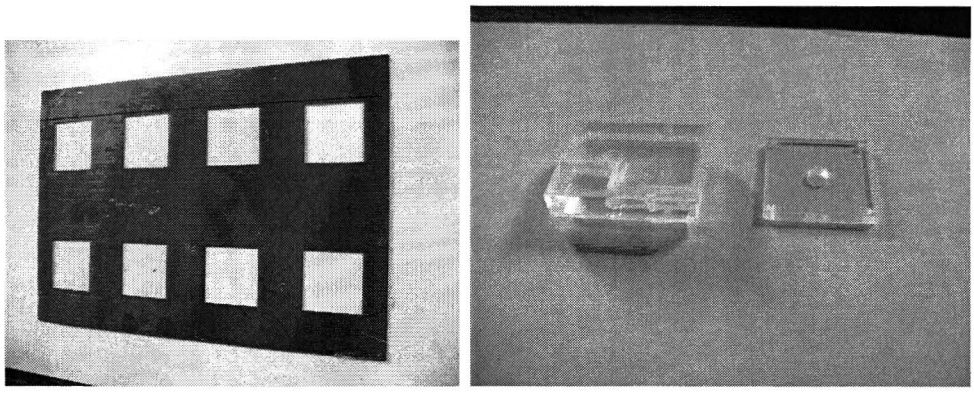

(a) Mold with PDMS membrane (b) Base micro valve with top

Figure 4.26: Mold for production membrane and the base of the micro valve

The chamber of the micro valve is made out of PMMA and can be seen in figure 4.26(b). On top of the base of the micro valve a plate with a hole of PMMA is screwed with the flexible PDMS membrane between the base and the top. The top can also be seen in figure 4.26(b). The micro valve is connected to the cross slot chip with messing nipples and placed inside the holder, which can be seen in figure 4.27(a).

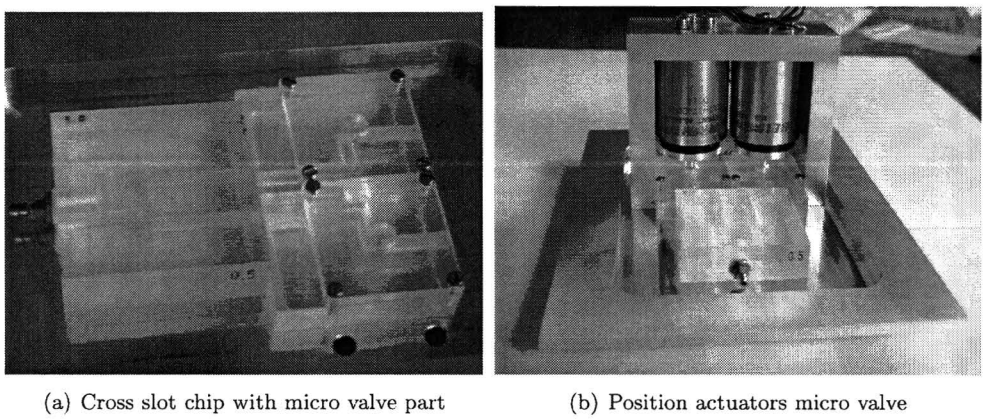

(a) Cross slot chip with micro valve part (b) Position actuators micro valve

Figure 4.27: Connection micro valves to chip and position actuators of micro valves

On top of this membrane a voice coil actuator is positioned with an aluminium bridge, see figure 4.27(b). At the end of the actuator a tip is mounted that can indented the flexible membrane. The tip and actuator assembly of the tip can be seen in figure 4.28(a) and 4.28(b).

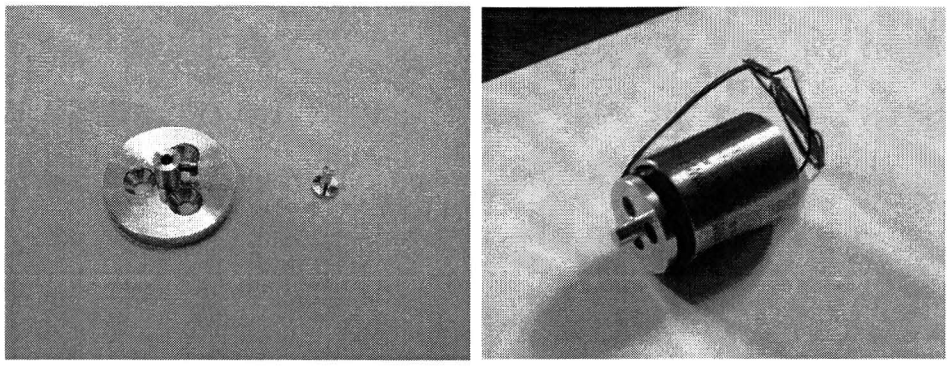

(a) Tip (b) Actuator with tip

Figure 4.28: Tip of actuator and assembly

Inside the tip of the actuator, a smaller tip can be fixate with a small screw. This small aluminium tip is attached to the PDMS membrane with glue. A test has been done, with the expertise of C. van der Vleuten at Philips, to determine how to connect the aluminium tip to the PDMS membrane. For this test, several ultra violet hardening glues, locktide, silicon based glues and even tape were used. All those kinds of glues did not connect the aluminium tip to the PDMS, except one. The silicone based glue did. For the attachment of the Aluminium tip a transparant silicone glue was used. The nippel is connected to the membrane so that not only the membrane can be pushed but also pull on the membrane. Beter control of the membrane should be possible if the tip of the actuator is connected to the membrane, in stead of indenting only on the membrane. An image of the tip of the membrane and assembly on the membrane can be seen in figure 4.29(a) and 4.29(b).

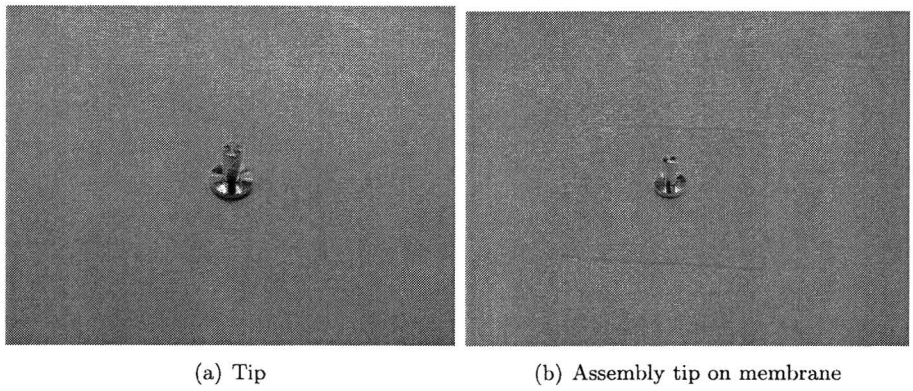

(a) Tip (b) Assembly tip on membrane

Figure 4.29: Tip and assembly of PDMS membrane

4.3.6 Software to control micro valve

The micro valves should be controlled real time the position a cell in the stagnation point of the cross slot. To control the micro valves real time, the position of the cell in the cross slot will be used as feedback for the control system. The imaging of the position of the cross slot will be with a digital camera, who has a speed of 60 fps. The control system will be build with Matlab Simulink. Lunix will be used in stead of Microsoft, because with Lunix faster frequency can be reached as with Microsoft. The Matlab Simulink has been made by R. van Aalst and B. van Daal. The model first reads the images from the camera through the computer. These images are used as input for the Matlab Simulink model. From the images the background is subtracted. By filtering the image with a certain threshold, the outer boundary of the cell can be found. With a boundary trace the boundary are found and the center mass of the cell can be determined. This information is used to position the center of mass of the cell on the stagnation point of the cross slot flow. A picture of the program for a cell flowing through a contraction can be seen in figure 4.30.

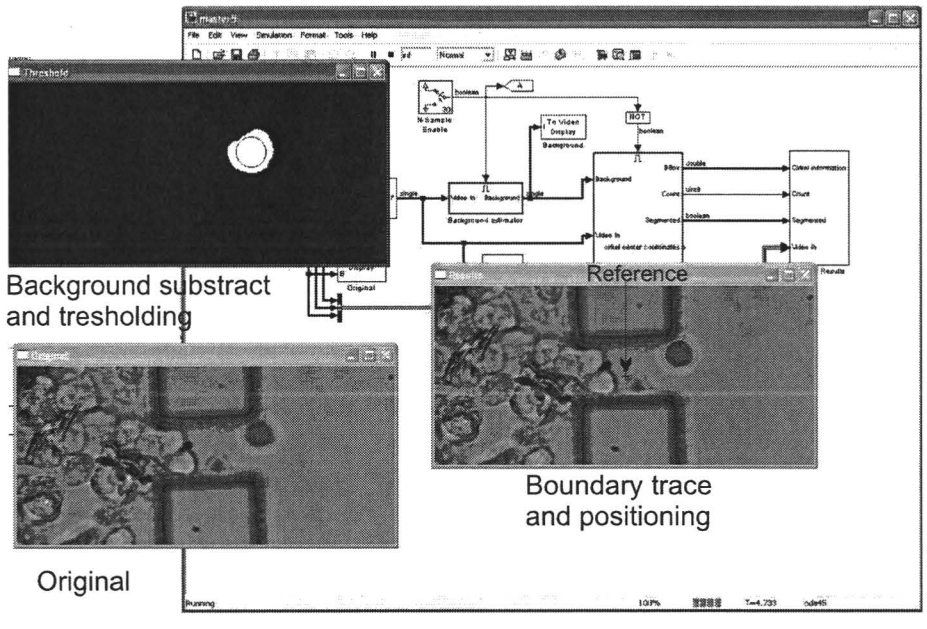

Figure 4.30: Picture of the Matlab Simulink model

This program can easily reach 60 fps, which assumed to be enough to control the flow in real time. The Matlab Simulink program controls the TU/e-dacs, which is connected to the computer. On the TU/e-dacs two amplifiers are connected to increase the voltage from the TU/e-dacs to the level needed for the micro valves. An image of the TU/e-dacs with the amplifier connected to the micro valves can be seen in figure 4.31.

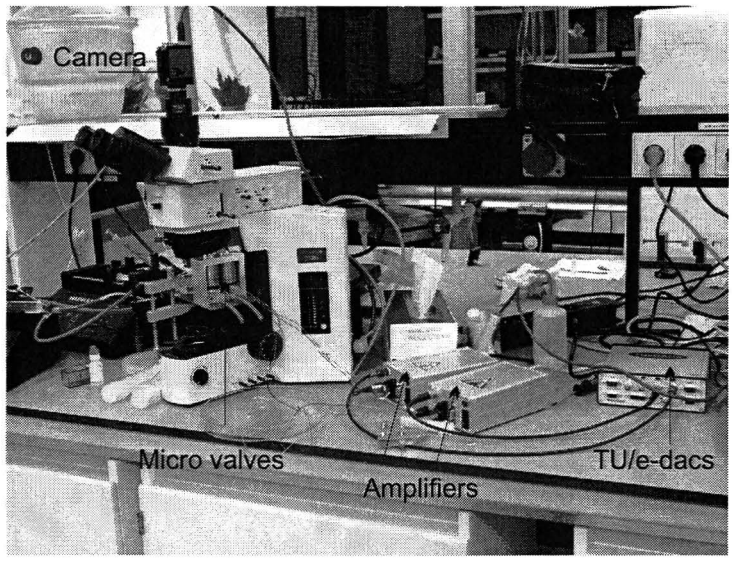

Figure 4.31: Image of TU/e-dacs connected to the micro valves

4.4 The optical system

The type of microscope used for the experiments is a Zeiss fluorescent microscope. Inside the Zeiss fluorescent microscope different lenses are used. For the experiments 20x 0.5 NA fluor phi 1 lens (Zeiss) and 40x 0.6 NA fluor phi 1 lens (Zeiss) are used. These lenses are specifically designed to look at biological cells. The lenses correct the abberation of the light from the spherical cells. The light shines from the top to the bottom, through an ocular phi 1. When it shines through the holder and contraction structure the image is captured by a camera attached to the microscope. For the image recording a Kodak motion corder analyzer SR series is used. This is a high speed camera which has a maximum image field of 512x480 pixels and a maximum speed of 1000 fps. The image size decreases if the speed of the camera increases. This is caused by the memory of the motion analyzer. If a speed of 500 fps is used the maximum image field is 512 x 240 pixels. The amount of images that can be recorded at this speed and image size is 1092, which means that the maximum measurement time is around 2 seconds. After the measurement, the recorded images must be transported to the hard disk of the computer. The time of exposure can be minimized to $\frac{1}{20000}$ sec.

If cell deformation will be measured with a microscope, it is important that the resolution of the optical system is sufficient to detect the deformation of the cell. Since cells have a diameter of around 10 μm, the cells can be observed with every wavelength of visible light. If particles must be observed that have a diameter smaller than the wave length of the observing light, fluorescent techniques can be used. Fluorescent techniques can also be used to enhance the contrast between the background and the cell for more accurate measurement of the cell size. The theoretical amount of detail and sharpness of an image obtained through a microscope is manly dependent on two factors:

- The absolute theoretical limit imposed by the wave length of the light being used for illumination
- The Numerical Aperture (NA) of the object lens which is a lens specification which denotes the collection efficiency of a lens

To explain the influence of NA on the maximum resolvable resolution, the concept of the diffraction limit need to be introduced. The definition of the NA can be found in appendix I. Besides these factors also the resolution of the image recorder is important for the measurement of the cell diameter and the deformation of the cell. The cells can be labeled with a fluorescent marker Cell Tracker Green. This marker emits light with a wavelength λ of 517 nm [Cambrex, 2005]. Further information of the fluorescent marker can be found in section §5.1.1.

4.4.1 Diffraction

When discussing diffraction, light is best considered as a wave phenomenon. Diffraction plays a major role in maximum image detail obtainable through a microscope. When a light of a coherent source is projected on a screen through a pinhole, a so called Airy disk diffraction pattern (figure 4.32) will appear on the screen instead of a point of light. The airy disk pattern is an effect of diffraction or scattering of light which occurs throughout the light path before it reaches the screen, following [Frank et al., 1993]:

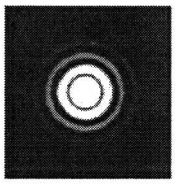

Figure 4.32: Airy disk pattern on screen [Lee, 2005]

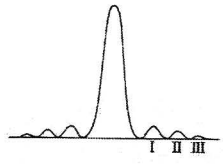

Figure 4.33: Gaussian light intensity distribution function plotted against radius r [Lee, 2005]

The circular Airy pattern is often referred to as the Airy disk and is defined by the region enclosed by the first minimum of the Airy pattern. The maximum is called the zeroth order maximum surrounding by concentric light circles (1^{st},2^{nd},3^{rd}, etc order maxima), with decreasing light intensity. (see figure 4.33). The more orders the lens can collect, the higher the intensity of the light becomes and better defined the Airy disk will become and higher the resolution become.

The diameter of the point spread function d_s of a circular aperture (pinhole) is defined as the diameter of the first dark ring in the image plane and is described by the equation 4.14, following [Frank et al., 1993, Meinhart and Wereley, 2003]:

$$d_s = 2.44\frac{s_i\lambda}{D_a} \tag{4.14}$$

Where:

s_i : Distance image plane form objective lens

λ : Wavelength of light

D_a : Diameter of the circular aperture

For a schematic view of the d_s see figure 4.34.

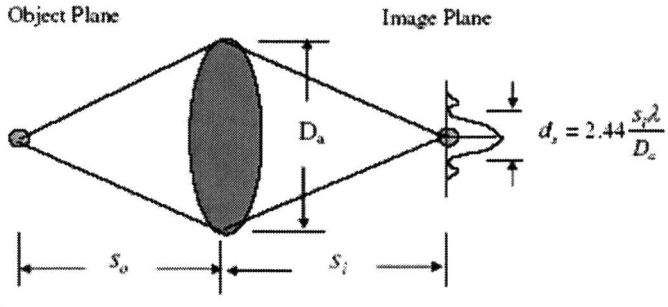

Figure 4.34: Schematic of the point spread function through a circular aperture [Meinhart and Wereley, 2003]

Two cases can be considered, namely using a single lens or an infinite corrected lens. The diffraction limited spot size through a single thin lens is described by equation 4.15.

$$d_{sp} = 2.44(M+1)\lambda\frac{f_o}{D_a} \tag{4.15}$$

The diffraction limited spot size of infinity corrected optics is described by equation 4.16, following [Meinhart and Wereley, 2003, Wereley et al., 1999, 1998]:

$$d_{s\infty} = 2.44M\lambda\frac{f_o}{D_a} \tag{4.16}$$

Where:

f_o : Focal length lens

D_a : Diameter of the circular aperture

The d_{sp} or $d_{s\infty}$ determines the smallest measured detail of a lens system and thus the maximum resolvable details. The determination of the equations 4.15 and 4.16 can be found in appendix J. Both expressions of the diffraction limited spot size d_{sp} and $d_{s\infty}$, the last term $\frac{f_o}{D_a}$ represent the f-number of the used lens system, which used to specify the speed of a single

photographic type lens [Lee, 2005]. The diffraction limited spot size determines the resolution of the optical system. From equation 4.15 and 4.16 its is clear if the resolution needs to be increased, the magnification (M), wave length of light (λ) and the focal length to aperture ratio ($\frac{f_o}{d_a}$) (or f-number) should be reduced. In table 4.1 lists values of f-number and diffraction spot sizes for various microscope lenses. (air immersion $n = 1.000$, water immersion $n = 1.330$, oil immersion $n = 1.515$)

Table 4.1: Characteristic values of f-number and diffraction spot size for various microscope lenses [Meinhart and Wereley, 2003]

M	n	NA	f_p	f_o	$d_{sp}(\mu m)$	$d_{s\infty}(\mu m)$
10	1.000	0.25	2.00	1.90	33.3	29.3
20	1.000	0.50	1.00	0.87	31.8	26.2
40	1.000	0.60	0.83	0.67	51.7	40.3
40	1.000	0.75	0.67	0.44	41.4	26.7
60	1.330	1.00	0.50	0.44	46.1	39.8
60	1,330	1.25	0.42	0.24	38.4	21.7
60	1.515	1.40	0.36	0.21	33.0	18.8

The $f - number$ or focal length to aperture ratio can be calculated with equation 4.17.

$$f - number = \frac{f_o}{D_a} \tag{4.17}$$

For the special case where the medium surrounding the lens is air ($n = 1$) and the objective is large compared to the aperture of the lens, NA can be approximately related to the $f - number$ by equation 4.18, following [Meinhard et al., 1998]:

$$f - number = \frac{1}{NA} \tag{4.18}$$

The actual recorded image of the cell, on the CCD camera, is the convolution of the diffraction limited point spread function for infinity corrected lens ($d_{s\infty}$) with the geometric particle image (Mdp) [Wereley et al., 1999]. Approximating $d_{s\infty}$ and Mdp as Gaussians, the effective cell diameter (d_e) can be expressed by equation 4.19, following [Meinhard et al., 1998]:

$$d_e = [M^2 d_p^2 + d_{s\infty}^2]^{\frac{1}{2}} \tag{4.19}$$

Where:

d_p : Diameter of the cell

For the setup an objective of Zeiss (LD Plan-Neofluar) is used with a magnification of 40 and a NA of 0.6 and for λ is taken the average wave length of 517 nm. The $d_{s\infty}$ becomes 84.1 μm, following equation 4.16. The effective cell diameter (d_e) of the cell on the CCD camera will be 408,7 μm, following equation 4.19

4.4.2 Dept of focus

The micro fluidic cell stretcher only takes a two-dimensional image of the flow. But the flow is 3-dimensional. Also cells that are out of focus are recording by the CCD camera. Depth of focus is the distance over the optical axis around the object plane where the resulting image will still be considered sharp. The depth of focus results in a depth of field where the image is recorded.

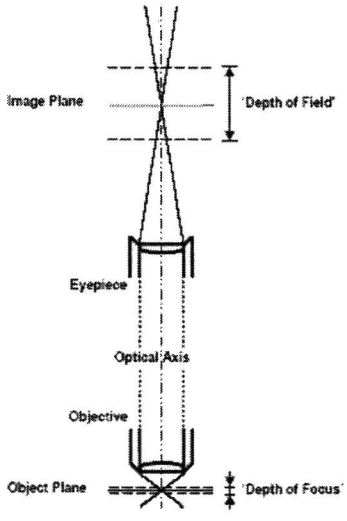

Figure 4.35: Overview of definitions of depth of focus and depth of field [Lee, 2005]

A cell that is out of focus appears blurred and larger. The greater the distance from the object plane the larger and more blurred the cell will appear. The size of the recorded cell is strongly dependent on magnification and NA, because the growth in image size of out of plane cells. This can be seen figure 4.36.

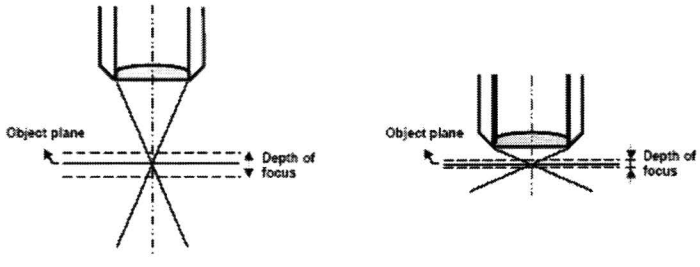

Figure 4.36: Overview of depth of focus (increasing NA left to right) [Lee, 2005]

The depth of focus can be calculated with equation 4.20, following [Frank et al., 1993]:

$$z_{focus} = \frac{\lambda}{2 \cdot (NA)^2} \tag{4.20}$$

In practice the dept of focus is much larger, because of the diffraction of the light (Airy disk). Depth of focus varies with NA and magnification. In practice high NA have high magnification and could have a lager depth of focus than low NA with low magnifications. In practice the total depth of field can be calculated with equation 4.21, following [Lee, 2005, Wereley et al., 1999].

$$z_{field} = \frac{\lambda \cdot n}{NA^2} + \frac{n}{M \cdot NA} \cdot e \tag{4.21}$$

Where:

e : The smallest resolvable distance of a detector that is placed in the image plane of a microscope objective (pixel size)

n : The refraction index of the immersion medium between the micro fluidic device and the objective lens

For the setup an objective of Zeiss (LD Plan-Neofluar) is used with a magnification of 40 and a NA of 0.6 and for λ is taken the average wave length of 517 nm. The immersion medium is air with a fraction index of 1.000. The camera has a 1/2 inch CCD chip inside. The maximum resolution of the image field of the camera is 512x480. The pixel size of the recorded images is 24.8 μm. The dept of focus z_{focus} will be 0.718 μm , following equation 4.20. The depth of field z_{field} will be 2.5 μm, following equation 4.21. So the location of the measuring plane is known within 2.5 μm.

4.4.3 Measurable deformation of the cell

The measurable deformation of the cell depends strongly on the pixel size of the recording images. The pixel size of the recorded images is 24.8 μm and the magnification of the lens is 40. The deformation can be measured with a step size of $\frac{24.8\mu m}{40} = 0.62$ μm. Every deformation below 0.62 μm can not be detected directly with the optical system described in this section. Figure 4.37 shows the influence of the pixel size on the measurable Taylor deformation rate of the cell.

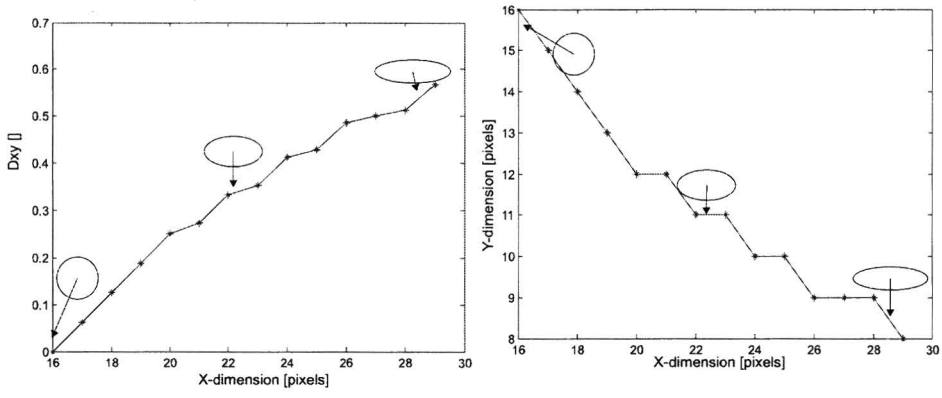

(a) D_{xy} against shape cell

(b) X-dimension against Y-dimension, area is constant

Figure 4.37: D_{xy} compared to the shape of the cell (x,y-dimension)

There are numerical ways to increase the detection on sub pixel level, following [Halir and Flusser, 1998]. This could increase the detection accuracy of the deformation. Also a camera with a higher resolution could increase the detection accuracy. An other possible solution will be to increase the magnification, so the recorded field a image is decreased and the deformation can be recorded in more detail. All images are stored on the computer, which is connected to the camera. If the resolution of the camera will be doubled, and the image field is the same as before, the pixel size will decrease to 0.31 μm, which will result in a more accurate measurement of the Taylor deformation rate, shown the figure 4.38

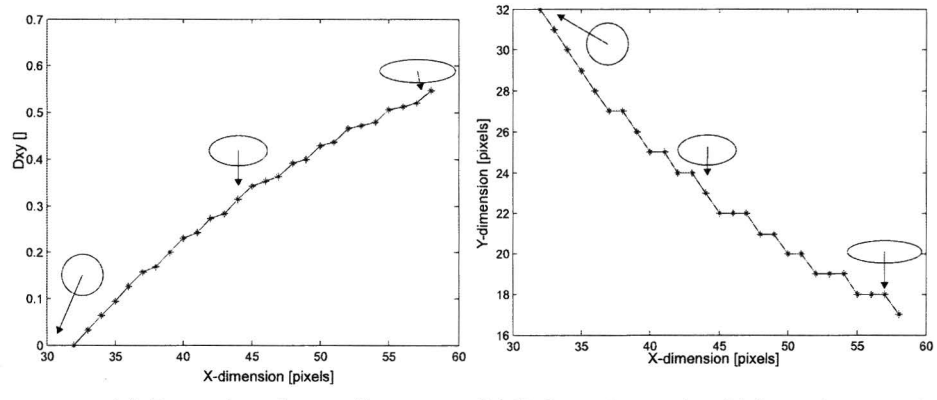

(a) D_{xy} against shape cell

(b) X-dimension against Y-dimension, area is constant

Figure 4.38: D_{xy} compared to the shape of the cell (x,y-dimension) for increased resolution

4.4.4 Single cell deformation analysis

For measuring the size of the cell a program is made with Matlab. Matlab can determine the cell diameter by counting the pixels of the image of the cell. If the actual size of one pixel is known, the real diameter of the cell can be determined by multiplying the diameter value in pixels with the real dimensions of one pixel. It the Taylor deformation rate needs to be determent, the actual size is not needed. The Taylor deformation rate can be determined from the pixel size of the cell in the x and y dimension. The program will be explained in figure 4.39 with an example of a C2C12 through a contraction of 1:16, where the smallest width of the contraction is 25 μm. A C2C12 is a muscle cell of a mice. The processing steps of the Matlab program are:

1. Figure 4.39(a): Load the image of the cell you want to measure.
2. Figure 4.39(b): Load the background of the image, without the cell you want to measure.
3. Figure 4.39(c): Subtract the background from the image with the cell you want to measure.
4. Figure 4.39(d): Select the area of interest of the image.
5. Figure 4.39(e): Enhance the contrast of the image.
6. Figure 4.39(f): Convert selected area to a binary image.
7. Figure 4.39(g): Fill the holes inside the binary image.
8. Figure 4.39(h): Find the boundary of the cell and fit an ellipse to the boundary that is found and return the Taylor deformation parameter D_{xy}.

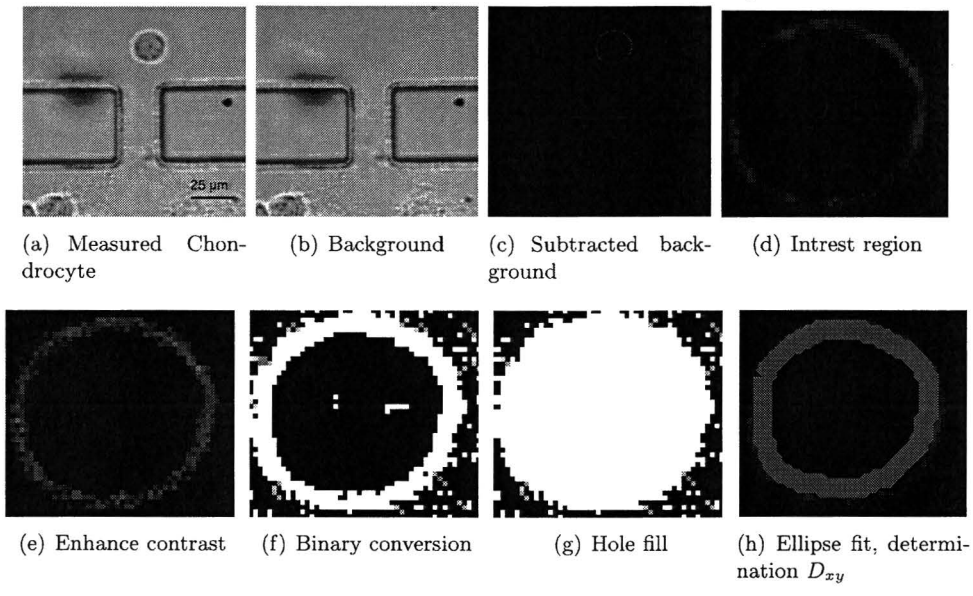

(a) Measured Chondrocyte (b) Background (c) Subtracted background (d) Intrest region

(e) Enhance contrast (f) Binary conversion (g) Hole fill (h) Ellipse fit, determination D_{xy}

Figure 4.39: Image proces Matlab for measuring cell Taylor deformation rate

In this example $D_{xy} = 0.0414$, which indicates that the chondrocyte is deformed a little due the flow of the contraction, before it enters the narrow part. If the cell was perfectly circular the Taylor deformation rate was ≈ 0). The ellipse fitting on the boundary of the cell is done by a numerically stable direct least squares fitting, following [Halir and Flusser, 1998]. This program can fit an ellipse from the data points of the boundary found with the Matlab program. Important for the Matlab program is that the contrast between the background and the cell is high otherwise the boundary of the cell can not be found with Matlab. The ellipse fit determined the Taylor deformation rate on sub pixel level, with an accuracy of 0.0001. The Matlab program used of image processing of the cell can be found in appendix K.

4.5 Flow generation

The flow will be generated with a syringe pump. Inside different syringes can be placed. The pump used is an infusion pump of Harvard apparatus type PHD 2000, see figure 4.40(a). The minimum flow rate, following the specifications, is 0.0001 μl/hr and the maximum flow rate is 220.82 ml/min, but this is strongly depended from the syringe used inside the pump. The maximum allowed syringe size is 140 ml and minimum size is 0.5 μl. The accuracy of the pump is $\pm$ 0.35 % with a reproducibility of 0.05 %. The push travel rate has a minimum of 0.18 μm/min and a maximum of 190.676 mm/min.

The precision of the pump is depending on the syringe used to create the flow. For example, if inside the infusion pump a glass syringe, model 1705 from Hamilton is used. The syringe is a gastight manual injection syringe with a volume ($volume_s$) of 50 μl. The stroke of the syringe($stroke_s$) is 50.8 mm. An image can be seen in figure 4.40(b). With a minimum travel rate ($v_{p_{min}}$) of 0.18 μm/min the minimum flow from the pump can be calculated with equation 4.22.

$$Q_{p_{min}} = \frac{volume_s}{stroke_s} * v_{p_{min}} \tag{4.22}$$

The minimum flow from the pump is $Q_{p_{min}} = 0.00018$ μl/min, which is between the minimum and the maximum flow rate of the pump defined by the specifications delivered from the supplier. This is the step of the flow induced by the minimum step size of the actuator of the pump. But if an ordinary laboratory syringe is used with a volume of 10 ml and a stroke of 50 mm, the minimum flow form the pump is 0.036 μl/min.

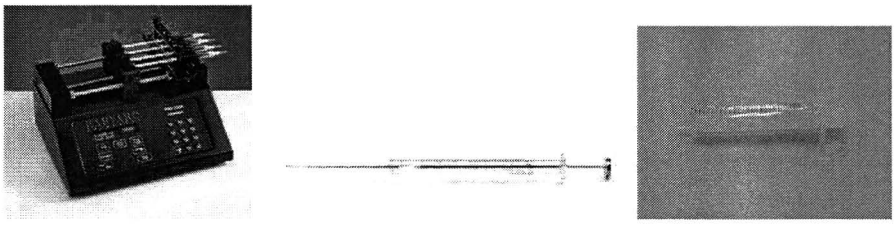

(a) Harvard apparatus infusion pump PHD 2000 (b) Hamilton GASTHIGHT manual injection GC syringe 50 μl (c) Laboratory syringe 10 ml

Figure 4.40: Pump and syringe

The pump is connected with tubes that are made of silicon rubber. The tubes have an inner diameter of 1 mm and an outside diameter of 4 mm. The tubing is flexible which results in a high impedance that could dissipate some pressure. The supplier of the silicon rubber tubes is Rubber b.v., which can be found at www.rubberbv.nl. The exit fluid of the micro fluidic cell stretcher is collected with a tumbler. The pump can be controlled manual or with a computer. Further investigation is needed to control the syringe pump with the computer and therefore the pump will be controlled by hand for the experiments.

Chapter 5

Experimental procedures and results

5.1 Experimental preparation

Because no experience was available in the field of micro fluidics, some difficulties have been encountered during the experiments. The procedures that were taken into account to solve some of the practical problems with experiments with micro fluidic structures are described in this section. Also the cell culturing and preparations are described.

5.1.1 Cell preparation

The cells that were used for the first test were fibroblasts from a mouse (3T3 fibroblasts). A fibroblast is a cell that forms the basic building block of the structural fibers and basic substance of connective tissue, like skin tissue. It has a branched cytoplasm surrounding and an elliptical nucleus. An image of a fibroblast attached to a substrate can be seen in figure 5.1.

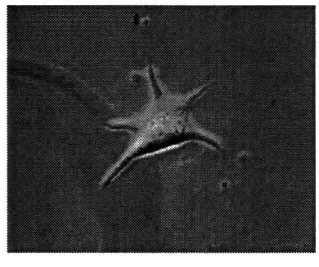

Figure 5.1: 3T3 fibroblast adherent to the surface of a fibrin gel [Janmey et al., 2001]

The fibroblast is chosen as a model cell, because many studies have already been carried out using these cells. Fibroblasts are easy to grow in culture and have a finite line of 50 generations. Also the fibroblasts have the property of immunofluorescence, which means that the properties of fibroblasts do not change if they are fluorescent and therefore they can live for a relatively long time if they are fluorescent. The cell's geometric properties are relatively constant between the cells, which gives better statistical results. Fibroblasts can survive even

after two or three subcultures [Spector et al., 1997]. The size of a 3T3-fibroblasts is around $10\mu m$ [Thoumine et al., 1999, Uhal et al., 1998]. The results of these previous studies provides information for the simulation of the cell deformation inside the micro fluidic cell stretcher.

The shear modulus of a fibroblasts 3T3 is 380 kPa, following [Peeters, 2004]. The shear modulus is determined with AFM and was based on a model of a hyperelastic isotropic deformation of a solid, and can be used as a reference for this model. Another advantage of using fibroblasts is that the elasticity of the cells is high, compared to other cells like chondrocyte. Chondrocyte have a Young's modulus of 2.7 kPa, which results in a shear modulus of 900 Pa. These values were also measured with AFM, following [Knight et al., 2002].

The fibroblasts are in vivo attached to a surface by tentacles (see figure 5.1). To grow fibroblasts, they are attached to a substrate. The fibroblast are put inside an incubator with a special growth environment (culture), and an exponential growth on the substrate will occur. The growing of the cells is done in an incubator, which provide an environment with:

- 37 °C
- 5% CO_2

Every 3 to 4 days the cells need a new culture, because the nutritive substances are absorbed by the cells. The culture is a combination of DMEM + 10% FBS + 1% glutamine + 1% penstrep (250 ml) and HAM's F12 + 10% FBS + 1% penstrep (250 ml) with a small fraction of fetal bovine serum (FBS)(50 ml), L-glutamine (2.5 ml) and penstrep (5 ml). Penstrep is a combination of antibiotic penicillin and streptomycin. The medium DMEM contains 100 units/ml penicillin, 100 μg/ml streptomycin (GIBCO/BRL 15140122), 2 mM glutamine (GIBCO/BRL 25030-081), 10 % donor bovine calf serum (JRH Bioscience 12143-78P) and 0.5 μg/ml tetracycline-hydrochloride [Spector et al., 1997]. HAM's F12 is a nutrient mixture of many inorganic salts, amino acids and vitamins. [Spector et al., 1997].

When a test is done with the fibroblasts, the tentacles are chemically detached from the substrate with trypsine. The fibroblasts are washed with Phosphate Buffered Saline (PBS) and become spherical cells floating inside the in situ solution [Spector et al., 1997]. Figure 5.2 shows an image of two fibroblasts floating inside their culture. Mention that the fibroblasts

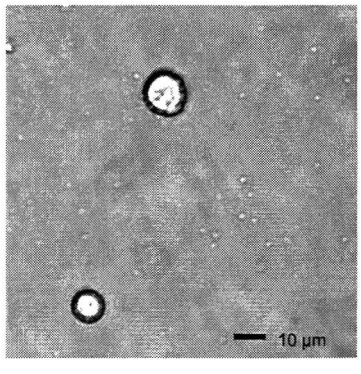

Figure 5.2: 3T3 fibroblast washed and floating inside the culture

in figure 5.2 are spherical. Before the fibroblasts are used for the test, the concentration of the fibroblasts is determined with a grid hemocytometer [Morgan and Darling, 1993]. To make the fibroblasts fluorescent Celltracker Green is used [Cambrex, 2005]. Celltracker Green passes freely through the cell membranes, but once inside the cell, is transformed into cell impermeable reaction products that may be retained in living cells. The Celltracker Green emits light with a spectrum of (517 nm) which can be detected with the fluorescence microscope of Zeis.

5.1.2 Closing the micro fluidic channels

The cross slot is closed with vacuum. The vacuum is applied with a membrane pump type MZ-2C of Vacuubrand, Germany. This pump is capable to suck air with a flow rate of 2.0 m^3/h. This results in a pressure difference around 9.0 mbar, which equals to 900 Pa. On the vacuum channels, a glass cover plate with a thickness of 0.17 mm is place on top of the cross slot chip. With a vacuum tube the connection between the vacuum pomp and cross slot chip has been made. With a pressure reduction of 900 Pa in the vacuum micro channel, the glass cover plate will be sucked on the surface of the cross slot chip and should close the micro fluidic channels. Images are shown in figure 5.3 of the cross slot chip with a cover glass, and the connection to the vacuum pump. A schematic view of the vacuum channels design can be

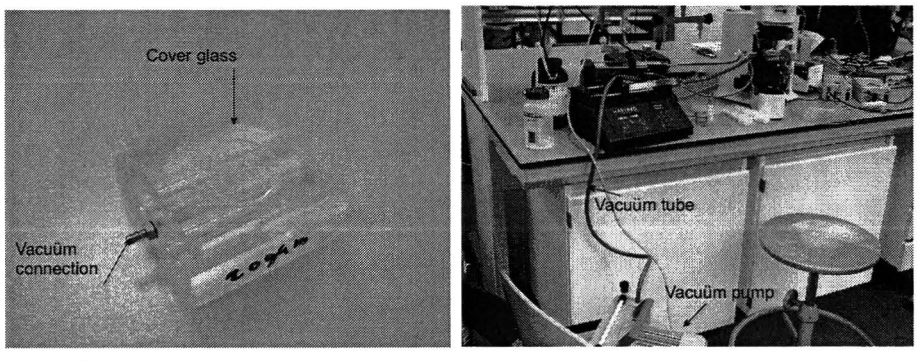

(a) Cross slot with cover plate (b) Vacuum pump with connection tube

Figure 5.3: Images of vacuum system cross slot

found in section §4.2.1.Because both designs of the vacuum systems did not close the micro fluidic channels, other possibilities were needed.

Another way to close the channels was to use some grease between the cover glass and the PMMA chip. With a small bar, some grease was put on the surface of the cross slot chip on both sides of the micro fluidic channels. When the whole surface, except the micro fluidic channels, was covered with grease, the thin cover plate was pressed on top of the chip. The grease induced a strong adhesion between the glass cover plate and the cross slot chip and closed any cap between the micro fluidic channel and the vacuum channel. With the grease it was possible to remove the cover glass after an experiment and clean the cross slot. A disadvantage was that grease could get inside the micro fluidic channels, which could clog the

channel. Also the cleaning of the chip was difficult. Ethanol and ultrasonic cleaning could remove the grease after several times. Also the grease did not always close the cross slot. During the experiment the cross slot could leak some fluid, because the cover glass became detached from the cross slot chip. For the experimental results of the 200 μm, grease had been used to close the micro fluidic channel.

Because the cross slot of 100 μm could not be closed with vacuum or with grease, another solution was needed to close the micro channels. On top of the 100 μm cross slot, a cover glas was glued with a ultra violet drying glue. The two holes of figure 4.14(e) and 4.14(b), where the PMMA was completely gone, where reconstructed with glue. An image of the reconstructed holes can be seen in figure 5.4.

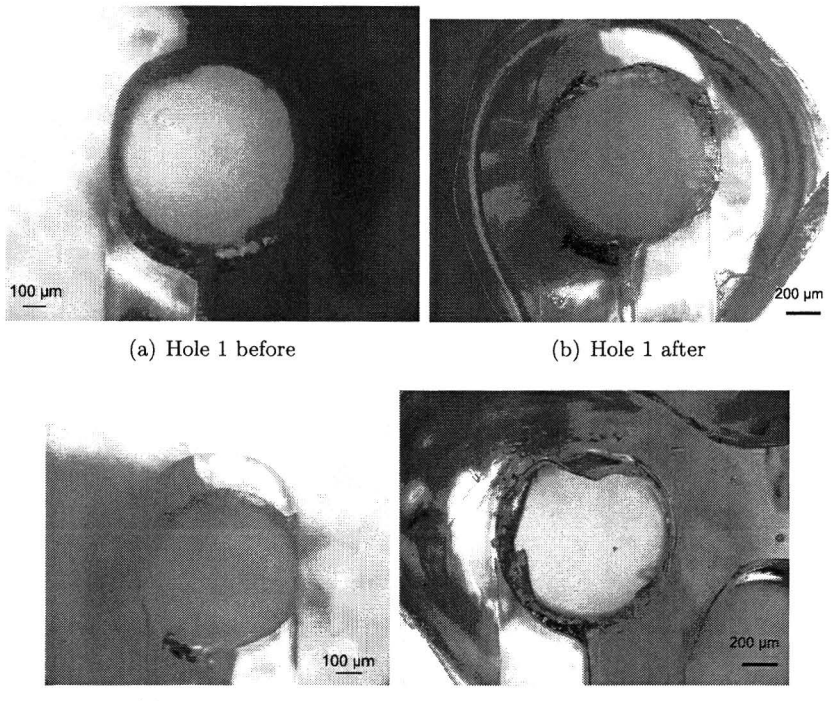

(a) Hole 1 before

(b) Hole 1 after

(c) Hole 2 before

(d) Hole 2 after

Figure 5.4: Holes of cross slot 100 μm before and after reconstruction

After the reconstruction the vacuum channel was filled with glue, the glass cover plate was placed on the cross slot chip and fixed with ultra violet light. This solution closed the micro channels properly and no leakage happened.

5.1.3 Filling of micro fluidic device

After the micro channels are closed, the system needs to be filled with PBS (Phosphate Buffered Saline). PBS has the same osmotic pressure as the culture of the cells which is used to grow the cells. If PBS is used it will prevent the cells to swell osmotically. The tumbler is filled with PBS and by using vacuum, the total system will be filled with PBS. The vacuum is applied by hand using two syringes on the inlet the cross slot. An image of the filling of the micro fluidic device is shown in figure 5.5.

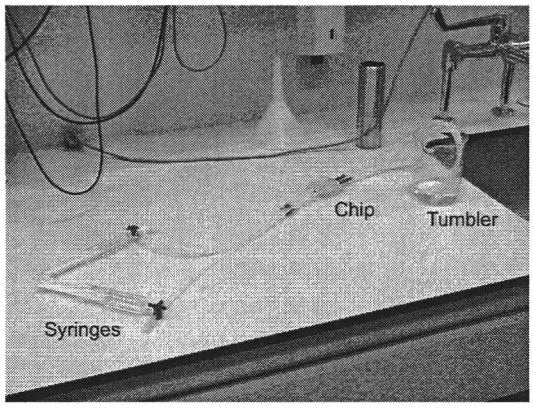

Figure 5.5: Filling of the micro fluidic device

Important is that all the air is removed from the micro fluidic system. If the tumbler, chip and syringe are held at the same height, the chance of air bubbles inside the system is minimized due the reduction of the height energy of the mass of the liquid. When the whole system is filled with PBS, both syringes, with a volume of 10ml, are filled with PBS and connected to the tubes. The micro fluidic cell stretcher is now ready for the experiment.

5.1.4 Control of the micro valves

The Matlab Simulink model for the control of the micro valves was tested on movies of cells flowing through sudden contractions and cross slot flows. The model had been designed to work under Lunix. Unfortunately the software to control the valves did not worked at the time of the experiments, because the camera real time imaging of the camera could not yet been done under Lunix. Because this problem was not yet solved the micro valves are controlled manually with feeding boxes for these experiments. An image of the actuators connected to the feeding boxes is shown in figure 5.6.

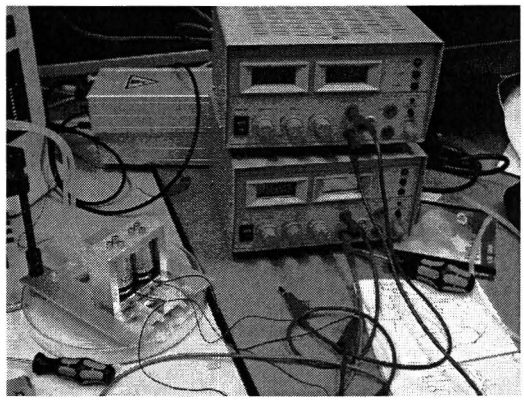

Figure 5.6: Feeding boxes for manually actuation of the micro valves

The Matlab Simulink program is still under development.

5.1.5 Input of the cells

The total system is filled with PBS. For the inlet of the cells, a valve is placed inside the tube. Here the cells can be inserted in the tube. To this tube another syringe is attached to control the input of the cells. From experience, filling the syringe at the pump takes a lot of time before cells are entering the cross slot flow, because of the fluid volume inside the tube that connects the pump to the chip. Therefore a practical solution was to place a valve inside the tubing close to the cross slot chip, which reduces the fluid volume between the cells and the T-junction. An image of the valve is shown in figure 5.7.

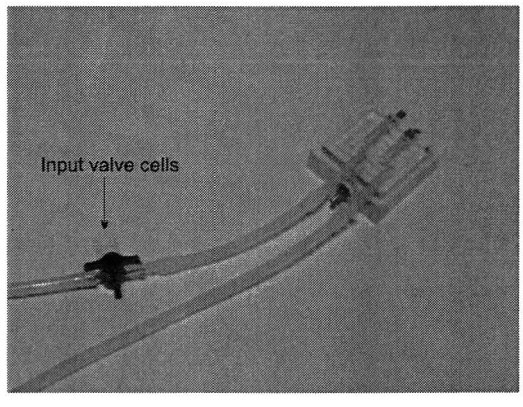

Figure 5.7: Valve for input of the cells inside the tube

5.1.6 Focus plane of the cells

The fibroblast are small but can easily be found with an objective with a magnification of ten. An way to find the middle of the cross slot channel is to focus on the top of the chip, count the turns needed to focus on the bottom of the channel. If the turns is dividend by two, the middle of the channel is found. Some microscopes have an displacement sensor for the

z-direction. When the focus plan is on the top or bottom of the channel, the z measurement can be read. If the dept of the channel is know the middle of the channel can be calculated. During the experiment the location of the fibroblast was still difficult to find. The best way was to look at the fastest moving fibroblast, and focus on that plane. Where the fibroblasts flow the fastest must be the middle of the channel due to the fluid dynamics.

5.1.7 Cleaning the experimental setup

After any experiment was done, the total system was cleaned by using ethanol. The effect is that all cells inside the system will die and be removed out of the micro fluidic system. Because biological cells are used, the waste needs to be removed with care. Cells need to be removed with the biohazard waste and the cleaning fluid at the chemical disposal in the cell lab. If wanted, ultrasonic cleaning can be used to remove any other dirt inside the micro fluidic channels. If grease was used to close the cross slot chip, a combination of ethanol and ultrasonic cleaning was needed to clean the micro fluidic channels.

5.2 Experimental results

For the experiments the flow rate on the inlet will be mention. For the main flow, this flow rate will be divided between the two main channels of the cross slot. The flow rate of the fibroblasts will go in only one channel. For the center of the cross slot different dimensionless numbers are calculated. The velocity of the cross slot center is assumed equal, because also in the simulations this is also the situation. This equal flow is the mean of the flow of the main channel and the flow of the fibroblast input. Because the fibroblasts are put inside the main channel with a certain flow, in reality the flow on both sides of the cross slot is different. This can be seen in the experiments, because the stagnation point is shifted to the channel with the least flow. Also images are taken from the input of the fibroblast in the main channel. The Reynolds number of both channels is calculated.

5.2.1 Cross slot 200 μm

An image of fibroblasts inside the cross slot of 200 μm can be seen in figure 5.8.

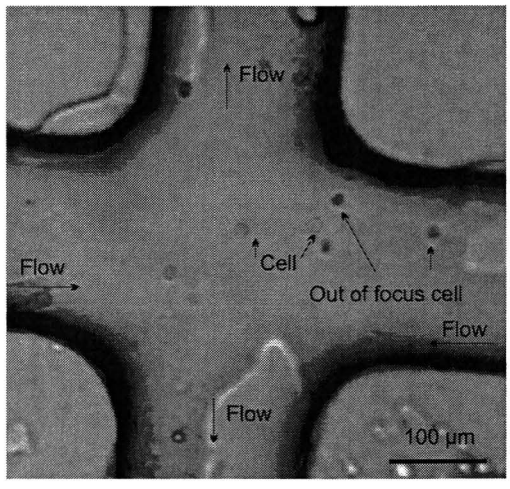

Figure 5.8: Image of cells inside cross slot 200 μm

In figure 5.8 it can be seen that some fibroblasts are not in the focus plane. In this experiment only fibroblasts were flowing through the cross slot, without trying to manipulate them to the stagnation point. The channel of 200 μm was still to big compared to the size of the cell. The fraction number for the cross slot is equal to F_{RW} 0.025. The T-junction was a good way for the input of the fibroblasts. Images are shown of the input of the fibroblasts inside the main channel in figure 5.9.

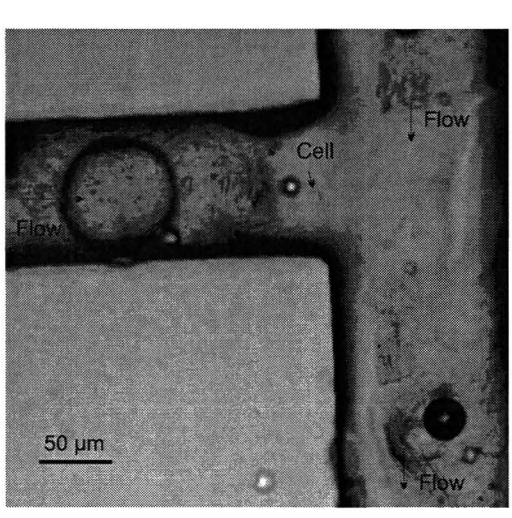

(a) t= 2.83 s

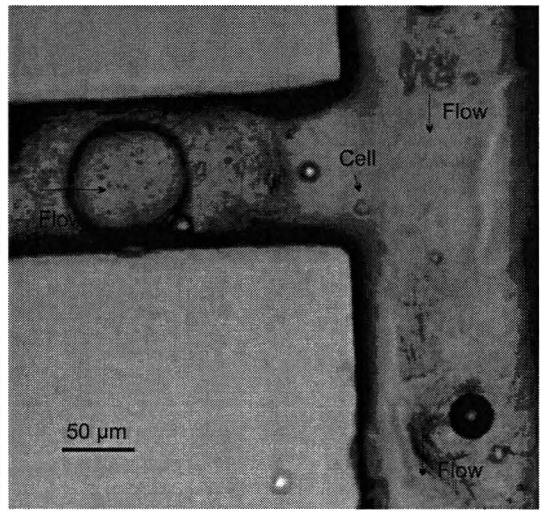

(b) t= 2.96 s

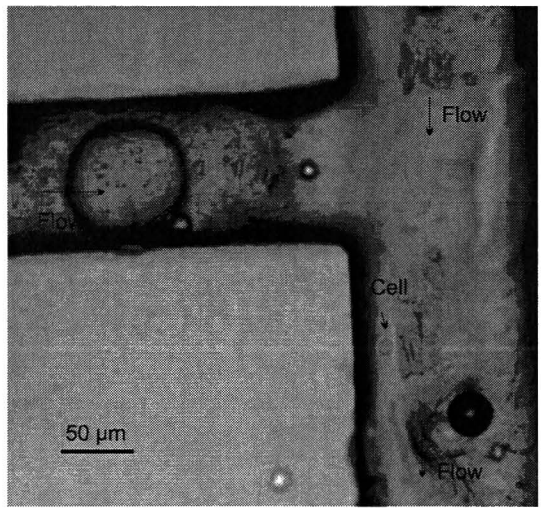

(c) t= 3.33 s

Figure 5.9: Input of fibroblasts with the T-junction of 200 μm cross slot

For this image the flow rate of the input channel was 0.6 μl/min and the flow rate of the main channel was 5 μl/min. This results in a fluid velocity in the main channel (200 μm) of 1.04 mm/s and the velocity inside the cell input channel of 1 mm/s. The Reynolds number for the input of the fibroblasts is 0.1. Where the Reynolds number of the main channel equals 0.21. It looks like the fibroblast deforms when it enters the main flow. The Matlab program to measure the deformation of the cell did not work on the images of figure 5.9, because the contrast between the back ground and the cell is not sufficient. In figure 5.8 and figure 5.9 the grease used to close the micro channels can be seen. Also some air bubbles can be seen in the channel.

When the fibroblasts are labeled with the Cell tracker Green, the fibroblasts become fluorescence and light up. An illumination source is needed and the reflected light needs te be filtered. This can be done with the fluorescent microscope of Zeiss. On the microscope a digital Kodac camera is placed to record the images. The high speed camera could not make images, because the intensity of light reflected from the fibroblast was not sufficient for recording. Images of the Kodac camera of the fluorescent labeled fibroblast can be seen in figure 5.10.

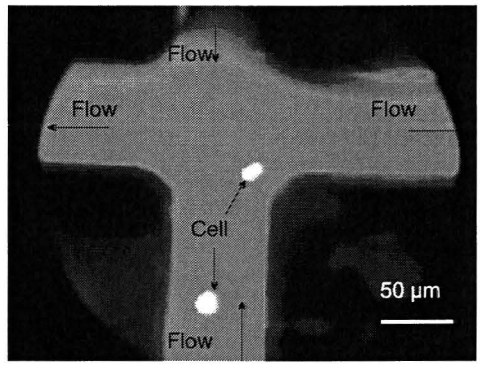

Figure 5.10: Image of fluorescence fibroblasts inside cross slot 200 μm

If the Taylor deformation rate is determined from the figure 5.10 fibroblast one has a Taylor deformation rate of $D_{xy} = 0.0826$ and the second fibroblasts has a Taylor deformation rate of $D_{xy} = 0.2065$. Although this are two different fibroblasts, this can give an idea of the possible deformation of a fibroblast under these circumstances. Because the flow was fast, no following image could be taken from the same fibroblast. Figure 5.11 shows the image from the Matlab program where the background is subtracted from the image in figure 5.10.

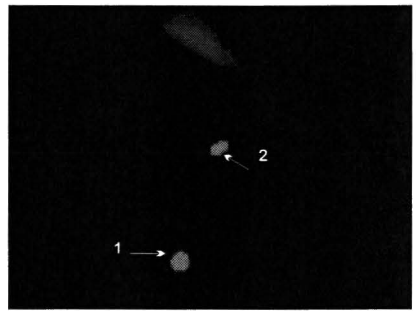

Figure 5.11: Determination of Taylor deformation rate fibroblasts 200 μm

From figure 5.11 it is clear that the contract between background and cell increases due the fluorescent label of the fibroblasts. The example of no fluorescent labeled fibroblast can be found in section 4.4.4. The flow rate of the main flow of this experiment was 5 μl/min and of the input of the fibroblasts the flow rate was 1 μl/min. The Reynolds number for the center of the cross slot in this experiment is 0.125. The Deborah number of this experiment is $3.29 \cdot 10^{-4}$ and the fraction number F_{RW} is 0.025.

Also some images are shown of the fluorescent labeled fibroblast entering the main channel with the T-junction in figure 5.12. For the figure 5.12, the main flow rate equals 5 μl/min

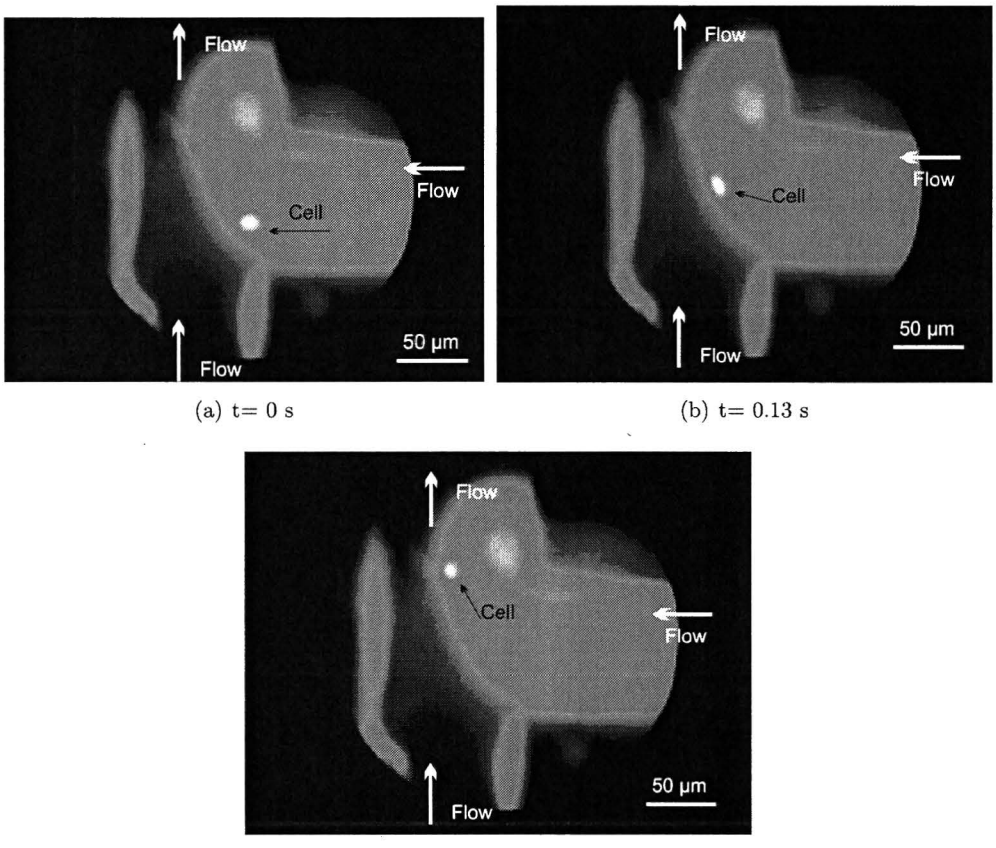

(a) t= 0 s

(b) t= 0.13 s

(c) t= 0.3 s

Figure 5.12: Input of a fluorescence fibroblast with the T-junction of 200 μm cross slot

and of the input of the fibroblasts the flow rate was 1 μl/min. The Reynolds number for the main channel is 0.104 and the Reynolds number of the input of fibroblasts equals 0.167. If the Taylor deformation rate of the fibroblast is calculated, the fibroblast of figure 5.12(a) has $D_{XY} = 0.1875$, figure 5.12(b) has $D_{XY} = 0.2117$ and figure 5.12(c) has $D_{XY} = 0.0340$.

An image of the micro channel of 200 μm with an air bubble just after the T-junction is shown in figure 5.13.

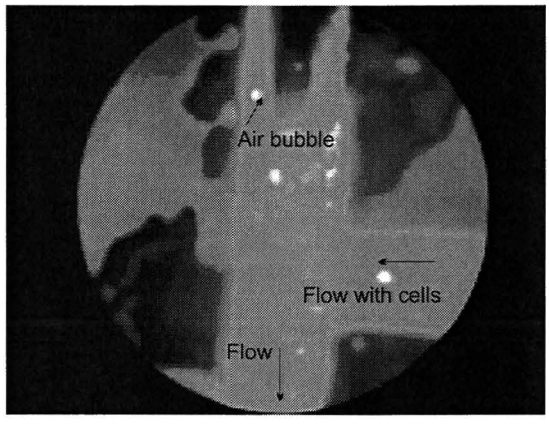

Figure 5.13: Image of air bubble inside main channel 200 μm with fluorescence fibroblasts

In figure 5.13 can be seen that the air bubble blocked the channel entirely and the main flow is going in the wrong direction. The fluid with cells is not able to push the air bubble out of place. Once an air bubble is inside the system, its very difficult to get this out of the micro fluidic system. This problem will be discussed in the conclusion of the experiments.

5.2.2 Cross slot 100 μm

With the cross slot of 100 μm the fibroblast was tried to positioned in the stagnation point with manual actuated micro valves. It was difficult to keep the fibroblast on the stagnation point manual because some back flow enters the cross slot when the valve is closed. In figure 5.14 two images of the fibroblast inside the stagnation point of the cross slot 100 μm can be seen.

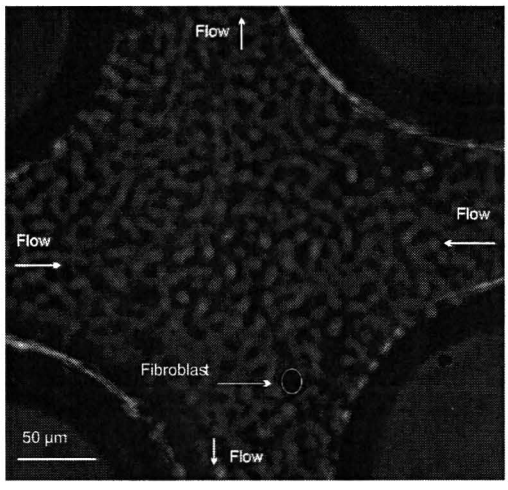

(a) Positioning, t = 1.83 s

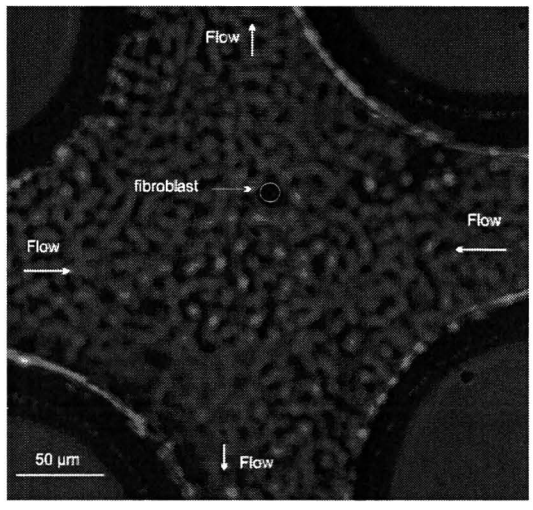

(b) Stagnation point, t = 3.17 s

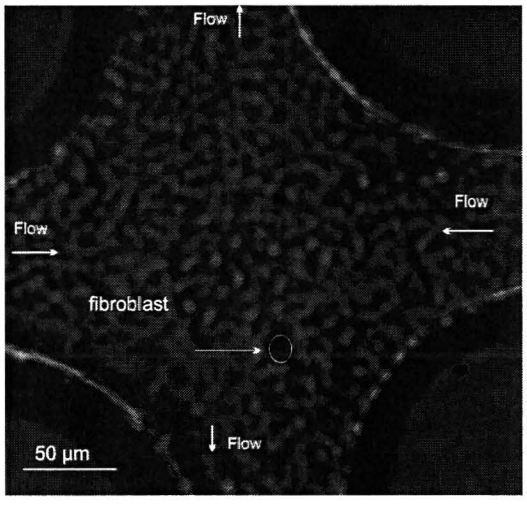

(c) Deformation near stagnation point, t= 3.33 s

Figure 5.14: Input of fibroblasts with the T-junction of 200 μm cross slot

In this experiment the flow rate of the main flow is 2 μl/min and the flow rate of the input of the fibroblasts was 0.6 μl/min. The Reynolds number for the center of the cross slot in this experiment is 0.11. The Deborah number is 5.71 $\cdot 10^{-4}$ and the fraction number F_{RW} is 0.05. If the Taylor deformation rate is determined by the Matlab program, the Taylor deformation rate of figure 5.14(a) is $D_{XY} = 0.1010$, figure 5.14(b) is $D_{XY} = 0.0525$ and of figure 5.14(c) is $D_{XY} = 0.1225$.

There is only little deformation of the fibroblast when the fibroblast is held in the center of the cross slot of 100 μm. The deformation of the fibroblast is the same as of a moving fibroblast through a straight micro channel. Unfortunately the velocity of the flow could not be increased since the cell needed to positioned manual in the cross slot. Every attempt to increase the flow, the fibroblast was already gone from the stagnation point.

Also some images where taken from the T-junction with the inlet of the fibroblasts. The flow rate of the main channel was 1.2 μl/min and the flow rate of the fibroblast input channel is 0.6 μl/min.

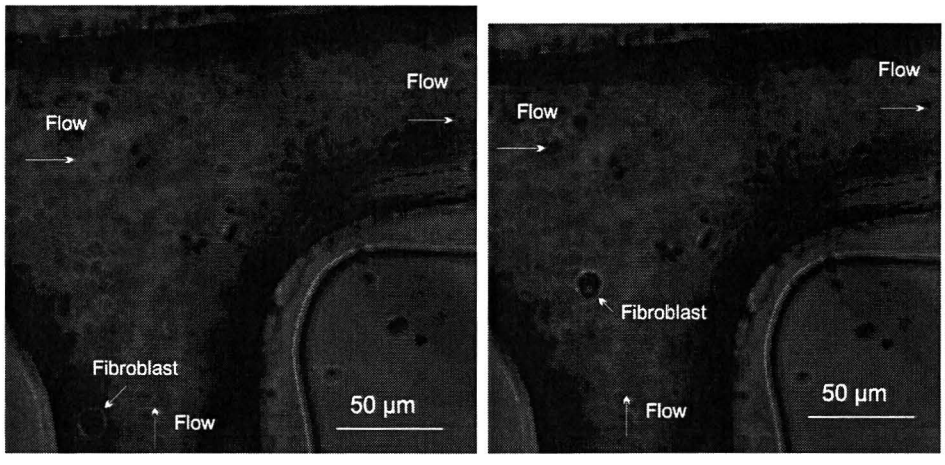

(a) t= 1.20 s (b) t= 1.44 s

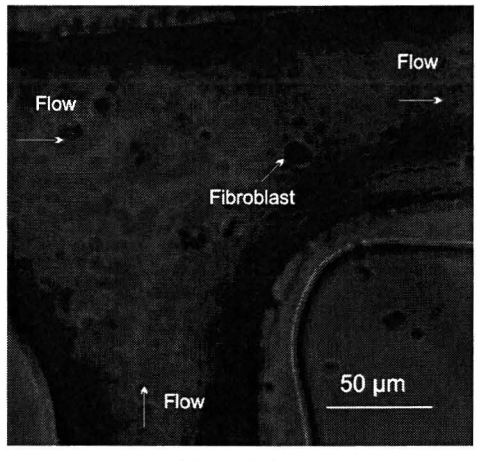

(c) t= 1.54 s

Figure 5.15: Input of fibroblasts with the T-junction of 100 μm cross slot

The Reynolds number of the main flow of figure 5.15 is 0.05, and the Reynolds number of the fibroblast input channel is 0.1. The Taylor deformation rate is determined form figure 5.15. For figure 5.15(a) $D_{XY} = 0.009$, figure 5.15(b) $D_{XY} = 0.0983$ and for figure 5.15(c) $D_{XY} = 0.1213$.

If the fibroblast were made fluorescence with cell tracker green. Also the fibroblast was tried to hold in the stagnation point manually. Because the high speed camera could not detect the fluorescence cell, a digital camera was put on the fluorescence microscope. With this camera movies where made. In figure 5.16 an image is shown of a fibroblast in the middle of the cross slot, with and without deformation.

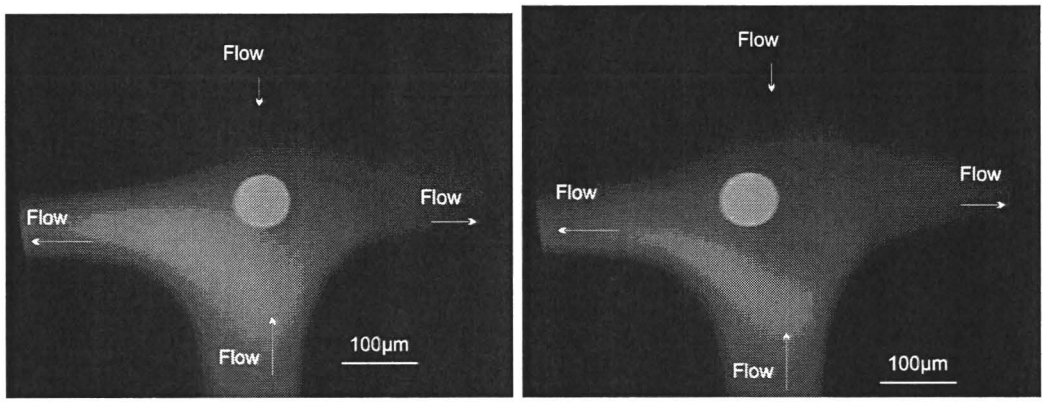

(a) Stagnation point, t = 24.5 s (b) Deformation near stagnation point, t= 24.9 s

Figure 5.16: Fluorescent fibroblast inside the cross slot of 100 μm

The flow rate of this experiment was 6 μl/min for the main flow and 2 μl/min for the input of the fibroblasts. This results in an Reynolds number for the cross slot of 0.33. The Deborah number of this experiment is $1.75 \cdot 10^{-3}$ and the fraction number is $F_{RW} = 0.05$. The Taylor deformation rate, determined with the Matlab program was for figure 5.16(a) $D_{XY} = 0.0362$ and for figure 5.16(b) $D_{XY} = 0.0422$. Images of figure 5.16 with subtracted background from the Mathlab program can be seen in figure 5.17.

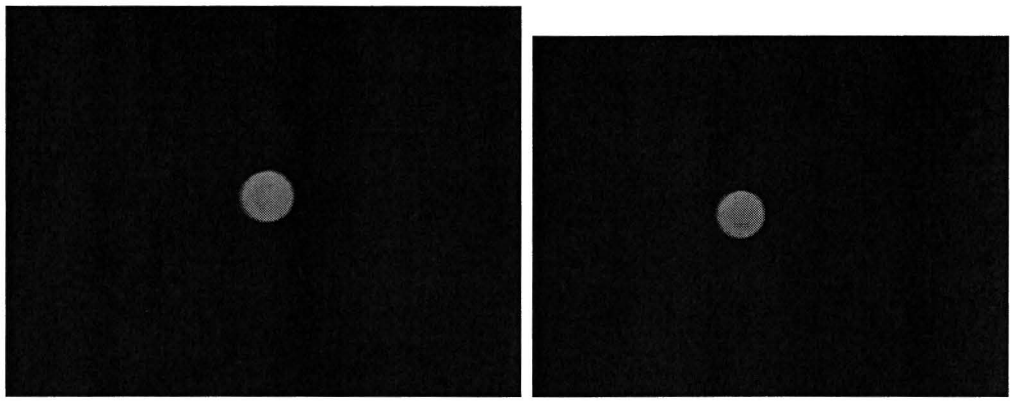

(a) Stagnation point, t = 24.5 s (b) Deformation near stagnation point, t= 24.9 s

Figure 5.17: Fluorescent fibroblast inside the cross slot of 100 μm

This means a small deformation happen, but this can also be a result of the out of focus of the fibroblasts. If the length scale is taken into account the fibroblasts are around 50 μm, which can not be the dimension of the fibroblast. This image shows the blurred image of a fibroblast that is out of focus. The Taylor deformation rate is not depending on the length scale of the fibroblast, because it is dimensionless. Thats why these images could be used to determine the Taylor deformation rate of the fibroblast inside the cross slot of 100 μm.

Also images are taken from the T-junction and the inlet of the fibroblasts. For this experiment the flow rate of the main channel was 3 μl/min and of the fibroblast input channel was 1 μl/min. The Reynolds number of the main flow is 0.125 and the Reynolds number of the fibroblast input channel is 0.167. Images of the input of a fibroblast can be seen in figure 5.18.

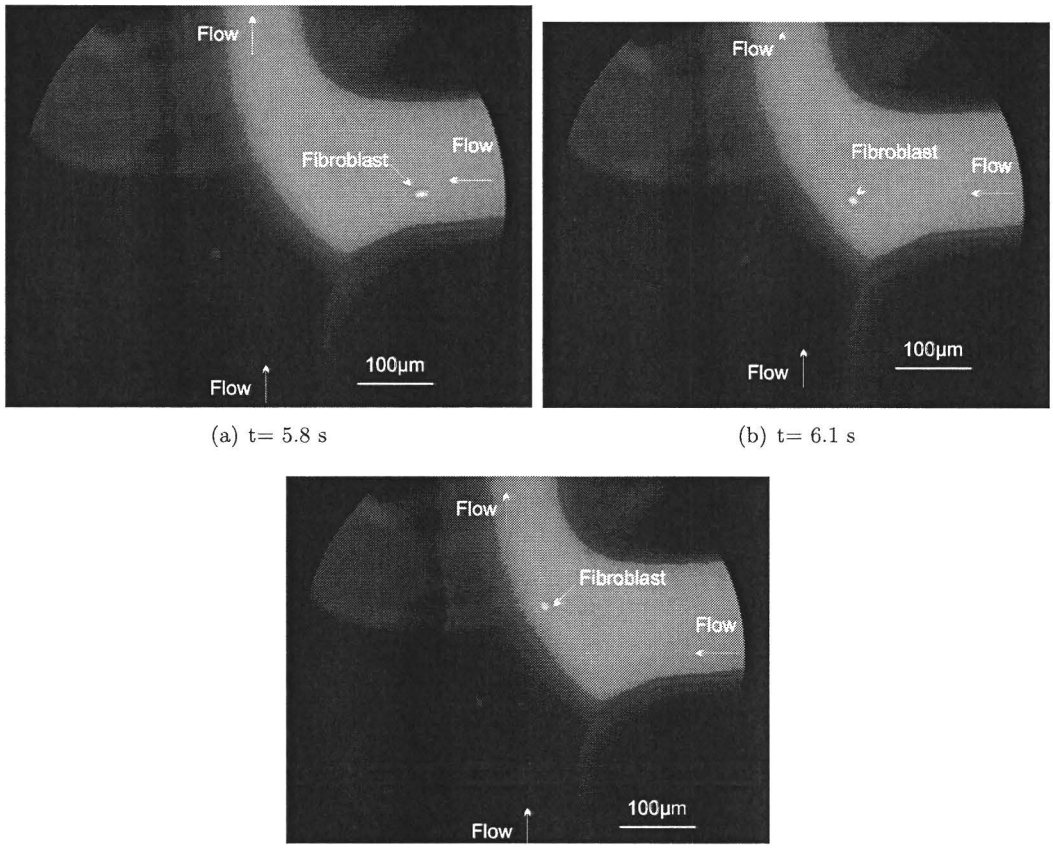

(a) t= 5.8 s

(b) t= 6.1 s

(c) t= 6.3 s

Figure 5.18: Input of fluorescent fibroblasts with the T-junction of 100 μm cross slot

The Taylor deformation rate is determent for figure 5.18. For figure 5.18(a) is $D_{XY} = 0.2185$, for figure 5.18(b) is $D_{XY} = 0.1012$ and for figure $D_{XY} = 0.4668$.

5.3 Conclusions experiments versus simulations

Many experiments have been done to proof the principle of the micro fluidic cell stretcher. Also experiments with a single contraction which can be found in appendix C. The key component from the experimental setup was not ready to use. The control system for the micro valves to position the cell in the stagnation point did not yet worked. Manual control of the flow was possible, only the flow could not be increase because full attention was needed to keep the cell in the stagnation point. If the flow was increased manually, the cell was removed from the stagnation point and gone. The Reynolds numbers of the experiments are relative high for micro fluidic systems but still small enough for a laminair flow. The experiments of the 100 μm cross slot can be used to compare with the numerical results, since the fraction number of this cross slot is $F_{RW} = 0.05$. The Reynolds number of this experiment was 0.33 and the Deborah number was $1.75 \cdot 10^{-3}$. The dimensionless numbers from the simulation were Re $= 0.1$, the De $= 0.000526$ and the $F_{RW} = 0.05$. The numerical model predicted a Taylor deformation rate of $D_XY = 0.00128$ at time 2. This was a steady state situation. Because the fibroblasts are put inside the main channel with a certain flow, in reality the flow on both sides of the cross slot is different. In the simulation the velocity of the cross slot on both sides is equal. This has been corrected by taken the mean flow of the cells and main flow and divided them over both channels. The numerical deformation of the cell is shown in figure 5.19(a).

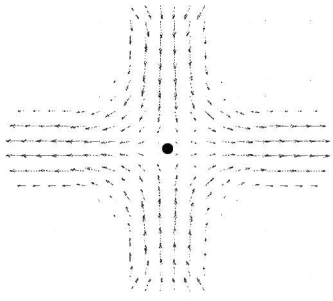

(a) Numerical results

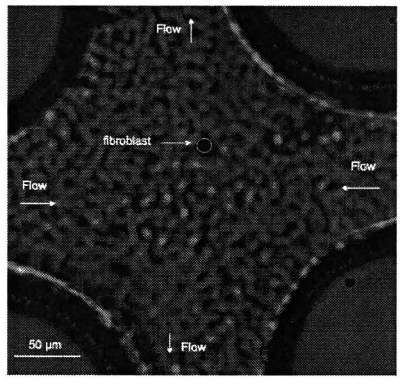

(b) Deformation cross slot 100 μm

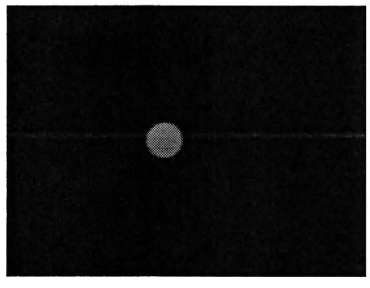

(c) Deformation fluorescent cross slot 100 μm

Figure 5.19: Compare numerical results to the experiments

In the experiment of figure 5.19(b) the situation was described with Re = 0.11, De =5.71 $\cdot 10^{-4}$ and F_{RW}= 0.05. The Taylor deformation rate of the fibroblast when it was just in the stagnation point was D_{XY} = 0.0525. After some time the Taylor deformation rate of the fibroblast in the stagnation point was D_{XY} = 0.1225. Mention that the deformation of the fibroblast before entering the cross slot was measured to be D_{XY} = 0.1010. This is much higher than what the simulation predicts. Because of the dimensionless number are a little higher, more deformation can be expected, but not a factor of 100. The fibroblast seems to be in the focal plane of the optical system. The dimension of the fibroblasts equals the dimension of the simulation. An explanation can be that the cell is not in the middle of the cross slot, but at the cover glass height. At the glass, the fibroblast will attached and therefore a deformation could had happend. Another explanation can be that the Matlab program does not accurate predict the Taylor deformation rate, but this is not the case. The boundary trace and the least square ellipse fit of the program are both often used to determine the size of the cell. The question is if this deformation of really from the fibroblast or is from the blurred image of the camera. The increasing speed of the fibroblast could lead to a longer imaged fibroblast. This is an effect of the imaging time of the camera. The imaging time of the camera was set on $\frac{1}{20000}$ and the speed inside the cross slot channel was 2.16 mm/s. This results if the displacement is in the x-direction, to a displacement of 0.108 μm during the imaging time. The influence on the Taylor deformation rate is $D_{XY(influence)}$ = 0.0054 if the fibroblast is not deforming. It can be concluded that the fibroblast must be deforming, since the deformation inside the cross slot is D_{XY} = 0.0525 and D_{XY} = 0.1225. The corrected values of the Taylor deformation rate for the error of the imaging time are D_{XY} = 0.0471 when just inside the stagnation point and D_{xy}= 0.1171 for figure 5.16(b). Due the manipulation of the flow, this velocity could be a little different, but from this corrected Taylor deformation rate it can be concluded that there will be some measurable deformation in the stagnation point.

In the experiment of figure 5.19(c) the situation was described with Re = 0.33, De = 1.75 $\cdot 10^{-3}$ and F_{RW} = 0.05. The Taylor deformation rate of the fibroblast when it was just in the stagnation point was D_{XY} = 0.0362. After some time in the stagnation point the Taylor deformation rate of the fibroblast was D_{XY} = 0.0422. In the experiments the Reynolds number is higher and the Deborah number is also higher. A higher Deborah number should lead to more deformation of the cell. However de deformation of the cell is still to large compared to the results from the model. Figure 5.19(c) shows a very large fibroblast, compared to the model shown in figure 5.19(a). This can be explained because the fibroblast was not in the focal plain of the objective. If the fibroblast is out of focus the image of the fibroblast gets blurred and the fibroblast appeared as a big dot. However the amount of deformation should not be effected, because the Taylor deformation rate is dimensionless. Because of the camera used to make the movie, the imaging time was limited. The high speed camera could not been used because of the amount of light reflected from the fibroblast. The frame rate of the camera was 15 fps. If the fibroblasts moves through the cross slot and the imaging time is to slow, the fibroblast image will be stretched to that direction. This can be implemented by the Matlab program as the deformation of the fibroblast. For the figure 5.19(c) the fibroblast was almost steady in the stagnation point and the value may be seen as the real deformation of the fibroblast. However no hard conclusions can be made, because the image was blurred so the fibroblast can be seen properly.

Images of the input of the fibroblasts through the T-junction are analyzed. The images of one example of a fibroblast through the T-junction is shown in figure 5.20(a). The Reynolds

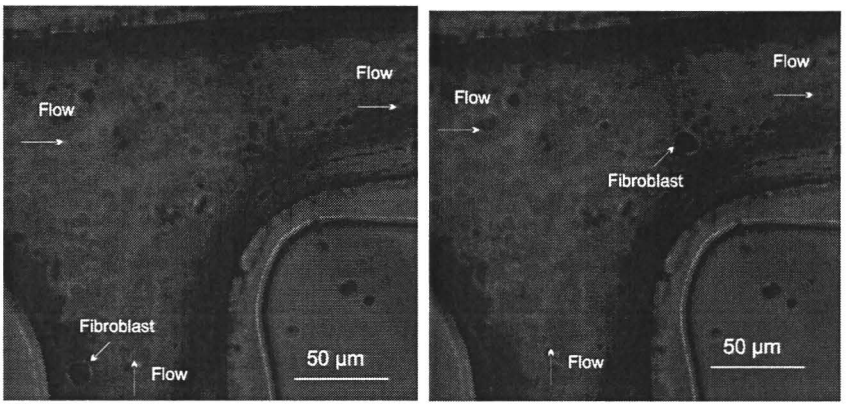

(a) t= 1.20 s (b) t= 1.54 s

Figure 5.20: Input of fibroblasts with the T-junction of 100 μm cross slot

number of the main flow of figure 5.20 is 0.05, and the Reynolds number of the fibroblast input channel is 0.1. The Taylor deformation rate of the fibroblast in figure 5.20(a) is $D_{XY} = 0.009$, which means that the fibroblast is initially almost circular $D_{XY} \approx 0$. When the fibroblast has enter the main channel, shown in figure 5.20(b), the Taylor deformation rate is $D_{XY} = 0.1213$. The question is if this deformation of really from the fibroblast or is from the blurred image of the camera. The increasing speed of the fibroblast could lead to a longer imaged fibroblast. This is an effect of the imaging time of the camera. The imaging time of the camera was set on $\frac{1}{20000}$ and the speed inside the main channel was 2 mm/s. The influence on the Taylor deformation rate is $D_{XY(influence)} = 0.005$ if the fibroblast is not deforming. It can be concluded that the cell must be deforming, since the deformation inside the main channel is $D_{XY} = 0.1213$. If this value is corrected with the error of the imaging time there is still een Taylor deformation rate of D_{XY}= 0.1163.

During the experiments something other happend once. The fluid flow inside the cross slot went to a hydro focus flow, which means three flows out and one flow goes through this hydro focus. Images are shown of the hydro focusing of a fluorescent labeled fibroblast inside the micro fluidic channel of 200 μm in figure 5.21. Here fibroblasts are fluorescent

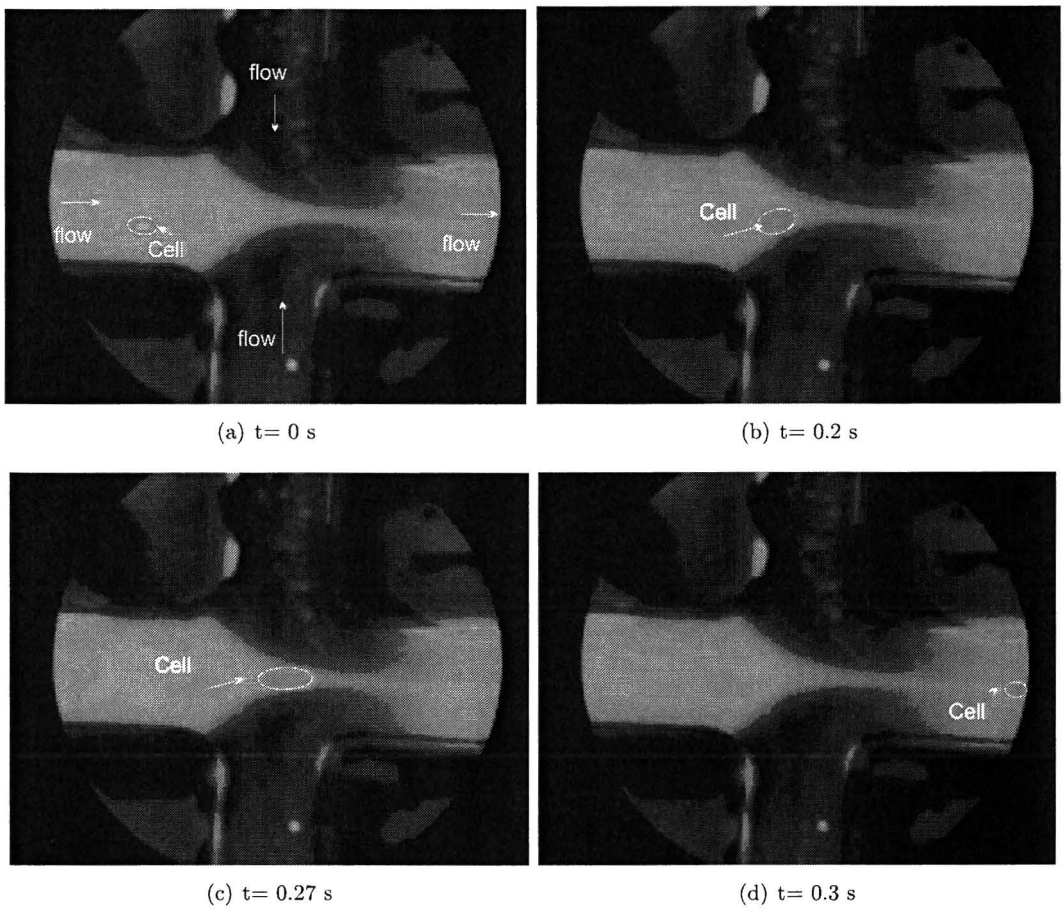

(a) t= 0 s (b) t= 0.2 s

(c) t= 0.27 s (d) t= 0.3 s

Figure 5.21: Cells through hydro focus

labeled with Cell tracer Green. The Taylor deformation rate is determined by the Matlab program. In figure C.11(a) $D_{XYx} = 0.2238$, in figure 5.21(b) $D_{XY} = 0.2568$, in figure 5.21(c) $D_{XY} = 0.4180$ and in figure 5.21(d) $D_{XY} = 0.2346$. The deformation in the figures C.11(a) and C.11(d) can be caused by the velocity of the flow and the limited imaging time of the camera. Since the flow was not defined, there can not be determined if the deformation is caused by the limited imaging time of the camera. But through the hydro focus the Taylor deformation rate changed ≈ 0.2, so it is assumed that the fibroblast will also deform inside the hydro focus flow.

The numerical results concluded that the fibroblast will only deform much if the viscosity and velocity is increased with a factor 10. This is not yet tested with the experiments and further investigation and study on this subject is needed. From test with the 100 μm cross slot of the T-junction shown in figure 5.20 and the cross slot 5.19(b) it can be concluded that a deformation of the fibroblast is possible even at low Reynolds numbers ($\approx$ 0.1). The fibroblast was in focus and even after correction of the imaging time of the camera, the Taylor deformation rate equals D_{xy}= 0.1163 for the cross slot and D_{XY} = 0.1171 for entering the main flow through the T-junction. Also the hydro focus flow shows a increase in the Taylor deformation rate, But the flow velocity inside the the hydro focus was not well defined. Because the fibroblast is deforming when entering the main flow and deforming when held manually inside the stagnation point, it can be concluded that it will be possible to measure the deformation of cells with the micro fluidic cell stretcher. Important is that the control system for the micro valves will be automated. The micro valves can work because the fibroblasts could also be manipulated manual to the stagnation point. If the control system works, cells can be positioned in the stagnation point even if the flow is increased until the fibroblast deforms.

In reality there could be some scaling effects that could also influence the deformation of the cell, but are not mention in the model. Because the control system of the micro valve is not working yet, the numerical results can not be tested if the parameters are valide or not. Because the deformation of the fibroblast can already be detected, I assume that the shear modulus found in the literature, is not valide for this experimental setup. The shear modulus of the fibroblast measured with micromanipulation can be different, because of the way of probing, environmental parameters or cell model. Also the surface tension could play a role on the deformation of the fibroblast and have not be taken into account. If the experimental setup is working, further study can be done on the experimental data to improve the numerical simulation.

5.4 Evaluation and improvement experimental setup

The experimental setup is still not ready to measure the deformation of the cell. There are several problems with the micro fluidic cell stretch experimental setup. The problems will be discussed in this section.

5.4.1 Cross slot chip

Both vacuum systems did not close the micro fluidic channel properly. The first vacuum system only had a vacuum channel far away from the micro fluidic channel. The water leaked almost instantly to the vacuum channel. The first vacuum design had a rough surface between the cover glass and the chip, this is not wanted if the micro fluidic channels need to be closed with vacuum. The second vacuum system worked better, but was still leaking fluid from the micro channels to the vacuum channels. Two holes of the 100 μm cross slot where to big, so the wall between the micro fluidic channel and the vacuum channel was gone and leakage happend. The sealing of the 100 μm cross slot with glue was a succes. There was no leakage of the micro fluidic channel to the outer world. The only disadvantage is that the cover glass can not be removed anymore for cleaning of the channels. For the micro fluidic cell stretcher this is no problem since cells can be removed with ethanol. But if the cover glass needs to

be removable, an elastic material have to be constructed between the glass cover plate an the PMMA chip. This elastic material can function as a sealing and small defects should have no effect on the sealing. Another solution could be to make the cross slot geometry out of PDMS. PDMS microstructure can be closed with a cover glass due the adhesion of the PDMS to glass. If the cross slot is made out of glass, anodic binding can be used to close the micro fluidic structure.

Besides leaking of fluid to the vacuum channel also leakage between the cross slot chip and the micro valve causes problems. The location is show in figure 5.22. A temporary solution

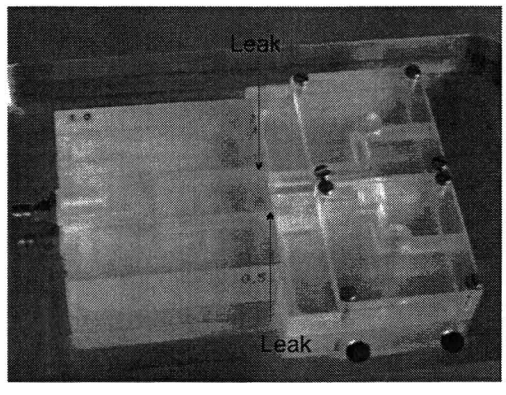

Figure 5.22: Location of leak experimental setup

was found with small connection tubes between the cross slot chip and the micro valve. The problem with this solution was that there was no space on the holder between the micro valve and the cross slot to create this connection. The best solution will be to intergrade the micro valve into the cross slot geometry, so no leakage can happen.

The input of the fibroblasts with the T-junction was good. The fibroblasts where entering without difficulty, only a lot of cells where getting stuck at the entrance of the cross slot. An image of the 100 μm cross slot entrance is shown in figure 5.23 The distance of the T-junction

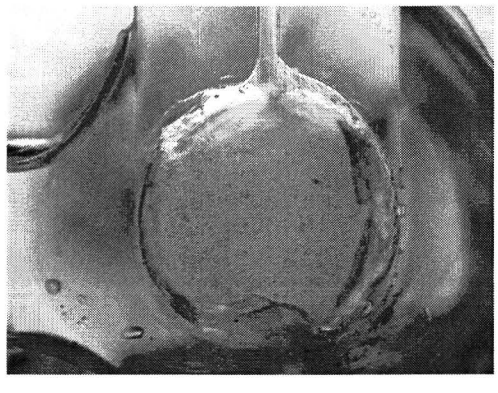

Figure 5.23: Image of fibroblasts stuck on the bottom of the entrance of 100 μm cross slot

from the cross slot center was long enough to get a fully developed flow. The pump can be programmed to a certain flow volume and injection time. With this control of the flow is should be possible te put small amount of cells inside the cross slot main flow and stop the flow of the cell input.

Another problem in the experimental setup is the possible air bubbles entering the system. This is not only a problem in the experimental setup only, but also in the whole micro fluidic science. Air bubbles can be reduces in the micro fluidic system if it is filled with certain care, however if there is some air inside the system it can cause problems. Air bubbles can not stuck inside a parallel channel, unless the roughness of the channel is high [Cubaud and Ho, 2004]. The channels of the cross slot are small and an air bubble could easily clog a channel. When the air bubble clogs the channel, an external pressure is needed to clear the channel. The clogging pressure equals the pressure drop over the bubble. A schematic model and an image of a bubble clogging the 100 μm cross slot in the center can be seen in figure 5.24. The

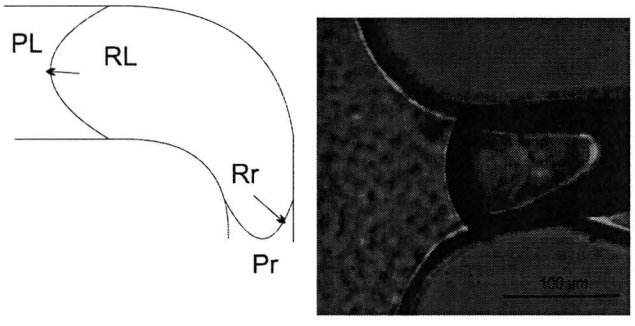

(a) Model bubble clogging (b) Image of air bubble inside cross slot 100 μm

Figure 5.24: Bubble clogging

pressure drop over a bubble can be calculated with equation ??.

$$\Delta P_b = P_r - P_l \tag{5.1}$$

Where P_l and P_r is the pressure on the left and right side of the air droplet. The pressure drop over the interface between the water and the air bubble is given by the equation:

$$\Delta P = \gamma_{lg}(\frac{1}{R} + \frac{1}{R}) \tag{5.2}$$

Where γ_{lg} is the surface tension of the liquid gas interface and R is the radius of the interface. The surface tensions between water and air equals 73.6 mN/m, following [Bruus, 2005]. If the radius of the drop on the left side is chosen $R_r = 50$ μm and the radius on the right side is chosen $R_l = 75$ μm, the pressure drop over the bubble equals 981 Pa. This means a pressure of 981 Pa is needed to push the bubble through the contraction and clear the channel. Since the cross slot has two inlet flows, the channel with a bubble inside can clog because the fluid will take the other channel, cause of the low resistance of the other channel. The places of the cross slot geometry where bubbles can clog the channel are shown in figure 5.25.

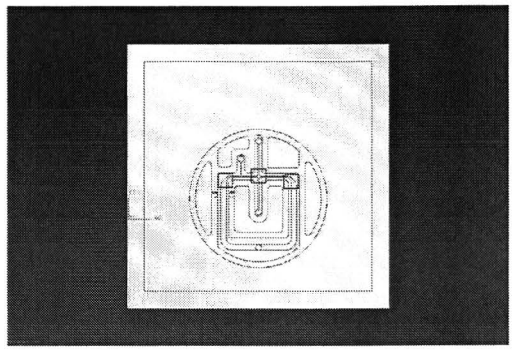

Figure 5.25: Problem areas of bubble clogging

The problem with the clogging air bubbles can be solved if the geometry of the cross slot is adapted. All the channels should have an equal width. Besides these places where the channels decreases or increases in width, also the inlet and outlet construction to the geometry can be improved. The entrance of the cross slot chip has a diameter of 4 mm and inside a chip the diameter goes from 4 mm to 1 mm. If an air bubble needs to go through this contraction. A clearance pressure is needed to push the bubble through this contraction. Also the inlet and outlet of the cross slot should be adapted, so air can easily leave the system is necessary. The inlet and outlet to the micro fluidic channels was horizontaal. If a certain angle can be used to remove air bubbles inside the inlet or outlet to the micro channels. If there was no air in the micro fluidic system the geometry of the cross slot was good. There was a steady flow inside the cross slot with a constant stagnation point.

The material used for the cross slot chip can also be improved to prevent air bubbles inside the micro fluidic system. PMMA is hydrophobic, which means that the water is not attracted to the PMMA. The way to measure if a material is hydrophobic or the opposite (hydrophilic) is to measure the contact angle of a droplet of liquid with the material [Port, 1999]. An image is show in figure A.37 of what is meant with the contact angle θ of a material.

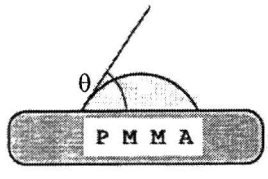

Figure 5.26: Contact angle θ [Port, 1999]

The manufacturing proces, surface treatment or surface roughness all influence the contact angle of a material. [Port, 1999]. The contact angle between water and PMMA is around 70 °, following [Nordstrom et al.]. There are ways to decrease the contact angle of PMMA, which will increase the attraction of water and will decrease the possible development of air bubbles in the micro channels. Following [Boricia et al., 2006] a plasma treatment (He + 10 % N_2) of the surface could reduce the contact angle of PMMA from 70 °to 45 °. An other

material could also be a solution to decrease the contact angle of the micro channel system. If SU-8 is used and treated with ethanolamine, the contact angle is around 25 °, following [Nordstrom et al.]. An disadvantage is that SU-8 can only be fabricated in thin sheets of material and is commonly used for lithography processing of micro structures. Glass will also be a good solution to decrease the contact angle. Glass has a contact angle with water of 14 °, following [Leijendeckers et al., 1998]. Only the proces to construct micro channels in glass is more complex and expensive than in a polymer. Besides the contact angle of PMMA, another problem are some sharp corners inside the construction of the micro valve and cross slot chip. These sharp corners could lead to trapping of air bubbles. Also the control of the flow inside the micro fluidic system is influenced if air bubbles are inside the system. The air can dissipate the pressure and influence the control of the flow inside the cross slot with the micro valve.

The channel structure of the cross slot chip are made using mechanical speed milling. The consequence is that the surface roughness is relatively high, Ra = 0.23404 μm, which could lead to secondary flow inside the micro channel. Because of the high surface to volume ratio of the micro fluidic cells stretcher, the bulk Poiseuille flow is typically accompanied by other surface-related physical or biochemical phenomena in the fluid [Bruus, 2005]. Therefore the roughness of the surface inside the channel could influence the flow inside the channel. From literature [Hsieh et al., 2004] it can be seen that the surface of the micro channel has influence on the Reynolds number, which leads to an earlier secondary flow than expected from the theoretical study. This could influence the flow field inside the cross slot and could lead to an instable stagnation point. A better fabrication proces is lithography in glass, but for the proof of principle a quick and easy way to make structures is speed milling in PMMA. An other improvement could be to make the micro channel structure in PDMS. First a negatieve mask of silicon has to be made and this can be used to fill with PDMS and cure, see reference [Mcdonald and Whitesides, 2002].

The middle of the cross slot is not easy to find. If a marker is made on the middle of the hight of the channel, with the microscope the marker can be used to focus in the middle of the cross slot. This will reduce the time needed to find the middle of the cross slot significantly.

In the end, a clinical solution is wanted for a quick and easy lab on chip analyses. Some features need to be constructed for a better measurement of the elasticity of the cell. The temperature of the experimental setup is room temperature 20 °C, but for better behavior of the cell the temperature should be 37 °C. Possible LED-lighting can be used to control the temperature of the cross slot chip. D. Gawlitta at the University of Eindhoven uses this technique for her thesis to keep the experimental setup at constant temperature. Another solution could be to integrate heating channels in the chip, through which hot liquid can transported heating the chip. Also a way to obtain disposable cross slot chip has to be found. The experimental setup needs to be cleaned after every experiment, which will cost a lot of time. Possibly the geometry can be produced with lithography. The actuators could be replaced by piezoelectric actuators designed on the chip. Piezoelectric actuators are already used for making micro pumps [Olsson, 1998], but also some concepts are designed for flow control [Roberts et al., 2003]. This can lead to a disposable chip which can be thrown away after every experiment.

5.4.2 Micro valve

The actuators of the micro valves where determined on the basis of assumptions that, later turned out to be not applicable. The total force needed to actuate the valve will be 0.4933 N. Because of this mistakes in the first calculations of the pressure inside the micro channels, another actuator was used for the micro valve. The moving mass of the actuator was assumed to be 0.6 Kg, which in reality is 0.01 Kg. Also the pressure inside the channel was calculated wrong. All these assumptions lead to a to strong actuator compared to the force needed to actuated the real valve. This leaded to the A12-17-000A of Bei Kimco. This choice was based on a required force of 10 N. This leaded to a piek force of 11.2 N. However the actuators are too strong, the accuracy of the voice coil actuator is still good for the actuation of the micro valve. Therefore no other actuator is needed to control the micro valve. For a new valve possibly a less strong actuator could also create enough force to actuate the micro valve membrane of PDMS. Bartels mikrotechnik is also working on a possible active flow control valve which will be commercial available in the spring of 2006. An advantage will be that even higher viscous fluids can be used inside the cross slot geometry, which can be helpful for other applications for the micro fluidic cell stretcher.

The PDMS membrane sealed well during actuation. The aluminium tips could be glued with silicone based glue but during tests some tips were broken of the PDMS membrane, because of the force applied by the actuator. Further investigation to improve the connection between the membrane and the actuator will be needed.

The Matlab simulink model to control the micro valves with the position of the cell inside the cross slot has to be finished. The system worked well for the movies and implementation in lunix works as well. The real time images from the camera should be should also be constructed under lunix. Further investigation on this subject is done by R. van Aalst and B. van Daal. The control of the micro valves manually worked als long as no air was inside the cross slot system. If one valve was closed, the stagnation point shifted almost instantly. Manually it was already possible, at low velocity of the flow (Re $\approx$ 0.1) to held a cell in the stagnation point. But increasing the flow and holding the cell in the stagnation point did not worked, because continuously the flow has te be controlled. If the micro valves can be used with automatically control, it can be concluded it will be possible to position the cell in the stagnation point with these micro valves. For the control of the system it is preferred to have one actuator that can control both micro valves at ones. With the two identical micro valves it is hard to control the flow lineair, this means that the total flow through the cross slot stays equal. Another kind of valve is designed. The membrane micro valve of the micro fluidic cell stretcher are controlling the system non-lineair. By the membrane the channel is squeezed, while the other channel is not opende equally. This causes pressure difference inside the micro fluidic system. If both channels are opened and closed, but the total exit area will be the same, the total flow through the system is constant and the pressure inside the micro fluidic system is constant. This means that the total flow through the cross slot is constant, but the stagnation point can be shifted with the micro valves. The flow can than be controlled lineair. This could contribute to a more stable stagnation point in the cross slot channel. A design has been made for a new valve that controls the flow linearly. A sketch of the principle of the lineair micro valve can be seen in figure 5.27.

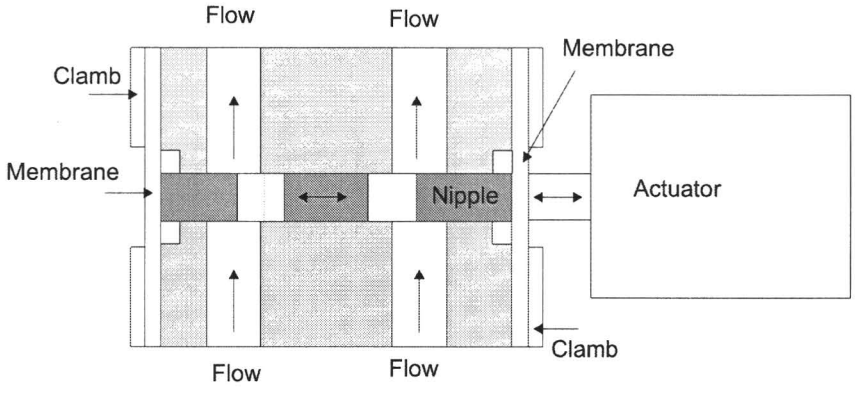

Figure 5.27: Principle lineair micro valve

In this concept a nippel is connected to two flexible membranes, which moved with a voice coil actuator. If the nippel is moved one fluidic channel is opened and the other is closed. When the valve is in it's center position, both channels are equally opened and the flow is the same in both channels. Drawings are shown in figure 5.28 for the concept of a new valve.

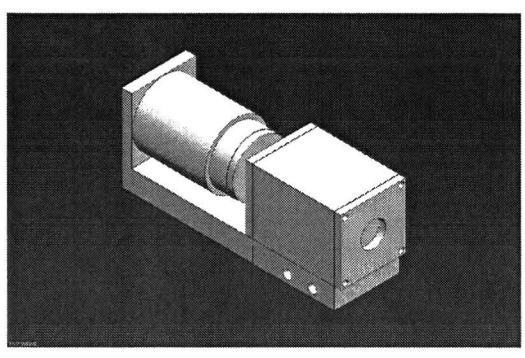

(a) d

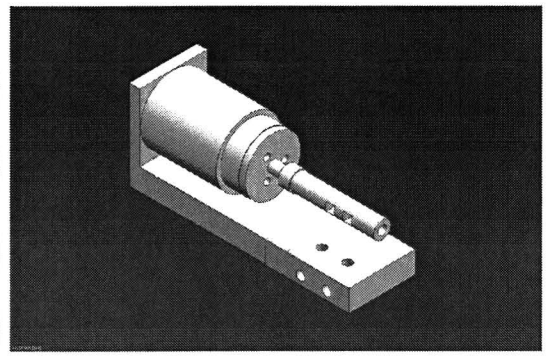

(b) d

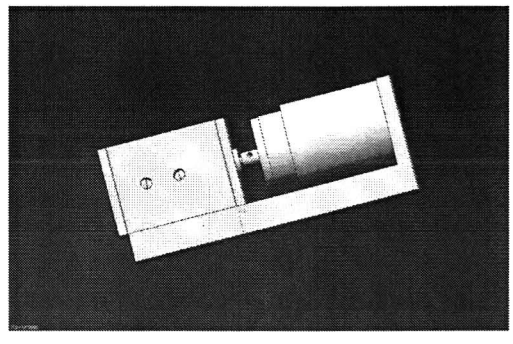

(c) d

Figure 5.28: Drawings of design of lineair micro valve

5.4.3 Other systems

The syringe pumps did provide a contant flow. The step size of the syringe pump is small enough for testing with micro fluidic devices. If the step size is seen in the micro fluidic channel, a small syringe can be used to decrease the volume a step size of the syringe pump. The syringe pumps can be controlled from a computer, but further investigation is needed how this can be constructed in the Matlab Simulink program of the control of the micro valves. If this program is ready it can be used to control the whole experimental setup or even program all the test conditions. The inlet of the cells can be programmed and the flow can be increased with the computer, in stead of manual.

The deformation of the cell can be measured on sub pixel level using the Matlab program for the determination of the Taylor deformation rate of the cell. The contrast between the background and the cell is sufficient, even if no fluorescent marker is used. However if no fluorescent marker is used, the cell has to be in the focal plane to have a good contrast between the background and the cell. This contrast is needed for the boundary trace of the Matlab program. If the cell is fluorescent, the boundary of the cell can easily be found. The program estimated from the boundary trace, the Taylor deformation rate with an accuracy of 0.0001.

Chapter 6

Discussion and conclusions

The micro fluidic cell stretcher is designed to deform single cells. Most of the mammalian cells form matrix clusters in the in vivo environment. For the micro fluidic cell stretcher the cells need to be chemically detached from other cells to stretch a single cell. The mechanical properties of a cluster of cells is different from the mechanical properties of a single cell, because the cells inside the cluster also interact with each other. This should be kept in mind when measuring the mechanical properties of cells with the micro fluidic cell stretcher.

The goal of designing an experimental setup for clinical application to measure cell elasticity is almost reached. The experiments prove that a fibroblast can be deformed with low Reynolds numbers inside a contraction of 400 μm to 25 μm. Also fibroblast deform inside a cross slot of 100 μm in the stagnation point, but also at the T-junction when flowing into the main channel of the cross slot. The flow can also be manipulate manually and the cell can be positioned in the stagnation point manually. If the micro valves can be controlled through the Matlab Simulink model, I assume the cell can also be held in the stagnation point of the cross slot. If the cell can be held in the stagnation point automatically, the flow can be increased and a deformation of the cell should be observed. An image can be made and afterwards the deformation of the cell can be determined. The deformation of the cell can be measured with a high speed camera or normal camera, depending on the imaging time needed for the experiment. With a magnification of 40, a Taylor deformation rate of 0.25 can be determined between 4 levels of deformation. With the Matlab program, deformation detection on sub-pixel level can be preformed, which increases the number of levels to detect the Taylor deformation rate. The measured Taylor deformation rate is determined with a accuracy of 0.0001. To measure the deformation of the cell will not be a problem. From literature the elasticity of the cell will correlated to the health state of the cell. The Young's modulus of a cancerous cell is even one order lower than of the same healthy cell. From the simulation it can be expected that the deformation of a cell, with shear modulus of 38 Pa is $D_{XY} = 0.2375$ and with a shear modulus of 380 Pa is $D_{XY} = 0.0245$. The difference of 0.213 can easily be detected with the Matlab program to determine the Taylor deformation rate of the cell.

From the numerical results the micro fluidic cell stretcher will work for the dimensional numbers Re = 0.1, De = 0.0526 and F_{RW}=0.05. The fibroblast, with a shear modulus of 380 Pa and a diameter of 10 μm will deform to D_{XY} = 0.0245. But if a cancerous cell will be used, the deformation will be D_{XY} = 0.2375. The experimental setup need to have the following features:

- Width of cross slot is 50 μm
- Velocity of the flow is 10 mm/s
- Density of the fluid is 1000 Kg/m^3
- Viscosity of the fluid is 0.01 Pa·s

The kind of cells needed for this experiment are fibroblasts. The viscosity of the PBS used inside the micro fluidic cell stretcher can be increase by using Dextran. To reach a velocity of 10 mm/s the flow rate of the syringe pump has te be equal to 1.74 μl/min. This is no problem for the syringe pump, almost the same flow rate already used for the experiments. This flow rate results in a pressure gradient inside the micro fluidic cell stretcher is of $\approx$ 26.6 Pa, following the numerical model. If the micro channels are close permanent with glue or even anonic bounding, this pressure will not be a problem for the cross slot chip. This pressure results in a tension on the cover plate of $\approx$ 26.6 mN/mm^2. Following the numerical model the pressure induced by the elongational flow on the surface of the cell is 26.6 Pa which induced a force on the cell of 0.42 mN. The stress in the cell induced by the elongational flow external on the cell equals 5.7 mN/mm^2. If this is compare to the optical tweezer, the pressure on the cell is three times smaller than induced by the optical stretcher. The optical stretcher can induce a stress on the cell surface of 1 Pa to 150 Pa caused by a laser power of 0.2 to 1.4 W, following [Cunningham et al., 2002]. The pressure on the surface of the cell is around the same order of magnitude as induced with the optical tweezer. The pressure of the fluid flow can be increased if the velocity is increased. This can be done because the Reynolds number was 0.1 and can be increased to a maximum of 1. Further investigation is needed to determine the loading range of the micro fluidic cell stretcher.

In practise, from experimental results it can be concluded that the cell will deform faster than predicted in the numerical model. From the comparison between the numerical results and the experimental results can be concluded that the cell is already deforming, while the numerical model predicts much lower deformations. More experiments need to be done with the cross slot chip of 100 μm needs to be preformed to be sure if the deformation of the cell can be measured with the 100 μm geometry. If the control system of the micro valves is ready, the micro valves can be glued to the cross slot chip to prevent the leakage between the cross slot chip and the micro valve. If the cell is held in the stagnation point with the micro valves and the fluid flow is increased, the cell may already be deforming due the elongating flow. The cells also deform when the cells enter the main flow of the cross slot and with hydro focusing. I would prefer further investigation with the 100 μm cross slot and if this does not give enough deformation of the cell, follow the numerical features for the new experimental setup and make a cross slot geometry with a main channel of 50 μm.

In the future if a reliable measurement is needed the experimental setup. Before the micro fluidic cell stretcher is reliable, first needs to be calibrated. The micro valves need to be calibrated to the displacement of the stagnation point. More PIV measurements are to know the flow velocity inside the cross slot at a several flow rates of the syringe pump. This provides the information needed for the numerical model to determine how the cell will deform inside the micro fluidic cell stretcher at certain flow rates of the pump. The numerical model needs to be calibrated on the real deformation observed with the experiments. If the numerical model is working properly, the deformation of the cell can be predicted with the numerical model at several flow rates. The first test that needed to be done is to measure two different cells, where the elastic properties are different known from literature. For example a fibroblast and an chondrocyte can be used. The chondrocyte has a higher elastic modulus than the fibroblast and will deform less in the micro fluidic cell stretcher. This measurement should result in an significant different Taylor deformation rate between the two cells for the same flow rates. Important for the reliable measurement is that all the circumstances are equally. This means that:

- Flow rates of the experiments are equal.
- Osmotic pressure of fluid between experiments is equal.
- Temperature of the environment is equal between experiments.
- Imaging time and resolution of the image is equal between experiments.
- Imaging the same focal plane between experiments, this is the middle of the height of the channel.

If everything is controllable the samples needed to measure the illness of the cells needs to be determined. The more cells needed to measure, the longer the experiment will taken, the less distribution of the measurement. The deviation of the measurement has to be investigated due the measurement of an single kind of cell and study the spreading of the measured deformations. For the determination of a significante difference between cells, sufficient samples (measurements of cells) are needed to test the hypothese. For an reliable measurement also the shape of the cells need to be identified, the cell is chosen to have an initial spherical shape. In reality the cell could have another shape. If the cell is turning around in the micro fluidic channel, a deformation can be measured due the shape of the cell. This required further investigation to determine the spherically of the cell in the fluid and study the influence of the shape of the cell on the measured Taylor deformation rate.

6.1 Recommendations

For the future work some recommendations can be made with respect to the experimental setup:

Air bubbles The design and material have to be improved to decrease the chance of clogging the micro fluidic system by air bubbles. All the micro fluidic channels should have equal width and depth, so no air bubble can clog the channel. Also the inlet and the outlet of the cross slot chip to the micro structure can be improved. The channels can be made under a certain angle, so air can be removed when it is in the inlet or outlet of the cross slot chip. In the design all sharp edges inside the channels need to be replaced by smooth edges, so no air bubble could get trapped inside corners. The material PMMA could be replaced by US-8 or glass to decrease the contact surface angle. Also an integration of the micro valves is recommended for a disposable chip and properly closed system. For the actuation of the membrane a piezoelectric actuation could give a solution.

Temperature control The experimental setup needs to have a temperature controlled environment at 37 °C. This can be done with LED-lighting or heating channels.

Dextran If the deformation of the cell is too small, Dextran can be used in the culture to increase the viscosity of the culture, which will increase the deformation of the cell according to the simulations. Tests has to be done to study the influence of the Dextran on the cell behavior.

Marker z-position Marker on the cross slot chip, to use as reference to focus in the middle of the height of the channel.

Permanent closed micro channels The micro channels can be closed with an ultra violet hardening glue. If the chip is made out of glass, also anonic binding can be used to close the micro channels. The micro channels can easily be cleaned with ethanol. If the cover glass do need to be removed the vacuum system needs to be improved. I suggest to make first a rubber like material on top of the chip (like PDMS), then make the micro channels inside the material. Vacuum channels should be on both sides of the micro fluidic channel. The rubber like material seals the micro fluidic channels and thus leakage will not happen between the micro fluidic channel an the vacuum channel.

Improve control micro valve The Matlab Simulink model needs to be improved. The model worked properly only the interaction with the camera had to be solved. If the Matlab Simulink model works, the micro valves need to be characterized on the displacement of the stagnation point. The syringe pumps should be able to be controlled from the computer. This function is possible with the syringe pumps used for the experiments, but further investigation is needed to implement the control in the Matlab Simulink model. Also can the micro valve itself can be optimize from a non-lineair valve to a lineair valve, so better control of the flow can be reached. The two separately valves need to be replaced by one valve that keeps the total flow through the cross slot constant.

If the experimental setup is working, more test with the experimental setup need to be done. First two different cells can be used to study the deformation at the same flow rate. For example a fibroblast and a chondrocyte cell can be used. From the literature a significant difference should be observe. If this is working, a healthy and a cancerous cell can be used for the experiment. Of key important is to determine the shape of the cell in the fluid. Important for the reliable measurement is how spherically the cell really is. A study needs to be done on the shape of cells inside fluids and the influence of different shapes on the measured Taylor deformation rate needs to be done.

For the model the following recommendations can be made:

Three dimensional The two dimensional model needs to be expanded to a three dimensional model.

Structural model In the numerical model the cell should be modeled with a structural model, which contains the several filaments and their mechanical properties. Also the interaction between the several filaments needs to be modeled and characterize.

Surface tension cell From experiments it should be found if the surface tension of the cell has influence on the deformation inside the micro fluidic cell stretcher. From the dimensional analysis it has been found that the shear modulus is equally important than the surface tension. However the characterizing length scale used to determine the dimensionless numbers could also be different in reality.

Mesh adaptation Mesh adaptation can be used to make the boundary between the fluid and solid interface conforming during the simulation.

If the micro fluidic cell stretcher setup is working. The measured deformation of the cell can be compared to the numerical results. Test needs to be done to study if the parameters are validate for the micro fluidic cell stretcher. First I should take a look at the shear modulus of the system, because every measure technique results in different elastic properties for the same kind of cell. Kind of measurement, environment and model all have influence on the value of the shear modulus of the cell. No reference could be found for this measurement technique, because it has been never preformed before, micromanipulation had been chosen as reference for the shear modulus. Since micromanipulation has been used as a reference for this model, this could explain the difference between the numerical and experimental results. The second thing that have to be investigated is the influence of the surface tension of the cell on the deformation inside the micro fluidic cell stretcher. Important is that if the experimental setup is working, the numerical model can be improved to a validate model of the micro fluidic cell stretcher.

6.2 Opportunities

In the future the micro fluidic cell stretcher can be used to determine if possible disease will develop or not. Not only cancer can be detected, but also other diseases could be possibly detected with this device. It will be a less destructive way to measure the cell elasticity. With the cross slot geometry also durability test can be preformed on the cells. For a high through put, the automatic control of het valve could help to increase the through put of the cross slot flow. Also hydro focusing could give a very high throughput, but the imaging time for the deformation of the cell is limited, and the cells need to be in the focal plane, which is difficult to define.

If it is possible to deform cells, it maybe also can be possible to stretch cells beyond the adaptive region. So the cell wall will break an cell lysing can be possible. When the cell wall break, DNA is released from the cell. The DNA can be used for further analysis. This technique can be integrated in a micro fluidic system for a controlled way of cell lysing.

Another application for the micro fluidic cell stretcher is for the research of droplets coalescence and break up on micro scale. Here the cross slot chip with a main channel of 500 μm can be used. W. Buysse, R. van Aalst, B. van Daal and M. Thissen are working on a project to use the micro fluidic cell stretcher for the droplets coalescence and break up on micro scale. Some experiments are already done with the micro fluidic cell stretcher to make droplets inside the cross slot. Figure 6.1 shows droplets of water dispersing inside Wacker AK1000, which is a silicon oil is a viscosity of 1 Pa·s.

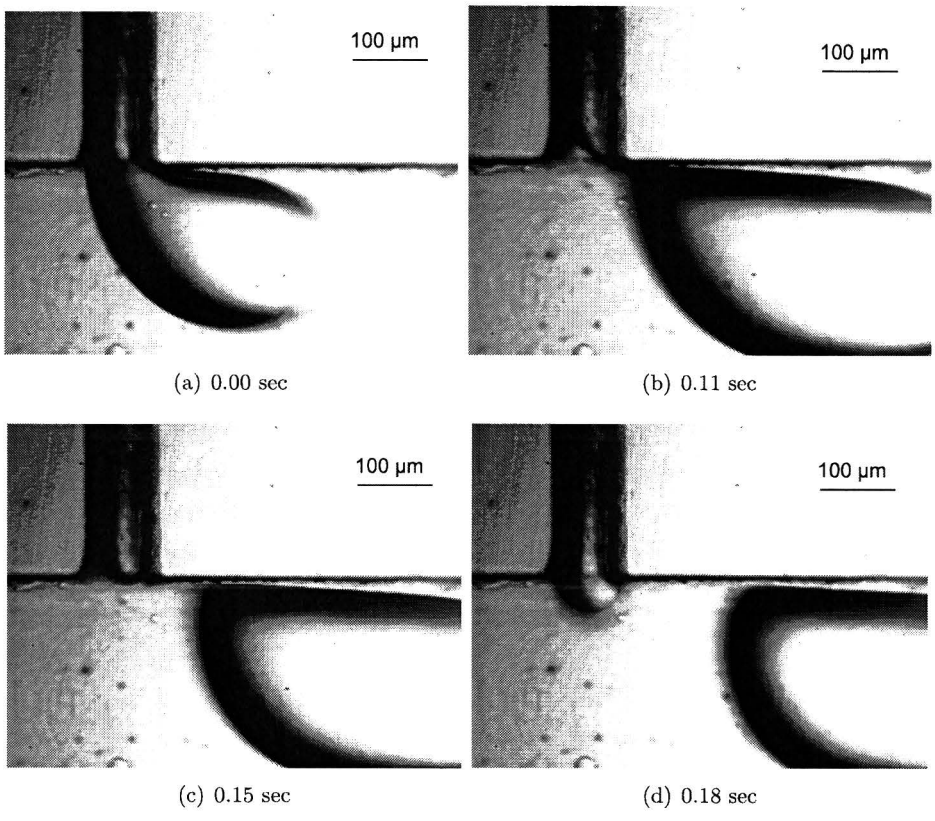

(a) 0.00 sec (b) 0.11 sec

(c) 0.15 sec (d) 0.18 sec

Figure 6.1: Formation of a water droplet in Wacker AK1000 with the T-junction

Because highly viscous fluids are used to research the coalescence and break up of droplets, an advantage of the strong actuator is that the valve can also be used for these high viscous liquids. The vacuum system on one side of the micro fluidic channel closed the fluidic system worked for the relative high viscosity of 1 Pa·s. Only sometimes during the experiments the cover glass came detached from the cross slot chip. For this application the cross slot structure needs to be opened, because the high viscous liquid can not easily be removed out of the micro fluidic system. The only difference between this application and the micro fluidic cell stretcher is that droplets are positioned inside the stagnation point instead of cells. An advantage of droplets break up and coalescence on micro scale compared to other experimental setups is the use of small amount of materials, which are relative expensive. Some images of air bubbles deforming and breaking up inside the cross slot of 500 μm can be seen in figure 6.2.

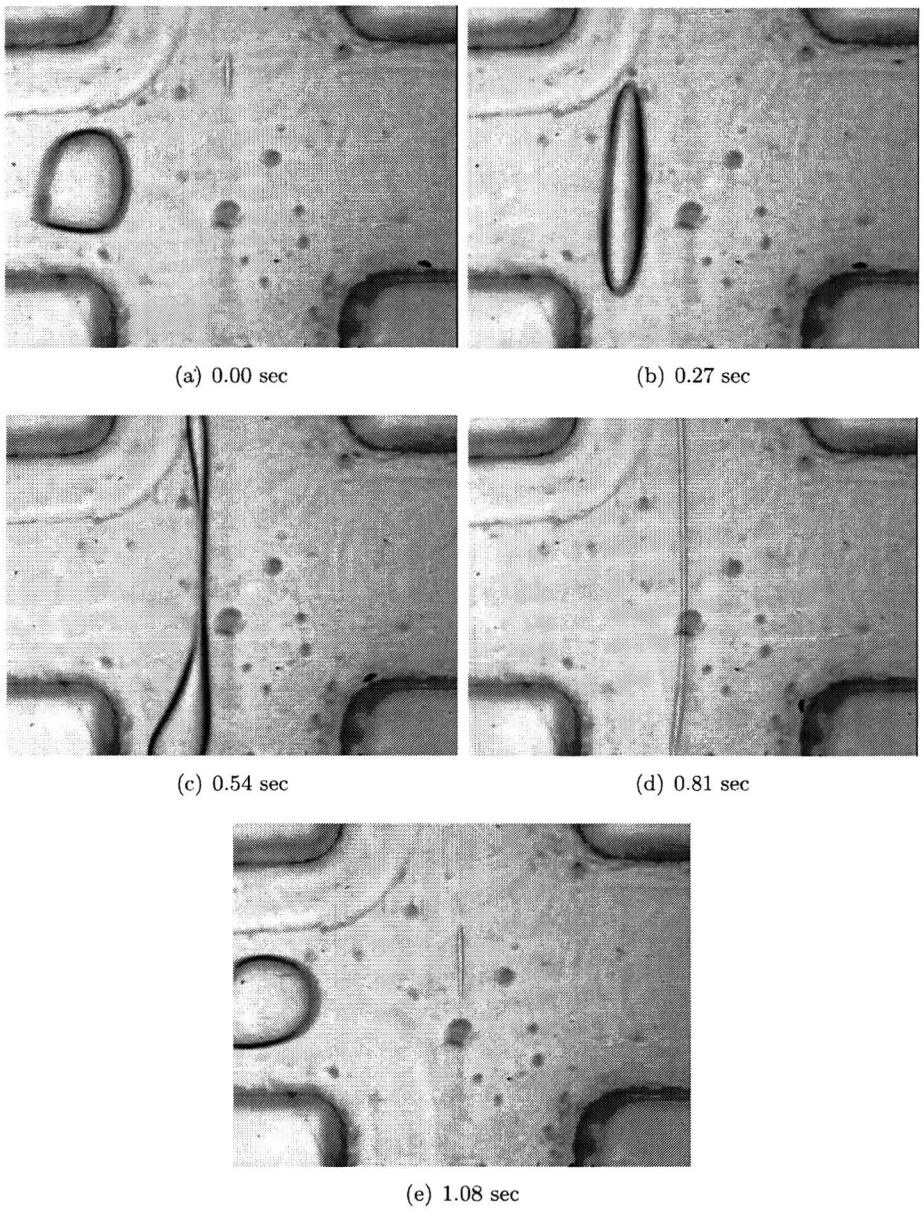

(a) 0.00 sec (b) 0.27 sec

(c) 0.54 sec (d) 0.81 sec

(e) 1.08 sec

Figure 6.2: Break up of air droplet in Wacker AK1000 in cross slot of 500 μm

Bibliography

K.M. Ainslie, J. S. Garanich, R. O. Dull, and J. M. Tarbell. Vascular smooth muscle cell glycocalyx influence shear stress-mediated contractile response. *Journal of applied physiology*, 98, 2005.

R. Ananthakrishnan, J. Guck, F. Wottawah, S. Schinkinger, B. Lincoln, M. Romeyke, and J. Käs. Modelling the structural response of an eukaryotic cell in the optical stretcher. *Academy of sciences of the Czech Republic*, 1998.

M.D. Antonik, N.P. D'Costa, S. Nageswaran, C. Schoenenberger, E. A-Hassan, W.F. Heinz, and J.H. Hoh. Relative microelastic mapping of living cells by atomic force microscopy. *Biophysical Journal*, 74, 1998.

D. Armani, C. Liu, and N. Aluru. Re-configurable fluid circuits by pdms elastomer micromachining. *Micro Electro Mechanical Systems Journal*, 1, 1999.

K.A. Athanasiou, E.J. Koay, and A.C. Shieh. Creep indentation of single cells. *Journal of biomechanical engineering*, 125, 2003.

D.J. Beebe, G.A. Mensing, and G.M. Walker. Physics and applications of microfluidics in biology. *Annual Review of Biomedical Engineering*, 4, 2002.

G. Boricia, N. Dumiutrascu, and G. Popa. Interaction of biological liquids with medical polymer films treated by dielectric barrier discharge. *Plasma physics laboratory, Romania*, Topic 10, 2006.

C.V.C. Bouten. Cell mechanica lecture notes. *Eindhoven University of Technology*, 2004.

H. Bruus. *Theoretical microfluidics.* Departement of micro and nanotechnology, technical university Denmark, 2005.

Cambrex. Cambrex bio sience walkersville inc. Website, 2005. `http://www.cambrex.com`.

T. Cubaud and C. Ho. Transport of bubbles in square micro channels. *Journal of physics of fluids*, 16, 2004.

C.C. Cunningham, J. Guck, R. Anathakrishnan, and J. Käs. Stretching biological cells with light. *Journal of physics: condensed Matter*, 14, 2002.

J.A. Dantzig and C.L. Tucker. *Modeling in materials processing.* Number ISBN 0-521-77923-5. Cambridge University Press, 2001.

J. de Hart, G.W.M. Peters, P.J.G. Schreurs, and F.P.T. Baaijens. A three dimensional computational analysis of fluid structure interaction in the aortic valve. *Journal of biomechanics*, 36, 2003.

Dextran. Dextran properties. Website, 2005. http://www.dextran.net.

J. Donea, A. Huerta, J.P.h. Ponthot, and A. Rodriquez-Ferran. Arbitrary lagrangian eulerian methods (ale). *Encyclopedia of computational mechanics*, 1, 2004.

Y.F. Dufrêne. Atomic force microscopy, a powerful tool in microbiology. *Biotechnology Letter*, 22, 2000.

C.D. Eggleton and A.S. Popel. Large deformation of red blood cell ghosts in a simple shear flow. *Physics of fluids*, 10, 1998.

A. Engler, L. Bacakova, C. Newman, A. Hategan, M. Griffin, and D. Disher. Substrate compliance versus ligand density in cell on gel responce. *Biophysical journal*, 86, 2004.

S.J. Frank, L. Pedrotti, and L.S. Pedrotti. *Introduction to optics second edition.* Number ISBN 0-13-501545-6. Prentice Hall, 1993.

D. Gil, J. Lekki, Z. Stachura, M. Lekka, P. Laidler, and A.Z. Hrynkiewicz. Elasticity of normal and cancerous human bladder cells studied by scanning force microscopy. *Eur Biophys J*, 28, 1999.

W.H. Goldmann. Mechanical manipulation of animal cells: cell indentation. *Biotechnology Letter*, 22, 2000.

R. Halir and J. Flusser. Numerically stable direct least squares fitting of ellipses. *Academy of sciences of the Czech Republic*, 1998.

R.M. Hochmuth. Micropipette aspiration of living cells. *Journal of biomechanics*, 33, 2000.

S. Hsieh, C. Yi Lin, C. Feng Huang, and H. Hsiu Tsai. Liquid flow in a micro channel. *Journal of micromechanics and microenginering*, 14, 2004.

J. James and H.J. Tanke. *Biomedical light microscopy.* Number ISBN 0-7923-0946-4. Kluwer Academic Publishers, 1991.

P.A. Janmey, T. Yeung, and L.A. Flanagan. Effect of substrate stiffness on cell morphology. *Bioengineering conference ASME*, 50, 2001.

J.G.M. Janssen. *Super critical fluid chromalo graphy in packed and open tubular columns.* Technical University Eindhoven, 1991.

J. Kas and J. Gunk. Stretching cells to detect cancer. *Internet journal of emerging medical technologies*, 20 June, 2005.

Bei Kimco. *Application guide voice coil actuators, Bei Kimco.* Bei kimco, 2005.

M.M. Knight, D.A. Lee, D.L. Bader, T. Ohashi, and M. Sato. Deformation properties of articular chondrocytes: A critique of three saparate techniques. *Biorheology*, 39, 2002.

P. Lamoureux, D.E. Ingber, S.R. Heidemann, and R.E. Buxbaum. Opposing views on tensegrity as a strutural framework for understanding cell mechanics. *J Appl Physiol*, 89, 2000.

T.A. Laursen, L.G. Alexopoulos, W.R. Trickey, F.P.T. Baaijens, and F. Guilak. Determination of the piosson's ratio of the cell: Recovery properties of chondrocytes after release from complete micropipette aspiration. *J. Biomech.*, Accepted, 2005a.

T.A. Laursen, F.P.T. Baaijens, W.R. Trickey, and F. Guilak. Large deformation finite element analysis of micropipette aspiration to determine the mechanical properties of the chondrocyte. *Annals of Biomedical Engineering*, 33, 2005b.

K.N. Lee. A study on the feasibility of a micro piv test setup for the investigation of flow through micro channels. *Eindhoven University of Technology*, 2005.

P.P.H. Leijendeckers, J.B. Fortuin, F. van Herwijnen, and H. Leegwater. *Poly Technisch zakboekje.* Number ISBN 90-6228-266-0. koninklijke PBNA polyboekjes, 1998.

J. Lewis, M. Raff, K. Roberts, B. Alberts, D. Bray, and J. D. Watson. *Molecular biology of the cell third edition.* Number ISBN 09-8153-1619-4. Garland publishing inc, 1994.

H. Mahmood, T.J. Moon, C.C. Cunningham, J. Guck, R. Ananthakrishanan, and J. Käs. The optical stretcher: A novel laser tool to micro manipulate cells. *Center for Nonlinear Dynamics, Department of Physics, University of Texas at Austin*, 81, 2001.

R.M. Markosyan, G.B. Melikyan, and F.S. Cohen. Tension of membranes expressing the hemagglutinin of ilfuenza virus inhibits fusion. *Biophysical journal*, 77, 1999.

B.S. Massey. *Units, dimensional analysis and physical similarity.* Number ISBN 0-442-05178-6. Van Nostrand Reinhold Company, 1971.

J.C. Mcdonald and G.M. Whitesides. Polydimethylsiloxane as a material for fabricating microfluidic devices. *Accounts of chemical research*, 35, 2002.

C.D. Meinhard, D.J. Beebe, J.G. Santiago, S.T. Wereley, and R.J. Adrian. A particle image velocimetry system for microfluidics. *Experiments in fluids*, 25, 1998.

C.D. Meinhart and S.T. Wereley. The theory of diffraction limited resolutionin microparticle image velocimetry. *Meas. Sci. Technol.*, 14, 2003.

E. Mitsoulis and S.G. Hatzikiriakos. Bagley correction: the effect of contraction angle and its prediction. *Rheol Acta*, 42, 2003.

T.J. Moon, C.C. Cunningham, J. Guck, R. Ananthakrishnan, and J. Käs. Optical deformability of soft biological dielectrics. *Center for Nonlinear Dynamics, Department of Physics, University of Texas at Austin*, 84, 2000.

S.J. Morgan and D.C. Darling. *Animal cell culture.* Number ISBN 1-872748-16-3. BIOS scientific publishers limited, 1993.

C.E. Morris and U. Homann. Cell surface area regulation and membrane tension. *Journal membrane biology*, 179, 2000.

T. Nisisako, T. Torii, and T. Higuchi. Formation of liquid droplets in a microchannelnetwork for microreactor applications. *Department of precision engineering, University of Tokyo*, 2002.

M. Nordstrom, R. Marie, M. Calleja, and title= A. Boisen.

A. Olsson. *Valve-less diffuser micropumps.* Number ISSN 0281-2878. Departement of signals, sensors and systems, Royal institute of technology, 1998.

E.A.G. Peeters. *Biomechanics of single cells under compression.* Number ISBN 90-386-2925-7. Technical University Eindhoven, 2004.

N.O. Petersen, W.B. McConnaughey, and E.L. Elson. Dependence of locally measured cellular deromability on position on the cell, temperature and cytochalasin b. *Cell Biology*, 79, 1982.

E. Planus-Redouan, F. Martial, B. Daniel, I. Valérie, M. Laurent, S. Hénon, and F. Gallet. Assessment of mechanical properties of adherent living cells by bead micromanipulation: Comparison of magnetic twisting cytometry vs optical tweezers. *Journal of biomechanical engineering*, 124, 2002.

M.J.A. Port. Contact lens surface properties and interactions. *Optometry today*, 1, 1999.

C. Pozrikidis. *Modeling and simulation of capsules and biological cells.* Number ISBN 1-58488-359-6. Chapman and Hall CRC, 2003.

D. Raucher and M.P. Sheetz. Cell spreading and lamellipodial extansion rate is regulated by membrane tension. *Journal of cell biology*, 148, 2000.

D.C. Roberts, H. Li, J.L. Steyn, O. Yaglioglu, M. Spearing, M.A. Smidt, and N.W. Hagood. A piezoelectric microvalve for compact, high frequency, high-differential pressure hydraulic micropumping systems. *Journal of microelectromechanical systems*, 12, 2003.

S. Schinkinger, F. Wottawah, D. Mitchell, S. Ulvick, C. Bilby, B. Lincoln, H.M. Erickson, and J. Guck. Deformability-based flow cytometry. *Institute for soft matter physics, University of Leipzig, Leipzig, Germany*, 2003.

J.F.M. Schoonen. *Determination of rheological constitutive equations using complex flows.* Number ISBN 90-386-0740-7. FEBO druk, 1998.

P.P.J.M. Schram, G.J.F. van Heijst, and M.E.H. van Dongen. *Fysische transportverschijnselen voor werktuigbouwkunde.* Number College dictaat. Technical University Eindhoven, 1994.

G. Segal. *Sepran.* Technical University Eindhoven, 2004.

A.C. Sheih and K.A. Athanasiou. Principles of cell mechanics for cartilage tissue engineering. *Annals of biomedical engineering*, 31, 2003.

J.P. Shelby, J. White, K. Ganesan, P.K. Rathod, and D.T. Chiu. A microfluidic model for single cell capillary obstruction by plasmodium falciparuminfected erythrocytes. *PNAS*, 100, 2003.

S. Shoji and M. Esashi. Microflow devices and systems. *Journal microenginering*, 4, 1994.

D.L. Spector, R.D. Goldman, and L.A. Leinwand. *Cells a laboratory manual.* Number ISBN 0-87969-522-6. Cold Spring Harbor Laboratory Press, 1997.

T.M. Squires and S.R. Quake. Microfluidics: fluid physics at the nanoliter scale. *Reviews of modern physics*, 77, 2005.

Y.W. Stegeman. *Time dependent behavior of droplets in elongational flows.* Number ISBN 90-386-2953-2. Technical University Eindhoven, 2002.

Y. Tardy, J. Meister, N. Caille, and O. Thoumine. Contribution of the nucleus to the mechanical properties of endothelial cells. *Journal of biomechanics*, 35, 2002.

O. Thoumine and A. Ott. Time scale dependent viscoelastic and contractile regimes in fibroblasts probed by microplate manipulation. *Journal of cell science*, 110, 1997.

O. Thoumine, O. Cardoso, and J. Meister. Changes in the mechanical properties of fibroblasts during spreading: a micromanipulation study. *Eur Biophys J*, 28, 1999.

B.D. Uhal, C. Ramos, I. Joshi, A. Bifero, A. Pardo, and M. Selman. Cell size, cell cycle, and a-smooth muscle actin expression by primary human lung fibroblasts. *American Physiological Society*, 1040-0605/98, 1998.

C.C. van Donkelaar, M.A. Danils, and J.M.R.J. Huyghe. Cell deformation in responde to long term hyperosmotic loading. *Acta Bioeng Biomech*, 5, 2003.

R. van Loon. *A 3d method for modelling the fluid structure interaction of heart valves.* Number ISBN 90-368-2687-8. Universiteitsdrukkerij TU Eindhoven, 2005.

R. van Loon, P.D. Anderson, F.N. van de Vosse, and F.P.T. Baaijens. A combined fictious domain adaptive meshing method for fluid structure interaction of heartvalves. *International Journal for Numerical Methods in Fluids*, 46, 2004.

S.T. Wereley, C.D. Meinhard, and J.G. Santiago. Micron resolution velocimetry techniques. *Developments in laser techniques and applications to fluid mechanics*, 1998.

S.T. Wereley, C.D. Meinhard, and J.G. Santiago. Piv measurements of a microchannel flow. *Experiments in fluids*, 27, 1999.

J. Westerweel. Fundamentals of digital particle image velocimetry. *Meas Sci Technol*, 8, 1997.

C. Yamahata, C. Lotto, E. Al-Assaf, and M.A.M. Gijs. A pmma valveless micropump using electromagnetic actuation. *Journal microfluid nanofluid*, 1, 2005.

Z. Zhang, C.R. Thomas, and C. Cowen. Micromanipulation measurements of biological materials. *Biotechnology Letter*, 22, 2000.

M. Zivkovic-Ben, F. Srboljub, M. Mijailovich, M. Kojic, and J. Fredberg. A finite element model of cell deformation during magnetic bead twisting. *J Appl Physiol*, 93, 2002.

Appendix A

Loading of single cells: techniques

Partial or full micropipette aspiration

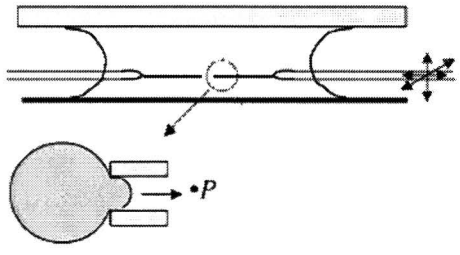

Figure A.1: Principle of micropipette aspiration [Hochmuth, 2000]

A cell is deformed using a micropipette and pressure to suck the cell inside the micropipette. See figure A.1 for the principle of micropipette aspiration. A cell is partially inside the micropipette, and there is a mathematical model that describes the theoretically predicted deformation of the cell. If the experimental data is fit with the theoretically predicted deformation, the Young's modulus (E) can be determined. In figure A.2 a chondrocyte cell is partially inside the micropipette.

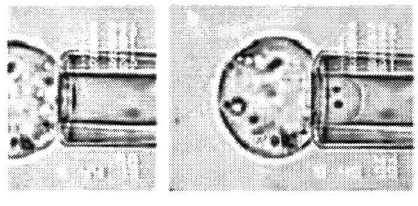

Figure A.2: Image chondrocyte partial micropipette aspiration [Laursen et al., 2005b]

Also full aspiration inside the micropipette can be described by a theoretical deformation model and can be used to estimate the Young's modulus of the cell. Figure A.3 shows pictures of two different cells (neutrophil and chondrocyte) before and after full aspiration.

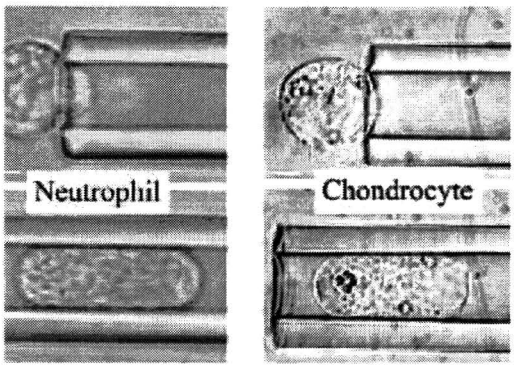

Figure A.3: Image full micropipette aspiration [Hochmuth, 2000]

Figure A.3 shows the difference between the two cells. The conditions are scaled such that the external force on the cell is the same. This needs to be done, because of the difference in diameter between Neutrophil (8 μm) and chondrocyte (12 μm $-$ 16 μm). Neutrophil expands more than chondrocyte which indicates that chondrocyte has a higher Young modulus compared to Neutrophil.

A nonlinear finite element analysis of the micropipette experiment was performed using several constitutive models. Neglecting the effect of inertia terms and body forces, the governing momentum equation is expressed as in equation A.1, following [Laursen et al., 2005a].

$$\nabla \cdot \boldsymbol{\sigma} = \mathbf{0} \tag{A.1}$$

For the cell a compressible Neo-Hookean model was used, see equation A.2 [Laursen et al., 2005a].

$$\boldsymbol{\sigma} = \kappa(J-1)\mathbf{I} + \frac{\boldsymbol{B}}{J}(\mathbf{B} - J^{\frac{2}{3}}\mathbf{I}) \tag{A.2}$$

Where:

$\mathbf{F}$: The deformation tensor is described by equation A.3

J : The volume ratio is described by equation A.4

$\mathbf{B}$: The Cauchy-Green tensor is described by equation A.5

κ : The compressibility modulus is described by equation A.6 (E is Young's modulus and ν is Piosson's ratio)

G : The shear modulus is described by equation A.7

$$\mathbf{F} = (\vec{\nabla}_0 \vec{x})^T \tag{A.3}$$

$$J = det\mathbf{F} \tag{A.4}$$

$$\mathbf{B} = \mathbf{F} \cdot \mathbf{F}^T \tag{A.5}$$

$$\kappa = \frac{E}{3}(1 - 2\nu) \tag{A.6}$$

$$G = \frac{E}{2(1+\nu)} \tag{A.7}$$

Incompressible behavior is assumed results that equation A.4 gives $J = 1$ or the Poisson's ratio is $\nu = 0.5$. The model for the micropipette experiment reduces to equation A.8, following [Laursen et al., 2005a]:

$$\boldsymbol{\sigma} = -p\mathbf{I} + \boldsymbol{\tau} \tag{A.8}$$

where:

$$\boldsymbol{\tau} = G(\mathbf{B} - \mathbf{I}) \tag{A.9}$$

Because cells have a time dependent behavior during micropipette aspiration, a two mode viscoelastic model is used to describe this behavior. The viscoelastic model is described by the equation A.10, following [Laursen et al., 2005a]:

$$\boldsymbol{\sigma} = \boldsymbol{\sigma}_e + \boldsymbol{\tau}_v \tag{A.10}$$

where:

$\boldsymbol{\sigma}_e$: The elastic response only described by equation A.2

$\boldsymbol{\tau}_v$: The viscoelastic response described by a compressible upper convected maxwell model, described by equation A.11

$$\frac{\nabla}{\boldsymbol{\tau}_v} + \frac{1}{\lambda}\boldsymbol{\tau}_v = 2G\mathbf{D} \tag{A.11}$$

Where:

$\mathbf{D}$: The deviatoric part of the rate of deformation tensor described by equation A.12

λ : The relaxation time of the viscoelastic mode.

$$\mathbf{D} = \frac{1}{2}(\dot{\mathbf{F}} \cdot \mathbf{F}^{-1} + \mathbf{F}^{-1} \cdot \dot{\mathbf{F}}^{T}) \tag{A.12}$$

The time depended behavior of the cell during micropipette aspiration can be captured by this theory. Assuming isotropic and constant permeability, the governing equations may be cast into, following [Laursen et al., 2005a]:

$$\nabla \cdot \boldsymbol{\sigma} - \nabla p = \mathbf{0} \tag{A.13}$$

$$\nabla \cdot \boldsymbol{v} - \nabla \cdot k \nabla p = \mathbf{0} \tag{A.14}$$

where:

$\boldsymbol{\sigma}$: The stress tensor of the solid phase

$\boldsymbol{v}$: The velocity of the solid phase

k : The permeability coefficient

p : The pressure

The interaction between the solid and fluid is described by the Darcy'Law by the equation A.15, following [Laursen et al., 2005a]:

$$\boldsymbol{v}_f - \boldsymbol{v} = -k \nabla p \tag{A.15}$$

where:

$\boldsymbol{v}_f$: The velocity of the fluid

The stress tensor for the solid phase may either be described by the compressible Neo-Hookean model (equation A.2) or the two-mode viscoelastic model (equations A.10 and A.11)

During the micropipette aspiration experiments, the cell is exposed to a fluid pressure, Δp, within the micropipette. The surface traction on the part of the boundary of the cell that is within the micropipette is therefore found from the hydrostatic pressure and the surface normal to the cell. As the cell is aspirated into the micropipette with increasing pressure, the surface normal vectors change with the evolving cell shape. Through iterations a numerical model is made for the deformation of the cell during micropipette aspiration. The normalized aspiration length for a viscoelastic model is described by the equation A.16. [Laursen et al., 2005b]

$$\frac{A}{R_p} = \frac{\Phi \Delta p}{\pi k_1}\left(1 - \frac{k_2}{k_1 + k_2} e^{-\frac{t}{\tau}}\right) \tag{A.16}$$

where:

t : Time

Δp : Applied pressure

A : Aspiration length

R_p : Inner radius of micropipette

Φ : Wall function identified as 2.1 from experimental research

k_1 , k_2 : Viscoelastic parameters

The parameters k_1, k_2 and τ where fitted to the experimental results. The Poisson ratio can be determent through complete aspiration inside the micropipette and subsequent sudden release of the cell [Laursen et al., 2005a]. The cell needs some time to return to its original shape. By fitting the experimental data to the theoretically predicted cell response, the Poisson's ratio and the viscoelastic recovery properties of the cell can be determined.

If a elastic model is used for the cell, the normalized aspiration length is described by equation A.17, following [Laursen et al., 2005b]:

$$\frac{A}{R_p} = \frac{3\Delta p \Phi}{2E\pi} \tag{A.17}$$

Where:

E : The Young's modulus

With equation A.17 the Young's modulus of the cell can be determined by fitting the experimental data to the numerical model.

Cell indentation or cell poking

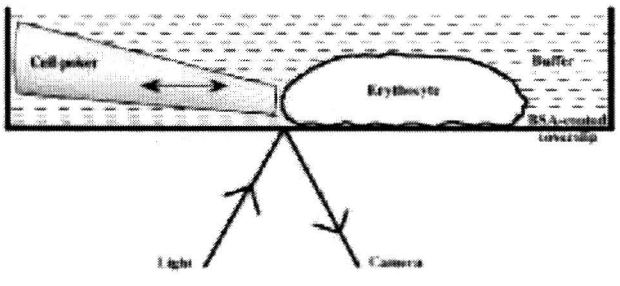

Figure A.4: Experimental setup cell indentation [Goldmann, 2000]

The principle of cell poking and its schematic representation is shown in figure A.4. The instrument is mounted on a microscope that focuses on the glass stylus. The deformation of the cell membrane, attached to a coated glass, is measured by a reflection interference contrast microscopy (RICM). A video was made during the poking of the cell with the glass stylus. From the movie, individual images (see figure A.5) [Goldmann, 2000] were taken to analyze the elastic response with the equation A.18, following [Goldmann, 2000]:

$$ln\Delta x_{(t_i)} = -k \cdot t_i \tag{A.18}$$

Where:

$\Delta x_{(t_i)}$: Time-depended lateral deformation relaxation

k : Rate of relaxation

t_i : Time

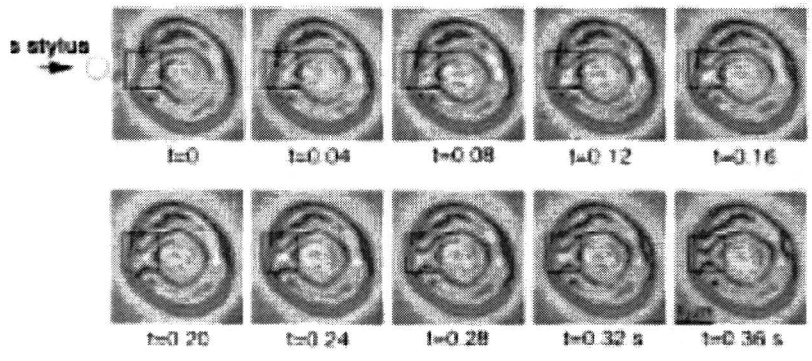

Figure A.5: Image cell indentation [Goldmann, 2000]

When the force on the cell and the displacement of the glass stylus are known, the elastic properties of the cell can be calculated.

Atomic force microscopy

Atomic force microscopy (AFM) imaging is performed not by means of an incident beam as in other classical microscopies, but by sensing the force between a very sharp probe and the sample surface. The sample or cell is mounted on a piezoelectric scanner, and can be positioned in three dimensions with high resolution. The force is measured through a beam attached to the probe. The bending of the beam is measured with a laser and indicates the force present on the cell [Antonik et al., 1998]. Image are made of the changing cell during loading. See figure A.6 for the principle of the AFM and see picture A.7 for sample preparation.

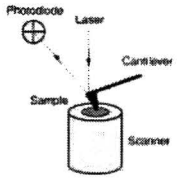

Figure A.6: Experimental setup [Dufrêne, 2000]

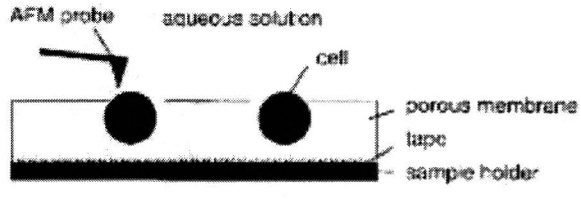

Figure A.7: Sample preparation of living cells [Dufrêne, 2000]

If a cell is loaded by the probe of the AFM, an image as figure A.8 can be obtained where:

A : Cell surrounded by an artifactual structure resulting from contact between the AFM probe and the pore edges.

C : The cell located in the center of the image.

M : Surrounding flat area represents the polymer membrane holding the cell.

S : Contact area of the AFM probe with the cell.

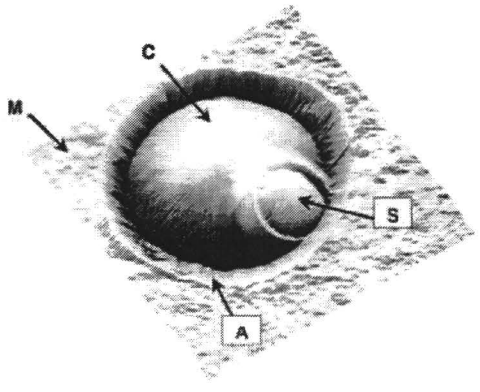

Figure A.8: Image cell under AFM force [Dufrêne, 2000]

With AFM the Young's modulus can be determined by the following model. The force acting F on the cell can be calculated with equation A.19, following [Gil et al., 1999]:

$$F = \frac{3}{4}\sqrt{R}E'\Delta z^{1.5} \tag{A.19}$$

Where:

R : Radius probe tip

Δz : Sample indentation

E' : Reduced Youngs modulus tip-cell sample system

E' can be calculated with equation A.20. [Gil et al., 1999]

$$\frac{1}{E'} = \frac{1-\mu_{tip}^2}{E_{tip}} + \frac{1-\mu_{cell}^2}{E_{cell}} \tag{A.20}$$

Where:

E_{tip},E_{cell}: Youngs modulus of the tip and the cell

μ_{tip},μ_{cell}: Poisson ratios of the tip and the cell

Taking into account that $E_{tip} \gg E_{cell}$, one obtains finally equation A.21, following [Gil et al., 1999]:

$$E' = \frac{E_{cell}}{1-\mu_{cell}^2} \tag{A.21}$$

Micromanipulation

The basic principle of the micromanipulation technique is the compression of a single cell between two parallel surfaces. Originally, these were the ends of two optic fibre probes, squeezing horizontally. A micromanipulation technique of single cells is developed by E. Peeters [Peeters, 2004]. With micromanipulation of x,y and z component a force is generated on the cell. The cell is compressed between a glass indenter with a relative large displacement (50 μm) and a glass plate. The shape of the deformed cell is measured with a confocal microscope. The principle of this technique is shown in figure A.9 and an image of the loading device is shown in figure A.10.

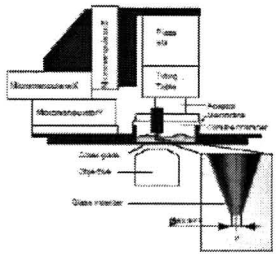

Figure A.9: Experimental setup loading device Peeters [Peeters, 2004]

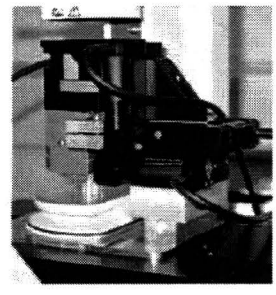

Figure A.10: Photo of loading device Peeters [Peeters, 2004]

When the glass indenter displaced more, the cell deforms more (see figure A.11).

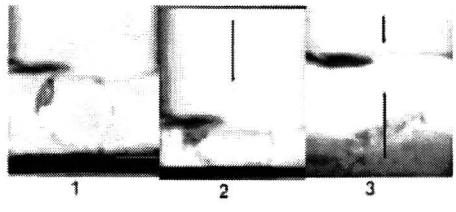

Figure A.11: Images of a compressed cell [Zhang et al., 2000]

Image are made of the cell, when the glass indenter displaced more into the cell. The cell deforms more with increasing displacement of the glass indenter (see figure A.12).

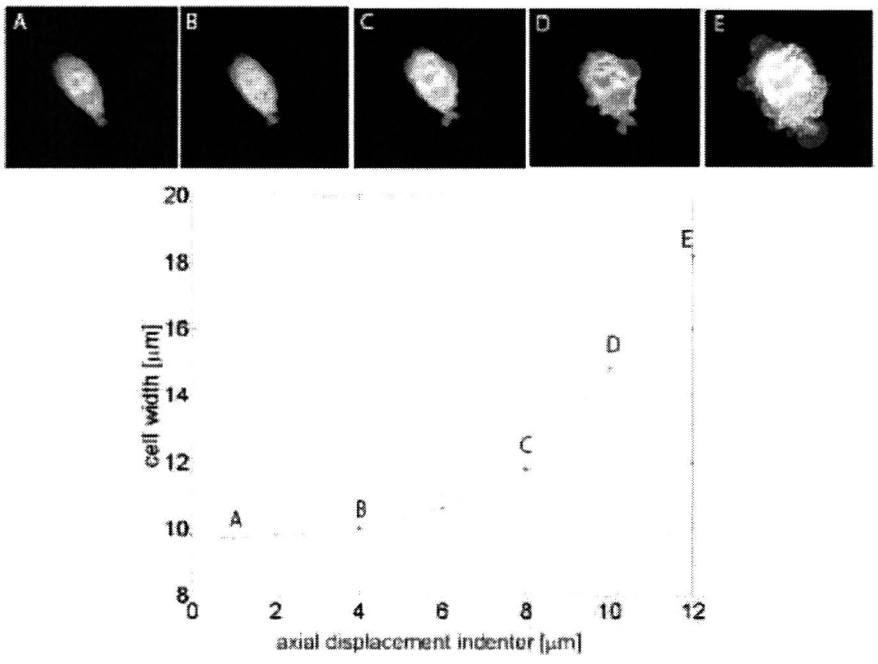

Figure A.12: Graphic shows increasing cell diameter with increasing indentation [Peeters, 2004]

With a confocal microscope the cell deformation can be visualized in three dimensions. The cell was modeled as an incompressible, Neo-Hookean material. The Gauchy stress tensor ($\boldsymbol{\sigma}$) can be calculated with equation A.22, following [Peeters, 2004]:

$$\boldsymbol{\sigma} = p\mathbf{I} + \boldsymbol{\tau} \tag{A.22}$$

Where:

p : hydrostatic pressure

$\boldsymbol{\tau}$: Extra stress tensor

$\mathbf{I}$: Unit tensor

Because the cell is modeled as a Neo-Hookean material, $\boldsymbol{\tau}$ is linear related to the right Gauchy-Green tensor $\mathbf{B}$ according to equation A.23, following [Peeters, 2004]:

$$\boldsymbol{\tau} = G(\mathbf{B} - \mathbf{I}) \tag{A.23}$$

Where:

G : shear modulus

B is related to the deformation tensor $\mathbf{F} = (\vec{\nabla}_0 \vec{x})^T$ according to $\mathbf{B} = \mathbf{F} \cdot \mathbf{F}^T$. The shear modulus can be calculated with equation A.24, following [Peeters, 2004]:

$$G = \frac{E}{2(1+\nu)} \tag{A.24}$$

Where:

E : Young's modulus

ν : Piosson's ratio

For an incompressible material the Poisson's ratio equals 0.5. Conservation of mass reduces in that case to the incompressibility constraint.

$$det(\mathbf{F}) - 1 = 0 \tag{A.25}$$

A finite element method was used to solve the balance of momentum equations A.22, A.23, A.24 and A.25. From the experiments a shear modulus can be estimated and fitted to the simulation. From the shear modulus the Young's modulus can be calculated with equation A.24.

Micro-plates

Micro-plates use a piezoelectric driven plate and a flexible micro-plates to squeeze cells or other small particles (see figure A.13). The deflection of the flexible plate is used to measure the uniaxial force on the cell. The deformation of the cell is recorded by a CCD camera and the images are imported in the image software. Figure A.14 shows pictures of a cell squeezed by micro-plates. The image software uses the deflection of the flexible micro-plate and the images to determine the Young's modulus.

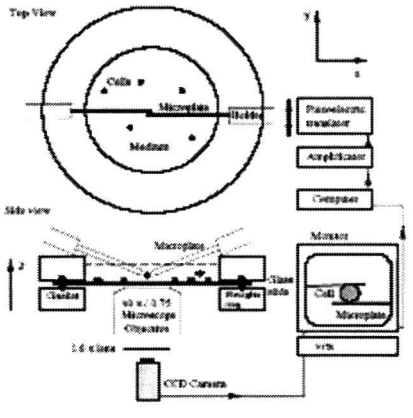

Figure A.13: Principle micro-plates [Thoumine and Ott, 1997]

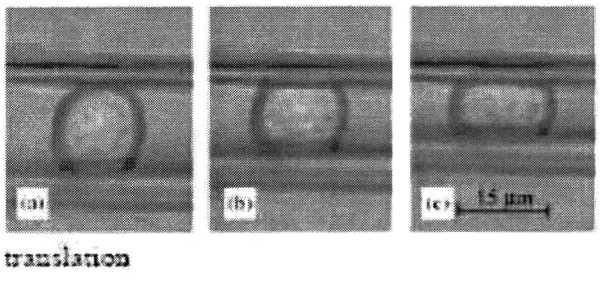

Figure A.14: Image squeeze cell micro-plates (a-b-c) [Tardy et al., 2002]

Optical tweezer

The optical tweezer uses a laser to stretch a cell. Figure A.15 shows the experimental setup of the optical tweezer.

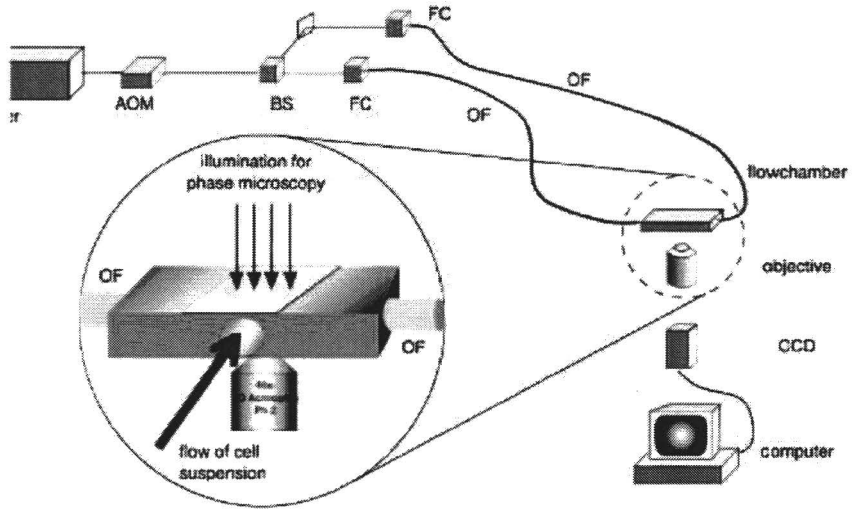

Figure A.15: Experimental setup optical tweezer [Mahmood et al., 2001]

The principle of the optical tweezer is based on the fact that, whenever light is absorbed, re-emitted, scattered, reflected and refracted by an object, there is a change in the momentum of the light. Conservation of momentum demands that radiation pressure generates a force on that interacting object. The amount of momentum p on the cell is proportional to its energy E and the refractive index n of the medium it travels in and can be calculated with the equation A.26, following [Cunningham et al., 2002]:

$$p = \frac{E \cdot n}{c} \tag{A.26}$$

Where:

c : speed of light

This momentum has to be conserved at the interface. When a light ray hits a particle, the momentum of the ray changes in direction and magnitude, and the difference is picked up by the particle which consequently feels a force. This can be calculated with the equation A.27, following [Cunningham et al., 2002]:

$$F = \frac{\Delta p}{\Delta t} = \frac{\Delta E \cdot n}{\Delta t \cdot c} = \frac{P \cdot n}{c} \tag{A.27}$$

Where:

P : Power of light ray

t : Time

Some of the light is reflected on the cell surface and some of the light goes into the cell and refract inside the cell. Depending on the incident angle, some light is always reflected backwards and not all energy enters the medium. The momentum of light inside the cell dominates over the momentum of the light that is reflected, causes the cell is almost transparent. The cell feels an outward force rather than an inward force. The change in momentum (Δp) can be described by equation A.28, following [Cunningham et al., 2002]:

$$\Delta \vec{p} = \vec{p}_1 - \vec{p}_2 - \vec{p}_r \tag{A.28}$$

Where:

p_1 : Momentum of the incident ray described by $\frac{En_1}{c}$

p_r : Momentum of the reflected ray described by $R_{(\theta)}\frac{En_1}{c} = R_{(\theta)}$

p_2 : Momentum of the transmitted ray described by $R_{(\theta)}\frac{En_2}{c} = T_{(\theta)}\frac{n_2}{n_1} = T_{(\theta)}n$

See figure A.16 for visualisation of momentum of light rays at interface.

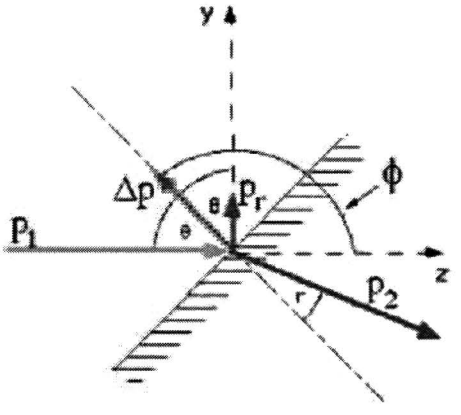

Figure A.16: Momentum of light at the interface between two media [Cunningham et al., 2002]

The reflection coefficients, $T_{(\theta)}$ and $R_{(\theta)}$, are described by equation A.29 and equation A.30, following [Cunningham et al., 2002]:

$$T_{(\theta)} = \frac{t_{\perp}^2(\theta) + t_{\parallel}^2(\theta)}{2} \tag{A.29}$$

$$R_{(\theta)} = \frac{r_{\perp}^2(\theta) + r_{\parallel}^2(\theta)}{2} \tag{A.30}$$

Where:

$t_{\perp}$, $t_{\parallel}$, $r_{\perp}$, $r_{\parallel}$; Fresnel coefficients

The components of the resulting change in momentum in z and y directions, as functions of the incident angle θ can be calculated with equation A.28, following [Cunningham et al., 2002]:

$$\Delta p_z = \Delta p \cdot \cos\phi = p - 1\cos(0) - p_2\cos(2\pi - \theta + r) - p_r\cos(\pi - 2\theta) = 1 - T_(\theta)\cdot n\cdot\cos(\theta - r) + R_\theta\cdot\cos(2\theta) \tag{A.31}$$

$$\Delta p_y = \Delta p \cdot \sin\phi = p - 1\sin(0) - p_2\sin(2\pi - \theta + r) - p_r\sin(\pi - 2\theta) = T_(\theta)\cdot n\cdot\cos(\theta - r) + R_\theta\cdot\cos(2\theta) \tag{A.32}$$

The magnitude of Δp can be calculated with equations A.31 and A.32, following [Cunningham et al., 2002]:

$$\Delta p = \sqrt{\Delta p_z^2 + \Delta p_y^2} \tag{A.33}$$

And the direction of the momentum can be calculated with equation A.34, following [Cunningham et al., 2002]:

$$\phi = arctan(\frac{\Delta p_y}{\Delta p_z}) \tag{A.34}$$

The stress on the cell can be calculated with the equation A.35, following [Mahmood et al., 2001]:

$$\sigma = \frac{F}{\Delta A} = \frac{n_1 \Delta p I}{c} \tag{A.35}$$

where:

I : Intensity of the light

The force on the cell can be calculated for differed incident angles θ on the spherical cell. See figure A.17 for the stretching force generated on the cell.

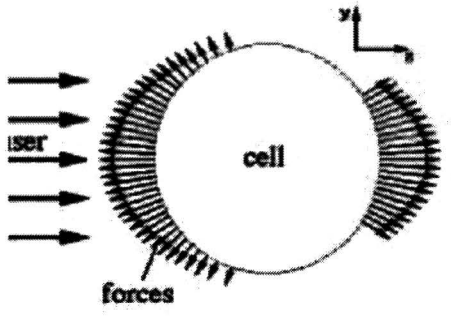

Figure A.17: Force on cell by laser [Cunningham et al., 2002]

Through this force the cell is stretched. The stretched profile in the optical stretcher is given by equation A.36, following [Cunningham et al., 2002]:

$$\mu_r = \frac{\rho\sigma}{2E}\left(\frac{m-2}{m+1} - \frac{8-14m}{5+7m}\right) \tag{A.36}$$

Where:

ρ : Radius of the cell

σ : Stress on the cell

m : Inverse of Poisson ratio (ν) (assuming incompressible material $\nu = 0.5$, $m = 2$)

E : Homogeneous Young's modulus of the cell

If the laser power is increased the force on the cell is increased, see equation A.27 , and the cell will stretch more because σ increase in equation A.36. A picture of the optical tweezer can be seen in figure A.18 where a stretched cell and un deformed cell are shown.

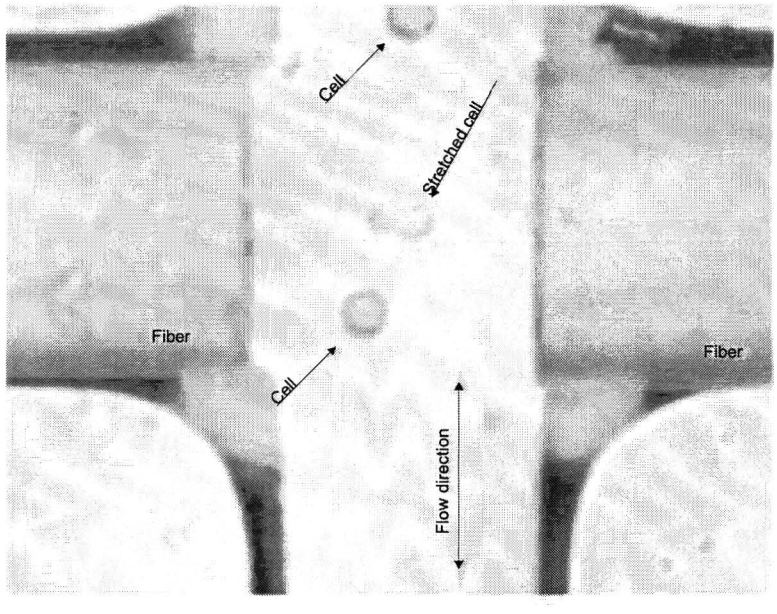

Figure A.18: Image optical tweezer [Schinkinger et al., 2003]

If pictures are taken from the cell when trapped and when deformed, a calculation can be made to determine the Young's modulus. The cell first needs to be trapped by the laser, before the power of the laser is increased to stretch the cell. See figure A.19 for images of a red blood cell (RBC) trapped by the laser and deformed by increased laser power with the optical tweezer.

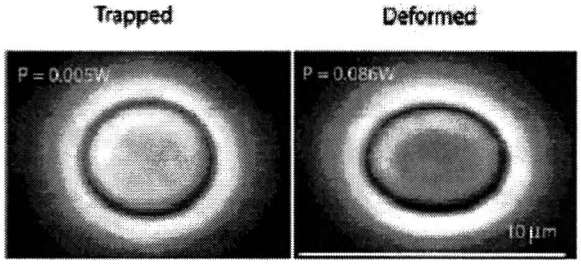

Figure A.19: Image RBC trapped and deformed with optical tweezer [Schinkinger et al., 2003]

Magnetic bead twister

A magnetic bead twister measures cytoskeleton mechanical properties of cells. This technique uses ferromagnetic micro beads, which are linked to the cell (see figure A.20 and figure A.21).

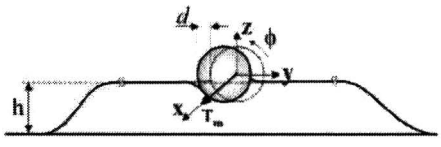

Figure A.20: Principle of magnetic bead twisting [Zivkovic-Ben et al., 2002]

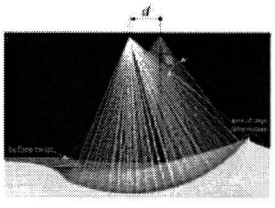

Figure A.21: Numerical model of magnetic twisting [Zivkovic-Ben et al., 2002]

With a magnetic twisting device a force is applied to the ferromagnetic micro bead, which generates a force on the cell. The cells are deformed by rotation of the beads. At equilibrium, the magnetic torque C is balanced by the elastic torque C_e, and using equation A.37, the angle of rotation of the bead is, following [Planus-Redouan et al., 2002]:

$$\theta_{eq} = \frac{3}{4\pi E} \frac{C}{R^3 \sin^3 \alpha} \tag{A.37}$$

Where:

E : Equivalent Young's modulus of intercellular medium

α : Angle micro bead immersion into the cytoplasm

R : Radius of micro bead

The magnetic torque C can be calculated with equation A.38, following [Planus-Redouan et al., 2002]:

$$C = \mu_o m H \sin(\frac{\pi}{2} - \theta_{eq}) \tag{A.38}$$

Where:

μ_o : permeability of free space

m : Micro bead magnetic moment

H : Magnitude of external magnetic field

When the bead is in equilibrium, images are taken from the deformed cell. With the recorded data from the experiment and equations A.37 and A.38, the Young's modulus can be estimated. In figure A.22 you can see a RGD coated ferromagnetic bead attached to a cell and twisted.

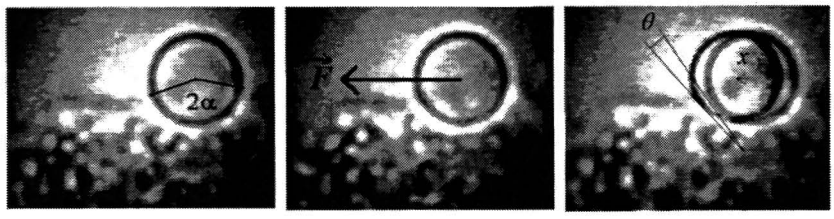

Figure A.22: Image recorded during an magnetic tweezer experiment [Planus-Redouan et al., 2002]

Appendix B

Tables of properties loading cells techniques

Table B.1: Characteristics of loading techniques designed for local loading of cells [Peeters, 2004]

	partial micropipette aspiration	cell poking	AFM	bead micro-manipulation
cell presentation	suspended cells	spread cells	spread cells	spread cells
physical principle	suction of part of cell	indentation	indentation	twisting (T) or moving (M) of attached microbeads with magnetic field or laser tweezers
control of	pressure	axial deformation	force or axial deformation	torque or force
size of load applicator	NA	2 μm	pyramid shape, radius of curvature <50 nm	bead diameter: 0.2-5.5 μm
force/pressure/ torque range	$\approx$ 0.01-1 kPa	5-400 nN	pN-nN	20 pN -10 nN (M), 0.1-10 Pa (T),pN $\cdot$ μm-nN $\cdot$ μm (T)
deformation range	depends on cell/pipette diameter ratio	max 50 %	max 10 %	max 2 μm (M),max 10 °C
resolution	0.2 μm, 0.1 Pa	0.02 μm, 5 nN	nm, pN	0.1 μm (M) ,1pN (M), 20 pN $\cdot$ μm (T)
visualization	brightfield microscopy	brightfield microscopy	brightfield, confocal microscopy	brightfield, fluorescence, confocal microscopy
operating temperature	RT	RT and 37 °C	RT and 37 °C	RT
controlled environment?	no	no	no	no

Table B.2: Characteristics of loading techniques designed for global loading of cells [Peeters, 2004]

	full micropipette aspiration	microplates	micro-manipulation	cyto-indentation
cell presentation	suspended cells	suspended and semi-spread cells	suspended and spread cells	spread cells
physical principle	suction of complete cell	unconfined compression and traction	unconfined compression	unconfined compression
control of	pressure	axial deformation	axial deformation	force
size of load applicator	NA	width=20 μm, length>100 μm	50 μm	5 μm
force/pressure range	$\approx$ 0.1-2 kPa	1-1.10^3 nN	10 nN-50 μN	1-100 nN
deformation range	depends on cell/pipette diameter ratio	max 50 %	total cell compression	NR
resolution	0.2 μm, 0.1 Pa	0.12 μm, 1 nN	0.2 μm, 10 nN	0.1 μm, 1 nN
visualization	brightfield microscopy	brightfield microscopy	brightfield microscopy	brightfield microscopy
operating temperature	RT	RT	37 °C	RT
controlled environment?	no	no	no	no

Appendix C

Contraction

For the measurements of deformation inside a contraction the following setup was used, see figure C.1:

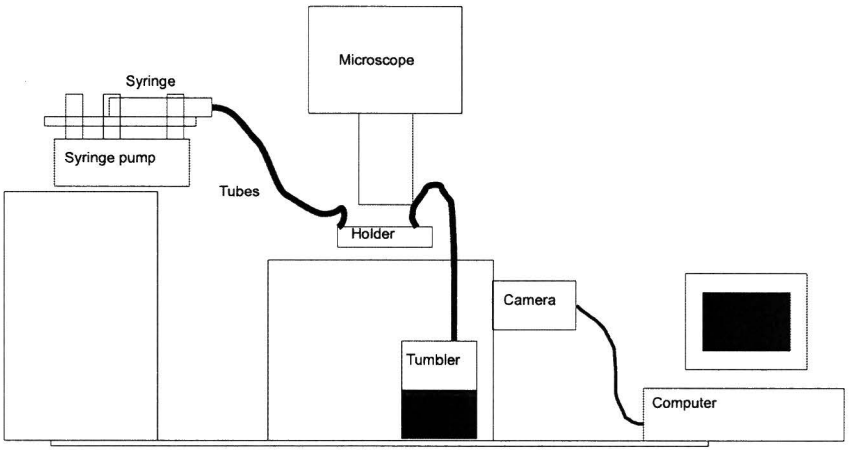

Figure C.1: Schematic experimental setup contraction

Contractions and holder

With the start of this project, Dr. P.D. Anderson had made micro structures into glass with a dry-etching technique. These micro structures were made at Mesa+ in cooperation with the Technical university in Twente. The top glass layer was fixed on top of the microstructure with anodic binding technique. These micro structures were used to carry out some first experiments to see what will happen with the cells in a contraction. Images of the micro structures can be seen in figure C.2.

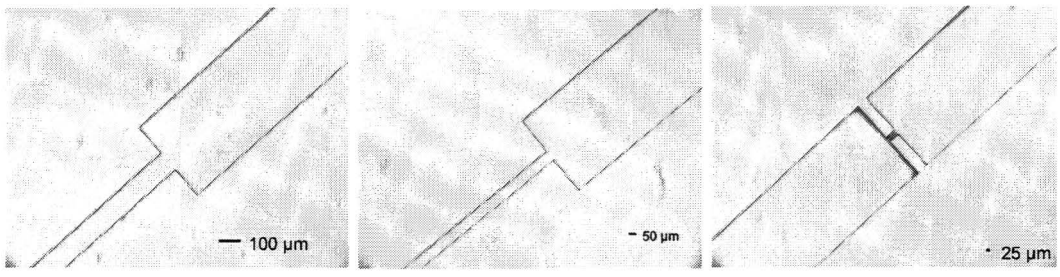

(a) $400\mu m$ to $100\mu m$ (b) $400\mu m$ to $50\mu m$ (c) $400\mu m$ to $25\mu m$

Figure C.2: Image of micro channel with different contraction

The holder is made out of Perpex and connects the contraction structure, from figure C.2, to the tubes. The design can be seen in figure C.3.

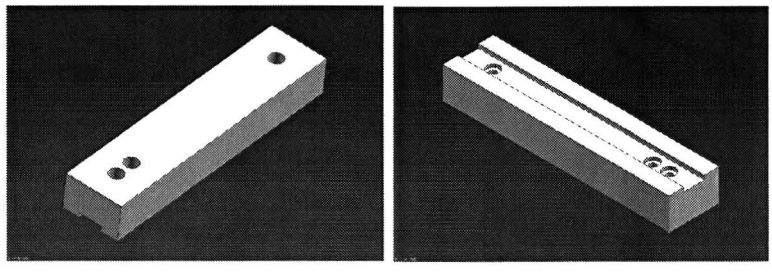

(a) Top view (b) Side view

Figure C.3: Design of holder for contractions

An image of the fabricated holder can be seen in figure C.4

Inside different micro channel structures can be placed. The connection from the holder to the micro channel is made with a rubber ring, which is seals the inlet of the micro channel to the holder. The micro channel clamp to the holder with screws.

Optical system

For the measurement of the deformation of the cell a Zeiss fluorescent microscope was used with different objectives, with magnifications of 10, 20 or 40. Also different kinds of cameras were used to record the deformation of the cell while flowing through the contraction. The first camera was a Zeiss AxioCam HRm and had an image field of 462x346 pixel at a maximum speed of 15 fps. At a speed of 15 fps the binning of the pixels is 5, which meas that 5 pixels are combined to one pixel. The exposure time of the image was 20 ms. This resulted into a blurred image cased by the fast movement of the cell and the exposure time of the image. Also the resolution of the camera is limited due the binning used to reach higher recording speeds. The second camera was a Kodak motion corder analyzer SR series. This is a high speed camera with a maximum image field of 512x480 pixels and a maximum speed of 1000 fps. The image size decreases if the speed of the camera increases. This is caused by the

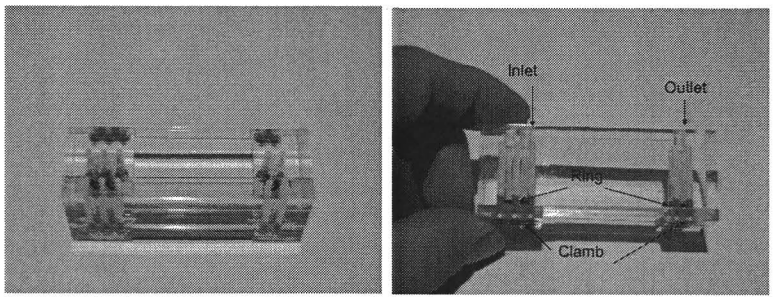

(a) Top view (b) Side view

Figure C.4: Holder for contractions

memory of the motion analyzer. If a speed of 500 fps is used the maximum image field is 512 x 240 pixels. The amount of images that can be recorded at this speed and image size is 1092, which meas that the maximum measure time is around 2 seconds. After the measurement, the recorded images must be transported to the hard disk of the computer. The time of exposure can be minimized to $\frac{1}{20000}$ sec.

Micro fluidic system

The flow is driven by a syringe pump. The tubes used were made from silicone rubber and had an inner diameter of 2 mm and an outer diameter of 4 mm. Before the experiments were started, the system was filled with water. Because osmotic swelling of the cells is not wanted, later PBS with the same osmotic value of the culture was used in the experiments. The cells were put inside the system by adding a valve in the tube just before entering the holder. An image of the valve is shown in figure C.5. This valve reduces the time needed for the cells to

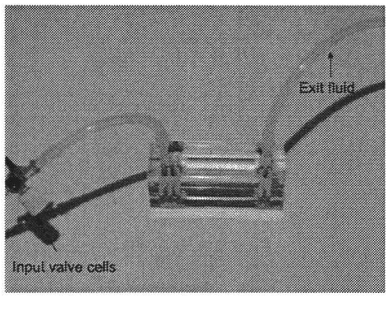

Figure C.5: Image of valve for input of cells

enter the contraction. A disadvantage was that by entering the cells with a syringe into the system, a high pressure was induced inside the system. After entering the cells the system needed some time to reach a stable flow which could be controlled with the syringe pump. The outlet of the holder was connected to a tumbler that could collect all exit fluid from the contraction.

Experiments

Contraction 1 : 4

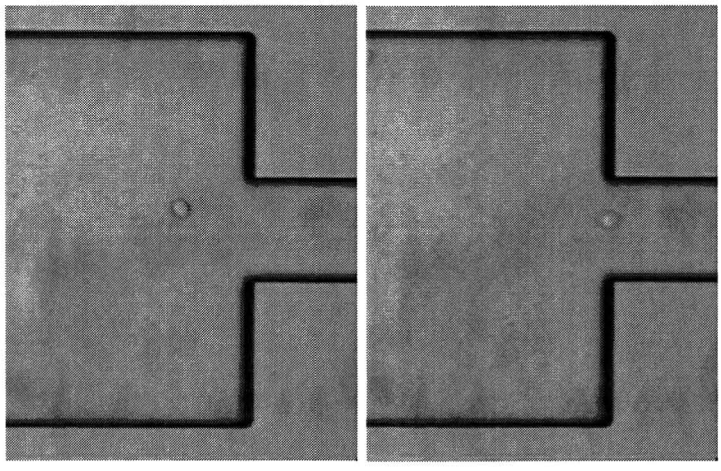

(a) Before (b) Inside

Figure C.6: Image of a fibroblast inside a contraction of 400 μm : 100 μm

The image in figure C.6 was taken with the Zeiss AxioCam HRm with a speed of 15 fps. The lens used was a 20x 0.5 NA fluor phi 1 form Zeiss. For this experiments fibroblasts were used, having an average diameter of 10 μm. The concentration of the cells in the solution is 200.000 cells/ml. The micro channel and tubes were filled with water before the entering of the cells. The cell solution was sucked with a syringe and connected to the Teflon tube, that enters the contraction. The syringe was placed inside the syringe pump. The syringe pump was set on a flow rate of 10 μl/min. Which leads to a velocity of the fluid in the smallest part of the micro channel of 0.033 m/s. Which leads to a Reynolds number of 3.33. During the flow of the cells images were recorded with a camera. Figure C.6(a) and figure C.6(b) show a cell flowing through the contraction.

The images of the cell are of sufficient quality to measure the cell in the wide part of the micro channel. However due the increasing speed of the cell, the image get blurred because of the limits of the speed of the camera. Because of the bad quality of the image it was not possible to determine the Taylor deformation rate inside the smallest part of the contraction. The Taylor deformation rate before entering the the small part is estimated on 0.0744. The estimation of the Taylor deformation rate is done with Matlab and the program can be found in appendix K. Also the fibroblasts (10 μm) are relatively small compared to the smallest channel width (100 μm). For the next experiment the camera is changed by a high speed camera and the micro channel is decreased in width. Also the type of cells are changed from fibroblasts (10 μm) to chondrocyte (30 μm), so the ratio between the width of the channel and the cell size decrease.

Contraction 1 : 8

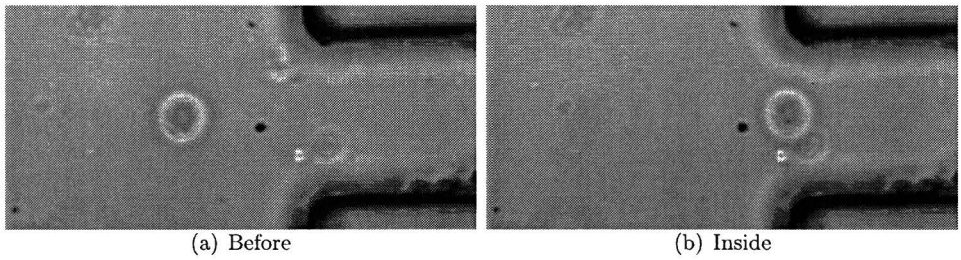

(a) Before (b) Inside

Figure C.7: Image of a chondrocyte inside a contraction of 400 μm : 50 μm

The image in figure C.7 was taken with a high speed camera, with a maximum speed of 1000 fps. In the microscope a lens type 40x 0.5 NA fluor phi 1 of Zeiss was used. For the experiment chondrocytes were used, which having an averaging diameter of 30 μm. An disadvantage is that the spreading of the diameter between different chondrocyte cells greater than the spreading of the diameter of Fibroblasts cells, which makes Chondrocyte a less ideal model cell. The Chondrocyte are from bones of pigs embryos. The micro channel and tubes were filled with water before the input of the cells. Between the inlet of the syringe of the pump and the entrance in the micro channel, a valve is placed. This valve is used to put the cells inside the water filled system. The benefits were, that the cells where more close to the entrance of the micro channel, so it takes less time to get the cells in the contraction. Also the leakage of cell solution was much less between the previous experiment en this test.

The cells were sucked inside a syringe and put, through the valve, inside the micro fluidic system. The syringe was placed inside the syringe pump. The syringe pump was set on a flow rate of 10 μl/min. Which leads to a velocity of the fluid in the smallest part of the micro channel of 0.066 m/s. Which leads to a Reynolds number of 6.66. During the flow of the cells images were recorded with a camera with 500 fps. Figure C.7(a) and figure C.7(b) show a cell going through the contraction.

The quality of the image is sufficient, however no deformation is detected when the cell is flowing through the contraction. A explanation can be that the micro channel is still to big compared to the size of the cell. A remark have to be made that fibroblasts are more elastic than the chondrocyte, which could also explain why the chondrocyte do not deform. For the next experiment a smaller micro channel will be used. Also the chondrocyte will be replaced, because of the long preparation to get chondrocyte cells. It takes a few days work to get some chondrocyte out of the bones of pigs embryos. An other type of cell is introduced, C2C12. This is a muscle cell of mice which can be grown in culture and has also a lager diameter than Fibroblasts. The average diameter of C2C12 is the same as Chondrocyte but the C2C12 it is possible that even larger cells exits in the solution.

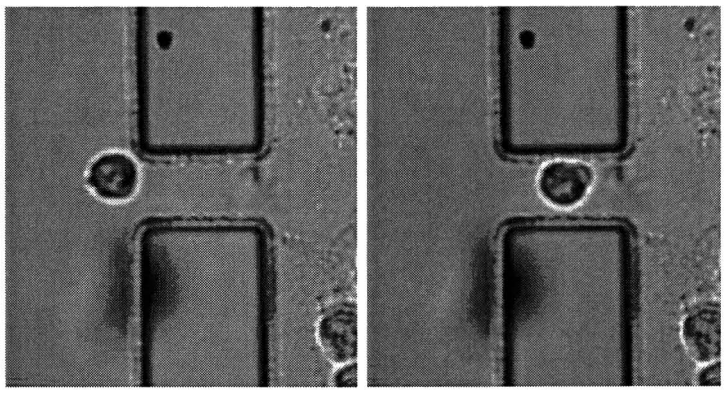

(a) Before (b) Inside

Figure C.8: Image of a muscle cell of a mice inside a contraction of 400 μm : 25 μm

Contraction 1 : 16

The figure C.8 was taken with a high speed camera, with a maximum speed of 1000 fps. In the microscope a lens type 40x 0.5 NA fluor phi 1 of Zeiss was used. For the experiment muscle cells of mice were used, which have an average diameter of 25 μm, but some cells should be greater than 25 μm. These cells where used to increase the fraction between the diameter of the cell and the smallest width of the channel. The input of the cell is the same as the experiment with the contraction 1 : 8. The cells were sucked inside a syringe and put, through the valve, inside the micro fluidic system. The syringe was placed inside the syringe pump. The syringe pump was set on a flow rate of 10 μl/min. Which leads to a velocity of the fluid in the smallest part of the micro channel of 0.132 m/s. Which leads to a Reynolds number of 13.2. During the flow of the cells images were recorded with a camera with 500 fps. Figure C.8(a) and figure C.8(b) show a cell going through the contraction.

The deformation of the cell is still very small. In image C.8(a) the Taylor deformation tensor is 0.0220 and in image C.8(b) the Taylor deformation tensor is 0.0781. Also the size of the muscle cells is almost the same as the chondrocyte and no bigger cells are seen. Smaller channels or higher flow rate could be a solution to deformatie the cell, only with higher flow rate also the time of imaging will decrease. The measurement time of the camera at 500 fps is around 1 second. In this time a cell needs to go through the contraction. The time to get the data from the high speed camera to the computer is around 10 minutes, which decreases the amount of measurement that can be done with a experiment. This should be improved to get more measurement data from the cell deformation experiments.

Design contraction

Based on experience with the experiments new designs were made to improve the cell deformation inside a contraction. Some features that could improve the contraction design are:

- Input of the cells
- Geometry of the contraction

These are discussed in the next section.

Input of cells

In the experiments the cells came random through the micro channel, which leads to a unidentified input of the cells. It is preferred that the cell should flow in the center of the contraction. To accomplish this, a fluidic centering was developed. A schematic principle can be seen in figure C.9(a). Because of the small dimensions of the micro channel and the slow velocity of the fluid, the Reynolds number will normal be $\ll 1$. The Reynolds number can be defined as equation C.1:

$$Re = \frac{\rho_f v_f W}{\eta_f} \tag{C.1}$$

Where:

W : Characteristic length of the channel (smallest height of the contraction)

Because the Reynolds number is $\ll 1$, the flow can be assumed laminar. If two fluid flows are place opposite on a middle flow, the two fluid flows will center the middle flow and so the cells. A image of a practical sample can be seen in figure C.9(b).

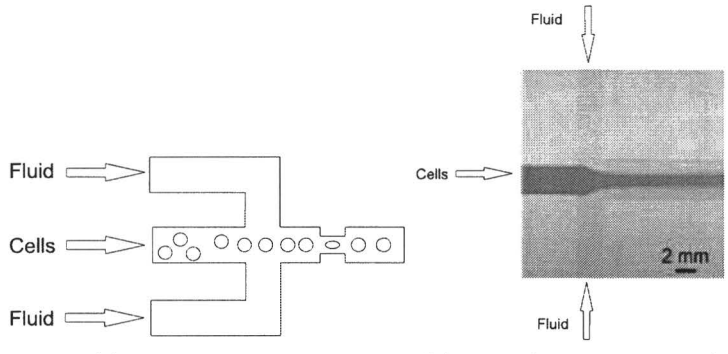

(a) Schematic principle (b) Image [Beebe et al., 2002]

Figure C.9: Micro fluidic centering of cells

Besides the benefit of centering the cells, also the side flows can be increase to increase the elongating inside the contraction. This can lead to higher deformation of cell inside the

contraction.

From the first experiments also could be concluded that the cells imaging was difficult. The focal plane of the cells was hard to find. A possible solution is to center the cells also in the focal plane direction. See figure C.10 for side plane of principle of centering cells in focal plane. The two fluid input channels are etched deeper than the cells input channel. Also the contraction part of the channel is less deep than the main channel. Since the flow is laminar, the cells are not concentrated in the whole channel, but only in the top side of the channel. This way the change of getting a cell in focus is higher, compared to a single input contraction.

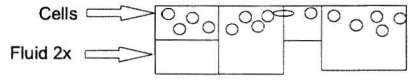

Figure C.10: Schematic principle fluid center focus plane (side view of figure C.9(a))

From experiments some image show the focusing of the cell to the center of the micro fluidic channel of 200 μm in figure C.11. Here fibroblasts are fluorescent labeled with Cell tracer Green.

The Taylor deformation rate is determined by the Matlab program. In figure C.11(a) $D_{XY} = 0.2238$, in figure C.11(b) $D_{XY} = 0.2568$, in figure C.11(c) $D_{XY} = 0.4180$ and in figure C.11(d) $D_{XY} = 0.2346$. The deformation in the figures C.11(a) and C.11(d) can be caused by the velocity of the flow and the limited imaging time of the camera. But the hydro focus the change in the Taylor deformation rate is ≈ 0.2, so the cell will deform inside the hydro focus flow.

Slight contraction

A sharp contraction can lead to detached of the flow, in notation of [Schram et al., 1994]. Secondary flow can develop at the begin of the contraction and just after the entrance of the contraction, see figure C.12.

This secondary flow leads to pressure losses inside the micro fluidic channel. The image of the flow field inside the simulation can be seen in figure C.14(a) and C.13(a). To prevent a secondary flow inside the contraction, the angle of the contraction (θ) can be changed, see figure C.12 [Mitsoulis and Hatzikiriakos, 2003]. Also a radius can be constructed on the edge of the contraction. To prove the difference in the flow a contraction with a radius and a slight contraction is simulated. An image of the flow field inside a contraction with a radius can be seen in figure C.14(b) and an image of the flow field inside a slight contraction can be seen in figure C.13(c).

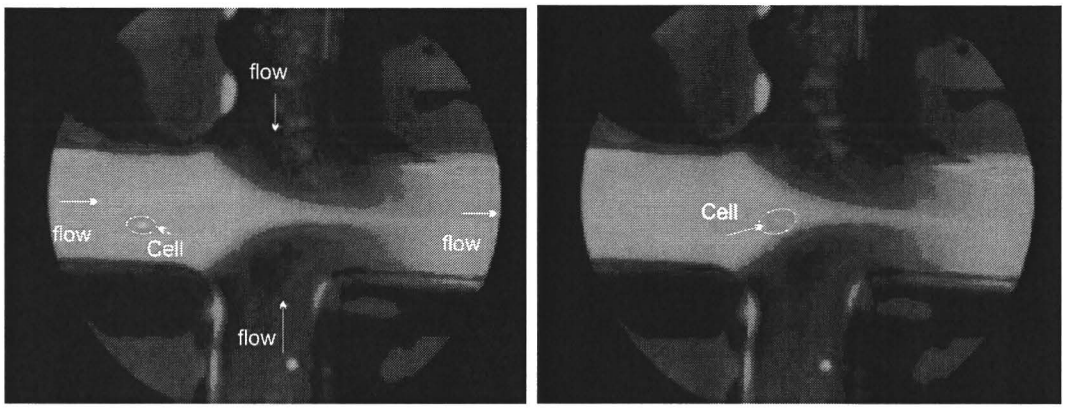

(a) t= 0 s

(b) t= 0.2 s

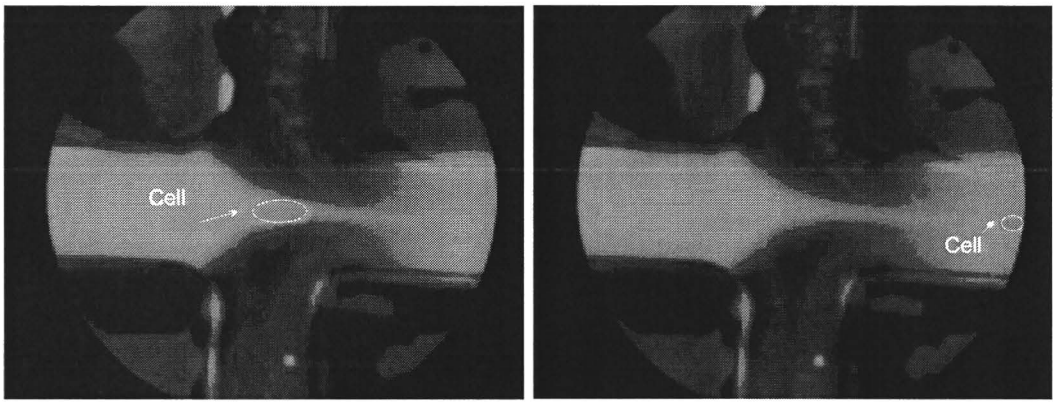

(c) t= 0.27 s

(d) t= 0.3 s

Figure C.11: Cells through hydro focus

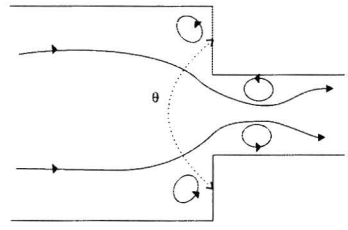

Figure C.12: Schematic flow through sudden contraction

For all these simulation the Reynolds number is 1. From figure C.13 there is no secondary flow inside any of the contraction, however the possible release of the flow is high with a sudden contraction compare to the other concepts. If the Reynolds number is increased there will be a secondary flow in the sudden contraction. In figure C.14 the Reynolds number is increased to 2000 and in the sudden contraction a secondary flow develops while the contraction with a radius no secondary flow can be seen.

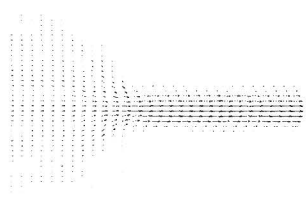

(a) Contraction sudden contraction

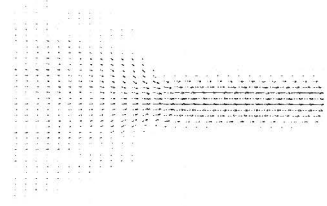

(b) Contraction with radius

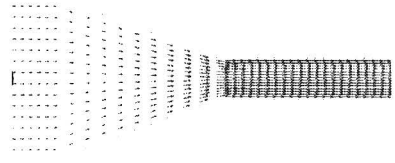

(c) Contraction with angle

Figure C.13: Velocity field flow inside different contractions with Re = 1

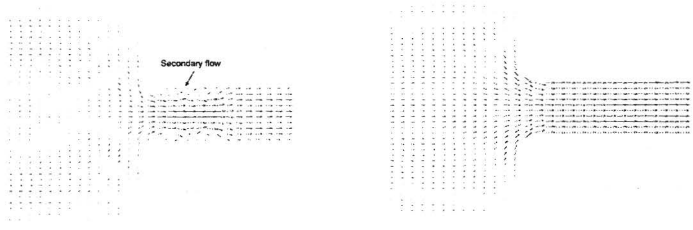

(a) Contraction sudden contraction (b) Contraction with radius

Figure C.14: Velocity field flow inside different contractions with Re = 2000

Geometry of contraction

Some channels with centering of the cells are constructed and some channels without centering of the cells are constructed. The schematic view of the contraction without centering of the cells can be seen in figure C.15(a) and the schematic view of the contraction with centering can be seen in figure C.15(b).

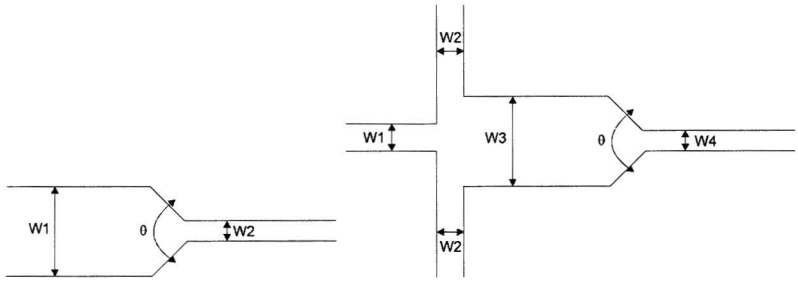

(a) Without centering of cells (b) With centering of cells

Figure C.15: Schematic contraction designs

The dimensions of the contractions used for the design can be found in table C.1.

Table C.1: Table dimensions contractions

Contraction	W1	W2	W3	W4	θ
1	200 μ m	50 μ m	-	-	90 °
2	200 μ m	25 μ m	-	-	90 °
3	200 μ m	25 μ m	-	-	90 °
4	150 μ m	15 μ m	-	-	90 °
5	100 μ m	100 μ m	200 μ m	50 μ m	90 °
6	100 μ m	100 μ m	200 μ m	25 μ m	90 °
7	100 μ m	100 μ m	200 μ m	25 μ m	90 °
8	100 μ m	100 μ m	150 μ m	15 μ m	90 °

The smallest possible channel was 15 μm because of the manufacturing technique with a foil mask. The resolution of the printer, used to print the mask, was around 15 μm. The length of the channel will be determined by the connection to the outer world. For the mounting a glass tube will be fixed on the micro channel. The inlet for the fluid to the micro channel will be a whole with a diameter of 1 mm. This space is also etched inside the micro channels. The schematic design of the channels in Corel draw can be seen in figure C.16.

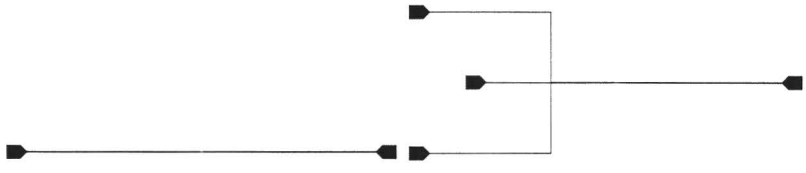

(a) Channel without cell centering (b) Channel with cell centering

Figure C.16: Total design contraction channels

The micro structures will be manufactured in silicon with lithography. First the design of the structures were made in Corel draw. The designs were positioned on a two wafers and were send to the mask manufacture. An image of the masks designs can be seen in figure C.17.

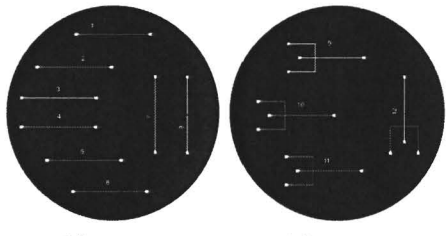

(a) Wafer1 (b) Wafer2

Figure C.17: Wafers contraction

The designs were printed on a foil mask. When the mask is developed, it can be used in a lithography machine. On a silicon wafer a positive photo sensitive layer is made. The wafer is placed inside the lithography machine and exposes through the foil mask. The places where the light hits the silicon wafer, a chemical reaction will happen. After the expose stage, the wafer is placed in a etching bath for several minutes, depending on the depth of the structures. The places where the chemical reaction happened during the exposes stage, will dissolve faster than the rest of the wafer. This creates the micro structures in the silicon wafer. When the wafer is ready, the structures are sawn out of the wafer. A glass top layer is made with entrance and exit holes of 1 mm diameter. This layer is glued on the silicon structure.

Unfortunately some problem happened during fabrication of the mask. Over the entire wafer were small holes, which will lead to problem in the expose step. See figure C.18 for image of holes in foil mask.

Figure C.18: Image of small holes in foil mask

Further development is not done on this subject.

Conclusion

For a new design of the contraction structure, should be taken in mind:

- Cells should be positioned in the center of the contraction.
- Cells should be positioned in focal plane, at a certain position in the z-direction.
- The dimensions of the contraction must be smaller. The dimensions of the cell are to small compare to the dimensions of the first contractions used. The main channel of the contraction used was 400 μm, this should be decreased to at least 200 μm. Through this reduction a higher magnification can be used to see the whole contraction and the cell. This leads to a better measurement of the cell deformation. The small channel should be decreased to 25 μm or less. The channel may not be smaller than the cell diameter, because the cell will not only be deformed through the flow but though the decreased channel wall.
- The sudden contraction should have a slight angle to prevent a development of a secondary flow [Mitsoulis and Hatzikiriakos, 2003]. It also prevents air from getting stuck inside the channel, which can block the micro fluidic channel due the surface tension of water versus air.

Appendix D

Dimensionless numbers

The model used for the determination of the dimensionless numbers for the micro fluidic cell stretcher can be seen in figure D.1. The geometry of the cross slot will be two input flows and two exit flows, with an equal width of W.

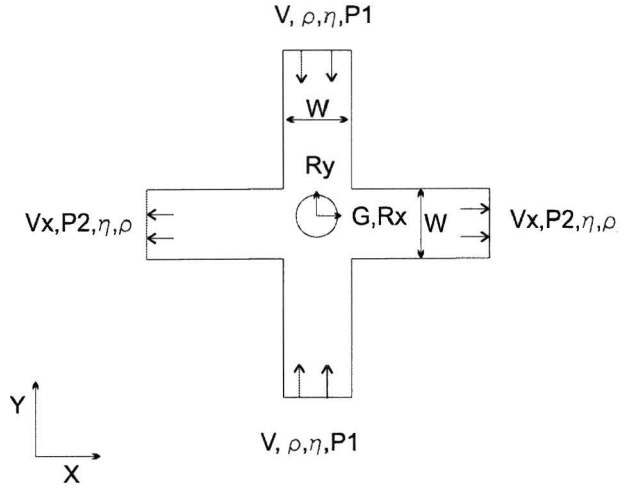

Figure D.1: Schematic model micro fluidic cell stretcher

The flow is stationary and the fluid is Newtonian with a constant density ρ and a constant viscosity η. The model is two dimensional in the x-y plane. Known parameters of the fluid are P_2, V, η and ρ. Unknown parameters of the fluid are P_1 and V_x. The solid is characterized as hyperelastic, Neo-Hookean and incompressible. Known parameters of the solid are the shear modulus G, dimensions of the solid in the x-y direction (R_x, R_y). Unknown parameters of the solid are the dimensions of the solid in the x-y direction after deformation (r_x, r_y), see figure D.2.

Governing equations and boundary conditions

The governing equation for the fluid inside the micro fluidic cell stretcher is:

$$\rho\frac{\partial \mathbf{v}}{\partial t} + \rho\mathbf{v}\cdot\nabla\mathbf{v} = \nabla\cdot(-p\mathbf{I}+\boldsymbol{\tau}) \tag{D.1}$$

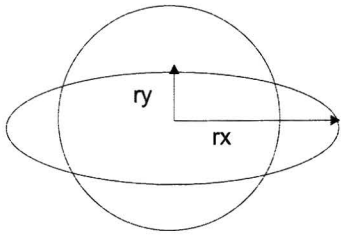

Figure D.2: Schematic r_x and r_y cell

The flow also has to obey the continuity equation, given by:

$$\nabla \cdot \mathbf{v} = 0 \tag{D.2}$$

The governing equation for the fluid and solid interaction is given by the force balance over the interface:

$$\boldsymbol{n}\boldsymbol{\sigma}_f - \boldsymbol{n}\boldsymbol{\sigma}_s = \Gamma k \boldsymbol{n} \tag{D.3}$$

Where $k = \dfrac{1}{R_r}$ is the curvature of the surface. For this model the surface tension of the solid will be negligible small [Laursen et al., 2005a]. Which leads to equation:

$$\boldsymbol{n}\boldsymbol{\sigma}_f - \boldsymbol{n}\boldsymbol{\sigma}_s = 0 \tag{D.4}$$

The solid also obey the incompressibility equation given by:

$$det(\mathbf{F}) - 1 = 0 \tag{D.5}$$

For equation D.4 look at figure D.3

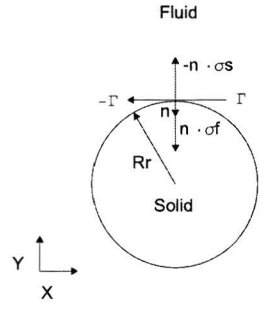

Figure D.3: Schematic model force solid

If the equation D.4 is combined with $\boldsymbol{\sigma} = -p\boldsymbol{I} + \boldsymbol{\tau}$ the equation becomes:

$$(p_s - p_f)\boldsymbol{n} + \boldsymbol{n}(\boldsymbol{\tau}_f - \boldsymbol{\tau}_s) = 0 \tag{D.6}$$

The $\boldsymbol{\tau}_f$ and $\boldsymbol{\tau}_s$ from equation D.60 are defined by:

$$\boldsymbol{\tau}_f = 2\eta_f \mathbf{D} \tag{D.7}$$

$$\boldsymbol{\tau}_s = G(\mathbf{B} - \mathbf{I}) \tag{D.8}$$

For a Newtonian fluid the rate of deformation tensor $\mathbf{D} = \frac{1}{2}(\nabla \mathbf{v}_f + (\nabla \mathbf{v}_f)^T)$. $\mathbf{v}_f$ is the velocity vector of the fluid. For a hyperelastic and isotropic according to a Neo-Hookean constitutive model. The Finger or Cauchy-Green strain tensor ($\mathbf{B} = \mathbf{F} \cdot \mathbf{F}^T$ where $\mathbf{F} = (\vec{\nabla}_0 \vec{x}_s)^T$). ∇_0 is the gradient operator and x_s is the cell position vector. If equations D.7 and D.8 are substituted in equation D.60 the equation becomes:

$$(p_s - p_f)\boldsymbol{n} + \boldsymbol{n}(2\eta \mathbf{D}) - \boldsymbol{n}(G(\mathbf{B} - \mathbf{I})) = 0 \tag{D.9}$$

To determine the dimensionless numbers of the governing equations, a good way is to look in a specific direction. In this model the Y-direction is interesting, because the flow on the cell comes from the Y-direction. The governing equation D.1 of the fluid in y-direction for the micro fluidic cell stretcher becomes:

$$\rho \frac{\partial v_y}{\partial t} + \rho(v_x \frac{\partial v_y}{\partial x} + v_y \frac{\partial v_y}{\partial y}) = -\frac{\partial \rho}{\partial y} + \eta(\frac{\partial^2 v_y}{\partial x^2} + \frac{\partial^2 v_y}{\partial y^2}) \tag{D.10}$$

Because the flow is assumed to be stationary, $\frac{\partial v_y}{\partial t} = 0$, the governing equation of the fluid flow in y-direction becomes:

$$\rho(v_x \frac{\partial v_y}{\partial x} + v_y \frac{\partial v_y}{\partial y}) = -\frac{\partial p}{\partial y} + \eta(\frac{\partial^2 v_y}{\partial x^2} + \frac{\partial^2 v_y}{\partial y^2}) \tag{D.11}$$

The governing equation D.9 for the force balance over the interface will be defined by:

$$(p_s - p_f)\boldsymbol{n} + \boldsymbol{n}\boldsymbol{\tau}_f - \boldsymbol{n}\boldsymbol{\tau}_s = 0 \tag{D.12}$$

The continuity equation of the flow (D.2) and solid (D.5) are defined in both directions and are shown here:

$$\frac{\partial v_x}{\partial x} + \frac{\partial v_y}{\partial y} = 0 \tag{D.13}$$

$$\frac{\partial r_x}{\partial R_x}\frac{\partial r_y}{\partial R_y} - \frac{\partial r_y}{\partial R_x}\frac{\partial r_x}{\partial R_y} - 1 = 0 \tag{D.14}$$

Scaling the problem

Each problem variable is divided by its characteristic value. For this model the dimensionless variables are:

$$y^* = \frac{y}{W} \tag{D.15}$$

$$x^* = \frac{x}{W} \tag{D.16}$$

$$v_y^* = \frac{v_y}{V} \tag{D.17}$$

$$v_x^* = \frac{v_x}{V_x} \tag{D.18}$$

$$p^* = \frac{p - p_2}{\Delta P_c} \tag{D.19}$$

$$p_{sf}^* = \frac{p_s - p_f}{\Delta P_{sfc}} \tag{D.20}$$

$$R_x^* = \frac{R_x}{R} \tag{D.21}$$

$$R_y^* = \frac{R_y}{R} \tag{D.22}$$

$$r_x^* = \frac{r_x}{R} \tag{D.23}$$

$$r_y^* = \frac{r_y}{R} \tag{D.24}$$

$$\boldsymbol{\tau}_f = \frac{\boldsymbol{\tau}_f^*}{\frac{\eta V}{W}} \tag{D.25}$$

$$\boldsymbol{\tau}_s = \frac{\boldsymbol{\tau}_s^*}{G(\frac{R^2}{R^2} + \frac{RR}{R^2} - \frac{R^2}{R^2})} \tag{D.26}$$

The dimensionless variables with $_c$ are unknown characteristic values and will be determined later. Assumed is that r_x, r_y and R_r scale with solid radius R. For very small deformations the solid radius after deformation is $\approx R$. This assumed can be used because no excessieve deformation is expected. $\boldsymbol{\tau}_s$ is calculated with the following equations:

$$G(\boldsymbol{B} - \boldsymbol{I}) = G(\frac{\partial r_y \partial r_y}{\partial R_y \partial R_y} + \frac{\partial r_y \partial r_x}{\partial R_x \partial R_x} - 1) = [G(\frac{R^2}{R^2} + \frac{RR}{R^2} - \frac{R^2}{R^2})](\frac{\partial r_y^* \partial r_y^*}{\partial R_y^* \partial R_y^*} + \frac{\partial r_y^* \partial r_x^*}{\partial R_x^* \partial R_x^*}) \tag{D.27}$$

Substitution of the dimensionless variables

The dimensionless variables are now substituted into the governing equations D.11,D.12 and continuity equations D.13 and D.14. First the equation D.13 of the continuity equations will be substituted, this gives:

$$[\frac{V_x}{W}]\frac{\partial v_x^*}{\partial x^*} + [\frac{V}{W}]\frac{\partial v_y^*}{\partial y^*} = 0 \tag{D.28}$$

Reverifying by multiply with $\frac{W}{V}$ gives the equation:

$$[\frac{V_x}{V}]\frac{\partial v_x^*}{\partial x^*} + \frac{\partial v_y^*}{\partial y^*} = 0 \tag{D.29}$$

Both $\frac{\partial v_x^*}{\partial x^*}, \frac{\partial v_y^*}{\partial y^*}$ need to be in an order 1 so V_x must be equal to V. If the equation D.14 of the boundary conditions is substitute, this gives:

$$[\frac{R}{R}\frac{R}{R}]\frac{\partial r_x^*}{\partial R_x^*}\frac{\partial r_y^*}{\partial R_y^*} - [\frac{R}{R}\frac{R}{R}]\frac{\partial r_y^*}{\partial R_x^*}\frac{\partial r_x^*}{\partial R_y^*} - 1 = 0 \tag{D.30}$$

Both $\frac{\partial r_y^*}{\partial R_x^*} = 0$ and $\frac{\partial r_x^*}{\partial R_y^*} = 0$, which leaves $RR = R^2$.

If the governing equation D.11 of the fluid is substitute, this gives:

$$[\frac{\rho V^2}{W}](v_x^*\frac{\partial v_y^*}{\partial x^*} + v_y^*\frac{\partial v_y^*}{\partial y^*}) = -[\frac{\Delta P_c}{W}]\frac{\partial p^*}{\partial y^*} + [\frac{\eta V}{W^2}](\frac{\partial^2 v_y^*}{\partial x^{*2}} + \frac{\partial^2 v_y^*}{\partial y^{*2}}) \tag{D.31}$$

If the governing equation D.12 of the solid interface is substitute, this gives:

$$[\Delta P_{sfc}]p_{sf}^*\boldsymbol{n} + [\frac{\eta V}{W}]\boldsymbol{n}\boldsymbol{\tau}_f^* - [G(\frac{R^2}{R^2} + \frac{RR}{R^2} - \frac{R^2}{R^2})]\boldsymbol{n}\boldsymbol{\tau}_s^* = 0 \tag{D.32}$$

The equation D.32 could be simplified by:

$$[\Delta P_{sfc}]p_{sf}^*\boldsymbol{n} + [\frac{\eta V}{W}]\boldsymbol{n}\boldsymbol{\tau}_f^* - [G]\boldsymbol{n}\boldsymbol{\tau}_s^* = 0 \tag{D.33}$$

Choose important term

Because the micro fluidic cell stretcher has a very small channel, with a low velocity of the fluid, it is chosen that the viscous terms are important. The validity of this assumption has to be checked afterwards. The equation D.31 of the fluid will be multiplied by $[\frac{W^2}{\eta V}]$ which leads to the equation:

$$[\frac{\rho V W}{\eta}](v_x^*\frac{\partial v_y^*}{\partial x^*} + v_y^*\frac{\partial v_y^*}{\partial y^*}) = -[\frac{\Delta P_c W}{\eta V}]\frac{\partial p^*}{\partial y^*} + (\frac{\partial^2 v_y^*}{\partial x^{*2}} + \frac{\partial^2 v_y^*}{\partial y^{*2}}) \tag{D.34}$$

The equation D.89 of the fluid-solid interaction will also be multiply by $[\frac{R}{\eta V}]$, because it is assumed that the viscous forces are important, which leads to the equation:

$$[\frac{\Delta P_{sfc} R}{\eta V}]p_{sf}^*\boldsymbol{n} + [\frac{R}{W}]\boldsymbol{n}\boldsymbol{\tau}_f^* - [G]\boldsymbol{n}\boldsymbol{\tau}_s^* = 0 \tag{D.35}$$

Determine unknown characteristic values

From the equation D.34 of the fluid, the unknown characteristic values are defined by:

$$\Delta P_c = \frac{\eta V}{W} \tag{D.36}$$

$$Re = \frac{\rho V W}{\eta} \tag{D.37}$$

Where equation D.36 is the characteristic pressure drop over the cross slot. The pressure drop is dominated by the viscous forces of the fluid. Equation D.37 is the Reynolds number. If the characteristic values are substitute into equation D.34 the governing equation for the fluid becomes:

$$[Re](v_x^* \frac{\partial v_y^*}{\partial x^*} + v_y^* \frac{\partial v_y^*}{\partial y^*}) = -\frac{\partial p^*}{\partial y^*} + (\frac{\partial^2 v_y^*}{\partial x^{*2}} + \frac{\partial^2 v_y^*}{\partial y^{*2}}) \tag{D.38}$$

From the equation D.35 of the fluid-solid interaction, the unknown characteristic values are defined by:

$$\Delta P_{sfc} = \frac{\eta V}{R} \tag{D.39}$$

$$De = \frac{\eta \frac{V}{R}}{G} \tag{D.40}$$

$$F_{RW} = \frac{R}{W} \tag{D.41}$$

If the characteristic values are substituted into equation D.35 the governing equation for the fluid-solid becomes:

$$p_{sf}^* \boldsymbol{n} + [F_{RW}] \boldsymbol{n} \boldsymbol{\tau}_f^* - [\frac{1}{De}] \boldsymbol{n} \boldsymbol{\tau}_s^* = [\frac{1}{Ca}] \frac{1}{R_r^*} \boldsymbol{n} \tag{D.42}$$

Control of the chosen important terms

The remaining dimensionless groups in the equations D.38 and D.42 must have a value between 0 and 1 if realistic values are substitute. Realistic values for the micro fluidic cell stretcher are ρ =1000 kg/m^3, η = 0.001 Pa/s, V =1 mm/s G =380 Pa, W =100 μm, R =5 μm and Γ =0.03 mN/m . Substitute these values inside the remaining dimensionless groups of the fluid gives:

$$Re = \frac{1000 \cdot 0.001 \cdot 0.0001}{0.001} = 0.1 \tag{D.43}$$

The dimensionless groups of the fluid are scaled properly because the Re-number in equation D.38 is $\ll 1$ and all other factors are equal to 1. Substitute the values inside the remaining dimensionless groups of the fluid-solid interaction gives:

$$F_{RW} = \frac{0.000005}{0.0001} = 0.05 \tag{D.44}$$

$$De = \frac{0.001 \cdot \frac{0.001}{0.000005}}{380} = 5.26 \cdot 10^{-4} \tag{D.45}$$

The dimensionless groups of the fluid-solid interaction are not scaled properly, because $\frac{1}{De} = 1.9 \cdot 10^3$ in equation ?? are $\gg 1$. If the right choice had been made in section D, then all the dimensionless numbers were around 1. Viscous force are not dominant, maybe the shear modulus is dominant.

Second choice, shear modulus dominant

If the equation D.89is multiplied with $[\frac{1}{G}]$ then the equation for the force balance over the fluid-solid interface becomes:

$$[\frac{\Delta P_{sfc}}{G}]p^*_{sf}\boldsymbol{n} + [\frac{\eta V}{WG}]\boldsymbol{n}\boldsymbol{\tau}^*_f - \boldsymbol{n}\boldsymbol{\tau}^*_s = 0 \tag{D.46}$$

To find dimensionless numbers, the equation D.89 is turned to equation:

$$[\frac{\Delta P_{sfc}}{G}]p^*_{sf}\boldsymbol{n} + [\frac{R}{W} \cdot \frac{\eta \frac{V}{R}}{G}]\boldsymbol{n}\boldsymbol{\tau}^*_f - \boldsymbol{n}\boldsymbol{\tau}^*_s = 0 \tag{D.47}$$

From the equation D.47 of the fluid-solid interaction, the unknown characteristic values are defined by:

$$\Delta P_{sfc} = G \tag{D.48}$$

$$De = \frac{\eta \frac{V}{R}}{G} \tag{D.49}$$

$$F_{RW} = \frac{R}{W} \tag{D.50}$$

If the characteristic values are substituted into equation D.35 the governing equation for the fluid-solid becomes:

$$p^*_{sf}\boldsymbol{n} + [F_{RW} \cdot De]\boldsymbol{n}\boldsymbol{\tau}^*_f - \boldsymbol{n}\boldsymbol{\tau}^*_s = 0 \tag{D.51}$$

The remaining dimensionless groups in the equations must have a value between 0 and 1 if realistic values are substitute. Realistic values for the microfluidic cell stretcher are ρ =1000

kg/m^3, $\eta = 0.001$ Pa/s, V =1 mm/s G =380 Pa, W =100 μm, R =5 μm. Substituting these values inside the remaining dimensionless groups of the fluid gives:

$$De = \frac{0.001 \cdot \frac{0.001}{0.000005}}{380} = 5.26 \cdot 10^{-4} \tag{D.52}$$

$$F_{RW} = \frac{0.000005}{0.0001} = 0.05 \tag{D.53}$$

The dimensionless groups of the fluid-solid interaction are scaled properly, because De and F_{RW} in equation D.51 are $\ll 1$.

Conclusion

If the model is simulated, the following dimensionless numbers must be taken in account:

$$Re = \frac{\rho V W}{\eta} = 0.1 \tag{D.54}$$

$$De = \frac{\eta \frac{V}{W}}{G} = 5.26 \cdot 10^{-4} \tag{D.55}$$

$$F_{RW} = \frac{0.000005}{0.0002} = 0.05 \tag{D.56}$$

The Reynolds number is low, which means that the flow is laminar. The Reynolds number is < 1, which means that the fluid flow is dominate by viscous forces. The Deborah number is low, which indicates that the resistance time of the cell against deformation is higher than of the resistance time of the fluid. The Deborah number has influence on the deformation of the solid because the stress of the flow $\boldsymbol{\tau}_f$ scale with an order $O(10^{-7})$ to the pressure difference over the surface p_{sf} and stress in the surface $\boldsymbol{\tau}_s$, following equation D.51.

$$[O(1)]p^*_{sf}\boldsymbol{n} + [O(10^{-7})]\boldsymbol{n}\boldsymbol{\tau}^*_f - [O(1)]\boldsymbol{n}\boldsymbol{\tau}^*_s = 0 \tag{D.57}$$

Dimensionless numbers with surface tension cell

The model used for the determination of the dimensionless numbers for the micro fluidic cell stretcher can be seen in figure D.4. The geometry of the cross slot will be two input flows and two exit flows, with an equal width of W.

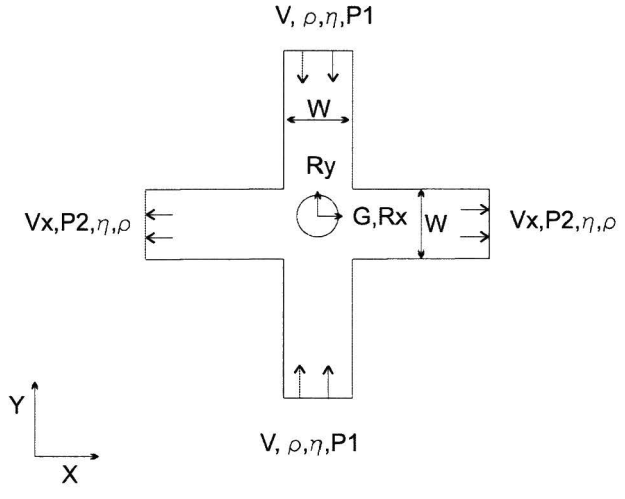

Figure D.4: Schematic model micro fluidic cell stretcher

The flow is stationary and the fluid is Newtonian with a constant density ρ and a constant viscosity η. The model is two dimensional in the x-y plane. Known parameters of the fluid are P_2, V, η and ρ. Unknown parameters of the fluid are P_1 and V_x. The solid is characterized as hyperelastic, Neo-Hookean and incompressible. Known parameters of the solid are the shear modulus G, dimensions of the solid in the x-y direction (R_x, R_y). Unknown parameters of the solid are the dimensions of the solid in the x-y direction after deformation (r_x, r_y), see figure D.5.

Governing equations and boundary conditions

The governing equation for the fluid inside the micro fluidic cell stretcher is:

$$\rho\frac{\partial \mathbf{v}}{\partial t} + \rho\mathbf{v}\cdot\nabla\mathbf{v} = \nabla\cdot(-p\mathbf{I}+\boldsymbol{\tau}) \tag{D.58}$$

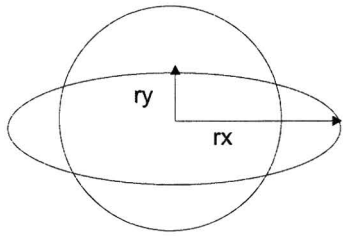

Figure D.5: Schematic r_x and r_y cell

The flow also has to obey the continuity equation, given by:

$$\nabla \cdot \mathbf{v} = 0 \tag{D.59}$$

The governing equation for the fluid and solid interaction is given by the force balance over the interface:

$$\boldsymbol{n}\boldsymbol{\sigma}_f - \boldsymbol{n}\boldsymbol{\sigma}_s = \Gamma k \boldsymbol{n} \tag{D.60}$$

Where $k = \dfrac{1}{R_r}$ is the curvature of the surface. The solid also obey the incompressibility equation given by:

$$det(\mathbf{F}) - 1 = 0 \tag{D.61}$$

For equation D.60 look at figure D.6

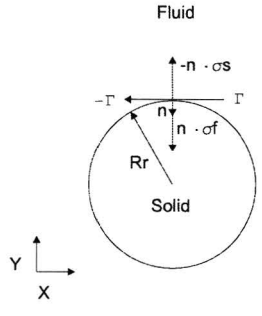

Figure D.6: Schematic model force solid

If the equation D.60 is combined with $\boldsymbol{\sigma} = -p\boldsymbol{I} + \boldsymbol{\tau}$ the equation becomes:

$$(p_s - p_f)\boldsymbol{n} + \boldsymbol{n}(\boldsymbol{\tau}_f - \boldsymbol{\tau}_s) = \Gamma k \boldsymbol{n} \tag{D.62}$$

The $\boldsymbol{\tau}_f$ and $\boldsymbol{\tau}_s$ from equation D.62 are defined by:

$$\boldsymbol{\tau}_f = 2\eta_f \mathbf{D} \tag{D.63}$$

$$\boldsymbol{\tau}_s = G(\mathbf{B} - \mathbf{I}) \tag{D.64}$$

For a Newtonian fluid the rate of deformation tensor $\mathbf{D} = \frac{1}{2}(\nabla \mathbf{v}_f + (\nabla \mathbf{v}_f)^T)$. $\mathbf{v}_f$ is the velocity vector of the fluid. For a hyperelastic and isotropic according to a Neo-Hookean constitutive model. The Finger or Cauchy-Green strain tensor ($\mathbf{B} = \mathbf{F} \cdot \mathbf{F}^T$ where $\mathbf{F} = (\overrightarrow{\nabla}_0 \overrightarrow{x}_s)^T$). ∇_0 is the gradient operator and x_s is the cell position vector. If equations D.63 and D.64 are substituted in equation D.62 the equation becomes:

$$(p_s - p_f)\boldsymbol{n} + \boldsymbol{n}(2\eta \mathbf{D}) - \boldsymbol{n}(G(\mathbf{B} - \mathbf{I})) = \Gamma k \boldsymbol{n} \tag{D.65}$$

To determine the dimensionless numbers of the governing equations, a good way is to look in a specific direction. In this model the Y-direction is interesting, because the flow on the cell comes from the Y-direction. The governing equation D.58 of the fluid in y-direction for the micro fluidic cell stretcher becomes:

$$\rho \frac{\partial v_y}{\partial t} + \rho(v_x \frac{\partial v_y}{\partial x} + v_y \frac{\partial v_y}{\partial y}) = -\frac{\partial \rho}{\partial y} + \eta(\frac{\partial^2 v_y}{\partial x^2} + \frac{\partial^2 v_y}{\partial y^2}) \tag{D.66}$$

Because the flow is assumed to be stationary, $\frac{\partial v_y}{\partial t} = 0$, the governing equation of the fluid flow in y-direction becomes:

$$\rho(v_x \frac{\partial v_y}{\partial x} + v_y \frac{\partial v_y}{\partial y}) = -\frac{\partial p}{\partial y} + \eta(\frac{\partial^2 v_y}{\partial x^2} + \frac{\partial^2 v_y}{\partial y^2}) \tag{D.67}$$

The governing equation D.65 for the force balance over the interface will be defined by:

$$(p_s - p_f)\boldsymbol{n} + \boldsymbol{n}\boldsymbol{\tau}_f - \boldsymbol{n}\boldsymbol{\tau}_s = \frac{\Gamma}{R_r}\boldsymbol{n} \tag{D.68}$$

The continuity equation of the flow (D.59) and solid (D.61) are defined in both directions and are shown here:

$$\frac{\partial v_x}{\partial x} + \frac{\partial v_y}{\partial y} = 0 \tag{D.69}$$

$$\frac{\partial r_x}{\partial R_x}\frac{\partial r_y}{\partial R_y} - \frac{\partial r_y}{\partial R_x}\frac{\partial r_x}{\partial R_y} - 1 = 0 \tag{D.70}$$

Scaling the problem

Each problem variable is divided by its characteristic value. For this model the dimensionless variables are:

$$y^* = \frac{y}{W} \tag{D.71}$$

$$x^* = \frac{x}{W} \tag{D.72}$$

$$v_y^* = \frac{v_y}{V} \tag{D.73}$$

$$v_x^* = \frac{v_x}{V_x} \tag{D.74}$$

$$p^* = \frac{p - p_2}{\Delta P_c} \tag{D.75}$$

$$p_{sf}^* = \frac{p_s - p_f}{\Delta P_{sfc}} \tag{D.76}$$

$$R_x^* = \frac{R_x}{R} \tag{D.77}$$

$$R_y^* = \frac{R_y}{R} \tag{D.78}$$

$$r_x^* = \frac{r_x}{R} \tag{D.79}$$

$$r_y^* = \frac{r_y}{R} \tag{D.80}$$

$$\boldsymbol{\tau}_f = \frac{\boldsymbol{\tau}_f^*}{\frac{\eta V}{W}} \tag{D.81}$$

$$\boldsymbol{\tau}_s = \frac{\boldsymbol{\tau}_s^*}{G(\frac{R^2}{R^2} + \frac{RR}{R^2} - \frac{R^2}{R^2})} \tag{D.82}$$

$$R_r^* = \frac{R_r}{R} \tag{D.83}$$

The dimensionless variables with $_c$ are unknown characteristic values and will be determined later. Assumed is that r_x, r_y and R_r scale with solid radius R. For very small deformations the solid radius after deformation is $\approx R$. This assumed can be used because no excessieve deformation is expected. $\boldsymbol{\tau}_s$ is calculated with the following equations:

$$G(\boldsymbol{B}-\boldsymbol{I}) = G(\frac{\partial r_y \partial r_y}{\partial R_y \partial R_y} + \frac{\partial r_y \partial r_x}{\partial R_x \partial R_x} - 1) = [G(\frac{R^2}{R^2} + \frac{RR}{R^2} - \frac{R^2}{R^2})](\frac{\partial r_y^* \partial r_y^*}{\partial R_y^* \partial R_y^*} + \frac{\partial r_y^* \partial r_x^*}{\partial R_x^* \partial R_x^*}) \tag{D.84}$$

Substitution of the dimensionless variables

The dimensionless variables are now substituted into the governing equations D.67,D.68 and continuity equations D.69 and D.70. First the equation D.69 of the continuity equations will be substituted, this gives:

$$[\frac{V_x}{W}]\frac{\partial v_x^*}{\partial x^*} + [\frac{V}{W}]\frac{\partial v_y^*}{\partial y^*} = 0 \tag{D.85}$$

Reverifying by multiply with $\frac{W}{V}$ gives the equation:

$$[\frac{V_x}{V}]\frac{\partial v_x^*}{\partial x^*} + \frac{\partial v_y^*}{\partial y^*} = 0 \tag{D.86}$$

Both $\frac{\partial v_x^*}{\partial x^*}, \frac{\partial v_y^*}{\partial y^*}$ need to be in an order 1 so V_x must be equal to V. If the equation D.70 of the boundary conditions is substitute, this gives:

$$[\frac{R}{R}\frac{R}{R}]\frac{\partial r_x^*}{\partial R_x^*}\frac{\partial r_y^*}{\partial R_y^*} - [\frac{R}{R}\frac{R}{R}]\frac{\partial r_y^*}{\partial R_x^*}\frac{\partial r_x^*}{\partial R_y^*} - 1 = 0 \tag{D.87}$$

Both $\frac{\partial r_y^*}{\partial R_x^*} = 0$ and $\frac{\partial r_x^*}{\partial R_y^*} = 0$, which leaves $RR = R^2$.

If the governing equation D.67 of the fluid is substitute, this gives:

$$[\frac{\rho V^2}{W}](v_x^*\frac{\partial v_y^*}{\partial x^*} + v_y^*\frac{\partial v_y^*}{\partial y^*}) = -[\frac{\Delta P_c}{W}]\frac{\partial p^*}{\partial y^*} + [\frac{\eta V}{W^2}](\frac{\partial^2 v_y^*}{\partial x^{*2}} + \frac{\partial^2 v_y^*}{\partial y^{*2}}) \tag{D.88}$$

If the governing equation D.68 of the solid interface is substitute, this gives:

$$[\Delta P_{sfc}]p_{sf}^*\boldsymbol{n} + [\frac{\eta V}{W}]\boldsymbol{n}\boldsymbol{\tau}_f^* - [G(\frac{R^2}{R^2} + \frac{RR}{R^2} - \frac{R^2}{R^2})]\boldsymbol{n}\boldsymbol{\tau}_s^* = [\frac{\Gamma}{R}]\frac{1}{R_r^*}\boldsymbol{n} \tag{D.89}$$

The equation D.89 could be simplified by:

$$[\Delta P_{sfc}]p_{sf}^*\boldsymbol{n} + [\frac{\eta V}{W}]\boldsymbol{n}\boldsymbol{\tau}_f^* - [G]\boldsymbol{n}\boldsymbol{\tau}_s^* = [\frac{\Gamma}{R}]\frac{1}{R_r^*}\boldsymbol{n} \tag{D.90}$$

Choose important term

Because the micro fluidic cell stretcher has a very small channel, with a low velocity of the fluid, it is assumed that the viscous terms are important. The validity of this assumption has to be checked afterwards. The equation D.88 of the fluid will be multiplied by $[\frac{W^2}{\eta V}]$ which leads to the equation:

$$[\frac{\rho V W}{\eta}](v_x^*\frac{\partial v_y^*}{\partial x^*} + v_y^*\frac{\partial v_y^*}{\partial y^*}) = -[\frac{\Delta P_c W}{\eta V}]\frac{\partial p^*}{\partial y^*} + (\frac{\partial^2 v_y^*}{\partial x^{*2}} + \frac{\partial^2 v_y^*}{\partial y^{*2}}) \tag{D.91}$$

From appendix ?? the shear modulus can be chosen as important term. This assumption will be checked afterwards. If the equation D.90is multiplied with $[\frac{1}{G}]$ then the equation for the force balance over the fluid-solid interface becomes:

$$[\frac{\Delta P_{sfc}}{G}]p^*_{sf}\boldsymbol{n} + [\frac{\eta V}{WG}]\boldsymbol{n}\boldsymbol{\tau}^*_f - \boldsymbol{n}\boldsymbol{\tau}^*_s = [\frac{\Gamma}{GR}]\frac{1}{R^*_\tau}\boldsymbol{n} \tag{D.92}$$

To find dimensionless numbers, the equation D.90 is turned to equation:

$$[\frac{\Delta P_{sfc}}{G}]p^*_{sf}\boldsymbol{n} + [\frac{R}{W}\cdot\frac{\eta\frac{V}{R}}{G}]\boldsymbol{n}\boldsymbol{\tau}^*_f - \boldsymbol{n}\boldsymbol{\tau}^*_s = [\frac{\Gamma}{\eta V}\cdot\frac{\eta\frac{V}{R}}{G}]\frac{1}{R^*_\tau}\boldsymbol{n} \tag{D.93}$$

Determine unknown characteristic values

From the equation D.91 of the fluid, the unknown characteristic values are defined by:

$$\Delta P_c = \frac{\eta V}{W} \tag{D.94}$$

$$Re = \frac{\rho V W}{\eta} \tag{D.95}$$

Where equation D.94 is the characteristic pressure drop over the cross slot. The pressure drop is dominated by the viscous forces of the fluid. Equation D.95 is the Reynolds number. If the characteristic values are substitute into equation D.91 the governing equation for the fluid becomes:

$$[Re](v^*_x\frac{\partial v^*_y}{\partial x^*} + v^*_y\frac{\partial v^*_y}{\partial y^*}) = -\frac{\partial p^*}{\partial y^*} + (\frac{\partial^2 v^*_y}{\partial x^{*2}} + \frac{\partial^2 v^*_y}{\partial y^{*2}}) \tag{D.96}$$

From the equation D.93 of the fluid-solid interaction, the unknown characteristic values are defined by:

$$\Delta P_{sfc} = G \tag{D.97}$$

$$De = \frac{\eta\frac{V}{R}}{G} \tag{D.98}$$

$$F_{RW} = \frac{R}{W} \tag{D.99}$$

$$Ca = \frac{\eta V}{\Gamma} \tag{D.100}$$

From equation D.70 was found that $R_{x1}R_{y2} = R^2$. If R_{y2} is replaced by R the unknown characteristic value of R_{xc} could be found:

$$R_{xc} = R \tag{D.101}$$

If the characteristic values are substitute into equation **??** the governing equation for the fluid-solid becomes:

$$p^*_{sf}\boldsymbol{n} + [F_{RW} \cdot De]\boldsymbol{n}\boldsymbol{\tau}^*_f - \boldsymbol{n}\boldsymbol{\tau}^*_s = [\frac{1}{Ca} \cdot De]\frac{1}{R^*_r}\boldsymbol{n} \tag{D.102}$$

Control of the chosen important terms

The remaining dimensionless groups in the equations D.96 and **??** must have a value between 0 and 1 if realistic values are substitute. Realistic values for the micro fluidic cell stretcher are ρ =1000 kg/m^3, η = 0.001 Pa/s, V =1 mm/s G =380 Pa, W =100 μm, R =5 μm and Γ =0.03 mN/m . Substitute these values inside the remaining dimensionless groups of the fluid gives:

$$Re = \frac{1000 \cdot 0.001 \cdot 0.0001}{0.001} = 0.1 \tag{D.103}$$

The dimensionless groups of the fluid are scaled properly because the Re-number in equation D.96 is $\ll 1$ and all other factors are equal to 1. Substitute the values inside the remaining dimensionless groups of the fluid-solid interaction gives:

$$De = \frac{0.001 \cdot \frac{0.001}{0.000005}}{380} = 5.26 \cdot 10^{-4} \tag{D.104}$$

$$Ca = \frac{0.000005 \cdot 380}{0.00003} = 63.3 \tag{D.105}$$

$$F_{RW} = \frac{0.000005}{0.0001} = 0.05 \tag{D.106}$$

The dimensionless groups of the fluid-solid interaction are scaled properly, because $\frac{1}{Ca}$,De and F_{RW} in equation D.102 are $\ll 1$.

Conclusion

If the model is simulated, the following dimensionless numbers must be taken in account:

$$Re = \frac{\rho V W}{\eta} = 0.1 \tag{D.107}$$

$$De = \frac{\eta \frac{V}{W}}{G} = 5.26 \cdot 10^{-4} \tag{D.108}$$

$$Ca = \frac{0.000005 \cdot 380}{0.00003} = 63.3 \tag{D.109}$$

$$F_{RW} = \frac{0.000005}{0.0001} = 0.05 \tag{D.110}$$

The Reynolds number is low, which means that the flow is laminar. The Reynolds number is < 1, which means that the fluid flow is dominate by viscous forces. The Deborah number is low, which indicates that the resistance time of the cell against deformation is higher than of the resistance time of the fluid. The Capillary number is high, which could indicate that the surface tension influence is very small, but from equation D.102 the Capillary number has significant influence on the deformation of the solid because the stress of the flow $\boldsymbol{\tau}_f$ and the curvature of the solid R_r scale with an order $O(10^{-7})$ to the pressure difference over the surface p_{sf} and stress in the surface $\boldsymbol{\tau}_s$, following equation D.102.

$$[O(1)]p^*_{sf}\boldsymbol{n} + [O(10^{-7})]\boldsymbol{n}\boldsymbol{\tau}^*_f - [O(1)]\boldsymbol{n}\boldsymbol{\tau}^*_s = [O(10^{-7})]\frac{1}{R^*_r}\boldsymbol{n} \tag{D.111}$$

Appendix E

Designs of cross slot chip and micro valve parts

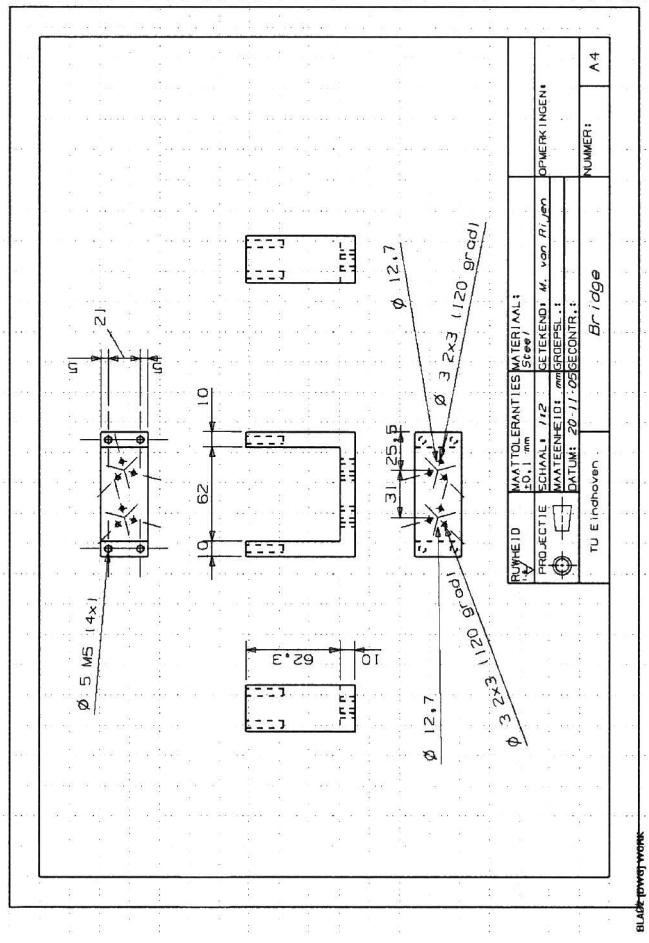

Figure E.1: Drawing of the holder of the actuators

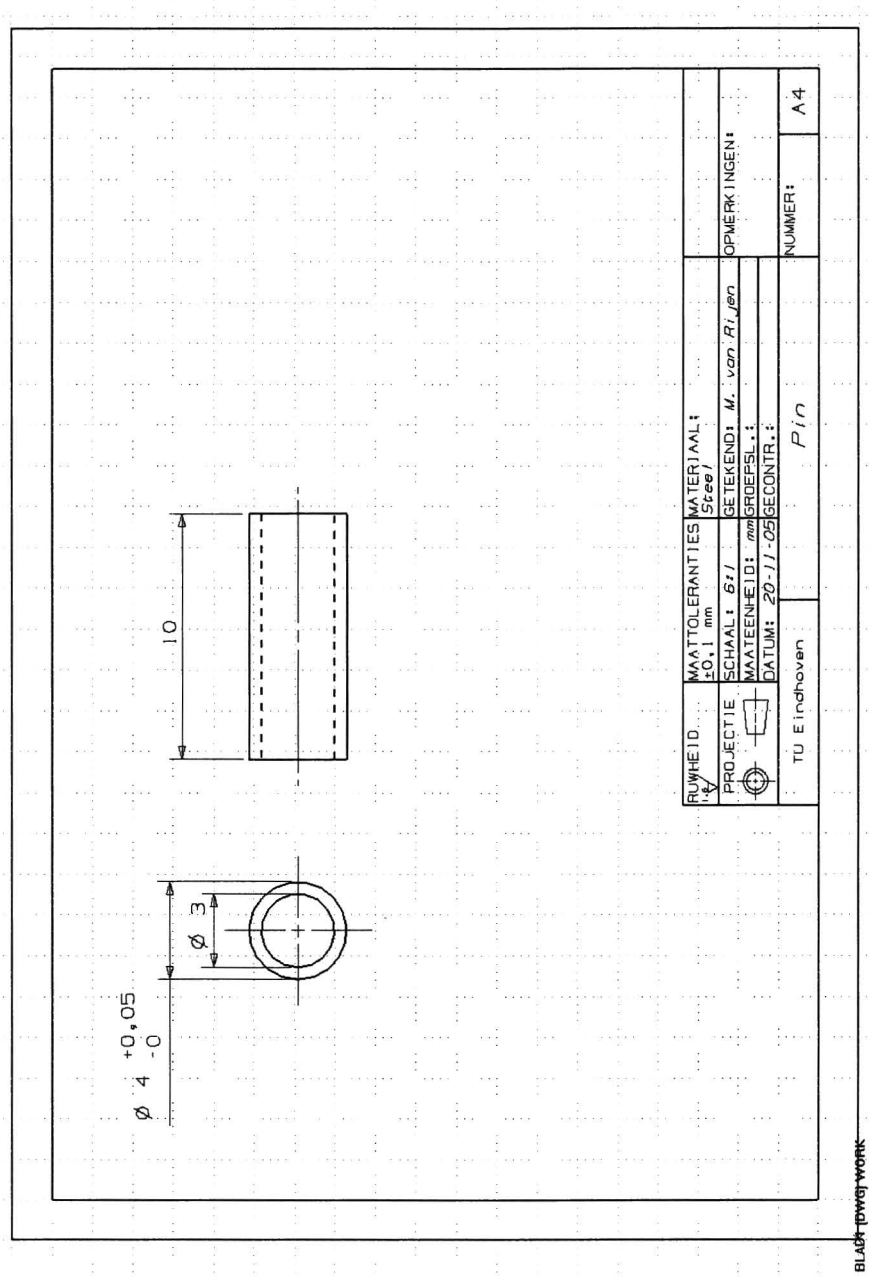

Figure E.2: Drawing of the connection nipple

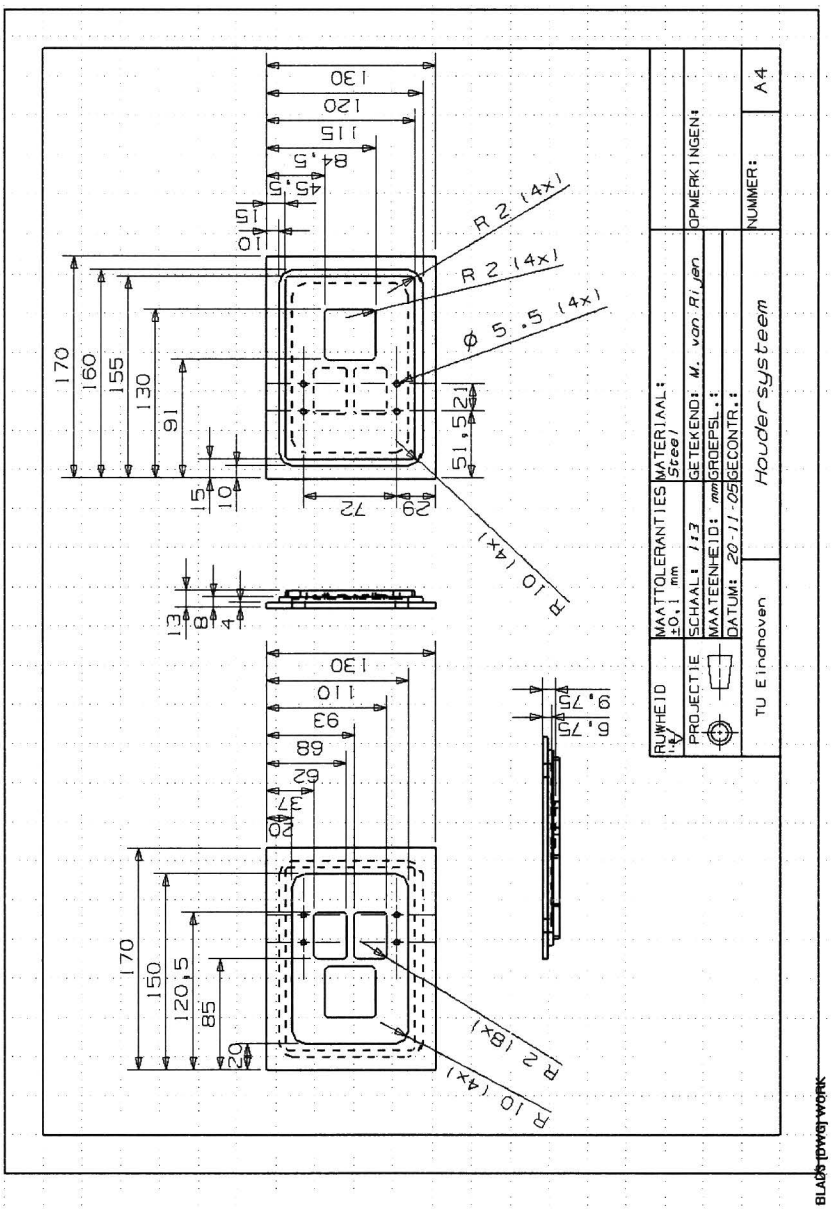

Figure E.3: Drawing of the base plate

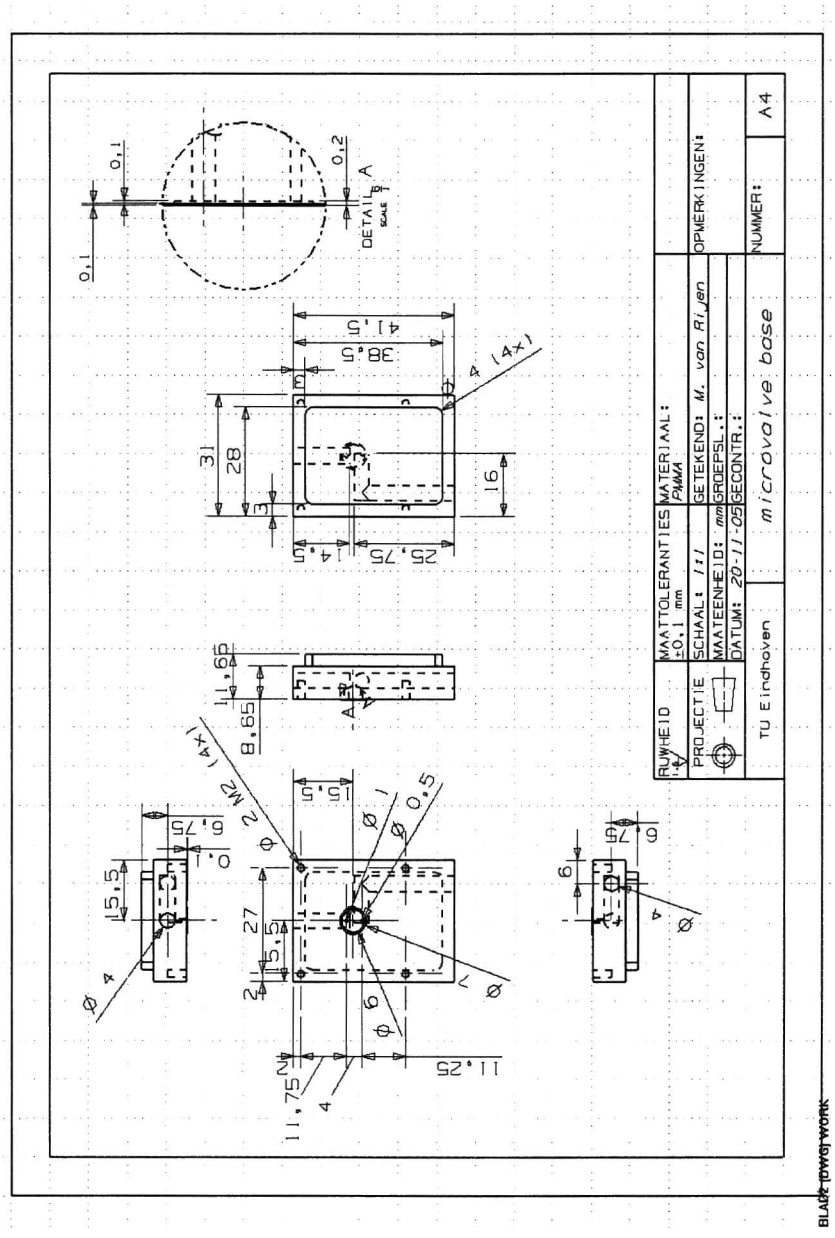

Figure E.4: Drawing of the micro valve base right

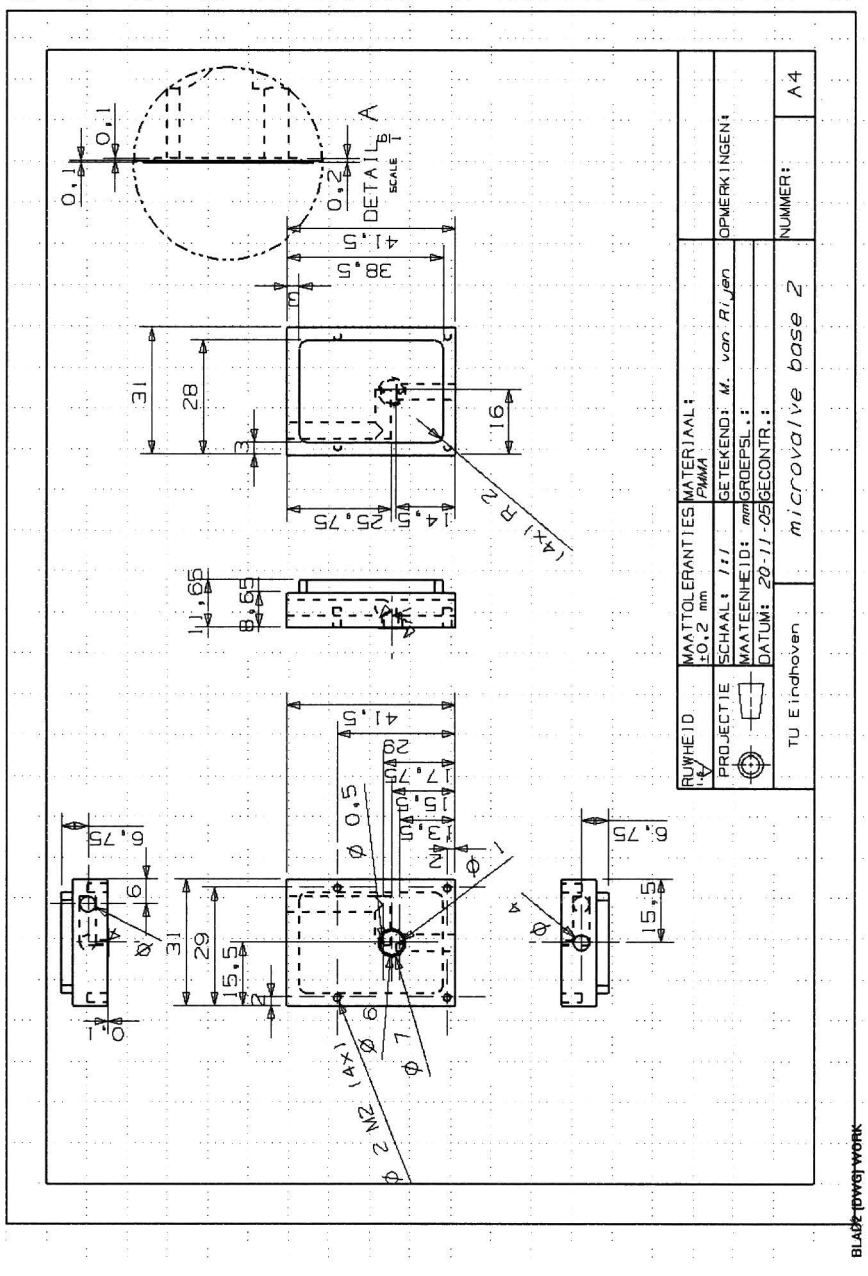

Figure E.5: Drawing of the micro valve base left

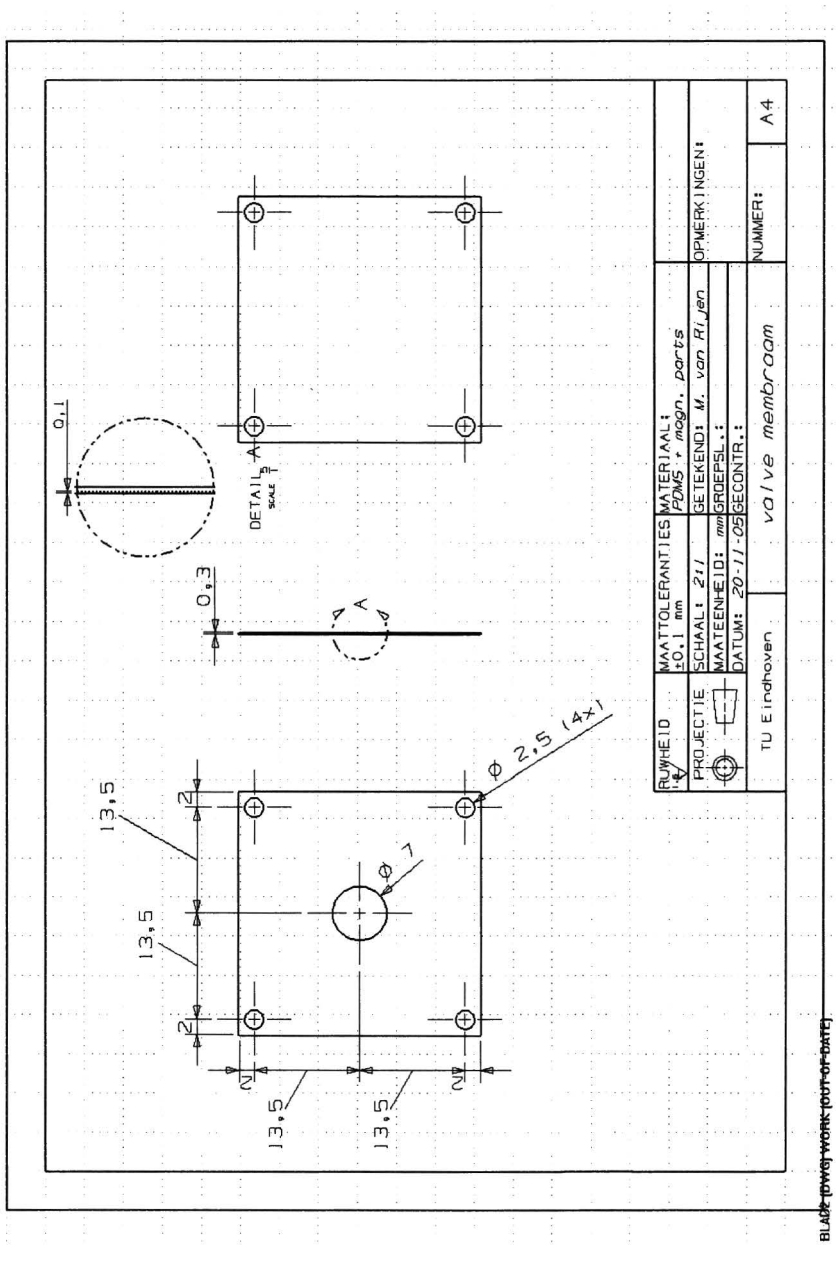

Figure E.6: Drawing of the micro valve membrane

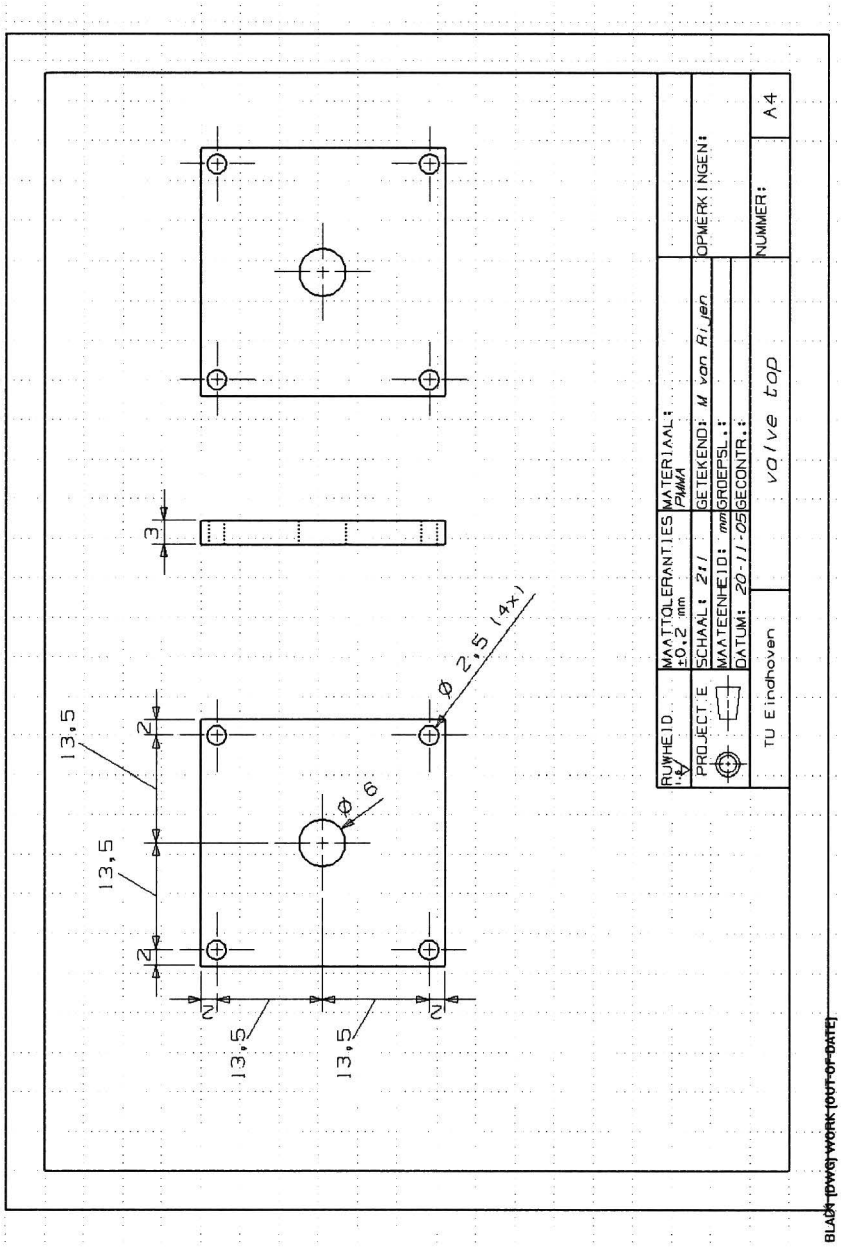

Figure E.7: Drawing of the micro valve top

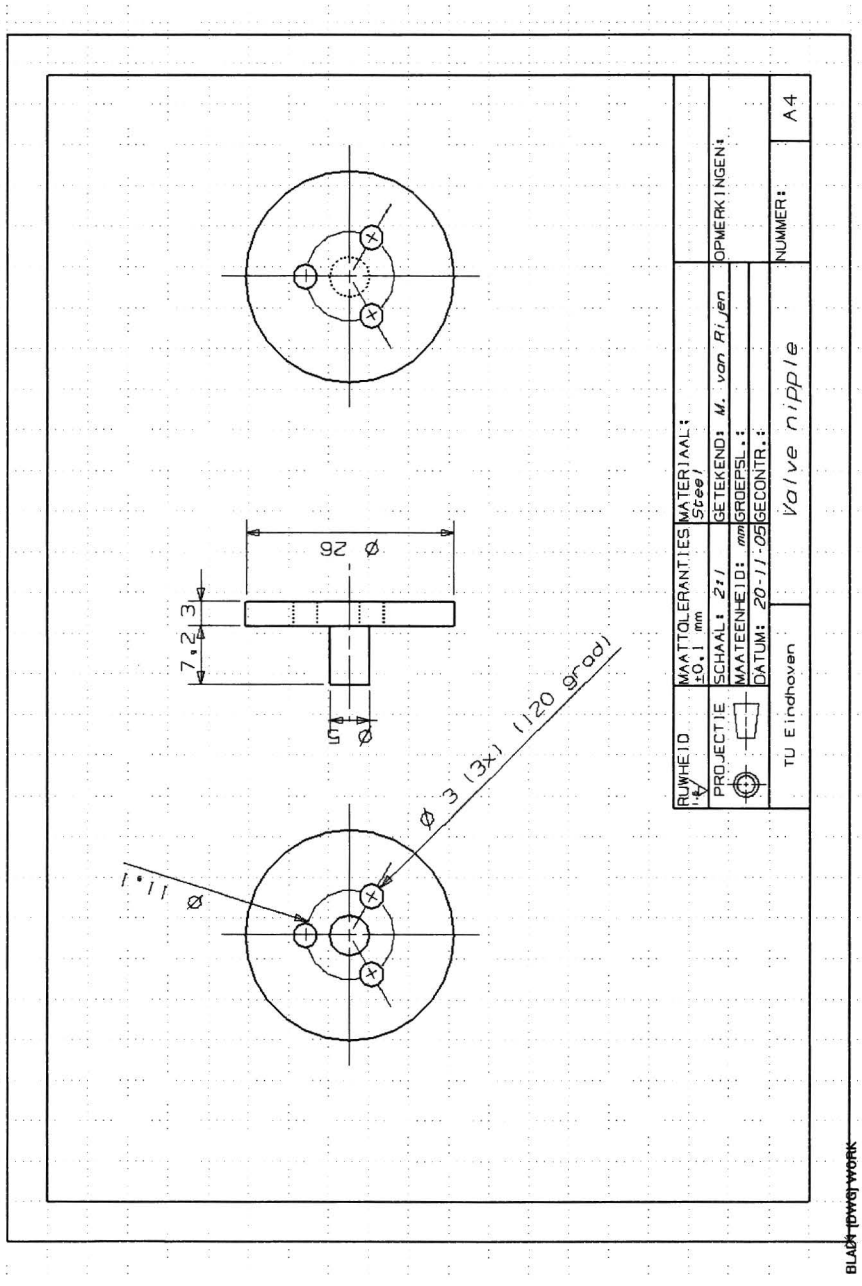

Figure E.8: Drawing of the micro valve actuator nipple

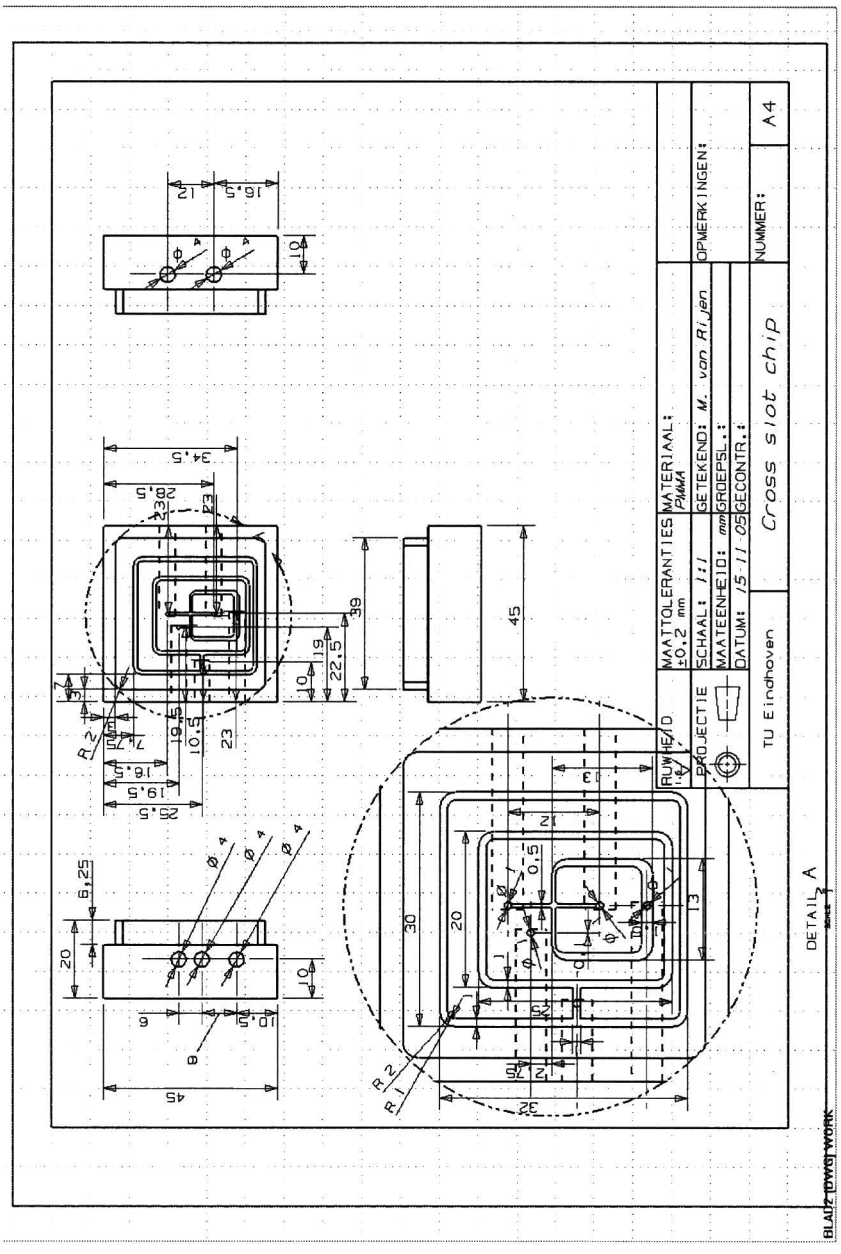

Figure E.9: Drawing of the cross slot chip

Appendix F

Other concepts micro valve

Because many ideas were generated in the course of the study, an overview of some concepts are given in this appendix. Some other ideas than the membrane micro valve will be shown in this appendix.

Nippel

For the control the flow inside the micro channel, a small change in resistance inside the channel can influence the velocity inside the cross slot chip. The principle of a nippel can be seen in figure F.1

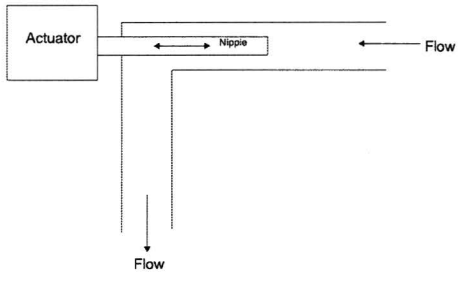

Figure F.1: Nippel micro valve

Here a nipple inside the micro channel can be actuated, so the resistance inside the micro channel changes with the length of the nipple inside the channel. This concept was not chosen, because of the moving part inside the micro channel and the sealing to the outer world.

Squeezing tubes

Here tubes are squeezed to change the resistance on the left or right side of the channel. The squeezing part will be an off axis axle which will be rotate with an Maxwell actuator, see figure F.2.

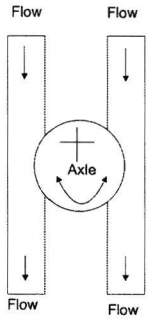

Figure F.2: Squeezing tube micro valve

The control of the rotation needs to be very accurate, in the order of less than one degree rotation. To reach this accuracy, a magnetic encoder was needed, because this encoder type are the most relegable. Besides the encoder, a gearbox is needed to reduce the rotation of the actuator. The margin of this gearbox needs to be removed, for example with a spring. This makes the change for an accurate control the axle even less. Beside the complex electric actuation of the axle, the tubes need to be close very thighs to get more resistance than the cross slot it self. Because of the margin in the actuation of the axle and the very tight closing of the tubes this concept was also not chosen.

Appendix G

Calculations micro valve

For the micro valve all the resistance of the cross slot system are calculated. The micro valve is located 'far' from the cross slot so the fluid resistance of the control valve needs to be higher than the cross slot own fluid resistance. First the resistance and pressure drop of all components of the cross slot system are calculated. Assumptions are that the liquid inside the fluid has the same properties as water and the velocity of the fluid inside the cross slot is $V_{crossslot}$= 1 mm/sec.

Resistance and pressure drop of cross slot

Since the width of the channel (W) and the hight of the channel (H) is the same ($W \approx H$), the resistance of the cross slot can be calculated with equation G.1, following [Beebe et al., 2002]:

$$R_{crossslot} = \frac{12\mu L}{WH^3}[1 - \frac{H}{W}(\frac{192}{\pi^5}\sum_{n=1,3,5}^{\infty}\frac{1}{n^5}\tanh(\frac{n\pi W}{2H}))]^{-1} \tag{G.1}$$

Where:

W : Width of the channel (500 μm)

H : Height of the channel (500 μm)

μ : Fluid viscosity, water (0.001 Pa·s)

L : Channel length (12.5 mm)

The length of the cross slot is the sum of inlet and outlet and the midsection of the cross slot. The resistance of the cross slot is $R_{crossslot} = 3.8 \cdot 10^9$ Pa·s·m^{-3}. The flow rate ($Q_{crossslot}$) can be calculated with equation G.2:

$$Q_{crossslot} = W \cdot H \cdot V_{crossslot} \tag{G.2}$$

The flow rate inside the cross slot is equal to 15 μl/min. The pressure drop in the cross slot can be calculated with Hagen-Poiseuille law defined by equation G.3.

$$\Delta P_{crossslot} = Q_{crossslot} \cdot R_{crossslot} \tag{G.3}$$

where:

$Q_{crossslot}$: Velocity of fluid inside cross slot

The pressure drop in the cross slot is $\Delta P_{crossslot} = 0.97$ Pa.

Resistance and pressure drop of tubing

The resistance of the tube can be calculated with the equation G.4.

$$R_{tube} = \frac{8\mu L}{\pi r^4} \tag{G.4}$$

Where:

μ : Fluid viscosity, water (0.001 Pa $\cdot$ s)

L : Channel length 100 mm

r : Channel radius 2 mm

If the length of the tube of the cross slot is estimated on 100 mm the resistance of the tube is $R_{tube} = 2.55 \cdot 10^8$ Pa·s·m^{-3}. The flow rate inside the tube (Q_{tube}) is the same as the flow rate inside the cross slot ($Q_{crossslot}$). The pressure drop in the tube can be calculated with Hagen-Poiseuille law defined by equation G.5.

$$\Delta P_{tube} = Q_{tube} \cdot R_{tube} \tag{G.5}$$

The pressure drop inside the tube is $\Delta p_{tube} = 0.064$ Pa.

Resistance and pressure drop of micro valve

The resistance of the cross slot must be $> R_{crossslot} = 3.8 \cdot 10^9$ Pa·s·m^{-3}. After some configurations a feasibility dimensions for the micro valve were found. For the micro valve the length will be L=2.5 mm. The width of the valve will be w =500 μm and hight of valve will be maximum h = 200 μm. The resistance of the micro valve can be calculated with the equation G.6.

$$R_{microvalve} = \frac{12\mu L}{WH^3}[1 - \frac{H}{W}(\frac{192}{\pi^5}\sum_{n=1,3,5}^{\infty}\frac{1}{n^5}\tanh(\frac{n\pi W}{2H}))]^{-1} \tag{G.6}$$

Where:

W : Width of the micro valve (500 μm)

H : Height of the micro valve (200 μm)

μ : Fluid viscosity, water (0.001 Pa·s)

L : Channel length (2.5 mm)

The resistance of the micro valve is $R_{microvalve} = 8.0 \cdot 10^9$ Pa·s·m^{-3}, which is higher than the resistance of the cross slot $R_{crossslot} = 3.8 \cdot 10^9$ Pa·s·m^{-3}. The flow rate inside the micro valve ($Q_{microvalve}$) is the same as the flow rate inside the cross slot ($Q_{crossslot}$). The pressure drop over the micro valve can be calculated with equation G.7.

$$\Delta P_{microvalve} = Q_{microvalve} \cdot R_{microvalve} \tag{G.7}$$

The pressure drop over the micro valve, at a hight of 200 μm, is $\Delta P_{microvalve} = 2.0$ Pa, following equation G.7.

Resistance and velocity of flow of micro valve during actuation

If the valve is decreasing the gab of 200μm the hydraulic resistance of the valve also will change. The hydraulic resistance dependence on the hight of the gab of the micro valve. If the hight of the gab is decreased form 200μm to 50μm and the pressure drop over the valve is constant ($\Delta P_{microvalve} = 2.0$ Pa), the resistance increases from $8.0 \cdot 10^9$ Pa·s·m^{-3} to $4.8 \cdot 10^{11}$ Pa·s·m^{-3} like shown in figure G.1, according equation G.6 and G.7.

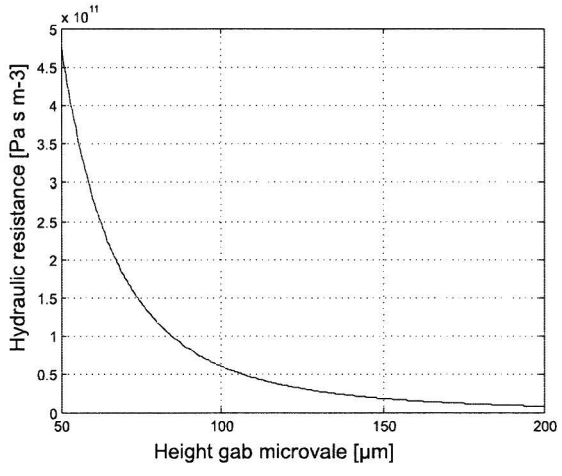

Figure G.1: Valve hydraulic resistance against height of the gab of the micro valve

If the pressure drop is constant ($\Delta P_{microvalve} = 2.0$ Pa), the flow rate through the micro valve decreases form 15 μL/min to 0.25 μL/min will be like figure ,according equation G.7:

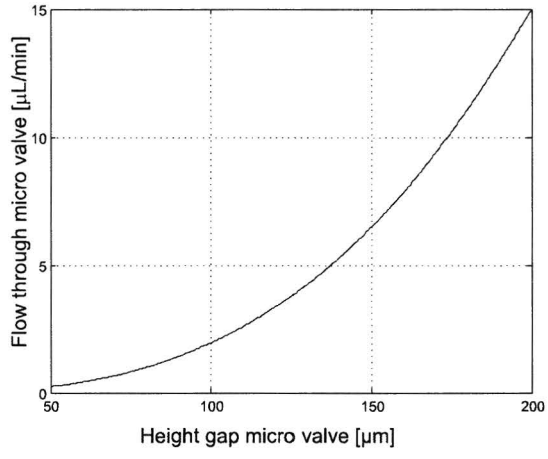

Figure G.2: Valve flow rate against height of the gab of the micro valve

Appendix H

Calculations voice coil actuator 1N

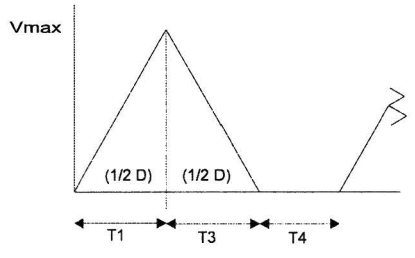

Figure H.1: Velocity profile of voice coil actuator

Where D is the distance of translation (200 μm), t_1 is acceleration time, t_3 is decelerations time and t_4 is dwell time. The frequency the voice coil actuator should translate up and down in assumed 50 Hertz. If is assumed that the voice coil actuator has a triangle velocity profile like figure H.1, the time to up or go down is 0.01 s. The time for accelerate t_1 and decelerate t_3 is 0.005 s. The maximum speed of the actuator can be calculated with equation, following [Kimco, 2005]:

$$v_{max} = \frac{D}{t_1 + t_3} = \frac{0.0002}{2 \cdot 0.01} = 0.01m/s \tag{H.1}$$

The maximum acceleration of the actuator can be calculated with equation:

$$a_{max} = \frac{v_{max}}{t_1} = \frac{0.01}{0.005} = 2m/s^2 \tag{H.2}$$

The force needed for this acceleration can be calculated with equation:

$$F_a = (m) \cdot a = (0.6) \cdot 2 = 1.2N \tag{H.3}$$

Where:

m : Mass on coil, assumed to be 600 gram

The piek force of the actuator can be calculated with equation.

$$F_p = F_a + F_{load} + F_{fric} = 1.2 + 1 + 0 = 2.2N \tag{H.4}$$

Where:

F_{load} : The force needed to deflect the membrane and close the valve $0.523N$ calculated in section 4.3.4. For a safety marge assume the force will be around 1 N.

F_{fric} : The friction force of the actuator guiding. This is assumed to be 0 N.

The root mean square (RMS) force of the actuator can be calculated with equation, following [Kimco, 2005]:

$$F_{rms} = \sqrt{\frac{(F_p^2 \cdot t_1) + (((F_a - F_{fric} - F_{load})^2)t_3)}{t_1 + t_3 + t_4}} = 1.562N \tag{H.5}$$

Choice of actuator

The displacement of the voice coil actuator is lineair and should be at least 200 μm. The peak force is at least 2.2 N and the F_{rms} is 1.562 N. From table H.1 a choice can be made which actuator satisfy these requirements.

10 Sec Peak Force (F_p) Lb.	Stroke ± In.	Force Constant (K_f) Lb. / AMP ±10%	Motor Contant (K_m) Lb. / √Watt	Resistance @ 25°C Ohms ±12.5%	Elec. Time Constant µ Sec.	Thermal Resistance of Coil °C / Watt	Weight-Coil	Total Weight	Envelope Dimensions In. Height	Width or Diameter	Length or Length at Mid Stroke
2.5	0.03	0.53	0.40	1.8	22	10.5	0.35 Oz	3.2 Oz	—	1.09	1.20
2.0	0.689	0.67	0.31	4.6	731	8.14	0.70 Oz	15.6 Oz	1.33	1.25	3.00
5.0	0.09	1.25	0.61	4.2	54	5.0	0.63 Oz	7.7 Oz	—	1.49	1.30
5.0	0.44	1.20	0.54	5.0	740	3.4	0.77 Oz	22.7 Oz	1.36	2.75	2.38
10.0	0.04	1.35	1.00	1.9	100	2.8	0.80 Oz	9.6 Oz	—	1.50	1.53
7.6	0.10	1.39	0.61	4.5	360	4.5	1.33 Oz	7.44 Oz	—	1.50	1.56
32.5	0.25	3.75	2.03	3.4	567	3.8	0.35 Oz	2.85 Oz	1.77	2.75	3.25

10 Sec Peak Torque (T_p) Oz. In.	Stroke Angular ± Degrees	Torque Constant (K_t) at Midpoint Oz. In. / AMP ±10%	Motor Contant (K_m) Oz. In. / √Watt	Resistance @ 25°C Ohms ±12.5%	Elec. Time Constant µ Sec.	Thermal Resistance of Coil °C / Watt	Weight-Moving Member	Total Weight	Outside Radius In.	Width In.	Length In.
11	15.0	5.5	2.4	5.2	540	30.6	2.9 Oz	3.6 Oz	0.81	1.94	0.76
25	16.0	16.0	4.19	14.6	180	9.7	1.2 Oz	6.8 Oz	1.43	1.84	2.86
120	15.0	19.0	13.8	1.9	730	5.2	0.75 Oz	15.6 Oz	3.12	1.19	3.75
60	20.0	11.0	10.5	1.1	250	6.6	0.60 Oz	14.6Oz	3.12	1.19	3.75
170	10.0	45.0	20.6	4.75	740	5.1	1.10 Oz	18.6 Oz	3.40	1.19	3.75
1536	15.0	230.4	63.4	13.0	2300	1.4	11.0 Oz	147.2 Oz	2.75	5.5	2.19

Table H.1: Voice coil actuator Bei Kimco 1

The A08-10-000A satisfy the requirements. The technical properties of the voice coil actuator are:

m_{coil} : Mass of coil, 0.00751 Kg

K_f : The force sensitivity, 1.15 N/A

K_b : Actuator back EMF, 1.15 V/m/s

v_{maxact} : Maximum voltage, 6.9 V

V_L : If is assuming that the coil inductance $L\frac{di}{dt}$ is nearly negligible or order 1 V

$V_{eleclos}$: The electrical losses is estimated, 1 V

R_{cold} : Resistance actuator cold, 1.2 Ω

R_{tol} : Tolerance on the resistance of the actuator, 12.5 %

R_{hot} : Resistance actuator hot, $(\frac{R_{cold}}{100} R_{tol}) + R_{cold} = 1.35\Omega$

A drawing of this actuator can be found an section H.

Control choice voice coil actuator

The new force needed for this acceleration can be calculated with equation:

$$F_a = (m + m_{coil}) \cdot a = (0.6 + 0.00751) \cdot 2 = 1.215N \tag{H.6}$$

This results in a new piek force, following equation H.4, of 2.215 N. Calculation of the generated back EFM results in:

$$v_b = v_max \cdot K_b = 0.01 \cdot 1.15 = 0.0115V \tag{H.7}$$

The force producing voltage can be calculate with equation.

$$v_c = v_{maxact} - v_b - v_L - v_{eleclos} = 0.01 - 0.0115 - 1 - 1 = 4.89V \tag{H.8}$$

The force producing current can be calculated with equation.

$$I_{max} = \frac{v_c}{R_{cold}} = \frac{4.89}{1.2} = 4.07A \tag{H.9}$$

For the worst case, when the resistance of the actuator is equal to R_{hot}, the force producing current can be calculated with equation.

$$I_{min} = \frac{v_c}{R_{hot}} = \frac{4.89}{1.35} = 3.62A \tag{H.10}$$

The maximum available force can be calculated with equation.

$$F_{max} = I_{min} \cdot K_f = 3.62 \cdot 1.15 = 4.16N \tag{H.11}$$

Conclusion

The peak force needed for the micro valve is estimated on 2.2 N, the voice coil actuator A08-10-000A has a maximum force of 4.16 N which is higher the the maximum force needed to close the valve. Also the stroke of 200 μ m is no problem for this actuator, which has a maximum stroke of $\pm$ 2.03 mm. The K_f value is constant over the entire stroke. The voice coil is constructed around the middle of the stroke length, where V=0. The voice coil actuator A08-10-000A satisfy the requirements. A drawing of the actuator with specifications can be seen in figure H.2.

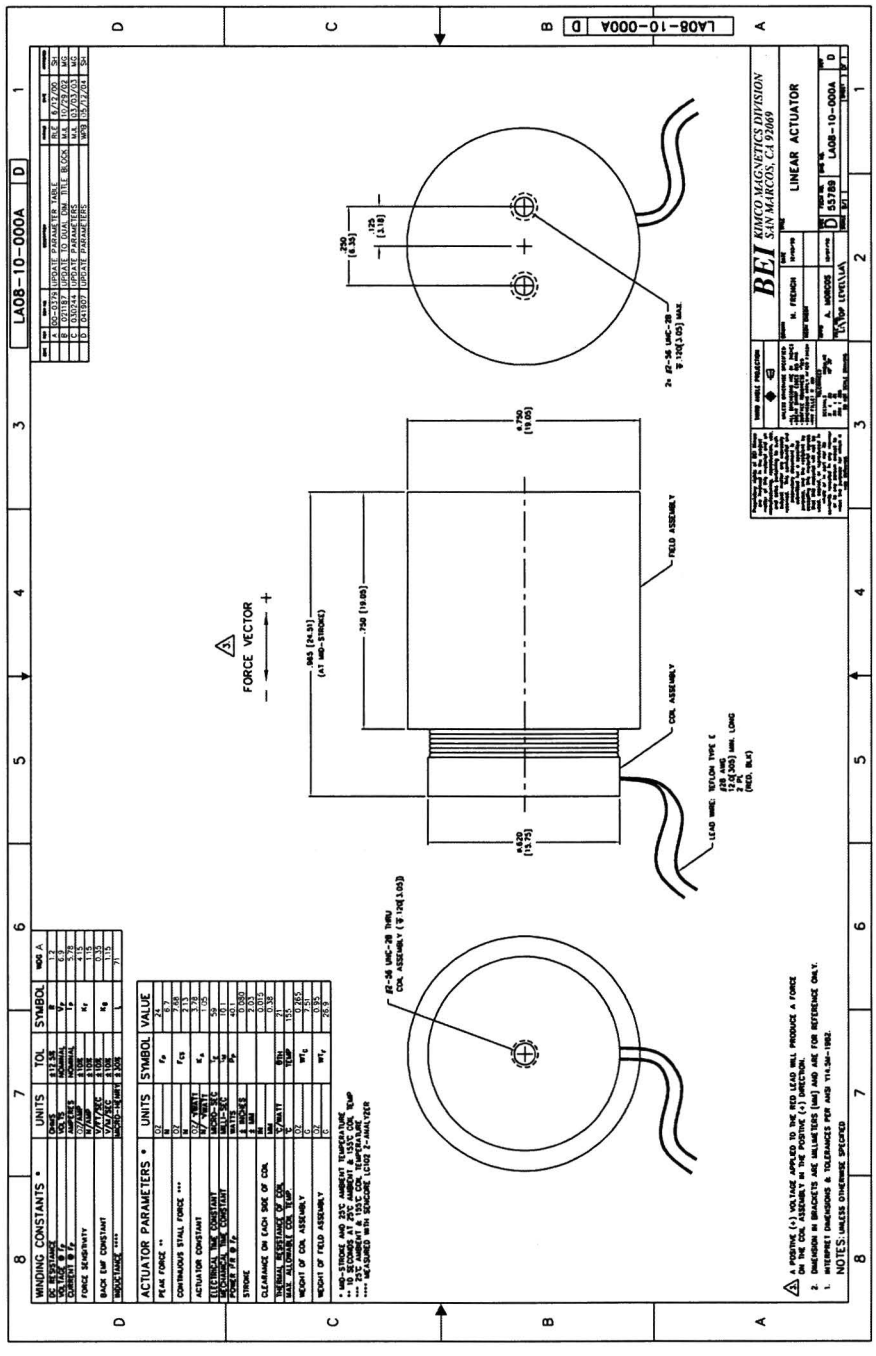

Figure H.2: Drawing of the voice coil actuator Bei Kimco LA12

Calculations voice coil actuator 10 N

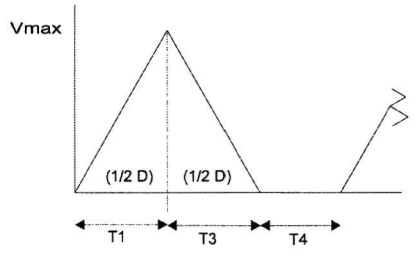

Figure H.3: Velocity profile of voice coil actuator

Where D is the distance of translation (200 μm), t_1 is acceleration time, t_3 is decelerations time and t_4 is dwell time. The frequency the voice coil actuator should translate up and down in assumed 50 Hertz. If is assumed that the voice coil actuator has a triangle velocity profile like figure H.3, the time to up or go down is 0.01 s. The time for accelerate t_1 and decelerate t_3 is 0.005 s. The maximum speed of the actuator can be calculated with equation, following [Kimco, 2005]:

$$v_{max} = \frac{D}{t_1 + t_3} = \frac{0.0002}{2 \cdot 0.01} = 0.01 m/s \tag{H.12}$$

The maximum acceleration of the actuator can be calculated with equation:

$$a_{max} = \frac{v_{max}}{t_1} = \frac{0.01}{0.005} = 2 m/s^2 \tag{H.13}$$

The force needed for this acceleration can be calculated with equation:

$$F_a = (m) \cdot a = (0.6) \cdot 2 = 1.2N \tag{H.14}$$

Where:

m : Mass on coil, assumed to be 0.6 Kg

The piek force of the actuator can be calculated with equation.

$$F_p = F_a + F_{load} + F_{fric} = 1.2 + 10 + 0 = 11.2N \tag{H.15}$$

Where:

F_{load} : The force needed to deflect the membrane and close the valve $5.36N$ calculated in section 4.3.4. For a safety marge assume the force will be around 10 N.

F_{fric} : The friction force of the actuator guiding. This is assumed to be 0 N.

The root mean square (RMS) force of the actuator can be calculated with equation, following [Kimco, 2005]:

$$F_{rms} = \sqrt{\frac{(F_p^2 \cdot t_1) + (((F_a - F_{fric} - F_{load})^2)t_3)}{t_1 + t_3 + t_4}} = 10.07N \tag{H.16}$$

Choice of actuator

The displacement of the voice coil actuator is lineair and should be at least 200 μm. The peak force is at least 11.2 N and the F_{rms} is 10.07 N. From table H.2 a choice can be made which actuator satisfy these requirements.

10 Sec Peak Force (F_p) Lb.	Stroke ± In.	Force Constant (K_f) Lb. / AMP ±10%	Motor Contant (K_m) Lb. / Watt	Resistance @ 25°C Ohms ±12.5%	Elec. Time Constant µ Sec.	Thermal Resistance of Coil °C / Watt	Weight-Coil	Total Weight	Envelope Dimensions In. Height	Width or Diameter	Length or Length at Mid Stroke
2.5	0.03	0.53	0.40	1.8	22	10.5	0.35 Oz	3.2 Oz	—	1.09	1.20
2.0	0.689	0.67	0.31	4.6	731	8.14	0.70 Oz	15.6 Oz	1.33	1.25	3.00
5.0	0.09	1.25	0.61	4.2	54	5.0	0.63 Oz	7.7 Oz	—	1.49	1.50
5.0	0.44	1.28	0.54	5.0	740	3.4	0.77 Oz	22.7 Oz	1.36	2.75	2.38
10.0	0.04	1.35	1.00	1.9	100	2.8	0.80 Oz	9.6 Oz	—	1.50	1.53
7.6	0.10	1.39	0.61	4.5	360	4.5	1.33 Oz	7.44 Oz	—	1.50	1.56
32.5	0.25	3.75	2.03	3.4	567	3.8	0.35 Oz	2.85 Oz	1.77	3.75	3.25

10 Sec Peak Torque (T_p) Oz. In.	Stroke Angular ± Degrees	Torque Constant (K_t) at Midpoint Oz. In. / AMP ±10%	Motor Contant (K_m) Oz. In. / √Watt	Resistance @ 25°C Ohms ±12.5%	Elec. Time Constant µ Sec.	Thermal Resistance of Coil °C / Watt	Weight-Moving Member	Total Weight	Outside Radius In.	Width In.	Length In.
11	15.0	5.5	2.4	5.2	540	30.6	2.0 Oz	3.6 Oz	0.81	1.94	0.76
25	16.0	16.0	4.19	14.6	180	9.7	1.2 Oz	6.8 Oz	1.43	1.94	2.86
120	15.0	19.0	13.8	1.9	730	5.2	0.75 Oz	15.6 Oz	3.12	1.19	3.75
60	20.0	11.0	10.5	1.1	250	6.6	0.60 Oz	14.6Oz	3.12	1.19	3.75
170	10.0	43.0	20.6	4.75	740	5.1	1.10 Oz	18.0 Oz	3.46	1.19	3.75
1536	15.0	230.4	63.4	13.0	2300	1.4	11.0 Oz	147.2 Oz	2.75	5.5	2.19

Table H.2: Voice coil actuator Bei Kimco 1

The A12-17-000A satisfy the requirements. The technical properties of the voice coil actuator are:

m_{coil} : Mass of coil, 0.0326 Kg

K_f : The force sensitivity, 7.34 N/A

K_b : Actuator back EMF, 7.35 V/m/s

v_{maxact} : Maximum voltage, 17 V

V_L : If is assuming that the coil inductance $L\frac{di}{dt}$ is nearly negligible or order 1 V

$V_{eleclos}$: The electrical losses is estimated, 1 V

R_{cold} : Resistance actuator cold, 2.8 Ω

R_{tol} : Tolerance on the resistance of the actuator, 12.5 %

R_{hot} : Resistance actuator hot, $(\frac{R_{cold}}{100} R_{tol}) + R_{cold} = 3.15\Omega$

A drawing of this actuator can be found an section H.

Control choice voice coil actuator

The new force needed for this acceleration can be calculated with equation:

$$F_a = (m + m_{coil}) \cdot a = (0.6 + 0.0326) \cdot 2 = 1.265N \tag{H.17}$$

This results in a new piek force, following equation H.4, of 11.265 N. Calculation of the generated back EFM results in:

$$v_b = v_max \cdot K_b = 0.01 \cdot 7.35 = 0.0735V \tag{H.18}$$

The force producing voltage can be calculate with equation.

$$v_c = v_{maxact} - v_b - v_L - v_{eleclos} = 0.01 - 0.0735 - 1 - 1 = 14.93V \tag{H.19}$$

The force producing current can be calculated with equation.

$$I_{max} = \frac{v_c}{R_{cold}} = \frac{14.93}{2.8} = 5.33A \tag{H.20}$$

For the worst case, when the resistance of the actuator is equal to R_{hot}, the force producing current can be calculated with equation.

$$I_{min} = \frac{v_c}{R_{hot}} = \frac{14.93}{3.15} = 4.74A \tag{H.21}$$

The maximum available force can be calculated with equation.

$$F_{max} = I_{min} \cdot K_f = 4.74 \cdot 7.34 = 34.78N \tag{H.22}$$

Conclusion

The peak force needed for the micro valve is estimated on 11.2 N, the voice coil actuator A12-17-000A has a maximum force of 34,78 N which is higher the the maximum force needed to close the valve. Also the stroke of 200 μ m is no problem for this actuator, which has a maximum stroke of $\pm$ 3.8 mm. The K_f value is not constant over the entire stroke, but because our stroke is very small, and the displacement is constructed around the middle of the stroke, the K_f can be assumed constant. The voice coil actuator A12-17-000A satisfy the requirements. A drawing of the actuator with specifications can be seen in figure H.4.

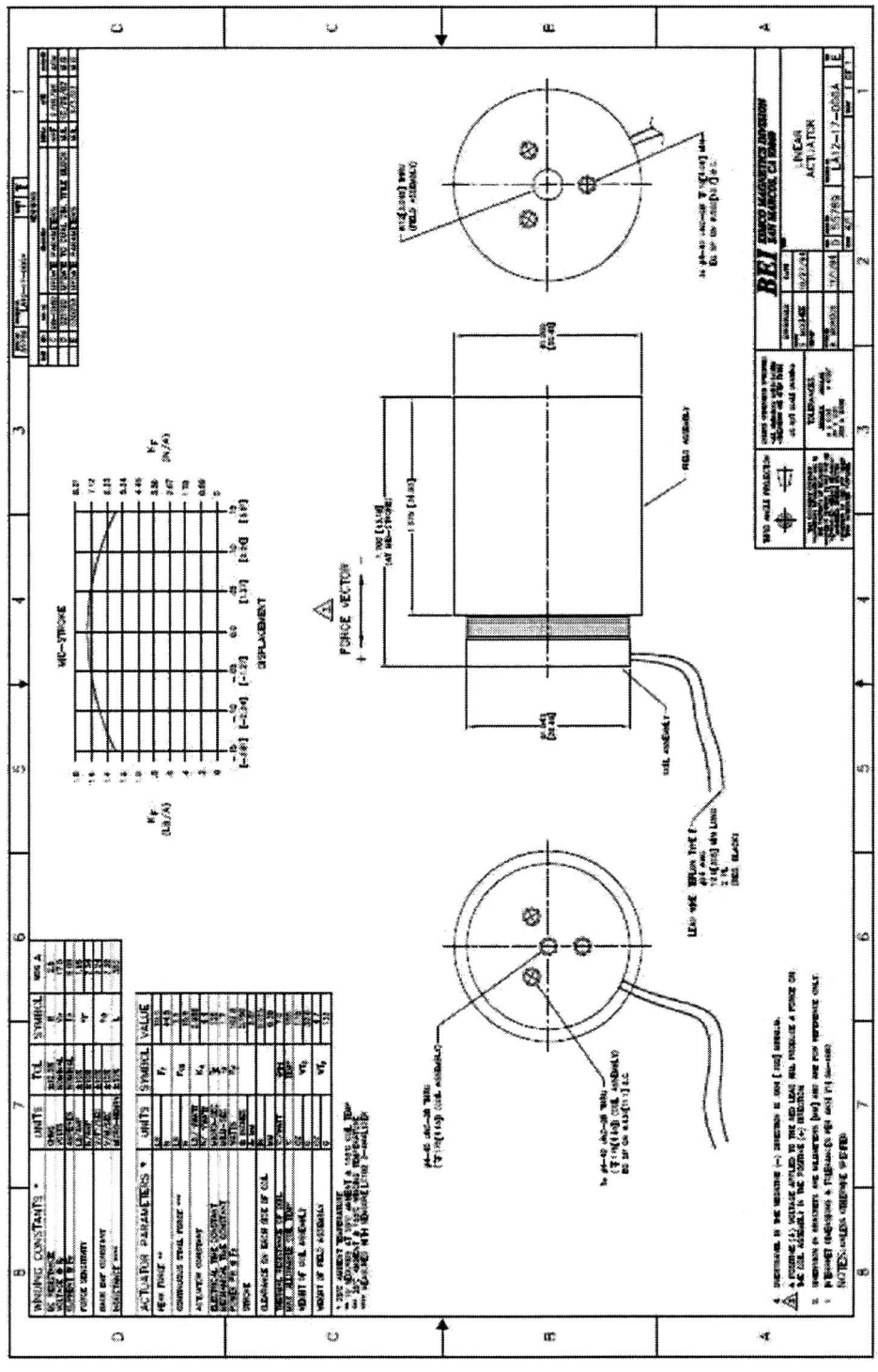

Figure H.4: Drawing of the voice coil actuator Bei Kimco LA12

Appendix I

Numerical Aperture

To collect more light and produce brighter images, cones of rays form the object, intercepted by the objective lens, should be large as possible. As magnifications increase and the focal lengths and diameters of the objective decrease correspondingly, the solid angle of useful rays from the object also decrease. For microscopy the typical measure of collection efficiency is the numerical aperture (NA). The NA can be calculated with equation I.1.

$$NA = n \sin \theta_{na} \tag{I.1}$$

Where:

n : Refractive index of the immersing medium between objective and lens

θ_{na} : Angular aperture of lens (half the value of the image forming cone ($= 2\theta_{na}$) aperture)

See figure I.1 for definition of θ_{na}. Two values limits the NA. The angular aperture θ_{na} and

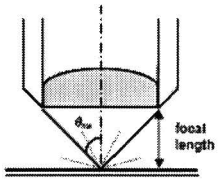

Figure I.1: Definition of θ_{na} [Lee, 2005]

the refractive index n. For air $n = 1.0$ the NA will not exceed 1.0, because the collection angle yields $\theta_{na} = 90$. Practical value of θ_{na} are 72, which corresponds to a NA of 0.95. Immersion lenses uses other immersion media to get a $NA > 1$.

Figure I.2 shows a microscope lens with fixed local lengths f (same magnification) and three increasing angular aperture sizes D_a. The value of NA increases with the increase of the light collection efficiency angle as is predicted with equation I.1.

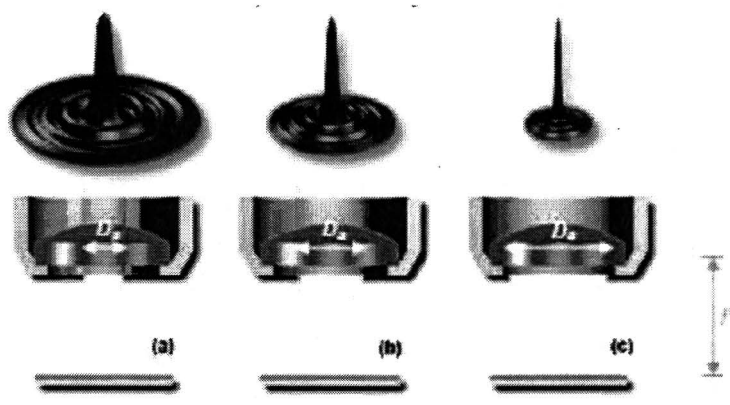

Figure I.2: Graphical representation of relation between NA, airy disk size and light collection capabilities of a microscope lens (increasing NA left to right) [Lee, 2005]

As the angle of the light collecting cone increases (increasing NA or decreasing $\frac{f}{Da}$ ratio) more orders of light scattered form the specimen will be collected and contribute to a smaller Air disk and narrower light intensity peak and thus results in a better separation in detail. This explains why higher values of NA results in sharper and brighter images with better detail.

NA usually increases with increasing magnification. For a microscope lens with a fixed aperture D_a and three decreasing focal lengths (increasing magnification) therefore the angle of the light gathering con also increases (increasing NA or decreasing $\frac{f}{D_a}$ ratio) and of course the resolution see figure I.3.

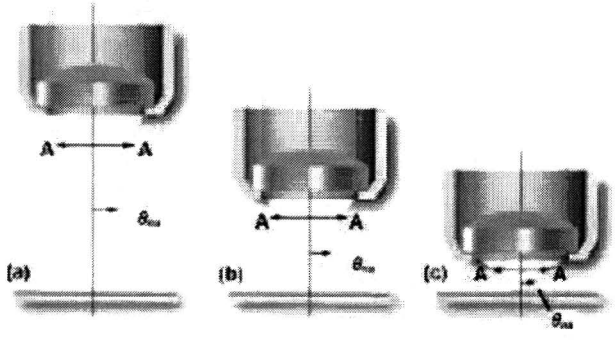

Figure I.3: Graphical representation of the influence of increasing magnification on the light gathering cone and NA value (increasing NA left to right) [Lee, 2005]

Appendix J

Diffraction limited spot size

single lens In case of a thin single lens, the Gaussian lens formula are given by equations J.1 and J.2.

$$\frac{1}{s_i} + \frac{1}{s_o} = \frac{1}{f_0} \tag{J.1}$$

$$M = \frac{s_i}{s_o} \tag{J.2}$$

Where:

M : Magnification of lens

f_o : Focal length of lens

s_o : Distance object plane to objective lens

If equation J.1 is substitute in equation J.2, we get the equation J.3

$$s_i = (M+1)f_o \tag{J.3}$$

If equation J.3 is substitute into equation 4.14 the diffraction limited spot size through a thin lens is described by equation J.4, following [Meinhart and Wereley, 2003].

$$d_{sp} = 2.44(M+1)\lambda\frac{f_o}{D_a} \tag{J.4}$$

The d_{sp} determines the smallest measured detail of a lens system and thus the maximum resolvable details.

Infinity corrected lens A optical system magnification is usually obtained through the combination of the objective lens and the ocular or eyepiece together. This is also called a infinity corrected lens. The advantage is that the distance between the objective and the image plane can be changed without effecting the magnification. The magnification M for a infinity corrected lens in terms of the focal lengths f_i, f_o , can be describes with the equation J.5.

$$M = \frac{s_i}{s_o} = \frac{f_i}{f_o} \tag{J.5}$$

If equation J.5 is substitute in equation 4.14, the diffraction limited spot size of infinity corrected optics is described by equation J.6 [Meinhart and Wereley, 2003, Wereley et al., 1999, 1998]

$$d_{s\infty} = 2.44M\lambda\frac{f_o}{D_a} \tag{J.6}$$

For schematic view of the $d_s\infty$ see figure J.1.

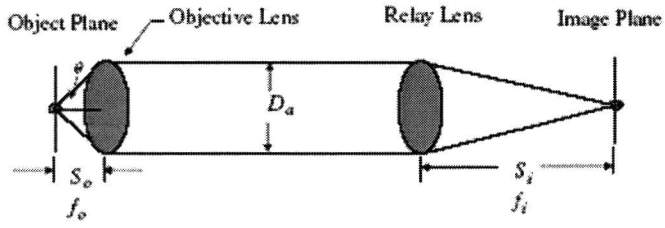

Figure J.1: Schematic view of infinity corrected lens [Meinhart and Wereley, 2003]

Appendix K

Matlab program determine cell Taylor deformation rate

```
clear all
hold off
close all

%%% number of cells to measure
cells= 1

%%% Read the image-file and background
I10 = imread('./serie3/f_000456.tif');
I11 = imread('./serie3/back.tif');


%%% subtract background
I = imsubtract(I10,I11);

%%% intrest region
I2 = imcrop;


sizeA = size(I2);
disp('Size original image:')
disp(sizeA)


%%% Filtering
alpha = 0.2;
h = fspecial('unsharp',alpha);
I3 = imfilter(I2,h);

%%% make image binairy
BW = im2bw(I3,0.05);
```

```
%%% fill holes
BW3 = imfill(BW,'holes');
figure, imshow(BW3)

%%% Edge detection:
BW2 = edge(BW,'canny');

%%% Boundary detection
boundaries = bwboundaries(BW2)
figure, imshow(I2)
hold on;


k=cells;
contour = boundaries{k};
plot(contour(:,2), contour(:,1),'g','linewidth',3);


%%% elliptical stable direct least squares fit of boundary cell
x=contour(:,1);
y=contour(:,2);

    if numel(x)~=numel(y) || numel(x)<5
        error('X and Y Must be the Same Length and Contain at Least 5 Values.')
    end

D1=[x.*x x.*y y.*y]; % quadratic terms
D2=[x y ones(size(x))]; % linear terms
S1=D1'*D1;
S2=D1'*D2;

[Q2,R2]=qr(D2,0);

    if condest(R2)>1.0e10
        warning('ellipsefit',...
            'Data is Poorly Conditioned and May Not Represent an Ellipse.')
    end


T=-R2\(R2'\S2'); % -inv(S3) * S2'

M=S1+S2*T;
CinvM=[M(3,:)/2; -M(2,:); M(1,:)/2];
[V,na]=eig(CinvM);
c=4*V(1,:).*V(3,:) - V(2,:).^2;
A1=V(:,c>0);
```

```
P=[A1; T*A1];

% correct signs if needed
P=sign(P(1))*P;

Phi=atan(P(2)/(P(3)-P(1)))/2;
c=cos(Phi);
s=sin(Phi);

% rotate the ellipse parallel to x-axis
Pr=zeros(6,1);
Pr(1)=P(1)*c*c - P(2)*c*s + P(3)*s*s;
Pr(2)=2*(P(1)-P(3))*c*s + (c^2-s^2)*P(2);
Pr(3)=P(1)*s*s + P(2)*s*c + P(3)*c*c;
Pr(4)=P(4)*c - P(5)*s;
Pr(5)=P(4)*s + P(5)*c;
Pr(6)=P(6);

% extract other data
XcYc=[c s;-s c]*[-Pr(4)/(2*Pr(1));-Pr(5)/(2*Pr(3))];
Xc=XcYc(1);
Yc=XcYc(2);
F=-Pr(6) + Pr(4)^2/(4*Pr(1)) + Pr(5)^2/(4*Pr(3));
AB=sqrt(F./Pr(1:2:3));
A=AB(1);
B=AB(2);
Phi=-Phi;
        if A<B % x-axis not major axis, so rotate it pi/2
            Phi=Phi-sign(Phi)*pi/2;
            A=AB(2);
            B=AB(1);
        end

S.Xc=Xc;
S.Yc=Yc;
S.A=A;
S.B=B;
S.Phi=Phi;
S.P=P;

        if nargout==1
            varargout{1}=S;
            else
            outcell=struct2cell(S);
            varargout=outcell(1:nargout);
        end
```

```
structuur = S
coeficientell= P;
P1 = P(1,1);
P2 = P(2,1);
P3 = P(3,1);
P4 = P(4,1);
P5 = P(5,1);
P6 = P(6,1);


%%% calculation Taylor deformation rate
Dxy= (A-B) / (A+B)
```

Output of the this file was:

```
cells =

     1

Size original image:
    47    54


boundaries =

    [127x2 double]
    [101x2 double]
    [ 13x2 double]
    [  7x2 double]
    [169x2 double]
    [129x2 double]


structuur =

     Xc: 25.1776
     Yc: 26.8207
      A: 22.8558
      B: 21.0382
    Phi: -1.3469
      P: [6x1 double]


Dxy =
```

0.0414